MODELLING IN THE ANALYSIS

OF ION EXCHANGE BETWEEN

BLOOD AND BONE

by

Simon Mark Willans B.Sc., M.Sc.

A thesis submitted for the Degree of :-

Doctor of Philosophy,

University of Edinburgh,

November, 1987.

to mam and dad, for support

and understanding

ACKNOWLEDGEMENTS

Having being a fortunate recipient of a Faculty of Medicine Scholarship, I would like to thank Professor S.P.F. Hughes for providing me with the opportunity to study at the University of Edinburgh, and for his encouragement during the course of the research.

I would also like to extend my thanks to my supervisor, Dr Ian McCarthy for useful suggestions, and for valuable help and guidance which was very much appreciated.

A special thanks to fellow colleagues for assistance during the course of the work. I must acknowledge the efforts of Bobby Fleming, who together with Ian McCarthy and Professor S.P.F. Hughes had performed multiple tracer outflow dilution experiments on the canine tibia. These experiments in fact provided me with the necessary data to be modelled. I am also grateful to Robin Strachan for performing the surgery in microsphere experiments involving the canine tibia.

Last, but not least, I am particularly indebted to Mike Devlin, Leslie Boyle (photography), and personnel at Medical Illustration (drawings) and Wm. Press Construction, Darlington, Co. Durham (tables and drawings).

DECLARATION

This thesis has been composed by myself. With the exception of the help and guidance as mentioned above, it is entirely my own work.

TABLE OF CONTENTS

Abstract

The principal objective of the research was to model the outflow results of multiple tracer outflow dilution (M.T.O.D.) techniques from the canine tibia so as to obtain a more precise understanding of the physiological mechanisms underlying mineral exchange in bone. To date, M.T.O.D. techniques have been performed on the tibiae of greyhound dogs but the subsequent outflow results have produced information mainly at the capillary level for the diffusible tracers concerned such as capillary permeability-surface area PS_C products from the widely used Crone-Renkin formulation. Back diffusion and heterogeneous capillary flow rates lacking from the formulation, however, have impaired the accuracy of PS_C.

Outflow results from two series of previously performed M.T.O.D. experiments were modelled. In the first experimental series, outflow results from the ipsilateral femoral vein concerning ^{125}I-albumin reference and ^{85}Sr (Ca analogue), ^{86}Rb (K analogue) diffusible tracers were used ; the tracers having being injected into the tibial nutrient arteries. In the second experimental series, ^{125}I-albumin and ^{85}Sr outflow results were used from parathyroidectomised dogs in which both tracers had been injected together before and after a dose of 0.0005 mg bovine parathyroid hormone (PTH).

The problem of back diffusion was alleviated by optimising a homogeneous flow model to M.T.O.D. data. The model produced informative parameter estimates for ^{85}Sr and ^{86}Rb concerning fluid spaces and associated boundaries in Haversian systems largely comprising the diaphyseal cortex. Exchange was assumed to take place there by virtue of injecting the tracers into the tibial nutrient artery.

Blood flow rates, known to be influential in governing the extent of tracer exchange in the diaphysis, were investigated using the microsphere technique. Flow rate heterogeneity was found to be substantial, as adjudged by distributions of relative deposition densities of microspheres in 40 pieces of cortex and 10 marrow samples in 6 tibiae. For the cortex, the distributions were positively skewed with a relative dispersion of around 40%. Additional work involving light microscopy suggested that the distribution of cortical flow rates were not attributable to particular changes in capillary density, which were relatively uniform at 2682 $\pm$ 510 capillaries/cm^2 (4 tibiae ; 240 observations).

The findings concerning flow rate heterogeneity, together with the deduction that the cortex and marrow respectively received 65% and 35% of tibial nutrient artery flow, prompted the development of a parallel multicapillary model in which 4 capillary systems were alloted to the cortex and 1 such system to the marrow. Input to the model was a suitable form of the reference tracer outflow profile which describes the large vessel transport behaviour assumed identical for all tracers concerned. Parameter estimates (mean $\pm$ s.d.) found by optimisation for ^{85}Sr and ^{86}Rb (n=6) were PS_C = 0.045 $\pm$ 0.021 and 0.047 $\pm$ 0.022 ml/s respectively. Apparent volumes of distribution (n=5) for the interstitial fluid were 0.90 $\pm$ 0.36 (^{85}Sr) and 0.69 $\pm$ 0.22 ml of diaphysis (^{86}Rb).

Additional studies involving gamma variates showed that model inputs were robust in terms of varying degrees of large vessel dispersion. Furthermore, simulation studies involving the effect of asymmetric transport on the resulting parameter estimates in the context of modelling the PTH data provided speculative evidence for the concept of a bone-lining cell membrane controlling uptake to bone surfaces.

LIST OF TABLES

LIST OF FIGURES

NOMENCLATURE

Symbol	Description	Typical units
C	Concentration	amount/ml
C_A	Arterial concentration	"
$C_B(x,t)$	Concentration of tracer in bone	"
$C_{B_j}(t)$	Concentration of tracer in the jth bone segment	"
$C_C(x,t)$	Concentration of tracer in the capillary	"
$C_{C_j}(t+)$	Concentration of tracer in the jth cap. segment	"
$C_I(x,t)$	Concentration of tracer in the interstitial fluid	"
$C_{I_j}(t)$	Conc. of tracer in the jth interstitial fluid segment	"
$C_{In}(t)$	Concentration of tracer in the arterial inflow	"
$C_{Out}(t)$	Concentration of tracer in the venous outflow	"
C_T	Tissue concentration	"
C_V	Venous concentration	"
$C_1(t)$	Concentration of compartment 1.	"
$C_2(t)$	Concentration of compartment 2.	"
C^*	Count rate	cts/min
C_{Co}^*	Diaphyseal cortex count rate	"
C_i^*	Count rate in sample i	"
C_{In}^*	Injected count rate	"
C_M^*	Diaphyseal marrow count rate	"
d_i	Microsphere deposition density in sample i	cts/g
D	Diffusion coefficient	cm^2/s
D_r	Radial diffusion coefficient of tracer	"
D_{Rb}	Free diffusion coefficient of ^{86}Rb	"
D_{Sr}	Free diffusion coefficient of ^{85}Sr	"

D_x	Axial diffusion coefficient of tracer	cm^2/s
E : E(t)	Extraction : extraction as a function of time t	-
E_{max}	Maximum extraction	-
$E_{net}(t')$	Net extraction after time duration t'	-
f_i	ith relative regional flow	-
Δf_i	ith class width of relative regional flows	-
$\Delta \hat{f}_{PS_C}$	Impact function for parameter PS_C	$5\ s^{-2}$
F_B	Blood flow rate of tracer	ml/s
F_{Bu}	Bicarbonate buffer flow rate of tracer	"
F_i	Regional capillary flow rate	"
F_P	Plasma flow rate of tracer	"
F_s	Solute/tracer flow rate (general)	"
FER(t')	Fractional escape rate after time duration t'	$5\ s^{-1}$
g_{Co}	Mass of diaphyseal cortex	g
g_i	Mass of sample i	"
g_M	Mass of diaphyseal marrow	"
h(t)	Whole system (bone) transport function	$5\ s^{-1}$
$h_A(t)$	Arterial transport function	"
$h_{A_i}(t)$	Individual artery/arterial system transport function	"
$h_C(t)$	Capillary transport function	"
$h_{C_i}(t)$	Individual cap./cap. system transport function	"
$h_{C/R}(t)$	Reference tracer capillary transport function	"
$h_D(t)$	Transport function of diffusible tracer	"
$h_{LV}(t)$	Large vessel transport function	"
$h_{LV_i}(t)$	Individual large vessel transport function	"
$h_R(t)$	Transport function of reference tracer	"
$h_R(t)_i$	Value of $h_R(t)$ for sample i	"
$h_V(t)$	Venous transport function	"

$h_{V_i}(t)$	Individual vein/venous system transport function	$5\ s^{-1}$
H	Fractional blood haematocrit	–
H(t")	Cumulative residence time after time t"	–
k_{12}	Rate constant from phase 1 to phase 2	min^{-1}
k_{21}	*vice versa* to k_{12}	"
k_{23}	Rate constant from phase 2 to phase 3	"
k_{32}	*vice versa* to k_{23}	"
KU	Coefficient of kurtosis	–
L_C	Length of a capillary	cm
L_{HC}	Length of a Haversian canal	"
m_r	Moment of order r	–
$n_{ms/Co}$	Number of microspheres in the diaphyseal cortex	–
n_{ms_i}	Number of microspheres in sample i	–
$\bar{n}_{ms_i}$	Number of microspheres in sample i if uniformly distributed in the cortex	–
$\bar{n}_{ms_i}'$	Newly derived $\bar{n}_{ms_i}$ value from random number generators	–
n_x	Number of axial capillary segments	–
NC	Number of capillaries counted	–
P	Permeability	cm/s
P_{12}	Permeability for tracer flux from phase 1 to 2	"
P_{21}	*Vice versa* to P_{12}	"
P_{23}	Permeability for tracer flux from phase 2 to 3	"
P_{32}	*Vice versa* to P_{23}	"
Pc_{Co}	Percentage of diaphyseal cortex, flow is supplied by the tibial nutrient artery	%
Pc_M	Percentage of diaphyseal marrow, flow is supplied by the tibial nutrient artery	%
PS_B	Permeability-surface area product of :- (^{86}Rb) :- bone cell (^{85}Sr) :- hypothetical bone surface binding pool	ml/s

$PS_{B/23}$	Permeability-surface area product for tracer influx from phase 2 (interstitial fluid) to phase 3 (bone)	ml/s
$PS_{B/32}$	*Vice versa* to $PS_{B/23}$	"
PS_C	Permeability-surface area product of capillary/ capillaries	"
$PS_{C/12}$	Permeability-surface area product for tracer influx from phase 1 (capillary) to phase 2 (interstitial fluid)	"
$PS_{C/21}$	*Vice versa* to $PS_{C/12}$	"
PS_i	Permeability-surface area product of barrier i	"
PS_{Tot}	Total permeability-surface area product	"
Pt_{Co}	Percentage partitioning of tibial nutrient artery flow to the cortex	%
Pt_M	Percentage partitioning of tibial nutrient artery flow to the marrow	%
qr	Radial flux	amount
qr_{B_j}	Radial tracer flux in the jth bone segment	"
Δqr_{BI_j}	Radial flux change in the jth bone segment whose neighbouring segment is that of the interstitial fluid	"
qr_{C_j}	Radial tracer flux in the jth capillary segment	"
Δqr_{CI_j}	Radial flux change in the jth cap. segment whose neighbouring segment is that of the interstitial fluid	"
qr_{I_j}	Radial tracer flux in the jth interstitial fluid segment	"
Δqr_{IB_j}	Radial flux change in the jth interstitial fluid segment whose neighbouring segment is that of the bone	"
Δqr_{IC_j}	Radial flux change in the jth interstitial fluid segment whose neighbouring segment is that of the capillary	"
r	Radial coordinate	cm
r-	Radial extreme of phase just before the barrier	"
r+	Radial extreme of phase just after the barrier	"

$\overline{rd}$	Mean relative deposition density	–
rd_i	Relative deposition density of sample i	–
Δrd_j	jth class interval width of relative deposition density values	–
R(t")	Residue function after time t"	–
R_C	Radius of capillary	cm
R_{CL}	Radius of cement line	"
R_{HC}	Radius of Haversian canal	"
S	Surface area	cm^2
S(x)	Surface area as a function of axial distance x	"
SD	Standard deviation	–
SK	Coefficient of skewness	–
t	Time	s
Δt	Time interval	"
t+	Time infinitely soon after the beginning of a time step occurring just after the shift of the capillary fluid downstream by one segment	"
t_{A_i}	Time delay for ith arterial system	"
t_i	Time taken for sample i	"
t_{LV_i}	Time delay for ith large vessel system	"
t_V	Time delay for venous system	"
t_{V_i}	Time delay for ith venous system	"
$\bar{T}$	Mean transit time for passage of tracer through whole organ/bone	"
T_C	Capillary transit time	"
$\bar{T}_C$	Average capillary transit time	"
T_{C_i}	ith capillary transit time	"
ΔT_{C_i}	Width of ith class of capillary transit times	"
T_{LV}	Large vessel transit time	"
$v_F(x,r)$	Velocity of flowing solute/tracer	cm/s

$V : V(x)$	Anatomical volume : Anat. volume as a fn. of exact position x	ml
V_C	Anatomical volume of the capillary/capillaries	"
$V_{C/Co}$	Anatomical volume of the cortical capillaries	"
$V_{C/M}$	Anatomical volume of the marrow capillaries	"
V'	Apparent volume of distribution	"
V_B'	Apparent volume of distribution of :- (^{86}Rb) :- bone cells (^{85}Sr) :- hypothetical bone surface binding pool	"
V_C'	App. vol. of distribution of the capillary/capillaries	"
V_I'	App. vol. of distribution of the interstitial fluid	"
V_T'	App. vol. of distribution of the whole tissue	"
w_i	Fraction of the organ/bone having a flow f_i	-
W(i) W_i	Overall weighting factor	-
x	Axial coordinate	cm

Greek letters

γ	Ratio of P_{21}/P_{12} (see P_{21}, P_{12})	-
$\sigma^2_{CASE\ 1}$ $\sigma^2_{CASE\ 2}$	Variances as defined in section 4.3.2.	-
σ_{Het}^2	Variance associated with a heterogeneous distribution of microspheres	-
σ_M^2	Variance associated with measurement (microsphere studies)	-
σ_{Ob}^2	Observed total variance (microsphere studies)	-
τ	Relaxation time	s
τ_r	Radial relaxation time	"
τ_x	Axial relaxation time	"

CHAPTER 1

INTRODUCTION

1.1. BONE STRUCTURE

Bone is a highly specialized form of connective tissue and is very hard and porous. It encapsulates the marrow and basically consists of organic and inorganic phases. The organic phase which constitutes around 35% of bone mass, consists of fibrous collagen and mucopolysaccharide ground substances, whereas the remaining inorganic mineral phase largely comprises compounds of calcium and phosphate called hydroxyapatites. There are basically two types of bone, depending on structure and shape. There are long bones which are tubular in structure, and bones that are short, flat and irregularly shaped. Bones such as the femur, tibia and humerus belong to the former type and bones such as the scapula and the vertebrae to the latter. In this thesis, interest will be solely confined to long bones.

1.1.1. Typical long bone structure

The long bone as illustrated in figure 1-1 is a major unit of the appendicular skeleton. It basically consists of a shaft (diaphysis) with an expansion (metaphysis) at each end.

In an immature animal, each metaphysis is surmounted by an epiphysis which is united to its metaphysis by a cartilaginous growth plate (epiphyseal plate). At the extremity of each epiphysis, a specialized covering of articular cartilage forms the gliding surface of the joint (articulation) which facilitates motion between the particular long bone and the adjacent bone in the skeleton.

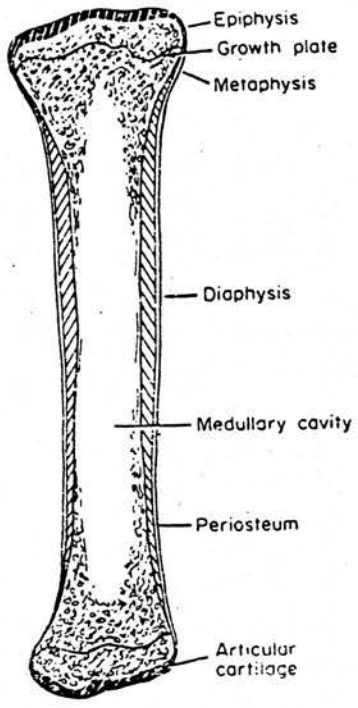

FIGURE 1-1 : Diagrammatic representation of the parts of a long bone.

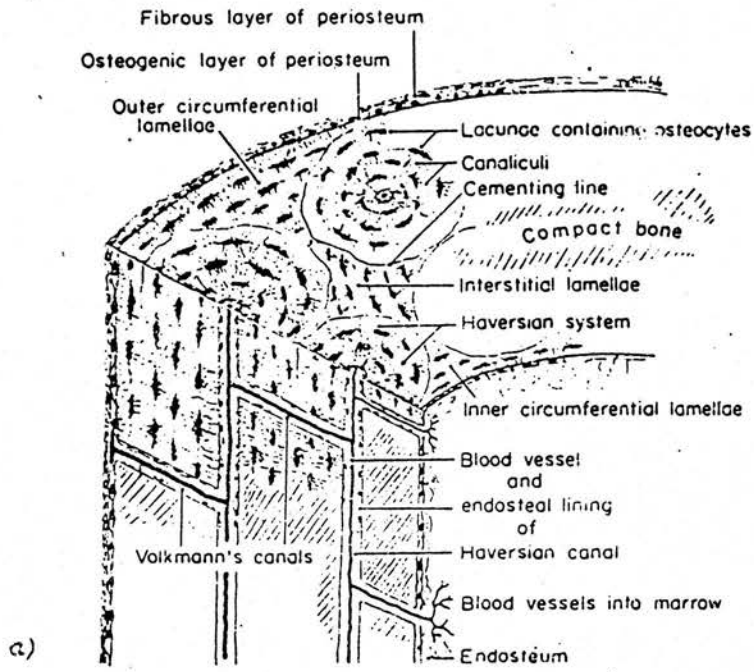

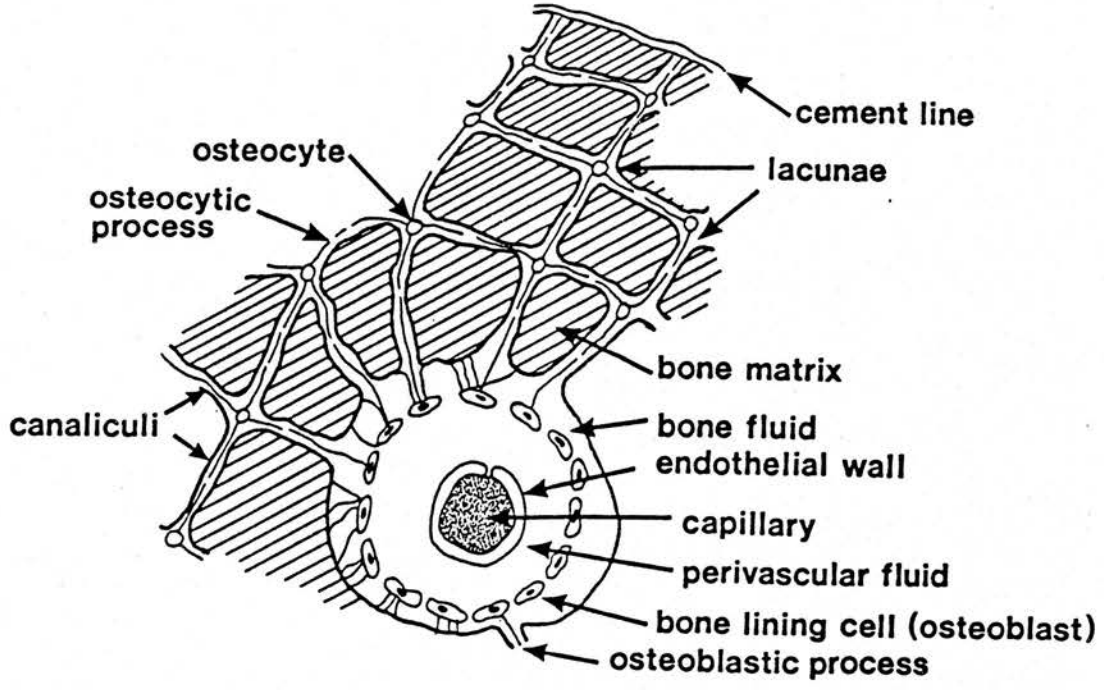

FIGURE 1-2 : a) Basic compact bone structure.
b) The Haversian system.

The diaphysis is a hollow tube. It's walls are composed of dense cortex which is thick throughout the extent of the diaphysis but tapers off to become the thin shell of each metaphysis. The central space (medullary cavity) within the diaphysis contains the bone marrow. The medullary cavity is present only in the diaphysis.

The metaphysis consists entirely, except for the cortical shell, of thin osseous spicules (trabeculae) in a lattice work of cancellous bone.

At the cessation of growth, the epiphyses composed of cancellous bone, become fused with the adjacent metaphyses at the sites of the previous growth plates. The outer shell of the metaphyses and epiphyses is a thin layer of cortical bone continuous with the compactum of the diaphysis.

Covering the entire surface of a mature long bone, except for the articulation is the periosteum which is composed of two layers. The main inner layer contains the highly active cells which produce circumferential enlargement and modelling of the growing long bone. The outer layer is fibrous and supporting and comprises almost the entire periosteum of a mature bone.

1.1.2. Compact bone

Figure 1-2a shows the internal structure of cortical bone as observed in man and also the dog. The inner surface of the cortex in contact with the marrow is called the endosteum. Located between the endosteum and periosteum are many osseous units called Haversian systems or secondary osteons.

The Haversian system contains a central Haversian canal which surrounds a single capillary in most instances, although there are occasions when there may be two capillaries. The Haversian systems tend to be aligned more or less

*The radii of bone capillaries have been observed to be variable in dogs (Cooper et al.1966); $R_c = 5 \times 10^{-4}$ cm was considered to be a suitably representative value for dogs and also man.

parallel to the long axis of the bone with a very gentle tendency to spiral (Cohen and Harris 1958). The capillaries which supply nutrients to the cortex communicate with each other via Volkmann canals ; this form of communication extends from the endosteum to the periosteum. The Haversian systems are bound by cement lines, and concentric layers of bone matrix fill in between the Haversian canal and the cement line. A more detailed picture of the Haversian system is shown in figure 1-2b and relevant morphometric measurements found by various investigators for man and dog in table 1-1.

TABLE 1-1

Morphometric measurements of Haversian systems in long bones of dog and man

Key references
Jow ; Jowsey (1966)
Joh ; Johnson (1963)
Atk ; Atkinson and Hallsworth (1982)

Description	Measurement x 10^{-4} cm		Key ref.
	Dog	Man	
Cement line radius R_{CL}	(77 ± 19)	(112 ± 25)	Jow : Jow
Haversian canal radius R_{HC}	(14 ± 6)	25	Jow : Joh,Atk
Haversian canal length L_{HC}	-	5000	: Joh,Atk
Capillary radius R_C*	5	5	-

The Haversian canal space outside the capillary contains interstitial fluid or perivascular fluid which is a medium for the passage of metabolites. At the outer reaches of the Haversian canal are bone lining cells often referred to as resting osteoblasts which are very occasionally involved in osteon formation. Beyond the osteoblasts is the layered bone matrix which contains numerous minute canals called canaliculi.

The canaliculi contain bone fluid which is a medium for the passage of

nutrients to deeper reaches of the matrix. Situated occasionally in the canaliculi are much larger structures called lacunae. The lacunae house other types of bone cell called osteocytes which are believed to originate from redundant osteoblasts. The osteocytes have very fine cytoplasmic processes which extend throughout the canaliculi and communicate with other osteocytes and osteoblasts.

Lacunae and canaliculi are also found in lamellar bone which fills in the rest of the cortex from the Haversian systems. Circumferential lamellar bone is located near the periosteal surface and interstitial lamellar bone is to be found between Haversian systems.

The structure of cortex in terms of lamellar bone and Haversian systems varies in different species. Men and dogs have very large numbers of Haversian systems, whereas rodents and rabbits have fewer numbers and higher proportions of lamellar bone.

1.1.3. Cancellous bone, woven bone & marrow

Referring to long bones in particular, the main location for cancellous bone is the metaphyses, where it forms a lattice work structure, the spaces of which are filled with marrow. Cancellous bone also exists to a lesser extent in an extremely thin layer on the endosteal surfaces of the cortex. Generally, Haversian systems are to be found in cancellous bone, but in much smaller numbers than in cortical bone. Exposed capillaries are to be found on cancellous bone surfaces.

Woven bone is immature bone that appears in embryonic development or in the repair of fractures. It is usually regarded as coarse bundled bone and is much more cellular than mature bone. Woven bone is replaced by mature

bone in growing animals.

Marrow which is encapsulated by bone occurs in two forms depending on colouration. Red marrow occurring predominantly in the short bones is responsible for red blood cell production and the production of some white blood cells, whereas yellow marrow occurring in long bones is a fatty adipose supporting tissue. Both forms of marrow are highly vascularised.

1.2. BONE BLOOD SUPPLY

1.2.1. The afferent vascular system

The number of afferent supply types to long bones is a controversial question. It is widely accepted that there are three types, which are the nutrient, metaphyseal and epiphyseal supplies, the question is whether a fourth afferent periosteal supply exists. Rhinelander (1968) on the basis of a great deal of experimental work considers that periosteal arterioles supply the outer third or quarter of the cortex only in localized areas of fascial attachments. On the other hand, Brookes (1971), and Lopez-Curto *et al* (1980) using Microfil techniques in adult dogs are not in favour of any significant afferent periosteal supply and consider that the bulk of the diaphyseal cortex is supplied by vessels that originate from the nutrient artery. An afferent periosteal supply may become prominent, but only in cases where blood vessels have been damaged in the medullary cavity (Nelson Jr. *et al* 1960). Descriptions of the nutrient, metaphyseal and epiphyseal artery groups follow.

The nutrient artery

The number of nutrient arteries supplying bone is dependent on the animal species and on the bone considered. Bones such as the tibiae in dogs tend to contain a single nutrient artery, whereas bones such as the femora in humans tend to contain two nutrient arteries.

The nutrient artery as in the case of the tibia, enters the diaphysis posterolaterally via a nutrient foramen and passes diagonally through the cortex in the nutrient canal in the presence of a nutrient vein. No branches emanate from the artery in the cortex and it finally enters the marrow cavity where it branches into ascending and descending medullary arteries. These

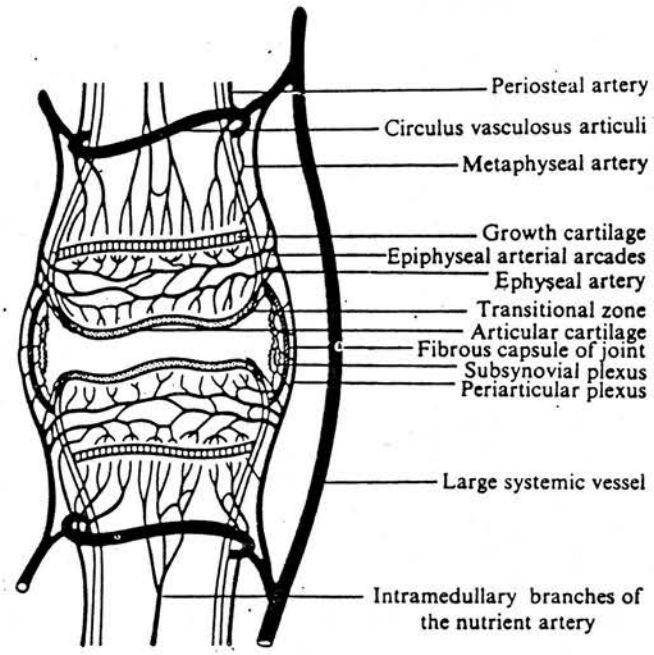

FIGURE 1-3 : Arterial arrangements at the extremities of long bone.

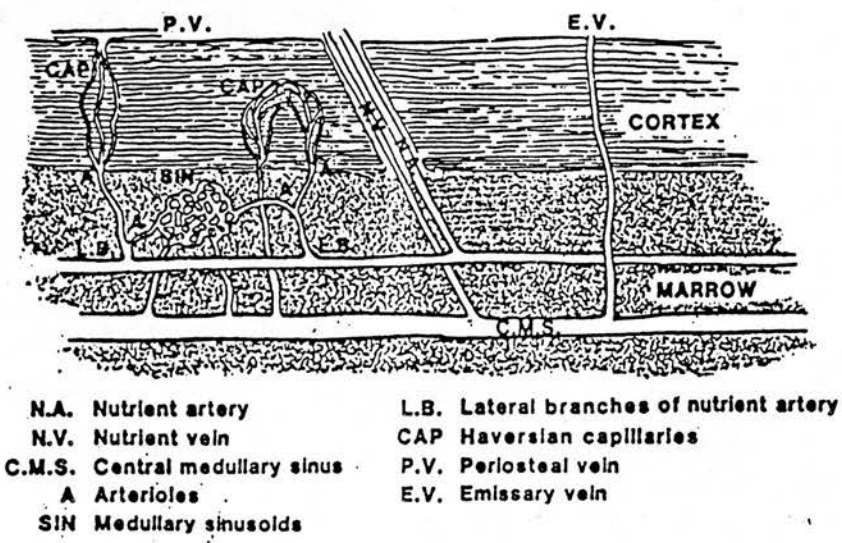

FIGURE 1-4 : Microvasculature of the canine tibial diaphysis

latter arteries divide further into arterioles which supply capillary networks in the cortex, and capillary and sinusoid networks in the marrow.

Metaphyseal arteries

Metaphyseal arteries are very numerous and in a mature long bone supply the bulk of the metaphyses via small foramina as shown in figure 1-3. By reference to their sites of entry into bone, they can be termed superior and inferior (Trueta and Harrison 1953). In mature long bones, metaphyseal arteries readily anastomose with epiphyseal arteries and intramedullary branches of the nutrient artery. They assume an important role in supplying nutrients to the diaphyseal cortex in situations of nutrient artery damage and obliteration (Brookes, 1971).

Epiphyseal arteries

As illustrated in figure 1-3, epiphyseal arteries supply the epiphyses with blood via small foramina, and by reference to their sites of entry can be termed medial and lateral (Trueta and Harrison 1953). They have been described in the adult human tibia by Nelson Jr. *et al* (1960) as being like the spokes of a wheel with many branches emerging at right angles forming a dense interlocking vascular network. This dense interlocking vascular network partly contributes an anastomoses to the metaphyseal vessels

1.2.2. The efferent vascular system

The components of the efferent vascular system are periosteal veins, cortical venous channels and the larger structures such as the central medullary sinus in continuity with nutrient and emissary veins. Most of these components are illustrated in figure 1-4 relating to the canine tibial diaphysis.

Periosteal veins

The drainage of the cortical capillaries in man and dog is principally to the periosteal venous complex and almost none drain to endosteal vessels (Lopez-Curto *et al* 1980). This situation may be different in rabbits and smaller animals, where Brånemark (1959) reported cortical capillary drainage to sinusoids or into collecting venules in the marrow.

Cortical venous channels

Cortical venous channels contribute to the drainage of marrow capillaries. They traverse the cortex directly often entering the cortex in the company of one or more arterioles.

Sinuses, nutrient and emissary veins

The other source of marrow drainage favoured by sinusoids is to collecting sinuses such as the central medullary sinus located in the bulk of the marrow substance. Nutrient and emissary veins located in the diaphysis, and epiphyseal-metaphyseal veins at the extremities are in continuity with the sinuses and provide drainage to the larger systemic veins.

1.2.3. Bone & marrow microvasculature

Lopez-Curto *et al* (1980) used the silicone elastomer Microfil to investigate the microvasculature of the adult dog tibia. They found that the tibial nutrient artery supplied the marrow and cortex via parallel, independent sets of arterioles and terminal capillary beds (figure 1-4). Furthermore, no arteriolar or capillary anastomoses were observed linking these separate beds. Brånemark (1959), however observed cortical and marrow vessels in rabbits that were in series and not in parallel as was seen in the dog.

The cortical capillaries are mainly located in Haversian systems, the main structural units of the cortex and are to a lesser extent found in Volkmann canals and lamellar bone. They are the nutrient exchanging vessels of cortical bone and by virtue of the fact that they are drained by periosteal vessels, the blood flow to the cortex is regarded as centrifugal. The capillaries to be found in cancellous bone are supplied by the metaphyseal and epiphyseal arteries and are located in sparsely populated Haversian systems and on cancellous bone surfaces.

With regard to the marrow, the functional vascular lattices are considered to be capillaries in yellow fatty marrow and sinusoids in red marrow. The capillaries and sinusoids are closed and continuous structurally (Trueta and Harrison 1953). Marrow capillaries can well be replaced by sinusoids when there is an increased demand for red blood cells as in states of anaemia. The sinusoids infact have been shown by direct vital microscopy, in the case of the rabbit fibula (Brånemark, 1959) to dilate and contract rhythmically, which could be a passive response to pulsatile blood flow in medullary arteries. This may suggest that sinusoids can to an extent control blood flow not only in the marrow but to the cortex as well. Sinusoids are supplied by more than one arteriole which has been demonstrated by the clumping of perfusates.

1.3. BONE PHYSIOLOGY & MINERAL EXCHANGE

1.3.1. Bone modelling & remodelling

Bone, as one might falsely conclude from its appearance is not a solid inert substance, but is infact a very dynamic tissue. It is continuously being formed (apposition) and destroyed (resorption) in response to homeostasis and external factors such as mechanical stress. The processes of apposition and resorption are collectively termed as modelling and remodelling when referring to endosteal-periosteal surfaces and osteons respectively.

Bone modelling is the more rapid of the two processes in terms of apposition and resorption rates, and is largely concerned with development, growth, repair and pathological processes in which bone shape and dimensions may significantly change. Concerning the modelling process in the normal mature diaphysis, resorption occurs at the endosteal surface and apposition at the periosteal surface ; both processes are continuous.

Bone remodelling by contrast, is a cyclical process and refers to the subtraction and addition to a bone surface regardless of location, timing, magnitude, purpose or mechanism (Parfitt 1984). It occurs to prevent the accumulation of fatigue damage and maintains an adequate supply of young bone to subserve mineral homeostasis. There are five stages to the cyclical process of remodelling which are termed quiescence, activation, resorption, reversal, formation, and return to quiescence. For the purpose of this thesis which deals largely with mature adult bones, salient features of the five stages of remodelling are mentioned to describe the existence of the predominant Haversian systems and to enforce the point that most bone surfaces are inactive or quiescent.

In adults of large animals such as man, about 80% and 95% of respective trabecular and intracortical bone surface is inactive with respect to bone remodelling (Parfitt 1984). Quiescent undeveloped bone surfaces tend to be covered by unmineralized connective tissue and extremely thin (0.1–1µm) flattened lining cells about 50 µm in diameter (Miller *et al* 1980). Activation, involving random bone surfaces may then occur.

During activation, precursor cells travel in the circulation to the sites of activation. These cells penetrate the covering of connective tissue and bone lining cells to reach the mineralized bone surface where they fuse into multinuclear cells called osteoclasts.

Once in contact with the bone, the newly formed osteoclasts begin to cause resorption. They tend to erode cavities of characteristic shape and dimensions, referred to in trabecular bone as a Howship's lacuna and in cortical bone as a cutting cone. The process of resorption is brought about by the secretion of acids which dissolve the bone mineral and release collagen fibres which are digested by other mononuclear cells. The rate of resorption occurs at about 5–10 µm/day perpendicular to the eroded surface and at about 20–40 µm/day parallel to and along the eroded surface. The resorption ceases when the subsequent cavity reaches a mean depth of around 60 µm from the surface in the trabecular bone and about 100 µm in cortical bone.

Once resorption ceases, then a state referred to as reversal is attained in which the resorbed site is prepared for the onset of new bone formation. During reversal, the osteoclasts disappear from the resorption cavity and are replaced by mononuclear cells which smooth over the ragged surface left by the resorptive process. The cells then deposit cement substance, thus preparing the surface for bone formation.

Bone formation takes place after the appearance of osteoblasts which are plump columnar cells containing single eccentric nuclei. The organelles of the osteoblasts produce synthesis reactions which contribute to the formation of bone matrix and the production of collagen and carbohydrate protein complexes. In both cortical bone and trabecular bone, the rate of matrix apposition is most rapid (2–3 µm/day) at the beginning when the osteoblasts are columnar and densely packed, and the osteoid seam reaches a maximum width of 20 µm just before or shortly after the onset of mineralization. The rate of mineral apposition is initially 1–2 µm/day and exceeds the rate of matrix apposition which tends to slow down. After the termination of matrix synthesis, mineralization continues slowly until the osteoid seam disappears, and the cells remaining on the surface complete the morphologic and functional transformation to lining cells. The surface has now returned to its original state of quiescence except that the bone is younger and Haversian systems or secondary osteons have subsequently been formed.

1.3.2. Mineral exchange

As mentioned previously, mineralization proceeds along with the formation of bone matrix, but it can also occur in quiescent states. The uptake of calcium (Ca^{2+}) in mineral exchange is particularly important because it is responsible for bone hardness and subsequent mechanical strength. Other ions that bind to the matrix are sodium (Na^{+}), magnesium (Mg^{2+}), carbonate (CO_3^{2-}), phosphates (PO_4^{3-}) and fluorine (F^{-}). Additionally, various radioactive ions such as ^{90}Sr from atomic fall out and ^{226}Ra in the case of the radium dial painters also have the ability to bind. Pathological conditions inevitably result from excesses or deficiencies of these ions in the matrix, such as rickets which occurs as a consequence of a deficiency of calcium ions. It is therefore very important to

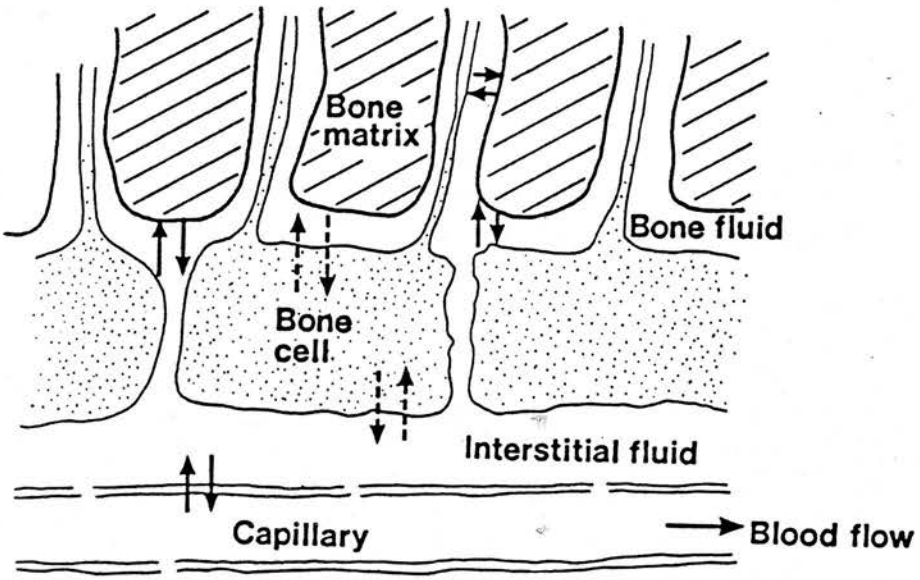

FIGURE 1-5 : Schematic diagram of pathways for mineral transport and sites for mineral exchange in a longitudinal section of a Haversian system.

understand the factors that affect ion movement and uptake in bone. For the purpose of this thesis, interest will be more concerned with the movement of Ca^{2+} and potassium K^{+} ions in compact bone by utilizing their respective tracer analogues of ^{85}Sr and ^{86}Rb.

Bone compartmentalization

Tracer uptake of ^{45}Ca a few minutes after injection has been shown by autoradiographs to be confined to surfaces that capillaries traverse (Pasternak *et al* 1968). In diaphyseal compact bone, these surfaces refer largely to bony layers surrounding the Haversian canal in osteons. To appreciate the pathways available to ion transport, figure 1-5 shows a schematic longitudinal section of a Haversian system which are predominant in compact bone. It can be seen that for ions to proceed to the bone matrix or bone cells they have at first to penetrate the capillary walls and then amass in sufficient a concentration in the interstitial fluid. This type of description of ion transport refers to different fluid spaces or compartments in which ions are allowed or prohibited in passing. The interstitial fluid can also be regarded as extravascular-extracellular or perivascular fluid depending on the interpretation of the compartments. Theories exist that are based on the bone lining cells (osteoblasts) forming an additional barrier and bone fluid compartment (Ramp and Neuman 1971), see figure 1-5. Ions that enter the bone fluid space such as ^{45}Ca can diffuse along the canaliculi so that they can bind to deeper bone structures. This has been demonstrated from autoradiographs of ^{45}Ca taken several days after administration, in which less intense uptake is seen between the Haversian canals (Rowland 1966). The volumes of distribution of the various compartments such as the capillary and interstitial fluid are important in relating to ionic and molecular concentrations and predicting uptake rates.

Bone capillaries

Only certain suitably sized ions and molecules can negotiate the first barrier, the capillary wall. Cooper *et al* (1966), from their electron microscopy studies of osteons from canine cortical bone, described the capillaries as being lined by one or more endothelial cells and a continuous basement membrane 400-600 Å thick. Small pores were observed in the endothelium in some specimens leaving the basement membrane to cover the resulting aperture. Furthermore, there were numerous cytoplasmic vesicles 600-1000 Å in diameter which were connected by pore-like openings to either the luminal or abluminal surface of the plasma membrane of the endothelial cell. The authors conclude that there are several mechanisms of molecular movement through the capillary, namely pinocytosis, passive diffusion and active transport. All three mechanisms necessitate passage across the basement membrane which could act as a rate limiting factor in the movement of certain ion species. Basement membranes, however have not been observed in long bones of rats (Hughes and Blount 1979) and mice (Döhler *et al* 1986).

In conclusion, capillaries of cortical bone seem to be of the unfenestrated, closed variety. For water soluble and hydrophilic ions such as Ca^{2+} and K^{+}, movement across them is by passive diffusion through the pores ; a process relying on concentration gradients and not requiring amounts of energy. Furthermore, passive diffusion describes the transport processes of lipophilic ions and molecules such as antipyrine which diffuse through the endothelial cell walls of bone capillaries, in addition to the pores. Other substances such as large protein molecules i.e. albumin traverse the capillary wall by pinocytosis. Infact, it is worth noting that large macromolecules such as horse-radish peroxidase (molecular weight 40,000) have been observed in

canaliculi after intravenous injection (Doty and Schofield 1972). Occasional large clefts which exist between the endothelial cells as well as the pores, and arise as a consequence of the confluence of chains of vesicles previously involved in pinocytosis, may facilitate the large macromolecular movement in addition (Renkin 1977).

Potassium in bone

The existence of another barrier, namely the bone lining cell membrane is a controversial question. Investigators such as W.F. Neuman (Cañas, Terepka and Neuman W.F. 1969 ; Ramp and Neuman W.F. 1971) have postulated such a membrane in order to explain why the bone fluid has much higher potassium levels than blood plasma. Neuman and his associates' views about the bone fluid phase stem from their discoveries that, potassium does not bind or concentrate on preformed crystals of calcium phosphate even in a potassium rich medium and that potassium in bone is rapidly and completely exchangeable (Neuman W.F. 1969). Furthermore, the cell phase in bone was found to be inadequate in accommodating the high levels of potassium. Neuman's findings led him to believe in blood/bone disequilibrium, the higher potassium concentrations in the bone fluid existing as a consequence of hydroxyapatite potentials (Brommage and Neuman W.F. 1979).

Contrary to the beliefs of Neuman, other investigators believe that all the described potassium can be accommodated entirely in bone cells rather than in bone fluid. Pinto and Kelly (1984), calculating fluid spaces in the canine tibia, demonstrated that ^{42}K content was by far the greatest in the cell phase, being around 10-15 times that of the perivascular phase. They also found that bone total and exchangeable potassium levels were similar, providing further

evidence that it does not bind to bone matrix. Pinto and Kelly suggest that, like other tissues, bone has a vascular space, an interstitial fluid space and an intracellular space, the only barrier being that of the capillary wall. Their views are the more believable in the light of the large molecule horse-radish peroxidase being found in the canaliculi after intravenous injection. If a membrane did exist it would have to contain large gaps between the cells to allow the movement of macromolecules such as the horse-radish peroxidase ; this in turn would not favour the disequilibrium between the fluid spaces, in particular the extremely high levels of potassium in bone fluid as compared to perivascular fluid.

Calcium in bone

The bulk of calcium in bone is to be found in the form of hydroxyapatites, complex microcrystalline compounds of calcium and phosphate of empirical form $Ca_{10}(PO_4)_6(OH)_2$. The crystals of hydroxyapatite are sparingly soluble and are believed to have a layer of water termed the hydration shell bound to their surfaces (Neuman W.F. and Neuman M.W. 1958). There are three zones in the crystal which present surfaces for ion exchange - crystal interior, crystal surface and the hydration shell. For Ca^{2+} ions, all three zones are accessible for ion exchange. The bone mineral apatite is highly imperfect structurally owing to small crystal size, internal crystalline disorder and lack of chemical perfection. The presence of carbonate, sodium and other ions and vital deficiencies in Ca^{2+} and OH^- make the bone metabolically active and in a state of disequilibrium (Posner 1978). In fact, small quantities of soluble amorphous forms of calcium phosphate are associated with the laying down of hydroxyapatite during calcification. Other locations for comparatively small amounts of calcium in bone are the bone cells, perivascular and bone fluid

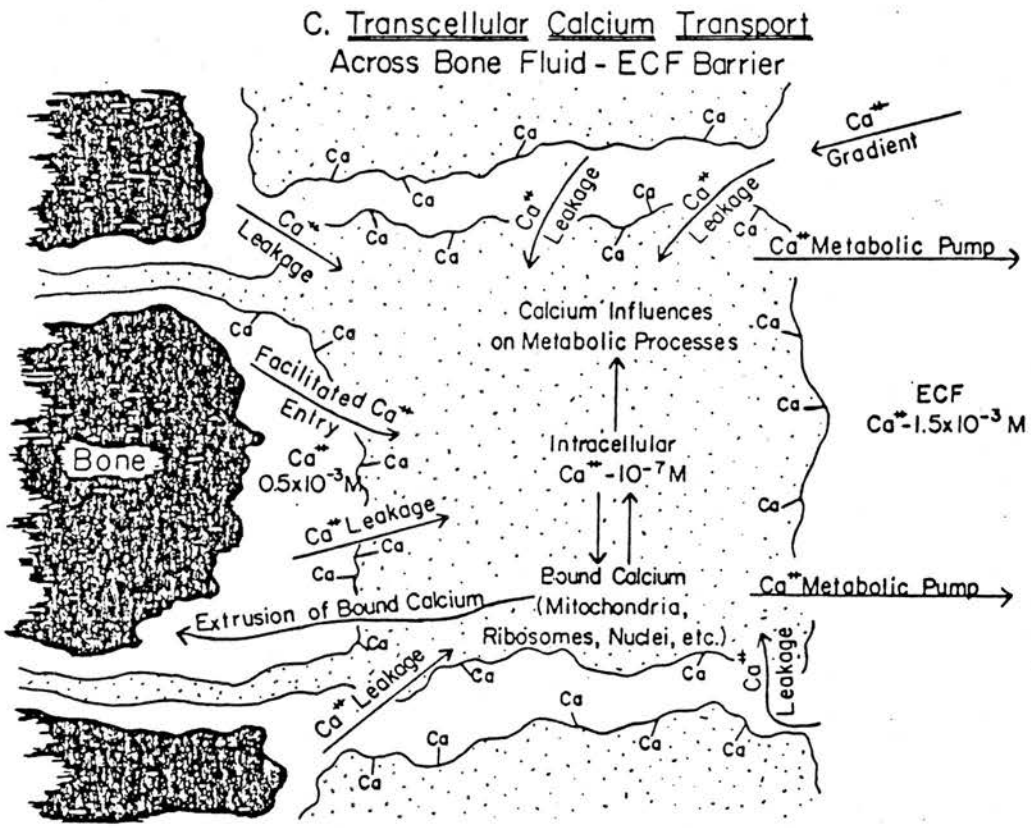

FIGURE 1-6 : Transcellular calcium transport in bone (Talmage, 1970).

phases.

These particular phases are important in our understanding of calcium exchange because it is thought that a disequilibrium exists between blood and exchangeable bone calcium levels. The disequilibrium aspect of such levels appears to be the only means of explaining why serum calcium concentration tends not to vary significantly with age and food intake. Furthermore, without calcium level disequilibrium, the mineralized bone could not resorb sufficiently and quickly enough to combat low serum calcium concentrations in instances of hypocalcaemia.

The ability of bone cells to store Ca^{2+} has led to the concept of a calcium pump (Talmage 1969). It has been considered that Ca^{2+} concentrations in the perivascular fluid phase are about three times higher than that of the bone fluid phase. This disequilibrium exists owing to activity in the bone lining cell layer. Talmage (1970) has postulated that Ca^{2+} influx between the two phases is by passive diffusion through the gaps between the cells. He also concludes that Ca^{2+} ions leak into the lining cell layer during the process (see figure 1-6). The intracellular calcium can then influence metabolic processes such that the cells can act as a pump and effectively pump out Ca^{2+} from the bone fluid. The efflux of Ca^{2+} ions between the two fluid phases thus results from an active transport mechanism and can take place even against large concentration gradients in these phases. The possibility of toxic effects, of having too much intracellular calcium is eliminated by calcium uptake to mitochondria to form calcium packages. These packages may then in turn move transcellularly along the cytoplasmic processes to other locations in the bone.

1.3.3. Biological factors in mineral homeostasis

The maintenance of bone can be thought of in terms of skeletal and mineral homeostases, but as the content of this thesis is concerned with the latter, only salient features of skeletal homeostasis will follow.

Skeletal homeostasis refers to the maintenance of the mechanical integrity of the skeleton and involves factors such as mechanical stress and pressure. It has long been known that patients who are confined to bed for long periods of time may be susceptible to a loss in bone mass. Furthermore, astronauts subjected both to recumbency and weightlessness tend to lose an appreciable amount of bone mineral. Thus it would seem, that to retain shape and structural strengths, bones have to be consistently stressed or weight bearing. It is now known that bone has electrical properties. In particular, streaming potentials can be produced by stress induced movement of ions through the fluid channels in bone.

Mineral homeostasis largely refers to the control of mineral ion concentrations in the plasma. The most important factors which involve bone are vitamin D_3 metabolites, parathyroid hormone (PTH) and calcitonin.

Vitamin D_3 metabolites

Vitamin D was first found to be responsible for intestinal calcium absorption which mainly contributes to plasma calcium levels. Diseases such as rickets in infants and osteomalacia in adults which stemmed from low plasma calcium levels were prevented by the consumption of high vitamin D products such as cod liver oil and dairy produce. The effect of vitamin D on two target organs, the intestine and the skeleton was clearly demonstrated and for many years,

interest was centred on its effect on intestinal absorption, assuming that it functioned in the body without alteration. However, it later became apparent once details of its chemical structure became available, that it was vitamin D in the form of metabolites of vitamin D_3 (cholecalciferol) that were responsible for the physiological interactions. The blood plasma calcium levels in normal and pathological conditions were infact controlled by various species of vitamin D_3 metabolites which were produced by way of the liver and kidneys. Under hypocalcaemic or hypophosphataemic conditions the kidney can produce the metabolite $1,25\text{-}(OH)_2D_3$ which on travelling to the intestines and bone can induce more intestinal transport of calcium and more bone calcium mobilization.

Vitamin D_3 is certainly implicated in the removal of calcium from bone to blood by osteoclastic resorption. In organ culture experiments, the metabolite $25\text{-}OHD_3$ has produced measurable bone resorption in which the vitamin D_3 by itself has produced no effect. Additionally, other investigators also believe that PTH is also associated with vitamin D_3 metabolites in bone resorption because only partial mobilization of calcium from body stores has been found to occur in thyroparathyroidectomised rats.

Parathyroid hormone (PTH)

PTH in increasing amounts is responsible for raising plasma calcium levels. It was found in early experiments, that surgical removal of parathyroid glands (parathyroidectomies) produced large falls in blood calcium associated with tetany and convulsions. The subsequent low blood levels of calcium could easily be restored following administration of PTH or bovine parathyroid extract PTE. Further studies revealed that a feedback mechanism existed to control the

secretion of the hormone ; hypocalcaemia stimulated its production whilst hypercalcaemia suppressed it (McLean 1957).

Difficulties however, are always present in the interpretation of experimental results involving PTH. For example, PTH-induced hypercalcaemia can be suppressed to certain extents in different species by endogenous PTH output and increased secretion of calcitonin, the hypocalcaemic hormone. Circulating levels of phosphate as well as calcitonin may also drastically affect PTH-induced mobilization of calcium. Furthermore, investigators such as Parsons *et al* (1971) have shown that plasma calcium levels actually fall transiently before beginning to rise after PTH administration. The fluctuations of the plasma calcium levels is also dependent on the size of the dosage of PTH and the period of study.

The effects of PTH administration are most pronounced in the kidneys, gastrointestinal tract and bones. In the kidneys, PTH administration causes increased urinary excretions of phosphate, sodium, potassium and bicarbonate and decreased excretion of hydrogen ions, ammonia, calcium and magnesium. Additionally, it may also control 25-OHD_3 metabolism in the kidney. The effect of PTH on the intestine is unclear. The most up to date answer available is that probably PTH has no direct effect on calcium absorption in the intestine but probably exerts an important indirect effect by its stimulation by synthesis of vitamin D_3 metabolites. In bones the effect of PTH is a rapid release of calcium, although much larger comparative doses to that of 1,25-$(OH)_2D_3$ are required. The rapid release of calcium is attributed to a direct action of PTH on bone cells. In tissue culture experiments it was found that the release of calcium is caused by increased chemical secretions by the osteoclasts which dissolved the matrix. In some cases the number of osteclasts and their precursors were found to increase as well. However, in intact animals it is

difficult to directly attribute the metabolic changes in the osteoclasts to the PTH because of possible contributions from vitamin D_3 metabolites. The effect of PTH on osteoblasts is a very puzzling question. Following PTH administration to a variety of species there is evidence of a rapid depression of the metabolic activity of osteoblasts. However, there is also evidence that PTH may have an anabolic effect. It has been found that osteoblasts and preosteoblasts can become more active ; increased mineralization has been observed after 3 weeks in thyroparathyroidectomised rats receiving daily doses of PTH. PTH may also affect the osteocytes because enlarged lacunae have been observed in the bones of experimental animals exposed to PTH.

Calcitonin

Calcitonin in increasing amounts is responsible for lowering plasma calcium levels and tends to oppose the action of PTH. It has been found in sheep and cows, that if the plasma calcium rises above its normal level for any reason, then the level of calcitonin in the plasma also rises, and as the plasma calcium falls the level of PTH rises. It is generally accepted that in mammals, calcitonin a peptide hormone arises in the C cells of the thyroid gland. Indeed, it was the discovery of rapid increases in plasma calcium following thyroparathyroidectomy in rats infused with PTE that provided evidence of its existence.

Calcitonin is far more effective in young than in old animals, since sensitivity to calcitonin is related to rates of bone turnover. It is believed to exert a direct action in reducing bone resorption. There have been reports of decreased numbers of osteoclasts in the vertebrae of parathyroidectomised rats which were subjected to calcitonin. Other investigators conclude that calcitonin

prevents the differentiation of new osteoclasts and decreases the effectiveness of existing ones. It is difficult though to conclude whether calcitonin affects both the mineral and matrix because there are still doubts about the full effects of preventing osteoclastic activity. The evidence that calcitonin may increase bone formation is not strong, even though some investigators have found increased amounts of new cortical bone as measured by tetracycline labelling in calcitonin treated rats.

Calcitonin has proved to be of use in the treatment of various bone dysplasias. It has assisted in the return of bone turnover rates to normality in patients with Paget's disease. Additionally it has proved to be useful in treating forms of hypercalcaemia, notably associated with malignant diseases, hyperthyroidism, hyperparathyroidism and vitamin D intoxication in both children and adults.

1.4. THESIS OBJECTIVES

1.4.1. Introduction

The purpose of this thesis is to study the short term kinetics of mineral exchange in bone. This can be achieved by studying the transport of important bone constituents such as calcium and potassium ions in bone capillaries and surrounding structures.

By virtue of the fact that it is extremely difficult to perform isolated blood vessel studies in bone, basically because of its hard and opaque structure, the best alternative that is available to us for studying mineral transport, is multiple tracer outflow dilution (M.T.O.D.) techniques. These techniques which have largely been performed on the canine tibia, have involved the usage of detectable tracer analogues of calcium and potassium such as ^{85}Sr and ^{86}Rb respectively. The subsequent outflow results have produced information concerning these two tracers mainly at the bone capillary level. However, many assumptions appertaining to capillary flow rates and the effect of the cortex-marrow inter-relationship on exchange had to be made.

The main objectives of this thesis were therefore to test these assumptions by developing detailed mathematical models to fit the outflow data in various circumstances and by so doing obtain a greater wealth of information concerning ion transport within internal bone structures. The models enabled one to allow for various important exchange processes within the bone thus making the system and findings more realistic. Hence, the outflow data regarding ^{85}Sr and ^{86}Rb in normal canine tibiae and ^{85}Sr data in the tibiae of parathyroidectomised dogs subjected to a fixed dosage of PTH was modelled to gain a further insight into bone physiology.

1.4.2. Objectives

To this end the objectives of this thesis were to :-

1. Review existing information on ^{85}Sr and ^{86}Rb uptake from M.T.O.D. techniques applied to the normal and PTH affected canine tibia.

2. Use morphometric data to develop a simple homogeneous flow capillary-interstitial fluid-bone (single capillary) model to interpret the short term M.T.O.D. data.

3. Assess blood flow contributions and heterogeneities of blood flow rates in the cortex and marrow by the microsphere technique for the benefit of a multicapillary model.

4. Develop a more complex cortex/marrow multicapillary model to interpret the short term M.T.O.D. data.

5. Investigate the effect of large vessel dispersion and active transport on model predictions.

CHAPTER 2

MULTIPLE TRACER OUTFLOW DILUTION (M.T.O.D.) TECHNIQUES

2.1. INTRODUCTION

2.1.1. Brief review of blood/bone ion exchange experiments

To date, many experiments have been carried out to study ion exchange between blood and bone. In the majority of them, radioactive tracer analogues of bone constituents have been used in *in vitro* and *in vivo* situations.

In the former situation, investigators have studied the movement of ions in bone chips and bone powder. For example, Harrison *et al* (1967) have studied the uptake and elution of ^{45}Ca, ^{85}Sr, ^{133}Ba and ^{223}Ra between a medium of stabilized concentration and a column of rat bone powder. Their results showed an increased retention of barium and radium as compared with strontium and calcium. However, this was the exact reverse of what occurred in *in vivo* experiments in which the heavier nuclides of ^{133}Ba and ^{223}Ra were excreted much more rapidly than ^{45}Ca and ^{85}Sr. This particular example throws doubt on *in vitro* experiments as a whole, notably that living and intact cellular systems may well be involved in ion exchange.

As far as *in vivo* experiments are concerned, Groer and Marshall (1973) investigated ^{45}Ca exchange by modelling serum and bone surface specific activity data obtained from Rowland (1966). This data was obtained over a fairly long period of time, up to around 500 hrs, by which time many complex structural ^{45}Ca exchanges may have taken place. Furthermore, the surfaces of bone used for specific activity determinations were questionable and were not specific enough as to relate to precise locations where ion exchange may be

taking place. Other investigators such as Makler Jr. and Charkes (1980) relied on more indirect methods to measure ion exchange in bone, which entailed modelling the results of blood and urine concentrations of an intravenously injected tracer. Knowing only these particular concentrations meant that many assumptions had to be made which culminated in a 5 compartment ion exchange model that was not very physiological.

Generally in most cases, bone seeking tracer experiments have been described for long term exchange (hours to days) with principal aims of finding bone turnover rates and associated rate constants determined from plasma tracer levels. Fewer experiments have been performed to examine the short term exchange (minutes) behaviour of tracers in bone which is largely in a quiescent state. For the former types of long term exchange experiment, compartment and non-compartment models have been employed.

2.1.2. Compartment models

The data from kinetic tracer studies generally relate to rates of change, in many instances being experimental plasma tracer concentration measurements as a function of time. The data have been found to be best described by exponential functions, in which certain kinds of such functions relate to exchange of tracer from well-mixed tanks or compartments.

Some investigators, such as Hughes *et al* (1978) analysing fluid spaces in bone have fitted the minimum necessary number of exponentials to their data and interpreted this number as being the number of compartments in bone. For ^{99m}Tc methylene diphosphonate (^{99m}Tc-MDP), they found that four exponential terms conveniently described outflow data from the femoral vein and inferred that cortical bone has 4 compartments, vascular, perivascular, bone fluid and

bone crystal.

Other investigators such as Cohn *et al* (1965) and Groer and Marshall (1973), both studying bone tracer kinetics, have fitted data to an already postulated compartment model which simulates the known physiology of the system. In the latter case, Groer and Marshall successfully fitted a two compartment model consisting of serum and bone surface to *in vivo* ^{45}Ca data supplied by Rowland, (1966). The rate constant (k) was found for dogs to be $k_{dog} = 0.0025$ min^{-1}, however they grossly assumed that the bone extracellular fluid equilibrates rapidly with the serum. Furthermore, they needed an extra compartment to describe *in vitro* data of ^{45}Ca uptake from aqueous solution into bone crystals.

Problems in deciding how many compartments to assign to tracer data probably result from the major flaw in compartment analysis which is the assumption of rapid compartment mixing. This may suffice in terms of the vascular compartment, but becomes less convincing in long term tracer uptake in bone where slower diffusion processes particularly in the bone fluid (canaliculi) may predominate. There follows a more detailed account of a quite recently used compartment system for studying tracer exchange in bone as used by Charkes and colleagues, to highlight problems in compartment analysis.

2.1.3. Compartment models of Charkes *et al* (1979) & Makler Jr. and Charkes (1980)

The above investigators utilised a 5 compartment model to study ^{18}F kinetics in rats in the former case and ^{99m}Tc-MDP in adult humans in the latter case. The 5 compartments were tubular urine, blood, none bone-extracellular fluid,

bone-extracellular fluid and exchangeable bone.

In the ^{18}F kinetic studies, they used experimental blood and skeletal ^{18}F uptakes at various times to fit the 5 compartment model and derive informative rate constants. The skeletal ^{18}F uptake was determined by multiplying the mean fraction of the administered ^{18}F dose per tibia or femur by conversion factors relating their weights to that of the skeleton which assumes that the kinetics of ^{18}F uptake in all the various types of skeletal bone is identical. The 5 compartment model produced good fits to the data as did a 3 compartment model consisting of blood, extracellular fluid and exchangeable bone. However, a 2 compartment model consisting of blood and bone mass was found to give poor fits. Derived rate constants for ^{18}F relating to regions of interest are shown in table 2-1.

TABLE 2-1

Computer-generated rate constants for five-compartment model of Fluorine-18 and Tc-MDP kinetics in min^{-1}

Description (const.)	Fluorine-18 (rats)	Tc-MDP (adult man)
blood to bone-ECF (k_{21})	0.307 ± 0.01	0.095 ± 0.003
bone-ECF to blood (k_{12})	0.640 ± 0.08 *	0.540 ± 0.038 *
bone-ECF to bone (k_{32})	2.335 ± 0.17	1.055 ± 0.037
bone to bone-ECF (k_{23})	0.0016 ± 0.0002	0.049 ± 0.001
$(k_{21})/(k_{12}) \equiv V_I'/V_C'$	0.48	0.18
$(k_{21})/(k_{23}) \equiv V_B'/V_C'$	191.88	1.94
$(k_{32})/(k_{23}) \equiv V_B'/V_I'$	1459.38	21.53

Notes

ECF :-Extracellular fluid
* ± 1 s.d.

The rate constants (min^{-1}) are inversely proportional to the compartment volume V, exchange is taking place from, hence one can relate ratios of such

constants to ratios of compartment volumes. The ratio $(k_{21})/(k_{12}) \equiv V_I'/V_C' = 0.48$ infers that the volume of the bone extracellular or interstitial fluid is roughly half that of the vascular volume. The rate constants referring to the bone surface reflects the considerable bone volume eligible for exchange.

The ^{99m}Tc-MDP kinetic studies were carried out with the intention of finding optimum times for obtaining the best bone images following intravenous injection in humans. Rate constants derived from the model fitting process are also shown in table 2-1.

Again, the ratio $(k_{21})/(k_{12}) \equiv V_I'/V_C' = 0.18$ was found to be less than unity reflecting larger vascular volumes. In reality, attributing exchange to bone from a generalized vascular volume is imprecise because such exchange emanates from bone capillary structures. Furthermore, morphometric measurements (see table 1-1) suggests that the bone fluid space in humans is infact much larger than the capillary vascular space involved in such exchanges. Although the rate constants refer to two different animal species, the ratio of rate constants for both isotopes appertaining to the bone are dissimilar by large orders of magnitude. These dissimilarities reflect the lack of physiological significance of the compartments.

2.1.4. Non-compartment models

Other approaches to the modelling of tracer data have included the use of non-compartment models which are generally mathematical formulations that include other terms such as power functions as well as exponentials. They have been described as in the case of most compartment models to describe long term behaviour of bone seeking tracers. Two examples of non-compartment models are those of Burkinshaw et al. (1969) (subscript B)

and Marshall (1964) (subscript M) that describe the fraction of injected radioactive plasma per g Ca (S) as a function of time (t). In particular,

$$S_B(t) = S_1 t^{-b}.\exp[k(1-t^{1-b})/(1-b)]$$

$$S_M(t) = (q b \varepsilon^b / \eta k).(t + \varepsilon)^{-b-1}$$

where :-

- S_1, is the value of S one day after calcium injection.
- b, is the power function exponent of time (dimensionless).
- k, is the rate constant of endogeneous calcium excretion.
- ε, is a constant (dimensions of time).
- q, is initial activity of tracer (mCi).
- η, is empirical excretion factor for the radioelement relative to calcium for a given physiological state.

Although these expressions may fit the observed data accurately, terms such as b and ε are hard to interpret physiologically.

2.1.5. Conclusions

In general, compartment and non-compartment models lack physiological and anatomical significance. For cases involving bone, their components and parameters are usually too crude to describe the system under study. The crudeness of the models stems from their use in analysing the many complex structural interactions of tracer involved in long term exchange behaviour. Furthermore, properties of the biological system such as flow and volume may well be subject to change i.e. be in non-steady states during such long periods of study which is not conducive to most model designs which are in essence

steady state.

Reeve *et al* (1978) in a review have emphasized approaches to steady-state tracer analysis. They rightly suggest that the best models to use are the ones which have the fewest assumptions, particularly unsupported assumptions, and have parameters that are realistic parameters of the system.

To achieve all these objectives, particularly the latter one, the best approach would involve isolating the organ of interest, and injecting tracers and making measurements local to it. Furthermore, by carrying out short term studies, the organ would be more likely to be in a steady state for purposes of modelling the data. These particular objectives can be best achieved for organs by applying the multiple tracer outflow dilution (M.T.O.D.) technique.

2.2. THE M.T.O.D. TECHNIQUE :- APPLICATION TO THE CANINE TIBIA

2.2.1. The M.T.O.D. technique

The M.T.O.D. technique which was introduced by Chinard *et al* (1955) has been used extensively to study the physiology of organs such as the heart (Tancredi *et al* 1975), kidney (Silverman and Trainor 1982), liver (Goresky 1963), salivary gland (Yudilevich and Smaje 1976) and bone (Kelly and Bassingthwaighte 1977). It is based on the use of two or more tracers of different characteristics which are mixed and injected as a bolus form, or infused at a constant rate into a major supply artery of the organ of interest. All the effluent blood from the organ is then collected at various intervals of time for a desired interval.

The tracers that are used are termed as reference and diffusible. The reference tracer is usually radioactively labelled albumin being of a large molecular size such that it does not escape from the blood. Hence the outflow results of the reference tracer is representative of all the dispersion within the vascular system. The diffusible tracer used can also be termed the test tracer and is the tracer whose physiological and kinetic behaviour one is interested in. The diffusible tracer is such that it diffuses or permeates through capillary walls to surrounding structures.

The reference and diffusible tracers can readily be assumed to be transported in the bloodstream in exactly the same way, such as having equivalent intravascular volumes of distribution. Effects of dispersion associated with their various molecular sizes in the bloodstream are very minimal. This is because the diffusion coefficients of most of the tracers are of the magnitude of 1×10^{-5} cm^2/s thus taking approximately $1 \times 10^5 s$ to diffuse through distances such as 1 cm which is very large in comparison with mean transit

times $\bar{T}$ for their passage through organs. For instance in M.T.O.D. techniques involving infusing tracers into the canine tibial nutrient artery at a physiological rate of 2 ml/min and collecting all effluent blood, $\bar{T}$ for ^{125}I-albumin reference tracer has been found to be 43.3 $\pm$ 30.8 s (n=5) (McCarthy *et al.* 1980).

The fact that the tracers are transported in the bloodstream in exactly the same way effectively means that the differences in the outflow profiles between the reference and diffusible tracers reflects differences in the permeable capillary system which is the main advantage of M.T.O.D. techniques. The intravascular reference tracer then serves well against which to estimate properties of the capillary system such as extraction and the capillary permeability-surface area product PS_C for the diffusible tracers.

By using appropriate combinations of tracer, additional information can be obtained for structures beyond the capillary system. Bassingthwaighte (1982) for instance, has used L-glucose as a reference tracer for D-glucose in M.T.O.D. studies concerning the heart. The L-glucose is confined solely to the capillary and the interstitial fluid space around it, whereas the D-glucose penetrates an additional barrier and space namely that appertaining to myocardial cells.

To conclude, M.T.O.D. studies are very useful in analysing the short term exchange behaviour of organs of interest. Suitable combinations of tracer can alleviate problems concerning large vessel dispersion in arteries and veins, and provide substantial information on internal organ function. However, there are disadvantages associated with M.T.O.D. studies which largely stem from the fact that it is an invasive technique. In situations where organs may have complex venous drainage i.e. bone, it is only possible at most to carry out two or three M.T.O.D. experiments on each animal owing to substantial blood loss

in the case of taking outflow venous blood samples. The process can be very wasteful in the sense that the animals may be largely intact when they are sacrificed at the ends of the experiments.

2.2.2. Experimental procedures

Introduction

Despite the disadvantages of the M.T.O.D. technique in general associated with invasiveness, it is still the only really creditable means of studying tracer (ion) exchange in bone. It is basically extremely difficult to perform isolated blood vessel studies in bone to analyse such exchange because of its hard and opaque structure.

Most of the M.T.O.D. studies that have involved bone have been performed on the canine tibia. In the mature canine tibia, Kelly (1966) described how the tibial nutrient artery could be exposed and cannulated by the transfibular approach. Consequently, many M.T.O.D. studies involving the isolated canine tibial diaphysis have followed, being largely carried out by Kelly and co-workers i.e. (Cofield, Bassingthwaighte and Kelly 1975 ; Davies, Bassingthwaighte and Kelly 1976).

In more recent times, investigators from the Department of Orthopaedic Surgery at the University of Edinburgh have built on the earlier work of Kelly *et al* The group mainly comprising Prof. S.P.F. Hughes, Dr. I.D. McCarthy and Mr. R.H. Fleming have performed M.T.O.D. procedures on adult greyhounds, approximately 25 kg in mass. Greyhounds were used because they are a pure breed, and have large tibiae with nutrient arteries that are relatively easy to cannulate. In general terms, the canine tibia is useful for study because the

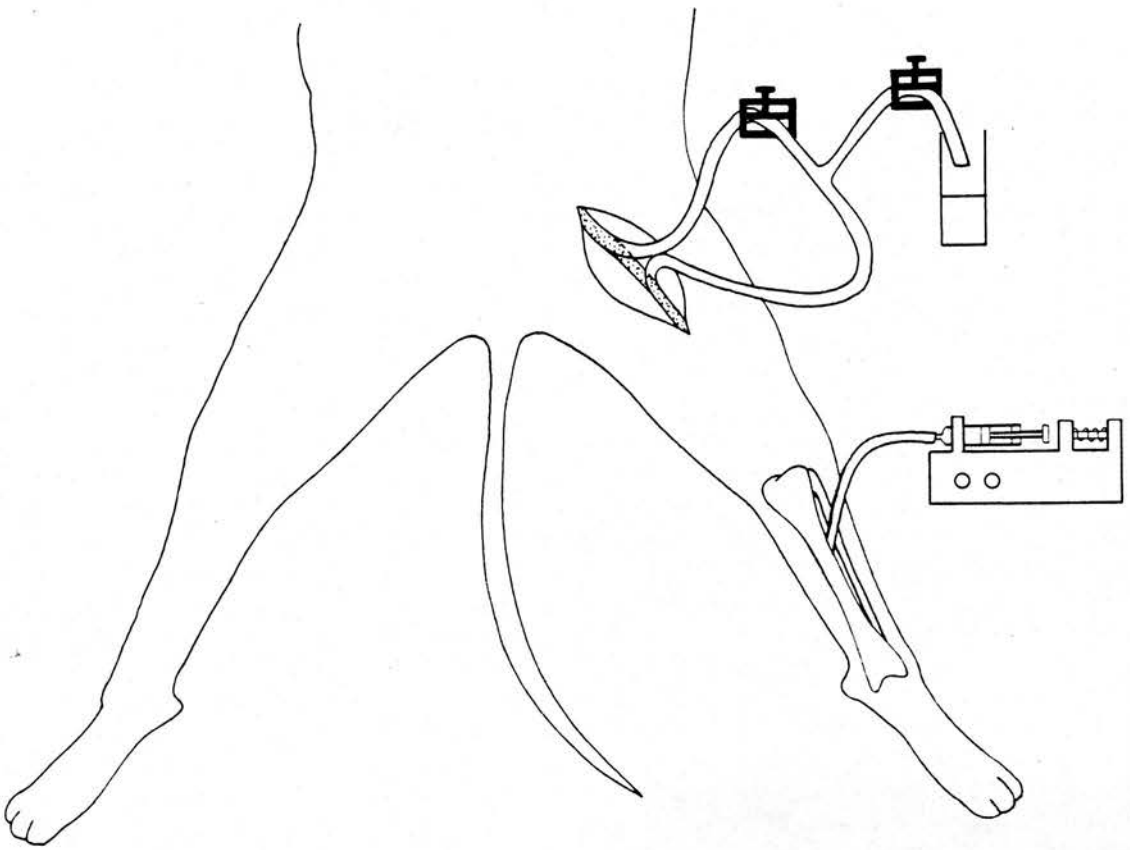

FIGURE 2-1 : Injection and sampling sites in M.T.O.D. procedures concerning the canine tibia.

structure of canine long bones is comparable to that of man and the vasculature of the tibia is less complex as compared with other bones.

The M.T.O.D. procedures as carried out by the above investigators on greyhounds is described in detail below because the content of this thesis largely deals with the subsequent results.

Preparation

The greyhounds were premedicated with 5 mg of acetopromazine and 0.6 mg of atropine sulphate which were injected subcutaneously, and then anaesthetized with intravenous sodium pentobarbitone. The tibial nutrient artery of one tibia was exposed by the transfibular approach as mentioned and was cannulated with a nylon intravenous cannula (3 F/G outside diam. 0.75mm). This catheter was connected to a 50 ml syringe containing Krebs-Ringer bicarbonate buffer as shown in figure 2-1. The syringe was placed in a Harvard infusion pump so that the tibia could be infused at a controlled rate. The ipsilateral femoral vein was cannulated with a Y-shaped cannula so that all the venous blood could be recovered when required. The venous blood will include that from other tissues besides the tibia under study, but this merely dilutes the tracers and does not change their amounts or relative concentrations. Earlier investigators (Cofield *et al* 1975) attempted to collect venous exiting blood from the nutrient vein but found that it represented only 10% of the total exiting blood.

An additional device (not illustrated in figure 2-1) used was a pressure transducer that was connected to the nozzle of the infusion syringe by means of a 3 way tap. The bicarbonate buffer was continuously perfused through the bone into the general circulation (base of Y-shaped cannula clamped) before

any tracers were injected. The pressure transducer was used to monitor the nutrient artery pressure or the resistance to the infusing bicarbonate buffer ; readings were displayed on a chart recorder. Once a stable pressure reading was established then the tracers were injected.

Injecting the tracers

^{125}I-albumin reference tracer and the diffusible tracers of ^{86}Rb and ^{85}Sr, each of activity 185 kBq (Amersham International plc) were injected simultaneously in a bolus form* via the 3 way tap into the bicarbonate buffer which was being continuously infused at a constant rate, usually of 2 ml/min. Blood samples containing the tracer washout were taken immediately from the ipsilateral femoral vein ; the collection time was 5 s with 60 samples being collected over a 5 min period. Heparinised saline in an intravenous drip replaced the blood that was collected. The blood samples were put aside for determining tracer content.

The whole experimental procedure was usually repeated on the same tibia after the bone physiology had been perturbed by administration of substances such as bovine parathyroid hormone PTH. For experiments involving PTH, parathyroidectomies were carried out on the greyhounds following anaesthesia and prior to exposing the tibial nutrient artery. For the second experimental run following the control run, fresh bicarbonate buffer containing 0.0005 mg of bovine PTH (Sigma Chemicals Ltd., Poole, Dorset) dissolved in 0.5 ml of normal saline was infused into the tibial nutrient artery one minute before the tracers were injected. For experiments in which PTH was used, the buffer flow was 1 ml/min.

*Typical tracer syringe volume was 0.15 ml requiring a dispensation time of 1 s.

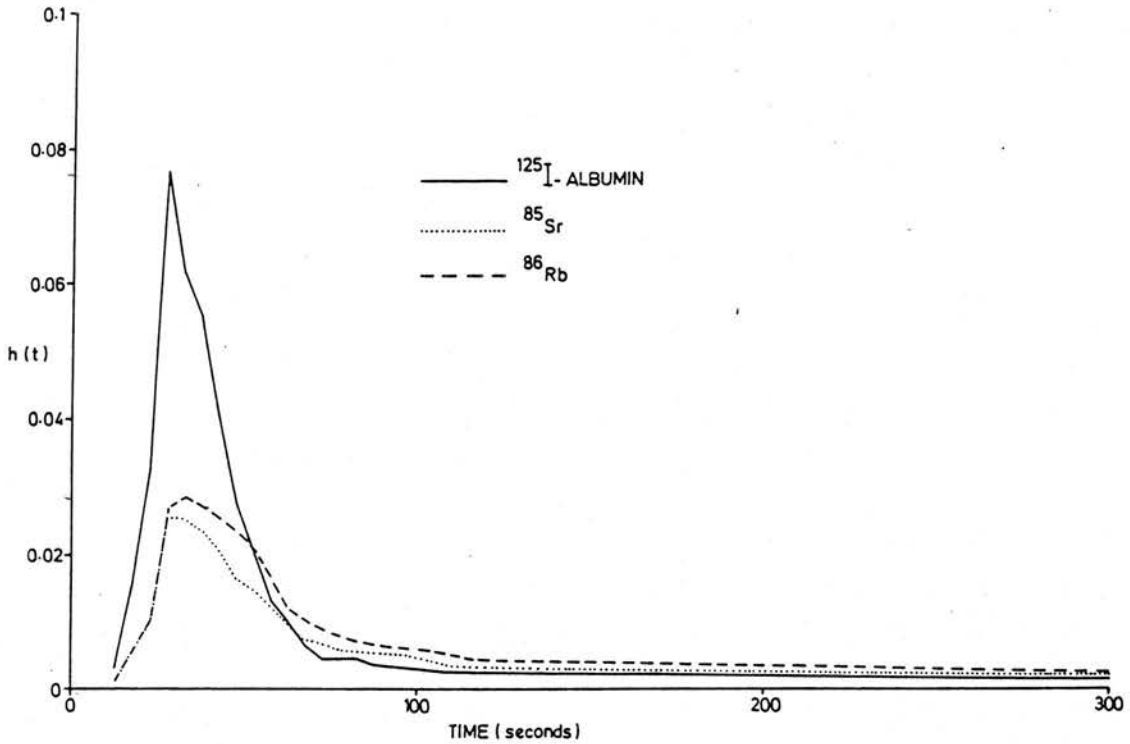

FIGURE 2-2 : Typical experimental outflow results for ^{125}I-albumin, ^{86}Rb and ^{85}Sr.

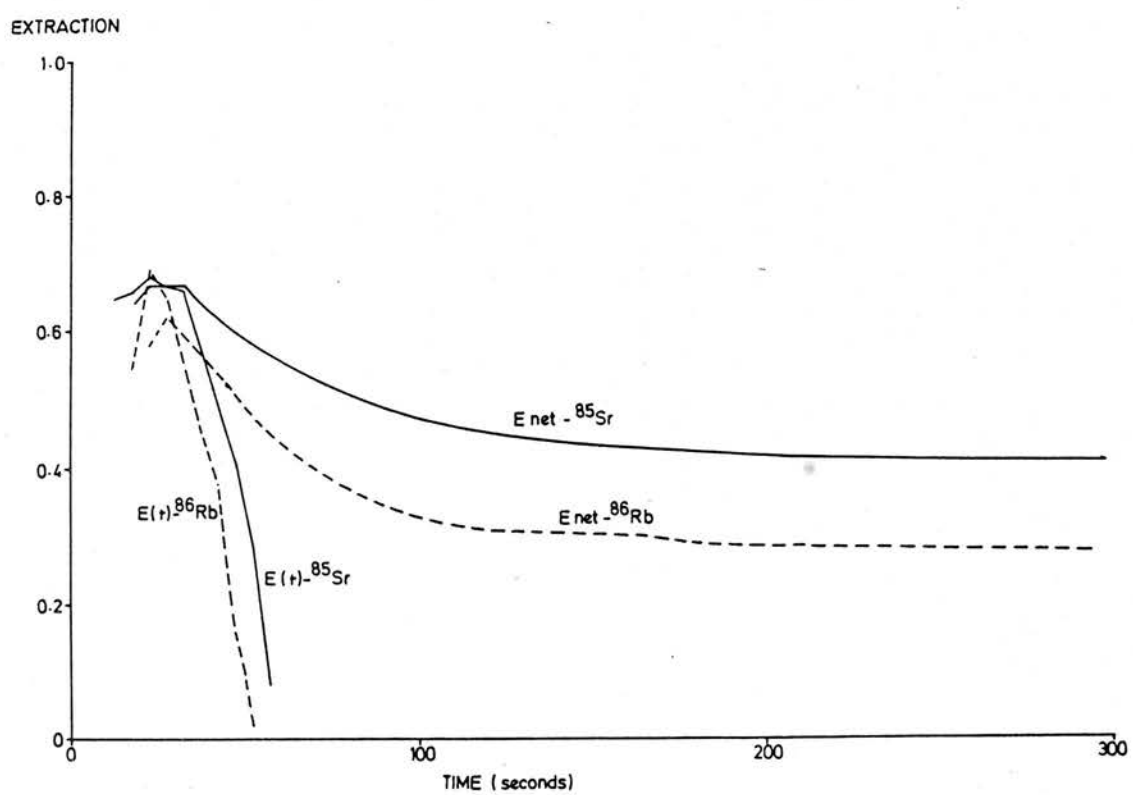

FIGURE 2-3 : Typical extraction profiles for ^{125}I-albumin, ^{86}Rb and ^{85}Sr.

Preparation of blood samples for radioactive assay

The volumes of each of the 60 blood samples which were typically around 7-8 ml were measured to an accuracy of 0.5 ml. The blood in each sample tube was thoroughly shaken and 1 ml aliquots of each sample were used for radioactive assay in a LKB-Wallac sample counter. The syringes containing mixtures of the 3 gamma ray emitting tracers were counted before and after the experiments with their individual standards. By allowing for background and calculating spillover energies, the total amounts of each isotope which was injected and amounts of each isotope in the venous blood samples was determined. This information enabled one to make measurements on the system (section 2.2.4.).

2.2.3. Theory associated with M.T.O.D. techniques :- the Crone & Renkin equation (model I)

Introduction

Figure 2-2 shows typical experimental outflow results for each of the tracers that was obtained from the canine tibia. The ordinate axis represents the transport function h(t) which is the ratio of the tracer counts in the sample collected over 5 s to the amount in counts that was injected. As was discussed in section 2.2.1., the differences between the reference ^{125}I-albumin tracer profile and each of the diffusible ones is interpreted as being representative of the exchanging capillary system and external volumes of distribution.

The magnitudes of the transport function for ^{86}Rb and ^{85}Sr are less than that

for the ^{125}I-albumin for quite a bit of the sampling period simply because they diffuse through the capillary walls. Magnitudes of the transport functions for ^{86}Rb and ^{85}Sr become greater than that for the ^{125}I-albumin at later stages of the sampling period because the diffusible tracers are returning to the blood without recirculation in a process called back diffusion.

Theory

As a consequence of confining our attention on tracer exchange to the capillary system, one can examine the mathematical description of capillary permeability considered by Kety (1951) and Renkin (1955).

The net exchange of a substance between blood and tissue depends on the substance flow rate F_s, the total surface area of capillary wall available for exchange S, and the permeability P of the capillary to the substance being studied. For an idealized capillary with uniform permeability and blood flow and constant concentration C of substances in tissue, then

$$(C_V - C_T) = (C_A - C_T).\exp(-PS_C/F_s) \qquad (2.1)$$

where the subscripts A,C,V,T refer to the artery, capillary, vein and tissue respectively. PS_C is the capillary permeability-surface area product.

The extraction E of the substance from unit volume of blood flowing through the capillary has been defined by Renkin (1959) as

$$E = \frac{(C_A - C_V)}{C_A} \qquad (2.2)$$

The extraction is simply a measure of the substance lost from the capillary in terms of the associated arterial and venous concentrations.

If one assumes that the tissue concentration of the substance is effectively zero i.e. the tissue volume is infinitely large so that back diffusion of the substance cannot occur, and substitute equation (2.2) in equation (2.1), one obtains the following equation derived independently by Renkin (1959) and Crone (1963)

$$PS_C = -F_s.\log_e(1 - E) \qquad (2.3)$$

In deriving the equation (2.3), attention has been focused on a single capillary. In practice, in particular to M.T.O.D. techniques the study of the permeability of bone capillaries to test tracers involves ensembles of many such capillaries. One has to assume that all properties of the capillaries relating to tracer kinetics such as the flow rates and permeabilities are identical to be able to use equation (2.3). Effectively this means that all the capillaries can be represented by a large single composite capillary of cumulative structural and kinetic properties. Thus for the requirements of M.T.O.D. techniques as described, one can write an analogous expression for extraction E(t) as

$$E(t) = \frac{h_R(t) - h_D(t)}{h_R(t)} \qquad (2.4)$$

where h(t) is the transport function (5 s^{-1}) of the reference (R) and diffusible (D) tracers.

Typical extraction E(t) versus time profiles for outflow results of ^{86}Rb and ^{85}Sr are shown in figure 2-3. The extraction can be seen to reach a peak early on in the outflow samples then it decreases to zero and negative values later on. The decrease in extraction occurs as a consequence of larger concentrations of tracer being established outside the capillary ; the concentration gradient from inside the capillary outwards is being reduced and back diffusion is taking place in ever increasing amounts. After the extraction has reached zero, more of the

tracer is returning to the blood than is leaving it, because convection has reduced concentrations in the capillaries.

To be able to utilize equation (2.3) effectively in M.T.O.D. techniques, it is necessary to use an extraction value E(t) that represents the unidirectional passage of tracer through the capillary wall. This is basically because equation (2.3) does not allow for back diffusion. Thus for M.T.O.D. techniques, equation (2.3) is utilised in the form

$$PS_C = -F_s.\log_e(1 - E_{max}) \qquad (2.5)$$

where E_{max} is the maximum value of extraction. In this thesis equation (2.5) will be referred to as model I.

2.2.4. Measurements relevant to M.T.O.D. techniques

E_{max} & PS_C

The maximum extraction E_{max} for diffusible tracers can be deduced from M.T.O.D. techniques using equation (2.4). The capillary permeability-surface area product PS_C (ml/s) can then be subsequently calculated from equation (2.5) using E_{max} and the infusing buffer flow rate F_{Bu} (ml/s) to represent F_s. If the tracers had been injected into arterial blood of flow rate F_B (ml/s), then

$$F_s \equiv F_P = F_B(1 - H) \qquad (2.6)$$

because the tracers are carried in the plasma whose flow rate F_P (ml/s) is determined using H the fractional haematocrit of the blood.

$E_{net}(t')$

The net extraction $E_{net}(t')$ or an averaged version of the instantaneous extraction E(t) which was introduced by Lassen and Crone (1970), can be calculated for the diffusible tracer from the outflow profiles for different periods of time t' i.e.

$$E_{net}(t') = \frac{\sum_{t=0}^{t=t'} [h_R(t) - h_D(t)]}{\sum_{t=0}^{t=t'} h_R(t)} \qquad (2.7)$$

Net extractions are close to instantaneous extractions in early stages of the sampling period. However in later stages, magnitudes of net extraction are useful in quantifying the uptake of tracers to structures beyond the capillary wall. In figure 2-3 for example, ^{85}Sr uptake to bone surface appears to be more abundant than ^{86}Rb uptake to bone cells.

FER(t')

The fractional escape rate FER(t') (5 s^{-1}) is that fraction of tracer present in the bone tissue that leaves the tissue per unit time. For our experimental use, this is defined by the equation

$$FER(t') = h(t')/R(t'') \qquad (2.8)$$

in which R(t") is the residue function or the amount of tracer still in the bone tissue at time t", where t" is the sampling period prior to a sample producing a transport function h(t') at time t', i.e. t" is always one sampling interval behind t'. Furthermore,

$$R(t'') = 1 - \sum_{t=0}^{t=t''} h(t) \qquad (2.9)$$

or

$$R(t'') = 1 - H(t'') \qquad (2.10)$$

where H(t") is the cumulative residence time distribution representing the amount of tracer that has left the bone tissue at time t".

In certain situations, for a tissue system in which the total conductance PS_{Tot} of the barriers is low relative to the flow (Tancredi *et al* 1975), FER(t') is approximated quite well by

$$FER(t') \approx PS_{Tot}/V_T' \qquad (2.11)$$

where V_T' is an apparent volume of distribution of the whole tissue (ml), which in the case of bone seeking tracers could readily apply to an apparent volume representing the large expanse of exchangeable bone surface. Additionally, the total conductance PS_{Tot} can be written in terms of the other n serial barrier conductances PS_i as

$$\frac{1}{PS_{Tot}} = \sum_{i=1}^{n} \frac{1}{PS_i} \qquad (2.12)$$

2.3. REVIEW OF M.T.O.D. RESULTS FOR THE CANINE TIBIA

2.3.1. E_{max} findings for ^{86}Rb & ^{85}Sr in the normal canine tibia

TABLE 2-2

Comparisons of E_{max} (mean ± s.d.) and F_s for ^{85}Sr in the normal canine tibia.

Set	Investigators	No. exps.	Sample time(s)	E_{max}	F_s (ml/min)	
1	Cofield et al. (1975)	12	30	0.53±0.08 (A)		
2	Davies et al. (1976)	14	10	0.69±0.11 (M)		
3	Lemon et al. (1980a)	7	5or10	0.59±0.13 (H)	0.65-1.69	ID,*,**
4	Lemon et al. (1982)	6	5	0.60±0.14 (H)	0.65-1.46	ID,*,**
5	McCarthy & Hughes (1986)	8	5	0.72±0.11 (M)	2.0	D
		5	5	0.71±0.13 (M)	2.0	D
6	McCarthy & Hughes, unpub.	5	5	0.79±0.10 (M)	1.0	D
		5	5	0.76±0.15 (M)	1.0	D
7	McCarthy & Hughes, unpub.	5	5	0.82±0.06 (M)	1.9	ID,*

Notes

E_{max} :- (A) :- average value obtained from E(t) at peak.
(M) :- maximum value.
(H) :- extraction value when half reference tracer emerges.

F_s D :- direct calculation $F_s \equiv F_{Bu}$
ID :- indirect calculation * :- $F_s \equiv F_P$ eqn.(2.6)
** :- assume 100 g tibia

Table 2-2 illustrates E_{max} values (mean ± s.d.) found by various investigators for ^{85}Sr in the normal mature canine tibia. The infusing flow rates are shown where possible ; missing values are from studies in which bone blood flow rates were not observed (set 2) or determined from external detection ^{125}I-4-iodoantipyrine techniques (set 1). In sets 5 and 6, F_s represents the infusing buffer flow rates, whereas in sets 3,4 and 7 whole blood was infused

and F_s is the calculated plasma flow rate. Furthermore, in sets 3 and 4, the investigators used adult mongrel dogs and it has been assumed that their tibiae are roughly 100 g being typical to that of greyhounds, so that F_s (ml/s) can be obtained for comparison purposes.

It can be appreciated from table 2-2 that E_{max} for ^{85}Sr has tended to increase over the years from around 0.5 up to about 0.8. The main reason for this increase, has been the way in which E_{max} has been calculated from M.T.O.D. techniques which deserves careful consideration.

Guller *et al* (1975) have found from myocardial sodium extraction studies that the most useful estimates of E_{max} were instantaneous extractions obtained from the later part of the upslope and the peak of the venous dilution curves. Further theoretical studies have tended to reinforce this view (Bassingthwaighte 1974). Other approaches of finding E_{max} have tended to be less successful. For instance, Martin and Yudilevich (1964) in an attempt to overcome the problem of back diffusion, extrapolated their outflow profiles to find the extraction at the appearance time of the tracers. The problem with their technique is that their lower extraction figures were more than likely to be associated with capillaries that had higher than average flow rates. In reality there are heterogeneities of flow rates in most organs and it is better to obtain E_{max} values that are likely to be associated with capillaries having average flow rates. This important latter point has influenced how the investigators cited in table 2-2 have attempted to obtain E_{max}.

In the earlier experiments, lower E_{max} values for ^{85}Sr were obtained when investigators obtained E_{max} by averaging the extraction values around the peak of the reference outflow profile or by obtaining E_{max} when half of the reference tracer had emerged from the system. These lower ^{85}Sr E_{max} figures probably

reflected substantial degrees of back diffusion which may have been minimized in cases of the more recent higher ^{85}Sr E_{max} figures. Furthermore, table 2-2 shows the trend of reducing sample duration times over the years in an attempt to minimize the extent of back diffusion in determining E_{max}.

TABLE 2-3

Comparisons of E_{max} (mean ± s.d.) and F_s for ^{86}Rb and other related isotopes in the normal mature canine tibia ; (sample time 5 s).

Isot.	Investigators	No. exps.	E_{max}	F_s (ml/min)	
K-42	Maltby et al. (1982)	12	0.58±0.10 (S)	0.79-1.62	ID,*,**
		7	0.53±0.05 (S)	0.79-1.62	ID,*,**
		9	0.50±0.13 (S)	0.79-1.62	ID,*,**
Rb-86	McCarthy & Hughes (1986)	8	0.68±0.11 (M)	2.0	D
		5	0.70±0.10 (M)	2.0	D
Na-22	McCarthy & Hughes, unpub.	5	0.81±0.03 (M)	1.9	ID,*

Notes

See table 2-2 otherwise,

E_{max} (S) :- smoothed value occurring during upslope or peak of reference tracer profile.

There appears to be no other ^{86}Rb E_{max} data for the normal canine tibia other than that obtained by McCarthy and Hughes (1986). They have found E_{max} values of around 0.7 for ^{86}Rb as shown in table 2-3. Also shown in this table are two periodically related isotopes ^{22}Na and ^{42}K whose E_{max} values can be compared. The much lower E_{max} findings for ^{42}K may be due to its mode of determination by smoothing extraction values on the upslope or at the peak of the reference outflow profiles.

2.3.2. Findings for PS_C products for ^{85}Sr and ^{86}Rb : exchange beyond the capillary wall

Estimates of PS_C products for diffusible tracers have been obtained using E_{max} and F_s figures in equation (2.5). These estimates have been particularly influenced by the infusing flow rates. For example, using data sets 5 and 6 derived from mature greyhounds (table 2-2), one can calculate for ^{85}Sr :- PS_C = 2.64 $\pm$ 0.78 ml/min (n=8, E_{max}=0.72$\pm$0.11, F_s=2.0 ml/min) and PS_C = 1.60 $\pm$ 0.77 ml/min (n=5, E_{max}=0.76$\pm$0.15, F_s=1.0 ml/min). Intuitively, one may expect PS_C to remain relatively constant for a range of flows F_s with there only being differences in extraction, however there is a tendency for PS_C to increase with flow. It is very unlikely that the capillaries can become more permeable or assume higher extraction values for increasing flow rates, so the only readily available explanation appears to be capillary recruitment at high flow rates. Cofield *et al* (1975) and Kelly and Bassingthwaighte (1977) have also encountered increased bone capillary PS_C products with increasing flow rates and have likewise attributed this to capillary recruitment.

A PS_C value using table 2-3 of 2.28 ml/min (n=8, E_{max}=0.68$\pm$0.11, F_s=2.0 ml/min) can be calculated for ^{86}Rb. This value is slightly less than the PS_C value for ^{85}Sr at the same flow rates. For comparison purposes with ^{86}Rb, another periodically related diffusible tracer ^{22}Na produces a PS_C value of 3.16 ml/min (n=5, E_{max}=0.81, F_s=1.9 ml/min) which is larger in magnitude.

Other investigators have been more interested in permeability ratios for two or more tracers rather than individual PS_C products. For a bolus containing two or more diffusible tracers, permeability ratios can be obtained by dividing equation (2.5) for both tracers. Only E_{max} values are required in the calculation because the flow rates and surface areas available for exchange are common

to both tracers and cancel.

Davies *et al* (1976) using a modified equation (2.5) to account for back diffusion found that the observed ratio of permeabilities (mean ± s.d.) of ^{85}Sr and ^{14}C-sucrose was 2.36 ± 0.46 (n=13) which was not substantially different from the ratio of their free diffusion coefficients, 2.55. This provided evidence that passive diffusion was the principal mechanism for moving ^{85}Sr and ^{14}C-sucrose through the bone capillary walls. Similarly, permeability ratios of ^{99m}Tc labelled ethane-1-hydroxy-1,1-diphosphonate (Hughes *et al* 1977) and $Na^{18}F$ (Kelly and Bassingthwaighte 1977) with ^{14}C-sucrose were also in close agreement with corresponding ratios of free diffusion coefficients reaffirming passive diffusion. However, for reasons that are rather puzzling, Maltby *et al* (1982) have found that the permeability ratio for ^{42}K and ^{85}Sr of around 0.83-0.89 was substantially less than the free diffusion coefficient ratio quoted as 1.50.

Another source of puzzlement is the logic in making direct numerical comparisons of PS_C/F_s for individual tracers with their free diffusion coefficients. Lemon *et al* (1980b) and Kelly (1983) have found that for many diffusible tracers with the exception of ^{42}K, such numerical comparisons have been very similar even though PS_C/F_s was dimensionless and the free diffusion coefficient had units of cm^2s^{-1}.

Exchange beyond the capillary wall has been quantified by calculating net extractions $E_{net}(t')$ for a particular time period t' using equation (2.7). For ^{85}Sr and ^{86}Rb, net extractions (mean ± s.d, n=8) after a 5 min period have been found to be 0.48 ± 0.11 and 0.38 ± 0.11 respectively (McCarthy and Hughes 1986). These net extraction values which are less than the corresponding maximum extraction values owing to back diffusion, show that a larger amount

of ^{85}Sr has been retained in the bone as compared to ^{86}Rb.

2.3.3. Findings from M.T.O.D. experiments involving the use of PTH

Davies *et al* (1976) were the earliest investigators to use PTH in M.T.O.D. techniques involving the canine tibia. However, they were more concerned with possible changes in permeability ratios of strontium and sucrose in separate groups of control and hypercalcaemic rendered dogs. They injected PTH (30 units/kg, parathormone, Lilly) intravenously 3 times a day for 3–5 days until until serum calcium concentrations were greater than 13 mg/dl. At this stage, the M.T.O.D. techniques were performed which resulted in permeability ratios of strontium and sucrose that were not significantly different from control dogs. Values obtained from E_{max} and E_{net} at 3 min were not really dissimilar between the control and hypercalcaemic dogs. They concluded that passive diffusion of ^{85}Sr across bone capillary walls was unhindered by hyperparathyroid conditions.

Lemon *et al* (1982) in a more detailed study examined maximum and net extractions and fractional escape rates (FER) of ^{85}Sr in the tibiae of dogs in various states of parathyroidism. Dogs were rendered hypocalcaemic by parathyroidectomy and hypercalcaemic by injecting bovine PTH (Eli Lilly), 10 U/kg 3 times daily, every day for 3 or 5 days preceding the study. Again as with the previous investigators, separate groups of dogs were used. They found that for each of the groups, ^{85}Sr E_{max} values of 0.6–0.66 were not significantly different. The only significant findings were for mean values of E_{net} (3 min) and FER (0–1 min) for data appertaining to the states of hyperparathyroidism and hypoparathyroidism. E_{net} (3 min) values (mean $\pm$ s.d.) between these two respective states were 0.39 $\pm$ 0.07 (n=5) and 0.53 $\pm$ 0.07 (n=6). Additionally, respective FER (0–1 min) values (mean + s.d.) were (408.8 $\pm$

74.1) x 10^{-3} (n=5) and (273.7 $\pm$ 66.3) x 10^{-3} min^{-1} (n=6). Control values which had a larger comparative scatter fell between these ranges. Increased levels of PTH which produced the lowest E_{net} (3 min) figures suggested a diminishment of the bone volume of distribution or the number of available binding sites for ^{85}Sr.

Research concerning the immediate effects of PTH in the canine tibia has been recently performed by McCarthy and Hughes (unpublished data). On parathyroidectomised greyhounds, two sets of outflow data concerning ^{85}Sr were obtained before and after injecting PTH. For the second set of data, 0.0005 mg (0.07 USP) of bovine PTH (Sigma Chemicals) was injected one minute before injecting the tracers. They found from paired student's t tests that E_{max} ^{85}Sr values were not significantly different between the two sets of data. However, E_{net} (5 min) ^{85}Sr values were significantly lowered after the administration of PTH. The authors conclude that PTH exerts a rapid and direct effect on blood-bone disequilibrium.

2.3.4. Conclusions

One can appreciate from the preceding sections, the problems in interpreting venous outflow results for the purpose of making measurements. These problems largely occur as a result of back diffusion and heterogeneous capillary blood flow rates which affects the outflow data. In using the formulations, notably equations (2.4) and (2.5) to make measurements one is assuming that back diffusion is negligible and that bone blood flow rates are homogeneous. Thus at best, one is trying to obtain average measurements for the system. The problem of obtaining E_{max} for the system is that one can never completely alleviate the effects of back diffusion and flow rate heterogeneity. For instance, in making the measurement of E_{max} one should

relate to average capillary blood flow rates by considering extractions on the upslope or at the peak of the reference tracer profile, but in doing so back diffusion may well be substantial.

Estimates of PS_C will also be vulnerable to inaccuracies owing to the determination of E_{max}. It has been seen that for the case of ^{85}Sr, PS_C increases substantially with increases in the infusing flow rate ($F_s \geqslant$ 1ml/min) which suggests capillary recruitment at higher flow rates. However, McCarthy and Hughes (1983) using similar M.T.O.D. techniques involving ^{99m}Tc-methylene diphosphonate (^{99m}Tc-MDP) found that above infusing whole blood flow rates of 1.9 ml/min, PS_C is constant. In terms of plasma flow F_s, assuming a fractional haematocrit of 0.45-0.5 it would appear that PS_C is constant for $F_s \geqslant$ 1 ml/min, suggesting that capillary recruitment does not occur as supposedly it does for ^{85}Sr.

The differences in these findings may be partly attributable to the fact that blood samples were taken every 5 s for ^{85}Sr and every 15 s for ^{99m}Tc-MDP. E_{max} values found for ^{99m}Tc-MDP (McCarthy and Hughes 1983) being approximately 0.3 at whole blood flow rates of 3.8 ml/min were much lower than such values for ^{85}Sr which were typically around 0.7 at comparative flow rates (F_s = 2.0 ml/min). The E_{max} values for ^{99m}Tc-MDP which were equivalent to three averaged 5 s sample values perhaps should have been higher owing to substantial back diffusion taking place. Generally, it is the errors that are associated with the determination of E_{max} from blood samples of different sampling intervals coupled with the errors associated with the fact that ^{85}Sr is more extractable than ^{99m}Tc-MDP that largely accounts for the discrepancies in the PS_C findings involving capillary recruitment.

Although the inaccuracies of estimating PS_C have been stressed, the good

agreement between the permeability and free diffusion coefficient ratios for the various tracers provides strong evidence for passive diffusion through capillary walls. As these diffusible tracers were injected together, any subsequent errors in E_{max} at particular flow rates F_s will largely cancel out. The disagreements in these ratios particularly for ^{42}K and ^{85}Sr is most likely due to the transport behaviour of ^{42}K. Complications may arise owing to ^{42}K uptake to endothelial cells and differing uptake rates to cellular types in the marrow and cortex.

To improve on the accuracy of making measurements concerning the canine tibia, more complex mathematical modifications to the existing formulations are necessary ; such mathematical modifications having already been accomplished on organs such as the heart (Rose and Goresky 1976 ; Rose *et al* 1980 ; Bassingthwaighte *et al* 1985).

The next important modification is allowing for back diffusion within the system, by having finitely sized spaces external to the capillary. These spaces will then provide a more physiological means of quantifying tracer exchange beyond the capillary wall other than the existing $E_{net}(t')$ and FER(t') parameters. Thus the emphasis is now on the development of anatomically and physiologically suitable models to describe ion exchange between blood and bone.

CHAPTER 3

SINGLE CAPILLARY DISTRIBUTED MODEL OF BLOOD-BONE EXCHANGE (MODEL II)

3.1. MODELLING METHOD

3.1.1. Pathways for tracer transport - fluid spaces

A mathematical model was developed to analyse the results of short term M.T.O.D. techniques applied to the canine tibia in order to obtain information about bone fluid spaces and their associated boundaries. Owing to the injection site of the tracers being the tibial nutrient artery, it is reasonable to assume that tracer kinetics will be solely confined to the tibial diaphysis. Although the intramedullary branches of the nutrient artery anastomose to an extent with the metaphyseal arteries, the consequent blood supply is considered negligibly small as compared to the supply to the cortex. Evidence to support this latter assumption is provided by Lemon *et al* (1982), whom in a number of dogs following M.T.O.D. procedures observed on average around 7-8 times more ^{85}Sr counts in isolated cortex than isolated cancellous bone.

By confining ones attention to the tibial diaphysis, use can be made of the fact (see figure 1-4) that the blood flows through the microvasculature of the cortex and marrow are in parallel. In this respect it is reasonable to treat the cortex and marrow independently, as has been the case in blood flow determinations using microspheres (Morris and Kelly 1980).

Although the cortex and marrow supplies are in parallel, it was further assumed that it was the cortex which received all the afferent tibial nutrient artery blood. This assumption was considered reasonable at the time, in view of the much

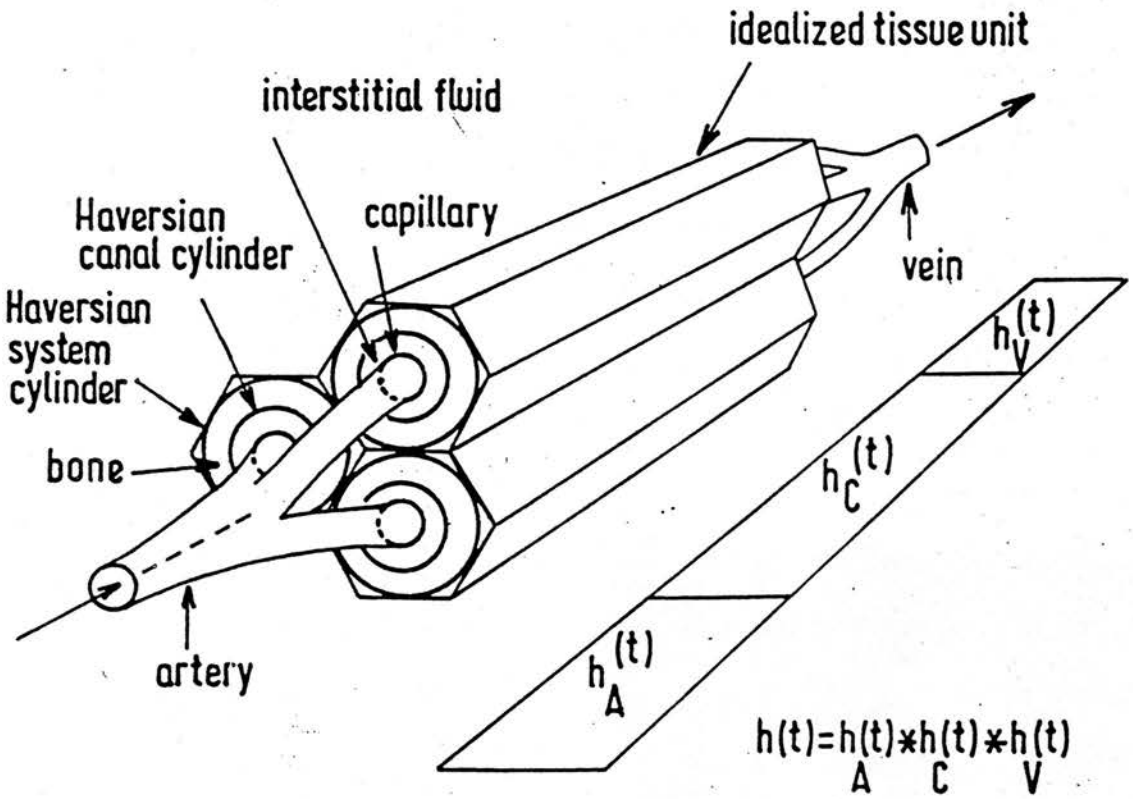

FIGURE 3-1 : Parallel hexagonal idealised tissue units responsible for tracer exchange, shown with artery and vein. These units consist of concentric cylinders of capillary, Haversian canal and Haversian system.

larger mass and volume contribution of cortex to the diaphysis. Cofield *et al* (1975) found that the cortex constituted 91% of the tibial diaphysis by mass. Thus the model was developed to describe the kinetics of tracers in the cortex, in particular the predominant Haversian systems whose capillaries were considered to be the exchanging vessels of the cortex.

With reference to figure 1-5 illustrating a schematic longitudinal section of a Haversian system, one can appreciate the fluid spaces available for tracer transport. The question as to whether the bone lining cells form an additional barrier and bone fluid compartment is debatable at this stage. As far as the modelling is concerned, the Haversian system was considered to be a concentric cylindrical unit which contained a central Haversian canal within which was a capillary. Figure 3-1 illustrates these Haversian systems which can be thought of in terms of Krogh cylinders of capillary, interstitial fluid and bone.

Krogh cylinder analysis has usually been adopted in organs of suitable geometry such as the heart and liver, i.e. having parallel arrays of long capillaries with uniform flow rates so there are no exchanges of tracer material between neighbouring capillaries. This was considered to be the case for the parallel aligned Haversian systems in the cortex, and structurally the Krogh cylinders were arranged in parallel idealized hexagonal tissue units which fitted together to make up the whole cortex. The volume between the outer Haversian system cylinder and the boundary of the hexagonal tissue unit was considered negligible.

Omissions from the modelling description of tracer exchange in Haversian systems, include Volkmann canals which connect neighbouring Haversian systems and lamellar bone. Furthermore, exchange processes in canaliculi to

deeper reaches of the Haversian bone matrix have been omitted to reduce the complexity of the model. This latter omission may be reasonable in view of modelling short term tracer exchange (minutes) in which the extent of tracer exchange in canaliculi may be small.

3.1.2. Derivation of model equations

In basic terms, a general outline for tracer exchange in a particular location in a phase or space may well be phrased (Bassingthwaighte and Goresky 1984),

$$\underset{\text{(local)}}{\text{concentration}} = -\underset{\text{(radial \& axial)}}{\text{diffusional flux}} - \underset{\text{(radial)}}{\text{permeation}} - \underset{\text{(axial)}}{\text{convection}} \qquad (3.1)$$

This description appertains to a geometrically uniform and straight cylindrical system in which radial fluxes are independent of axial fluxes. The minus signs indicate that in any particular phase location, the above processes result in tracer loss.

In terms of cylindrical geometry of variable radial r and variable axial x coordinates, the descriptive equation (3.1) translates to,

$$\frac{\partial C(x,r,t)}{\partial t} = + \underset{\text{(axial diffusion)}}{D_x \cdot \frac{\partial^2 C(x,r,t)}{\partial x^2}} + \underset{\text{(radial diffusion)}}{D_r \cdot \left[\frac{\partial^2 C(x,r,t)}{\partial r^2} + \frac{1}{r} \frac{\partial C(x,r,t)}{\partial r} \right]}$$

$$- \underset{\text{(permeation)}}{\frac{S(x)}{V(x)} [P_{12}(x) C(x,r-,t) - P_{21}(x) C(x,r+,t)]} - \underset{\text{(axial convection)}}{v_F(x,r) \frac{\partial C(x,r,t)}{\partial x}} \qquad (3.2)$$

The partial differential equation (P.D.E.) (3.2) describes exchange processes in a

phase with respect to a third variable time t. Hence, concentration C is a function of three variables x,r and t. Additionally, D_x and D_r are axial and radial free diffusion coefficients ; other terms are surface area S(x), volume V(x) and velocity $v_F(x,r)$. In the permeation part of the equation describing exchange across the barrier surrounding the phase, the term $P_{12}(x)$ denotes the apparent permeability for flux in an outward direction at position x and $P_{21}(x)$ that in the centripetal direction. The concentration at the radial extremes of the phase just before the barrier (coordinate r−) is C(x,r−,t) and C(x,r+,t) is the concentration just external to the barrier (coordinate r+).

For the prescribed Krogh cylinder system of capillary, interstitial fluid and bone, there are 3 phases involved. To reduce the complexity of the resulting 3 P.D.E.s, the following assumptions have been made.

1. The system to be modelled is considered to be uniform and straight geometrically, such that radial fluxes are independent of axial fluxes and the system is radially symmetric. One can appreciate from figure 1−2a that the parallel alignment of the Haversian systems and their contents, the Haversian canals and capillaries satisfies the geometrical criteria of this assumption.

2. The system is assumed to be linear and stationary, to ensure mass conservation when there is no consumption of tracer.

3. Permeable boundaries have negligible thickness so that tracer does not accumulate there and have axially uniform permeability−surface area products.

4. Capillary tracer movement is described by a flat velocity $v_F(x)$ profile which is reasonable in view of small bone capillary diameters being typically of the order of 10 µm. Flat velocity profiles ensure much easier solutions to the model.

5. Convection is assumed to occur only in the capillaries ; the interstitial fluid is regarded as a stagnant phase.

6. There are equal blood flow rates in capillary–tissue units such that there are no concentration gradients across the interfaces between units (see figure 3–1). In such a circumstance, the units can themselves be regarded as one single composite unit of cumulative structural properties, hence the description of single capillary model.

7. Radial diffusion is adjudged to be rapid on the basis of short relaxation times τ_r regarding the distance between a bone capillary and the extremities of a Haversian canal. For example, referring to table 1–1,

$$\tau_r = (R_{HC} - R_C)^2/D = 0.04 \text{ s}$$

using a typical diffusion coefficient D = 2.0 x 10^{-5} cm^2/s. This assumes that binding occurs only on the surface of the Haversian canal and that binding on internal canalicular and lacunar surfaces can be ignored which may well be justified in modelling the short term exchange behaviour of tracers over a period of minutes.

8. Axial diffusion is assumed to be negligible because the transit times for the vessels are short in comparison with relaxation times τ_x for diffusion along the axial distances involved. For example, if the length of the capillary L_C is equal to the length of a Haversian canal L_{HC} = 0.5 cm from table 1–1, then

$$\tau_x = L_C^2/D = 12{,}500 \text{ s}$$

using a diffusion coefficient D = 2.0 x 10^{-5} cm^2/s. τ_x is very much larger than capillary transit times T_C being of the order of 10 s, to be discussed later.

As a result of the assumptions, the concentrations of tracer in capillary (C), interstitial fluid (I), and bone (B) can be described by the following 3 P.D.E.s.

For the capillary of length L_C (cm), subject to a tracer flow rate F_s (ml/s),

$$\left.\begin{aligned}
\frac{\partial C_C(x,t)}{\partial t} &= \frac{PS_C[C_I(x,t) - C_C(x,t)]}{V_C'} - \frac{F_s L_C}{V_C'}\frac{\partial C_C(x,t)}{\partial x} \\
\text{For the interstitial fluid,} \\
\frac{\partial C_I(x,t)}{\partial t} &= \frac{PS_C[C_C(x,t) - C_I(x,t)]}{V_I'} - \frac{PS_B[C_I(x,t) - C_B(x,t)]}{V_I'} \\
\text{For the bone,} \\
\frac{\partial C_B(x,t)}{\partial t} &= \frac{PS_B[C_I(x,t) - C_B(x,t)]}{V_B'}
\end{aligned}\right\} \quad (3.3)$$

where PS is passive permeability-surface area product (ml/s) :- $P_{12}=P_{21}$ in equation (3.2), V' is apparent volume of distribution (ml) and C(x,t) is concentration (amount/ml) as a function of axial position x (cm) and time t (s). The apparent volume of distribution represents the anatomical volume accessible to the tracer multiplied by a factor which accounts for the compounded effects of parameters such as volume exclusion, phase partition coefficients, tracer binding and asymmetric transport ($P_{12} \neq P_{21}$) across boundaries. The concentrations are defined in terms of apparent volumes of distribution. The notation of PS_B and V_B' has been used for bone. These parameters apply to bone cells and to a hypothetical pool representing bone surface binding when describing the kinetics of ^{86}Rb and ^{85}Sr respectively.

In this thesis, this homogeneous single capillary model will be referred to as model II.

3.1.3. Solving the model equations

The 3 P.D.E.s (equation (3.3)) can be solved by analytical and numerical methods.

Rose *et al* (1977) have solved P.D.E.s of similar nature to equation (3.3) analytically, which have resulted in very complex solutions for $C_c(x,t)$ containing Bessel functions. The solutions for an impulse input function have been very useful in demonstrating the exact behaviour of the system. However, the analytical approach is not very pliable in dealing with the various types of input function. In addition, values for Bessel functions must be computed from polynomial approximations which really only makes the approach "semi-analytical".

The numerical method of solving the P.D.E.s as detailed by Bassingthwaighte (1974) is a much better approach and takes advantage of a computer's ability to perform tasks repeatedly and rapidly with reasonable accuracy. The numerical solution to the 3 P.D.E.s is in fact much quicker than obtaining analytical solutions (Bassingthwaighte, personal communication). Furthermore, by using the numerical method, solutions can easily be obtained for more complex P.D.E.s such as equation (3.2) (Bassingthwaighte *et al* 1970), and for various input functions i.e. lagged normal density function.

The numerical solution of the 3 P.D.E.s :- equation (3.3)

The equations were solved by a numerical technique described by Bassingthwaighte (1974). Firstly, they were reduced to ordinary differential equations (O.D.E.s) by dividing the phases up into a number of segments n_x along the vessel such that each equation described tracer exchange across a

permeable barrier in a segment. Thus for a segment j, the transport of a radial flux qr of tracer across the capillary membrane d(qr)/dt from the capillary (C) to the interstitial fluid (I) phase was given by the following 2 simultaneous O.D.E.s

$$\left.\begin{aligned} \frac{dqr_{C_j}}{dt} &= \frac{V_C'}{n_x}\cdot\frac{dC_{C_j}}{dt} = \frac{PS_C}{n_x}\left[C_{I_j}(t) - C_{C_j}(t+)\right] \\ \frac{dqr_{I_j}}{dt} &= \frac{V_I'}{n_x}\cdot\frac{dC_{I_j}}{dt} = \frac{PS_C}{n_x}\left[C_{C_j}(t+) - C_{I_j}(t)\right] \end{aligned}\right\} \qquad (3.4)$$

where t is time and t+ is the time infinitely soon after the beginning of a time step $\Delta t = T_C/n_x$, with T_C being the capillary transit time.

Equations (3.4) were solved in finite difference form for the time interval Δt in terms of the flux Δqr traversing the membrane during the interval t to $t+\Delta t$, (see appendix 1 ; case $\gamma = 1$). Hence,

$$\Delta qr_{CI_j} = \frac{V_C'}{n_x}\left\{1 - \exp\left[-\Delta t PS_C\left(\frac{1}{V_C'} + \frac{1}{V_I'}\right)\right]\right\} \cdot\left\{\frac{1}{(V_C' + V_I')}\left[V_C'C_{C_j}(t+) + V_I'C_{I_j}(t)\right] - C_{C_j}(t+)\right\} \qquad (3.5)$$

and

$$\Delta qr_{IC_j} = -\Delta qr_{CI_j} \qquad (3.6)$$

where Δqr_{CI_j} refers to the flux in the capillary segment j whose neighbouring segment is that of the interstitial fluid segment j ; *vice versa* for Δqr_{IC_j} . Equation (3.6) merely represents mass conservation of tracer between the two phases as invoked by assumption 2.

To obtain fluxes for the third phase (bone) which occurs owing to exchange

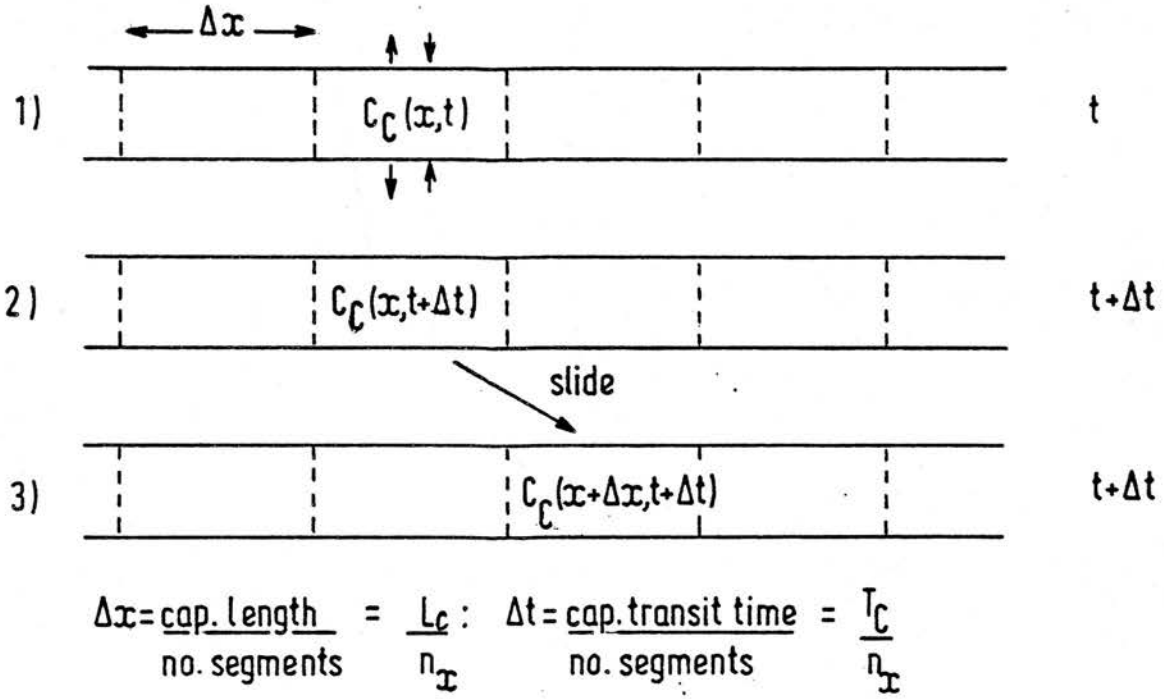

FIGURE 3-2 : Exchange of capillary fluxes, and convection in the numerical solution of the model.

between an interstitial fluid (I) segment and bone (B) segment, one can use the same solutions (3.5) and (3.6) with a change of subscripts. Hence referring to the j^{th} segments again,

$$\Delta qr_{IB_j} = \frac{V_I'}{n_x}\left\{1 - \exp\left[-\Delta t PS_B\left(\frac{1}{V_I'} + \frac{1}{V_B'}\right)\right]\right\} \cdot \left\{\frac{1}{(V_I' + V_B')}[V_I'C_{I_j}(t) + V_B'C_{B_j}(t)] - C_{I_j}(t)\right\} \quad (3.7)$$

and

$$\Delta qr_{BI_j} = -\Delta qr_{IB_j} \quad (3.8)$$

The calculated fluxes were used to obtain new segmental concentrations after a time interval Δt i.e.

$$C_{C_j}(t + \Delta t) = C_{C_j}(t+) + \frac{n_x \cdot \Delta qr_{CI_j}}{V_C'} \quad (3.9)$$

$$C_{I_j}(t + \Delta t) = C_{I_j}(t) + \frac{n_x}{V_I'}(\Delta qr_{IC_j} + \Delta qr_{IB_j}) \quad (3.10)$$

$$C_{B_j}(t + \Delta t) = C_{B_j}(t) + \frac{n_x \cdot \Delta qr_{BI_j}}{V_B'} \quad (3.11)$$

The process of convection was then achieved by sliding the capillary concentration values along by one segment in the direction of flow (see figure 3-2). The concentration in the n_xth segment then became the capillary outflow concentration. It should be clearer now, that it is the segmental concentration resulting from shifting the previous such segmental concentration that is used in the calculation of new fluxes at time t.

The processes of successively calculating fluxes and concentrations, then sliding capillary concentrations by one segment were repeated up to a prescribed time to meet the demands of a lengthy continuous input and changing concentration gradients. All calculations were accomplished on the University of Edinburgh's BUSH (ICL 2988) computer system using programs written in Fortran 77 (see Appendix 4 for details).

3.1.4. Application of the model to experimental data

To permit applications of the model to experimental data from bone, one should consider the transport functions (probability density function of transit times) of the arteries and veins $h_A(t)$ and $h_V(t)$, as well as the capillaries for the whole system (see figure 3-1). The transport function of the whole system h(t) is the convolution of the arterial, transcapillary and venous transport functions,

$$h(t) = h_A(t) * h_C(t) * h_V(t) \qquad (3.12)$$

or

$$h(t) = h_C(t) * h_{LV}(t) \qquad (3.13)$$

where $h_C(t)$ is the impulse response of the capillary tissue cylinder and $h_{LV}(t)$ is a large vessel transport function.

For M.T.O.D. techniques which involve inflow injections and outflow sampling, one can write

$$C_{Out}(t) = C_{In}(t) * h(t) = \int_0^t C_{In}(\alpha).h(t - \alpha)d\alpha \qquad (3.14)$$

where $C_{In}(t)$ and $C_{Out}(t)$ are inflow and outflow concentrations which can be expressed in terms of variable counts. α is a variable used for the integration.

For the purposes of this homogeneous model, it is assumed that all the capillary transit times T_C are equal, and that the large vessel transit times for each capillary unit are identical. The transport function $h_R(t)$ of an intravascular reference tracer such as ^{125}I-albumin can then be subsequently written

$$h_R(t) = h_{LV}(t - T_C) \qquad (3.15)$$

The reference transport function shifted left by one capillary transit time is used as input to the model. Parameters of the model may then be optimized such that the solutions or output fit the transport functions $h_D(t)$ of the diffusible tracers. The parameters in question are PS_C, PS_B, V_I' and V_B'. Their final estimates will provide an insight into the role of barriers and fluid spaces in bone for diffusible tracers.

3.2. MODEL ACCURACY & INFORMATIVE SIMULATIONS

3.2.1. Assessing the accuracy of model solutions

The accuracy in the numerical approach of solving the 3 P.D.E.s, equation (3.3) is dependent to a large extent on the number of segments, n_x the phases are divided up by ; the larger the n_x value the more accurate the solution. However, larger n_x values result in more calculations that have to be performed, which means for a given input function, longer central processor unit (CPU) times are needed to produce model solutions. The process of optimisation i.e. fitting the model to the experimental data requires repeated calculations of such model solutions and clearly model solutions taking large, perhaps unnecessary amounts of CPU times are impractical and wasteful of resources. It was therefore necessary to find a compromise between model accuracy and economical CPU times.

To assess the model accuracy, use was made of the more exact analytical solutions. Analytically at the capillary transit time T_C, the throughput fraction of tracer is always $\exp(-PS_C/F_s)$ as shown in equation (54) by Bassingthwaighte and Goresky (1984). The throughput fraction also corresponds to the unextracted part of the Crone-Renkin equation (2.5).

To test the accuracy of the model solutions, hypothetical reference $h_R(t)$ and diffusible $h_D(t)$ profiles with pre-assigned values were obtained for a spiked impulse response input function. Profile values at the capillary transit time were used to calculate E(t) (equation (2.4)) and PS_C (equation (2.5)). The calculated model PS_C values were compared with the pre-assigned true values of PS_C for various flow rate and structural values of the capillary.

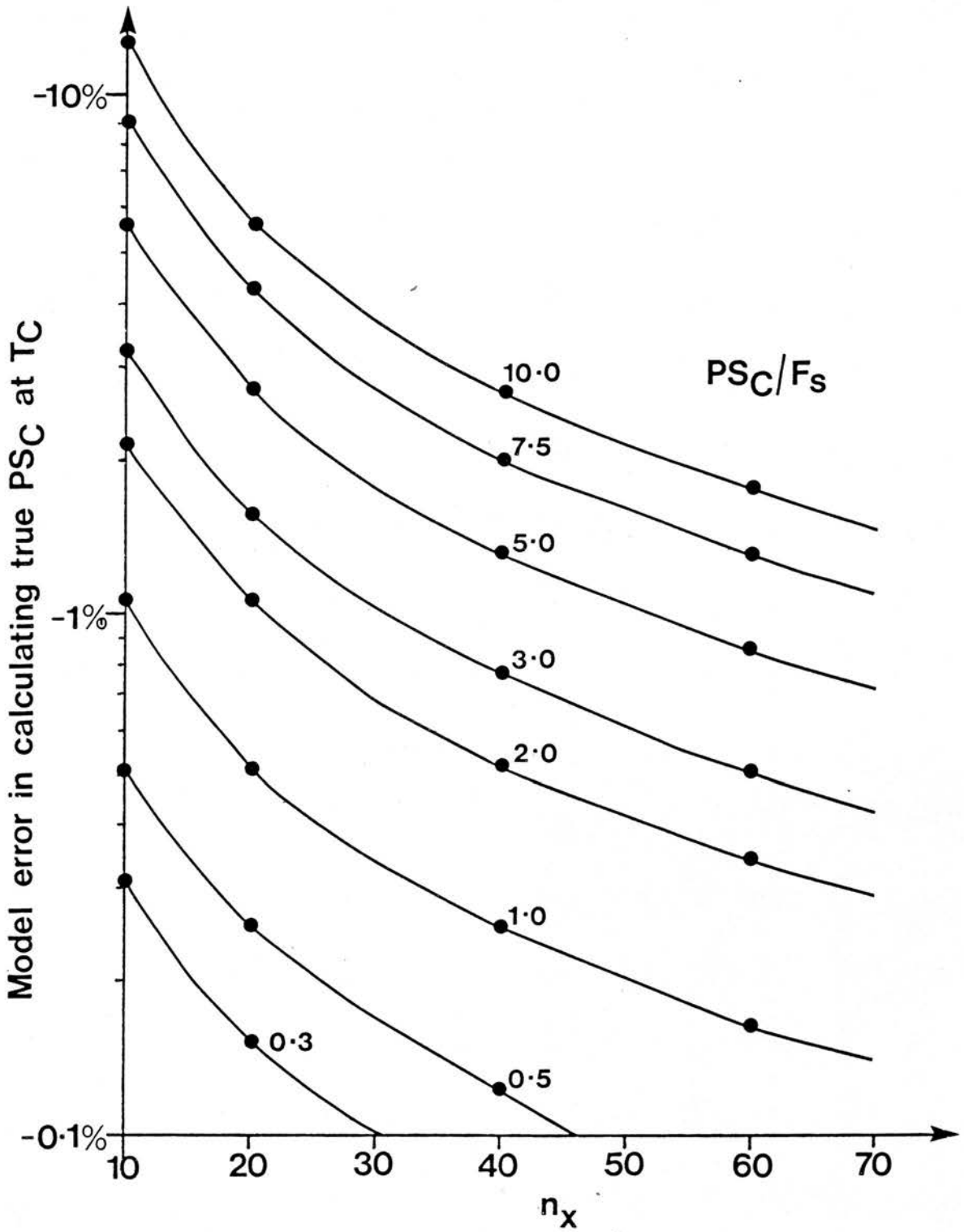

FIGURE 3-3 : Systematic errors in model PS_C values at the capillary transit time T_C as a consequence of the choice of n_x. $T_C=10^C$s, V_C'=0.4 ml, V_I'=2.ml, V_B'=4 ml, F_s=0.04 ml/s (fixed).

TABLE 3-1

Model predictions of PS_C at the capillary transit time T_C = 10 s from hypothetical outflow data as compared with the true varied pre-assigned values of PS_C. Fixed values :- n_x=10, F_s=0.04 ml/s, V_C'=0.4 ml, V_I'=2.0 ml and V_B'=4.0 ml.

True		Model	
PS_C (ml/s)	PS_C/F_s	PS_C (ml/s)	error(%)
4.0×10^{-3}	0.1	3.996×10^{-3}	-0.10
2.0×10^{-2}	0.5	1.99×10^{-2}	-0.51
4.0×10^{-2}	1.0	3.96×10^{-2}	-1.03
8.0×10^{-2}	2.0	7.83×10^{-2}	-2.11
1.6×10^{-1}	4.0	1.53×10^{-1}	-4.44
4.0×10^{-1}	10.0	3.49×10^{-1}	-12.69

Table 3-1 shows model predictions and associated errors for PS_C with n_x=10, when the true PS_C of the capillary is varied. All other parameters of the capillary system are fixed at values resembling those of the canine tibial diaphysis i.e. F_s = 0.04 ml/s ≡ F_s = 2.4 ml/min (close to F_{Bu}) ; V_C' = 0.4 ml is reasonable from tracer equilibration studies. It can be seen that generally all model PS_C solutions are underestimates of the true PS_C, with the degree of underestimation increasing when the capillary wall becomes "leakier" i.e. PS_C or PS_C/F_s increasing. One can appreciate that more permeable capillaries require larger n_x values to achieve accurate model solutions. Figure 3-3 illustrates how the systematic errors associated with model PS_C solutions at T_C can be reduced by increasing n_x. For example, if a capillary had a true PS_C/F_s ratio of 7.5, then by increasing the n_x value from 10 to 40 the error associated with the model solution would decrease from around 9% to 2%.

Table 3-2 shows model predictions and associated errors for PS_C/F_s (with n_x = 10), when the flow rate F_s is varied ; all other parameters being fixed. It can be seen that the error in calculating PS_C/F_s increases with decreasing flow F_s or increasing T_C. From tables 3-1 and 3-2 one can see that the errors are truly

dependent on the PS_C/F_s ratio of the capillary.

TABLE 3-2

Model predictions of PS_C/F_s at the capillary transit time T_C= 10 s from hypothetical outflow data as compared with the true varied pre-assigned values of PS_C/F_s (F_s varied only). Fixed values :- n_x=10, PS_C=0.04 ml/s, V_C'=0.4 ml, V_I'=2.0 ml & V_B'=4.0 ml.

True		Model		
F_s (ml/s)	PS_C/F_s	T_C (s)	PS_C/F_s	error(%)
0.080	0.5	5.0	0.497	-0.51
0.040	1.0	10.0	0.990	-1.03
0.020	2.0	20.0	1.958	-2.11
0.010	4.0	40.0	3.823	-4.44
0.004	10.0	100.0	8.730	-12.69

Tables 3-3 and 3-4 show the effect of varying V_C' and V_I' respectively on model solutions of PS_C with the other parameters fixed accordingly. From table 3-3, it can be seen that larger errors in model predictions of PS_C are associated with increases in T_C, caused by increasing V_C'. From table 3-4, it can be seen that the ratio V_I'/V_C' has an effect on model PS_C values. The higher the ratio the lower the percentage error and *vice versa*.

TABLE 3-3

Effect of V_C' on model predictions of PS_C at the capillary transit time T_C (s) for n_x=10. Fixed values of PS_C=PS_B=F_s=0.04 ml/s, V_I'=2.0 ml and V_B'=4.0 ml used in generating the hypothetical outflow data.

		Model		
V_C'(ml)	V_I'/V_C'	T_C (s)	PS_C (ml/s)	error(%)
0.04	50.00	1.0	3.996×10^{-2}	-0.10
0.10	20.00	2.5	3.990×10^{-2}	-0.26
0.20	10.00	5.0	3.979×10^{-2}	-0.51
0.40	5.00	10.0	3.960×10^{-2}	-1.03
0.60	3.33	15.0	3.939×10^{-2}	-1.53
0.80	2.50	20.0	3.918×10^{-2}	-2.04

TABLE 3-4

Effect of V_I' on model predictions of PS_C at the capillary transit time T_C = 10 s for n_x=10. V_C'=0.4 ml, otherwise other values as in table 3-3.

		Model	
V_I' (ml)	V_I'/V_C'	PS_C (ml/s)	error(%)
0.5	1.25	3.614×10^{-2}	-9.65
1.0	2.50	3.801×10^{-2}	-4.99
2.0	5.00	3.898×10^{-2}	-2.54
4.0	10.00	3.949×10^{-2}	-1.28
8.0	20.00	3.974×10^{-2}	-0.64
16.0	40.00	3.987×10^{-2}	-0.32

A value of PS_C/F_s for ^{85}Sr from the Crone-Renkin equation was found to be around 1.11 (Lemon *et al* 1980b). Furthermore, Lopez-Curto *et al* (1976) from tracer equilibration studies deduced that the average ratio of V_I'/V_C' (mean $\pm$ s.d.) was 3.62 $\pm$ 0.76 (n=6) at 3 hr and 3.84 $\pm$ 0.63 (n=6) at 4 hr. Using these figures with n_x=10 would produce an error of 3% in the model solution of PS_C at T_C, which was regarded as acceptable at the time. It was further realized that this error may be considerably less than 3%. This is because the tracer equilibration ratio V_I'/V_C' may be too small owing to tracer being distributed in larger blood vessels as well as the exchanging capillaries.

To conclude, a value of n_x = 10 was considered adequate in modelling the experimental data with reasonable accuracy.

3.2.2. Simulations of outflow profiles from varying the parameters

To appreciate the behaviour of the model it was necessary to examine the responses as a consequence of varying the parameters. A smooth input function was used in this study, obtained using a NAG E04FDF minimization routine to fit a lagged normal density curve to experimental ^{125}I-albumin reference data (see appendix 2). The lagged normal density curve simulated

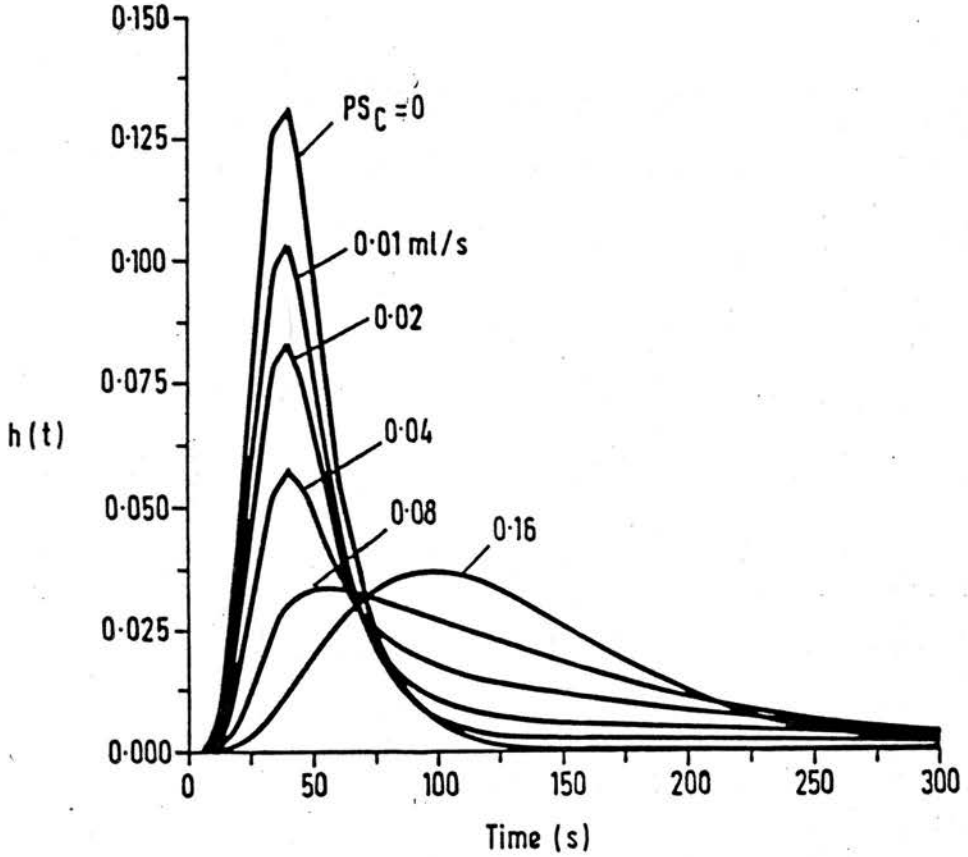

FIGURE 3-4 : Responses of the model specified as h(t), representing solutions every 5 s for changes in PS_C, with PS_B=0, F_s=0.04 ml/s, V_I'/V_C'=8.0 and T_C=10 s.

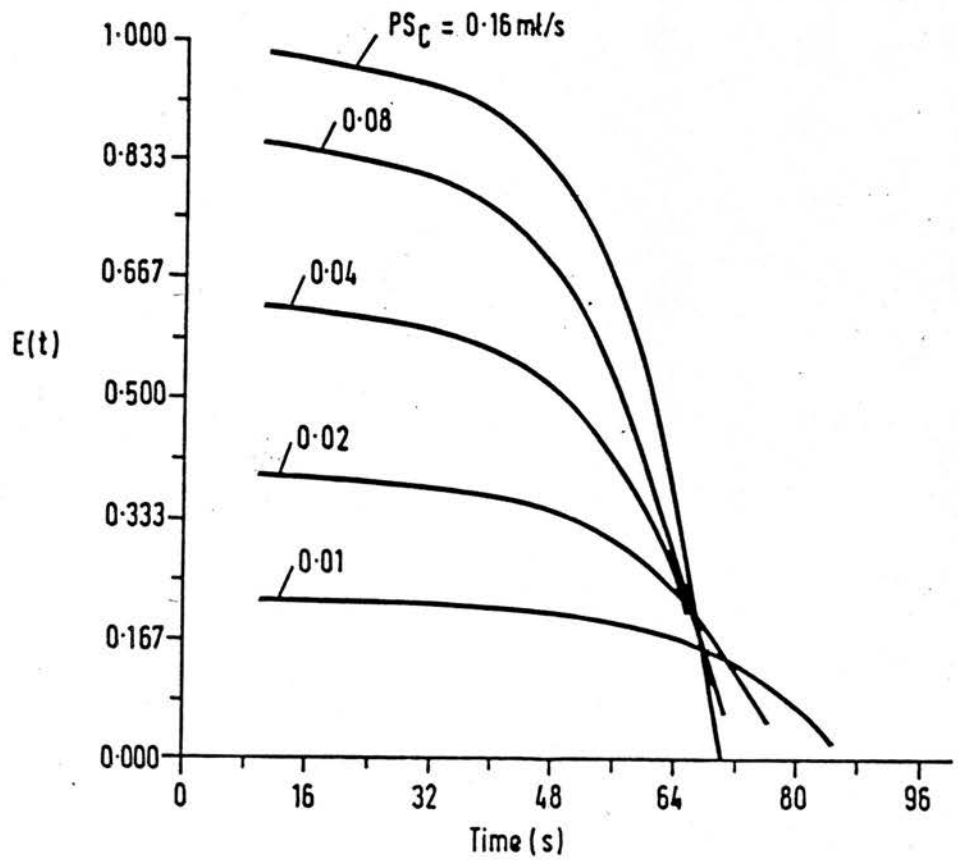

FIGURE 3-5 : Positive extractions calculated from the responses in Figure 3-4.

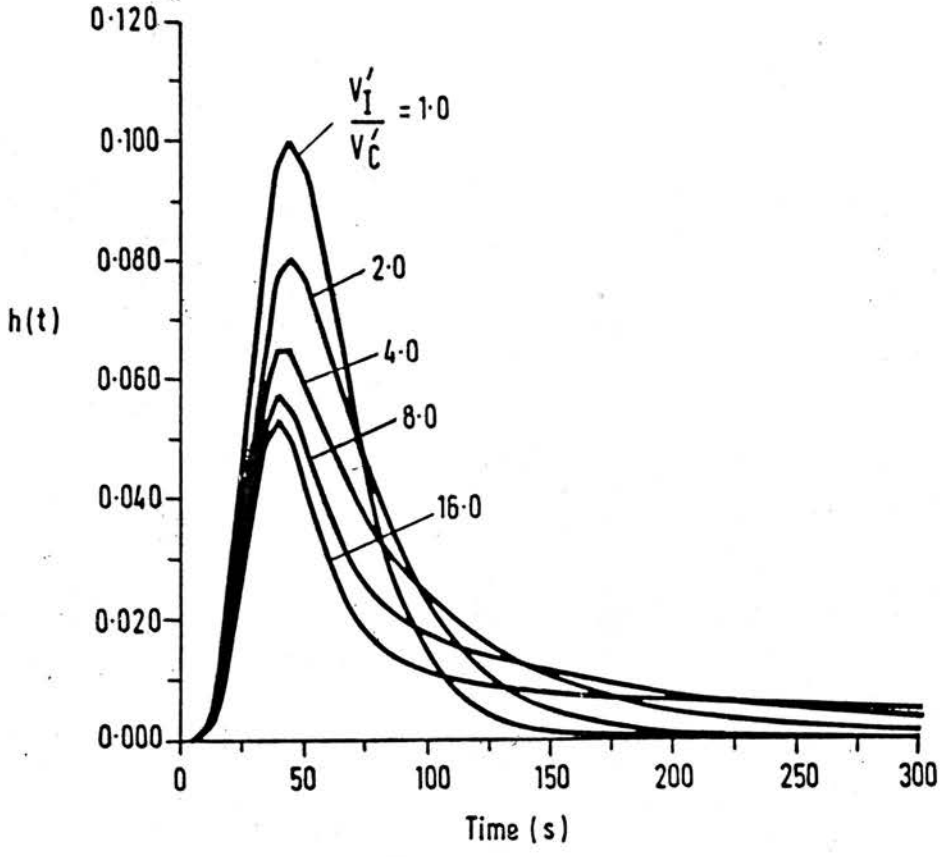

FIGURE 3-6 : Responses of the model specified as h(t), representing solutions every 5 s for changes in V_I'/V_C', with PS_C=0.04 ml/s, PS_B=0, F_s=0.04 ml/s and T_C=10 s.

the effects of tracer dispersion in the large vessels in a smooth form, and subsequent responses from the model were indicative of hypothetical outflow data. Input values of the lagged normal density curve were defined every 5 seconds and intermediate values in the calculation of model fluxes were obtained by linear interpolation ; outflow responses were subsequently calculated at 5 second intervals.

Figure 3-4 shows the responses of the model to changes in PS_C ; the response for $PS_C = 0$ is simply the input function appearing after the capillary transit time. The effect of PS_C is considerable, the peak of the response decreases with increasing PS_C. Also, the tail portions of the responses become more substantial, demonstrating increasing amounts of tracer returning to the vascular system i.e. back diffusion.

Figure 3-5 illustrates the positive extractions which can be calculated from the responses using equation (2.4). The maximum extraction always occurs at the capillary transit time and decreases as higher concentrations of solute are established in the interstitial fluid space. The rate of decrease is principally governed by the magnitudes of PS_C and V_I'. Smaller PS_C and higher V_I' values always produce slower rates of decrease and *vice versa*.

Responses of the model for changes in V_I'/V_C' are shown in figure 3-6. The responses for changes in PS_B and V_B'/V_C' are not as apparent when compared to the other parameters, although they do play a decisive role in the modelling of bone.

3.2.3. Impact functions

Impact functions are useful in demonstrating the effects of parameter estimations on the model (Levin *et al.* 1980). Considering the 3 P.D.E.s

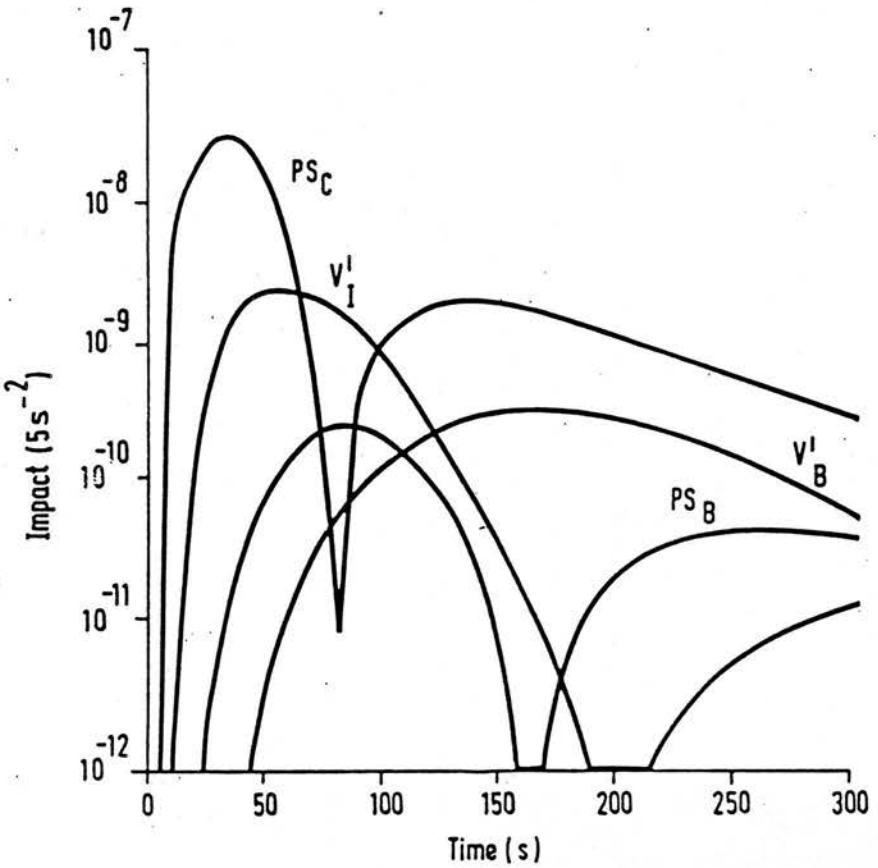

FIGURE 3-7 : Impact functions (log. scale) derived every 5 s, caused by 1% perturbations to the parameters $PS_C/F_s=PS_B/F_s$ =1.0 and $V_I'/V_C'=V_B'/V_C'$=7.5

(equation (3.3)) in the form of a general functional relationship

$$\hat{f} = \hat{f}(t;PS_C,PS_B,V_I',V_B') \qquad (3.16)$$

where $\hat{f}$ is the function calculated for values of an independent variable, time t. The impact function for each parameter is a measure of the change in $\hat{f}$ caused by a perturbation of that parameter. For example, the impact function $\Delta\hat{f}_{PS_C}$ caused by a perturbation ΔPS_C applicable to the PS_C product is

$$\Delta\hat{f}_{PS_C}^{\ 2} = [\hat{f}(t;PS_C+\Delta PS_C,PS_B,V_I',V_B') - \hat{f}(t;PS_C,PS_B,V_I',V_B')]^2 \qquad (3.17)$$

The two functions as illustrated in equation (3.17) in fact comprised simulated outflow values derived every 5 s up to 300 s after a lagged normal density curve as described, had been used as model input.

Figure 3-7 illustrates the impact functions of each of the parameters over the experimental time range for the smooth lagged normal density curve input function ; the size of the perturbations are 1% of the parameter values. It is interesting to observe the considerable effect of PS_C, particularly for early times when extractions are positive. The impact function for V_B' is larger in magnitude over the last half of the time range and emphasizes why so many blood count samples have to be taken. The maximum value for each input function gives one a good idea of the relative accuracies involved in obtaining parameter estimates.

3.2.4. Effects of noise on the parameter estimates

Simulations involving noisy hypothetical outflow data representing the variations in isotope activity in the blood samples were performed to test the robustness of parameter values in the optimisation process.

Firstly, a smooth test model curve with pre-assigned parameter values was

TABLE 3-5

Effects of noise on the parameter estimates from the homogeneous model using BMDP PAR :- optimising to 20, 40 and 60 data values. Final values, residual sum of squares (RSS) and coefficients of variation (c.v.) are averaged over given number of runs. No bounds applied.
Pre-assigned package values. T_C=10 s, n_x=10.

Parameter vector (PS_C/F_s, PS_B/F_s, V_I'/V_C', V_B'/V_C') : True values (1.20, 1.20, 9.00, 9.00)

Starting values (1.80, 1.80, 11.25, 11.25)

No. data values	Noise level (s.d.$_p$)	Number of runs /runs attempted	Final values parameter vector	c.v. (%) parameter vector	RSS
20	0%	1/1	1.20, 1.20, 9.00, 9.00	-	2.08×10^{-13}
	1%	5/5	1.21, 1.42, 8.51, 13.92	1.02, 29.39, 8.19, 88.33	1.75×10^{-6}
40	0%	1/1	1.20, 1.20, 9.00, 9.00	-	3.71×10^{-13}
	1%	5/5	1.20, 1.26, 8.77, 9.16	0.54, 6.73, 2.91, 2.45	2.70×10^{-6}
	5%	5/5	1.22, 1.28, 8.39, 9.54	4.08, 38.48, 15.37, 11.94	7.01×10^{-5}
60	0%	1/1	1.20, 1.20, 9.00, 9.00	-	5.36×10^{-13}
	1%	5/5	1.20, 1.25, 8.77, 9.16	0.52, 5.64, 2.69, 2.47	3.22×10^{-6}
	5%	5/5	1.22, 1.26, 8.42, 9.32	3.62, 27.03, 11.99, 11.12	8.14×10^{-5}
	10%	5/5	1.34, 1.50, 7.28, 11.60	6.79, 29.79, 28.83, 7.38	3.15×10^{-4}

produced using a lagged normal density curve as input. Then varying amounts of noise, which was obtained using two NAG routines G05CCF and G05DDF (see appendix 3) to produce a non-repeatable Gaussian distribution of random numbers, was subsequently added to the test model data. The noise was defined in terms of the standard deviation ($s.d._p$) calculated at the peak of the response $h(t)_{max}$, where

$$s.d._p = k\sqrt{h(t)_{max}}$$

The square root of $h(t)_{max}$ was found because the standard deviation associated with quantities of radiation so defining h(t) in general, relates to the Poisson distribution. Hence the constant k, to produce the required amount of noise at the peak of the response was calculated and used to derive the expected higher standard deviations associated with lower h(t) values. The noisy data along with the smooth input function was optimized using a BMDP PAR package (see appendix 3).

Table 3-5 illustrates the effects of noise on the parameter estimates for various numbers of data values, with 60 values being comparative to the 60 experimental sample values over a time period of 5 min. The optimisation routine was initiated using parameter estimates which were 50% higher than their true values. These results show the trend of higher coefficients of variation (c.v.) and residual sum of squares (RSS) with higher levels of noise. They also show that estimations of PS_C are much more accurate in comparison with the other parameters, which is what Levin *et al* (1980) found using a similar model to study coronary circulation. It can also be appreciated that for accurate estimations, particularly for parameters relating to the third phase (bone), many samples and long counting times are necessary.

Table 3-6 Parameter estimates of experimental ^{86}Rb data using ^{125}I-albumin as input to the model. Max. increment halvings = 100, otherwise preassigned BMDP package values. T_C = 10 s, n_x = 10.

Experiment number	1	2	3	4	5	6
Parameter vector $\left(\frac{PS_C}{F_s}, \frac{PS_B}{F_s}, \frac{V_I'}{V_C'}, \frac{V_B'}{V_C'}\right)$						
Starting values	1.818,0.303,1.515,1.515	1.818,0.303,1.515,1.515	1.061,0.303,1.515,1.515	1.212,0.303,1.515,1.515	0.757,0.303,1.515,1.515	0.909,0.303,1.515,1.515
Lower bounds	0.030,0.000,0.030,0.030	0.030,0.000,0.030,0.030	0.030,0.000,0.030,0.030	0.030,0.000,0.030,0.030	0.030,0.000,0.030,0.030	0.030,0.000,0.030,0.030
Final values	2.527,0.621,1.064,7.035	1.870,0.409,2.654,7.367	0.897,0.094,2.720,1.780	1.770,0.936,2.661,16.066	0.691,0.330,36.795,16.394	1.258,0.518,2.664,L
CV	11.090,8.505,8.682,15.057	6.877,11.215,6.247,20.005	10.203,137.663,13.143,11.867	4.212,5.613,6.608,10.309	0.856,20.242,13.752,188.000	3.784,6.874,5.631,L
RSS	4.425×10^{-4}	3.575×10^{-4}	5.764×10^{-4}	1.423×10^{-4}	1.413×10^{-4}	5.809×10^{-5}
CPU time (s)	39.46	37.07	611.17	80.70	504.87	105.36
Largest number of increment halvings required (No. of times for max)	5	3	100(6)	8	1100(4)	7

L:- large, value is larger than format specifications of package.

Table 3-7 Parameter estimates of experimental ^{85}Sr data using ^{125}I-albumin as input to the model. Max. increment halvings = 100, otherwise preassigned BMDP package values, T_C = 10 s, n_x = 10.

Experiment number	1	2	3	4	5	6
Parameter vector $\left(\frac{PS_C}{F_s}, \frac{PS_I}{F_s}, \frac{V_I'}{V_C'}, \frac{V_B'}{V_C'}\right)$						
Starting values	2.121,0.303,1.515,1.515	1.970,0.303,1.515,1.515	1.212,0.303,1.515,1.515	1.818,0.303,1.515,1.515	0.606,0.303,1.515,1.515	0.909,0.303,1.515,1.515
Lower bounds	0.030,0.015,0.303,0.303	0.030,0.015,0.303,0.303	0.030,0.015,0.303,0.303	0.030,0.015,0.303,0.303	0.030,0.015,0.303,0.303	0.030,0.015,0.303,0.303
Final values	2.052,1.042,2.644,22.498	1.909,0.770,3.714,20.712	0.985,0.094,7.189,2.064	1.764,1.279,3.934,27.012	*0.618,*0.015,*121.062,*292.623	1.242.0.964,5.501,149.542
CV	3.590,2.827,4.811,5.906	4.103,5.357,5.323,11.362	3.134,174.690,5.495,5.980	2.639,4.329,5.604,7.909	NA, NA, NA, NA	1.701,5.221,4.788,51.606
RSS	5.480×10^{-5}	1.271×10^{-4}	3.875×10^{-4}	6.592×10^{-5}	1.790×10^{-4} *	1.434×10^{-5}
CPU time (s)	118.76	67.27	926.87	52.11	-	35.23
Largest number of increment halvings required (No. of times for max)	11	8	100(9)	5	100(3)	2

* Last values obtained for an incomplete run.
NA:- Not available.

3.3. RESULTS OF SINGLE CAPILLARY MODEL OPTIMISATION TO M.T.O.D. DATA

3.3.1. Fitting the experimental data using BMDP PAR

Tables 3-6 and 3-7 show the results for parameter estimates of experimental ^{86}Rb and ^{85}Sr data respectively ; lower bounds as well as starting values are shown because they were required to prevent negative estimates and model solutions exceeding the computational range. Starting values were picked close to the limit nearer zero as advised in BMDP literature. The choice of a starting value for PS_C was found to be very influential in obtaining quick and meaningful results from the package. A PS_C value slightly less than an experimental value calculated from equations (2.4) and (2.5) was found to be the most suitable. The number of increment halvings cited in the tables gives an indication of the adequacy of the model, the higher the value the less adequate the model (see Appendix 3).

The fitting of data for experiments 3 and 5 is not very good, indicated by the fact that the pre-assigned maximum number of increment halvings has been reached several times. The CPU times and c.v.s for these experiments are also generally higher than for the others. For ^{85}Sr data, experiment 5, the final values shown represent the last parameter estimates which were obtained before the program failed owing to exponential terms in the analytical solution being out of computational range. The CPU time has not been cited and the c.v.s are not available because the run was incomplete ; additional runs using different starting values could not remedy the situation, hence the model is unsatisfactory for this data. Figure 3-8 shows the poor model fit to ^{86}Rb data of experiment 3.

The fitting of data for experiments 1,2,4 and 6 was considered satisfactory in

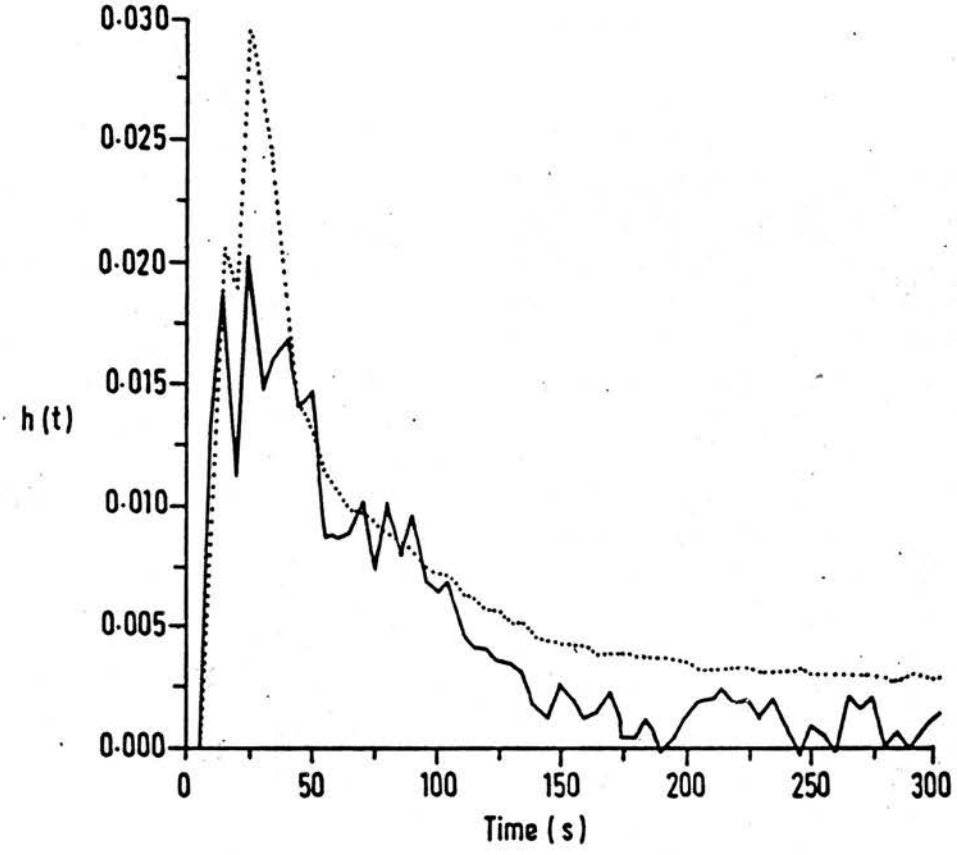

FIGURE 3-8 : Poor model fit (dotted line) to ^{86}Rb data of experiment 3 (solid line). Fitting is performed at 5 s multiples for 300 s.

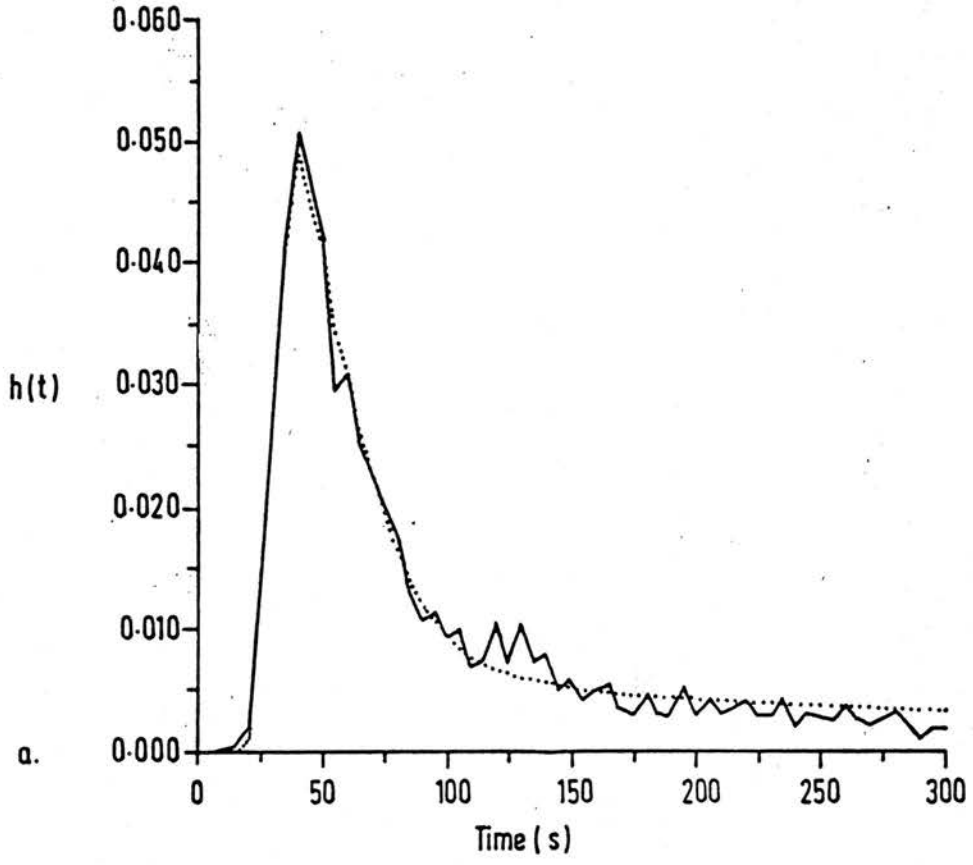

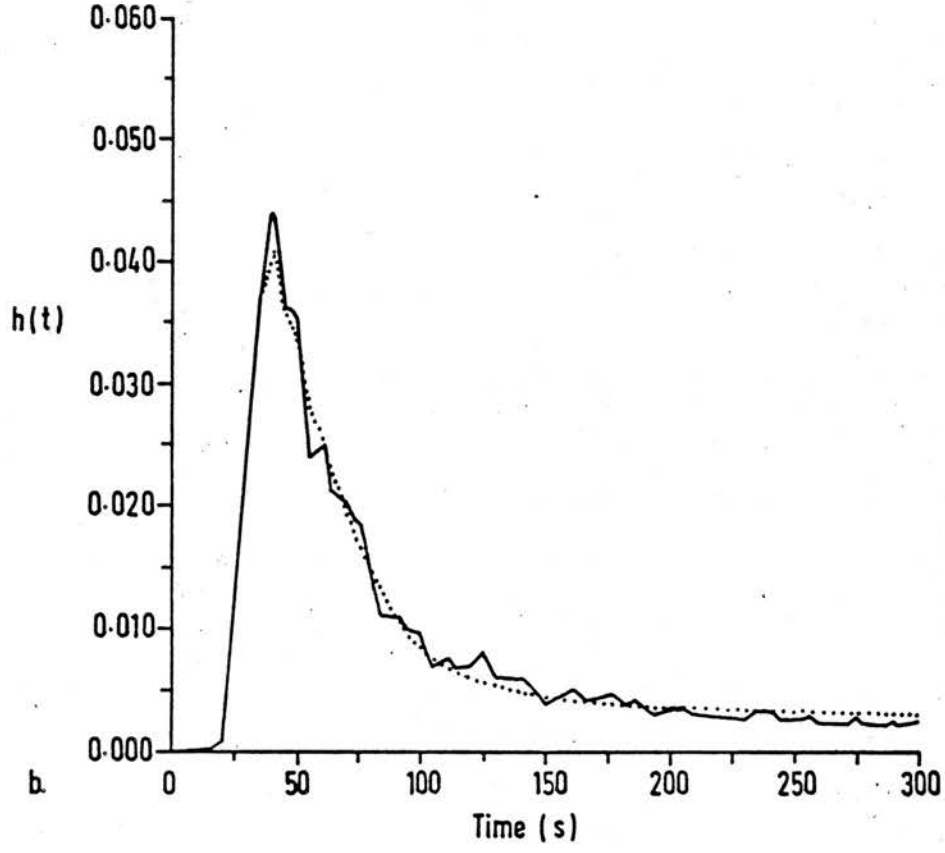

FIGURE 3-9 : Satisfactory model fits (dotted lines) to, a. ^{86}Rb and, b. ^{85}Sr data of experiment 4 (solid lines). Fitting is performed at 5 s multiples for 300 s.

TABLE 3-8

Checking the n_x accuracy on final parameter estimates and fit (^{86}Rb data ; expt. 1). T_C=10 s, max. increment havings=100, otherwise pre-assigned BMDP package values.

n_x	PS_C/F_s	PS_B/F_s	V_I'/V_C'	V_B'/V_C'	RSS	CPU (s)
10	2.527	0.621	1.964	7.935	4.425×10^{-4}	38.46
20	2.476	0.615	1.925	7.960	4.426×10^{-4}	110.58
40	2.452	0.612	1.907	7.973	4.427×10^{-4}	330.42

view of smaller c.v.s, CPU times and numbers of increment halvings used. Figures 3-9a and 3-9b illustrate the fitting of the model to ^{86}Rb and ^{85}Sr data respectively of experiment 4.

From section 3.2.1., it was stressed how the accuracy of model solutions depended on model parameters, particularly PS_C or PS_C/F_s ; higher n_x values were commended to the "leakier" or high PS_C capillaries. The PS_C/F_s prediction of around 2.5 for ^{86}Rb (experiment 1) which was the highest from all the data that was optimized to the model with n_x=10, was believed to be possibly inaccurate. However, table 3-8 which illustrates parameter estimates for ^{86}Rb (experiment 1) for model optimisation with higher n_x values shows that the differences in all parameter estimates are relatively small. If the most accurate estimate of PS_C/F_s = 2.452 (n_x=40) did resemble the realistic figure, then the estimate of PS_C/F_s = 2.527 (n_x=10) is only about 3% different. The latter estimate is all the more reasonable in view that only 38-39 s of CPU time was required to obtain it with the other parameter estimates ; the final parameter estimates (n_x=40) took around 330 s of CPU time. It would seem from table 3-8 that doubling the n_x values in the model optimisation process results in a trebling of the CPU time required to run that process to completion.

3.3.2. Comparisons of extractions & PS_C products between models I & II

Mean and s.d. figures for the PS_C products for ^{86}Rb and ^{85}Sr have been calculated from the single capillary model II predictions. All 6 sets of data for each of the tracers including the poorer model fits have been used in these calculations. The reason for doing this is that the PS_C parameter is by far the most dominant and stable parameter in the model as seen from the impact functions and the lower comparative coefficients of variation in the noise tests. Model II E_{max}s were calculated from their corresponding PS_C products and the

infusing flow rate F_s using equation (2.5). Means and s.d.s for E_{max} (model II) along with those for the PS_C products for ^{86}Rb and ^{85}Sr are shown in table 3-9. These figures are compared with calculated values using equations (2.4) and (2.5) - model I, utilizing the same outflow data. The methods refer to the ways in which E_{max} was deduced bearing in mind the need to obtain extraction values that are conducive to average capillary flow rates and are not impaired by back diffusion.

TABLE 3-9

Mean ± s.d. of E_{max} and PS_C for ^{86}Rb and ^{85}Sr (n=6) ; percentage coeffs. of variation in parentheses.

	^{86}Rb	^{85}Sr
MODEL I		
Method 1		
E_{max}	0.73 ± 0.11 (14.47)	0.76 ± 0.12 (16.05)
PS_C (ml/s)	0.046 ± 0.014 (30.15)	0.052 ± 0.018 (35.51)
Method 2		
E_{max}	0.65 ± 0.10 (15.65)	0.66 ± 0.17 (25.64)
PS_C (ml/s)	0.036 ± 0.010 (28.16)	0.039 ± 0.016 (41.32)
Method 3		
E_{net}	0.65 ± 0.11 (16.82)	0.66 ± 0.15 (22.70)
PS_C (ml/s)	0.036 ± 0.011 (29.05)	0.037 ± 0.013 (35.70)
MODEL II		
E_{max}	0.73 ± 0.16 (22.18)	0.73 ± 0.16 (22.00)
PS_C (ml/s)	0.050 ± 0.023 (45.56)	0.047 ± 0.019 (39.85)

A maximal value of instantaneous extraction is referred to as method 1. The average of instantaneous extractions up to the peak of the reference outflow profile constitutes method 2. Method 3 is the net extraction (equation (2.7)) up to the time of the peak of the reference outflow profile which occurs typically between 15-40 s into the sampling period. In all 3 methods, spurious results

occurring from low count rates in the first samples were avoided.

From table 3-9, one can see that the values from method 1 of around 0.73 agree best with model II predictions which tends to suggest that sensible values for E_{max} were found from the noisy instantaneous extraction data. Smoother model I values typically of 0.65-0.66 from the other 2 methods are lower than model II predictions owing to back diffusion. Extraction values obtained from both these methods are very similar and apply more to average capillary blood flow rates as compared to method 1.

Modified Crone-Renkin equations

TABLE 3-10

Correlation coefficients (r) between E_{max} model II (y) predictions and different forms of E_{max} calculated from model I (x) for individual sets of experimental data.

	^{86}Rb	^{85}Sr
E_{max} (method 1)	0.91	0.95
E_{max} (method 2)	0.98	0.99
E_{net} (method 3)	0.93	0.98

It is interesting to obtain correlation coefficients (r) between the various E_{max} values calculated from model I (x) and the model II (y) predictions. Table 3-10 illustrates these correlation coefficients, where it can be seen that higher correlation coefficients are associated with the more averaged and smoother approaches of calculating E_{max} using methods 2 and 3. As far as relationships between both models are concerned it is better to use averaged instantaneous extractions which have the highest correlation coefficients. Thus for the benefit of investigators who do not have access to the single capillary model II, modifications to the Crone-Renkin equation accounting for back diffusion is suggested as follows,

(^{86}Rb & ^{85}Sr) $$PS_C = -F_s.\log_e(1 - 1.12E_{max}) \quad (3.18)$$

The correction factors being 1.12 ± 0.09 (^{86}Rb) and 1.11 ± 0.07 (^{85}Sr) were of a similar size to a value of 1.14 which was found by Guller *et al* (1975) in correcting for back diffusion for sodium in perfused dog hearts.

Permeability ratios (P_{Rb}/P_{Sr}) were found by dividing the PS_C product for ^{86}Rb with that of ^{85}Sr. Model II and model I, method 1 ratios (P_{Rb}/P_{Sr}) were found to be 1.04 ± 0.11 and 0.90 ± 0.11 respectively. These values fall short of the free diffusion coefficient ratio (D_{Rb}/D_{Sr}) of 1.58 where D_{Rb} = 2.10 x 10^{-5} cm^2/s (Alvarez and Yudilevich 1969) and D_{Sr} = 1.33 x 10^{-5} cm^2/s (Maltby *et al* 1982) in water at 25°C. The model I (P_{Rb}/P_{Sr}) ratio around 0.9 is similar to (P_K/P_{Sr}) ratio ranges of around 0.83-0.89 found by Maltby *et al* (1982) who used potassium ^{42}K.

It is still however difficult to explain at this stage the low ratio values of (P_{Rb}/P_{Sr}) as compared to their corresponding diffusion coefficient ratios. It is encouraging that an increased ratio of 1.04 nearer to the figure of 1.58 was obtained from the more realistic model II.

3.3.3. Apparent volumes of distribution ; PS_B

TABLE 3-11

Mean ± s.d. of V_I'/V_C', V_B'/V_C' and PS_B/F_s for ^{86}Rb and ^{85}Sr. Experimental numbers used in parentheses (Model II).

	^{86}Rb	^{85}Sr
V_I'/V_C'	2.49 ± 0.35 (1,2,4,6)	3.95 ± 1.18 (1,2,4,6)
V_B'/V_C'	10.46 ± 4.87 (1,2,4)	23.43 ± 3.28 (1,2,4)
PS_B/F_s	0.62 ± 0.23 (1,2,4,6)	1.02 ± 0.21 (1,2,4,6)

Table 3-11 shows the mean ± s.d. values of parameter estimates V_I'/V_C' and V_B'/V_C' found for the diffusible tracers. The ratios quoted were calculated from the parameter estimates of satisfactory experimental fits and represent apparent volumes of distribution. The larger V_I'/V_C' ratio for ^{85}Sr compared with ^{86}Rb suggests that the interstitial fluid is more accessible to ^{85}Sr, if one assumes equal accessibilities for the tracers in the bicarbonate buffer flowing through the capillaries. Overall, the V_B'/V_C' and V_I'/V_C' ratios are higher for ^{85}Sr than they are for ^{86}Rb emphasizing the much greater capacity for longer term ^{85}Sr retention as compared with ^{86}Rb. The higher PS_B/F_s ratios for ^{85}Sr as compared with ^{86}Rb suggests that the process of ^{85}Sr uptake to the bone is quicker than cellular uptake of ^{86}Rb.

Model I estimates for PS_B were found using the equations (2.11) and (2.12). If one assumes that the total conductance PS_{Tot} of the system consists of the conductances of PS_C and PS_B in series, and that V_I' can be ignored owing to it being small in comparison with V_B', then $PS_B = FER(t)V_B'PS_C/(PS_C - FER(t).V_B')$. An average FER(t) value was obtained from the last 5 experimental FER values, calculated using equation (2.8). These latter FER values although noisy constituted the flatter portion of FER(t) versus time profiles between times of 275-300 s. Average values of V_B' = 3.45 ml (^{86}Rb) and V_B' = 7.73 ml (^{85}Sr) obtained from satisfactory fits of model II were used in the calculation along with model I PS_C products from maximum instantaneous extractions.

Table 3-12 illustrates the mean ± s.d. of the FER values used and the resulting values of PS_B (model I) obtained from the calculations. The model I PS_B predictions are about four times less than model II estimates and have much higher coefficients of variation. It would appear that higher values of FER(t) appertaining to shorter time periods would have been more suitable in the determination of PS_B.

TABLE 3-12

Comparisons of PS_B determined from average FER values (275-300 s) with model II PS_B predictions for ^{86}Rb and ^{85}Sr using satisfactory model fits (experimental numbers 1,2,4 and 6). All values quoted represent mean ± s.d. (n=4) ; percentage coeffs. of variation in parentheses.

	^{86}Rb	^{85}Sr
MODEL I (experimental data sets 1,2,4 and 6)		
FER s^{-1}	$(1.38 \pm 1.14)\times10^{-3}$	$(9.36 \pm 4.17)\times10^{-4}$
PS_B ml/s	0.0054 ± 0.0047 (86.50)	0.0083 ± 0.0038 (46.24)
MODEL II		
PS_B ml/s	0.021 ± 0.0075 (36.58)	0.034 ± 0.0070 (20.78)

3.3.4. Conclusions & future model developments

Although the single capillary model far from resembles the complex structure of bone it is considerably more advanced than the aforementioned compartment and non-compartment models that have preceded it. When optimisation procedures were used to derive parameter values by fitting to experimental data, the model was able to provide fits in the majority of cases. A choice of n_x=10 was found to be a suitable compromise in obtaining accurate model parameters and being economical with CPU time.

The single capillary model predictions of E_{max} for both ^{86}Rb and ^{85}Sr were similar to individual maximum instantaneous extractions obtained from the outflow data. It would thus seem from outflow profiles, that an individual maximum instantaneous extraction value as opposed to an average extraction value is a better estimate of the actual bone capillary extraction. However, in cases where the outflow extraction data are very noisy, one would be better

advised to use averaged measures of extraction and an empirical formula such as equation (3.18) which applies to both ^{86}Rb and ^{85}Sr. In table 2-2, it would appear that the latter estimates of ^{85}Sr E_{max} (sets 5-7) from M.T.O.D. techniques are the most meaningful because maximum instantaneous extractions were used.

The model II permeability ratio (P_{Rb}/P_{Sr}) of 1.04 was found to be less than the free diffusion coefficient ratio (D_{Rb}/D_{Sr}) of 1.58. This however is an improvement on the model I (P_{Rb}/P_{Sr}) ratio of 0.90. The lower permeability ratios may arise owing to complications of ^{86}Rb transport to endothelial cells and differing ^{86}Rb uptake rates to cellular types in the marrow as opposed the cortex.

The most significant advantage of fitting model II to the outflow data was obtaining finite apparent volumes of distribution for the phases within the bone. Ratios of these apparent volumes of distribution can only be compared with other ratios if the same tracers were used under the same experimental conditions. Nevertheless, the V_I'/V_C' ratios found for ^{86}Rb and ^{85}Sr are about the same order of magnitude compared with $V_I'/V_C' = 2.20 \pm 1.35$ calculated from data in which ^{99m}Tc-albumin (plasma), ^{99m}Tc-labelled red blood cells, and ^{14}C-sucrose (extravascular) tracers were used (Morris *et al* 1983). The ratio of $V_B'/V_C' = 10.46 \pm 4.87$ for ^{86}Rb with V_B' being applicable to bone cells, agrees quite favourably with $V_B'/V_C' = 6.00 \pm 1.15$ (mature dogs) and $V_B'/V_C' = 6.00 \pm 1.30$ (old dogs) calculated from data in which ^{99m}Tc-labelled red blood cells were used (Pinto and Kelly 1984). The high V_B'/V_C' ratio for ^{85}Sr indicates that it must be absorbed by the large bone surface area.

The use of fractional escape rates to obtain PS_B for both the diffusible tracers is not recommended. The use of such a technique relies on the fact that the

interstitial fluid phase is negligibly small in comparison with the bone phase and that the permeability of the associated barriers is low relative to capillary blood flow rates. These factors lend credence to the notion of a large bone tissue phase in which the rate of tracer efflux to the capillary is slow and consistent such that PS_B can be accurately predicted as mentioned. However, for the diffusible tracers of ^{86}Rb and ^{85}Sr, V_I' is not negligibly small as compared with V_B' and furthermore the permeability of the capillaries to these tracers is relatively high. Compound these effects with the possibility of heterogeneous capillary flow rates makes one realize that fractional escape rates are very unlikely to represent constant bone-capillary effluxes. Model I predictions of PS_B for ^{86}Rb and ^{85}Sr found from FER(275-300)s^{-1} were about four times less than the more realistic model II predictions. This is because, FER values were generally too low and were probably representing tracer effluxes from capillary tissue regions with below average flow rates.

The fact that some of the experimental data could not adequately be described by the model, indicated that further modifications were necessary. The next most important modification is allowing for heterogeneous blood flow rates which are known to exist in the cortex and marrow. Bassingthwaighte and Goresky (1984) reported that PS_C is consistently underestimated when a similar homogeneous model is used to fit heterogeneous data. The assessment of blood flow in the diaphyseal cortex and marrow was the next priority.

CHAPTER 4

EXPERIMENTAL ASSESSMENT OF DIAPHYSEAL BLOOD FLOW IN THE TIBIA

4.1. TECHNIQUES & MEASUREMENTS OF BONE BLOOD FLOW

Methods of determining bone blood flow have been suitably categorized in a review by Tothill (1984). These categories mainly include methods that use radioactive isotopes notably clearance of bone-seeking tracers, washout of highly diffusible tracers and indicator fractionation.

4.1.1. Clearance of bone-seeking tracers

This technique involves injecting bone-seeking tracers intravenously and using a measurement of their disappearance from the plasma to determine bone blood flow rates. Frederickson *et al* (1955) were amongst the earliest investigators to adopt this technique in which from intravenous injections of ^{45}Ca they found that bone blood flow rates in rats were between 0.1-0.3 ml/min/g tissue.

The experimental relationship between the disappearance or clearance of bone-seeking tracers from the blood and skeletal blood flow rate F_{sk} is given by the following equation (Weinman *et al* 1963)

$$F_{sk} = \%_{sk} / [\overline{\%}_{p} . DT . (1 - H)]$$

where

- $\%_{sk}$ is the percentage dose retained by the skeleton, usually per 100 g of skeleton.
- $\overline{\%}_{p}$ is the mean arterial percentage of dose per ml of plasma

during the duration DT of the experiment.

- H is the fractional haematocrit required to obtain plasma flow rates.

Weinman *et al* (1963) injected ^{85}Sr and ^{47}Ca tracers intravenously via the right jugular vein and obtained blood samples for the determination of $\bar{\%}_p$ from the left carotid arteries of dogs. $\bar{\%}_p$ was obtained from a plot of tracer disappearance per 100 ml carotid artery plasma versus time up to 10 minutes, the duration DT of the experiment. $\%_{sk}$ at 10 minutes for mature (^{85}Sr ; n=2) and immature dogs (^{47}Ca, ^{85}Sr ; n=5) was found to be around 25-30% and 40-44% respectively. They found that mean blood flow rates for mature and immature dogs were 5.6 and 7.7 ml/min.100g^{-1} respectively.

The main problem with the clearance technique however is that tracers are assumed to be completely extractable, with extractions being independent of flow rate. This is invariably not the case and additionally the net extraction of the bone seeking tracers is variable with successive recirculations of tracer. These views are reinforced by Copp and Shim (1965) who carried out clearance and extraction studies on ^{85}Sr over a 5 minute period in the tibiae of adult dogs. After having injected an intravascular dye with ^{85}Sr into tibial nutrient arteries they obtained E_{net} (5 min) = 0.76 which with corresponding clearances produced bone blood flow rates which were generally higher than those obtained by Weinman *et al* (1963).

It would appear that more reliable estimates of bone blood flow rates would be obtained if a tracer was completely extracted during single capillary passage. This was believed to be the case at one stage by Wootton (1974) who studied ^{18}F uptake in rabbit bones. He injected a mixture of ^{18}F and ^{51}Cr labelled microparticles into rabbit aortas and killed the animals 10 s later to avoid the possibilty of ^{18}F recirculation. The tibiae and femora were removed and

assayed for radioactivity. The mean ratio of ^{18}F activity to that of the ^{51}Cr particles which impacted in the capillaries on single passage was close to unity. Wootton interpreted this as implying 100% extraction and suggested that ^{18}F may be used for bone blood flow rate studies. However, Lemon *et al* (1980a) studying tracer uptake in canine tibiae have reported ^{18}F extractions between 18-70%.

Tothill and Hooper (1984) have recently examined the uptake of intravascular and diffusible tracers in the bones of rats and rabbits as a function of time. The animals were killed quickly at different times following the injection of tracers into their hearts and aortas. They found that at no time between 4 and 60 s after injection did the bone concentration of any of the tracers fall to negligible values. They proved conclusively that the tracer could not be completely removed in bones before recirculation started. It would thus seem that in Wootton's experiments, the ^{18}F may not have completely circulated through the various bones and may have been caught in transit causing high activity readings. Tothill and Hooper (1984) have proved that for tracers that are not completely extractable, the determination of bone blood flow rates from clearance and extraction measurements is invalid.

To conclude, it would seem that the clearance method of determining blood flow rates will only be valid if a bone-seeking tracer can be found that is completely extractable and is taken up very quickly such that back diffusion is minimal. Little and Bassingthwaighte (1983) have found that tritium labelled desmethylimipramine (DMI, mol. wt. 266.3) satisfies these criteria for reasonable lengths of time in perfused hearts. Thus [^{3}H]DMI may be of use in determining blood flow rates from clearances in the heart or perhaps even other organs.

4.1.2. Washout of diffusible tracers

The principle of this method is that the rate of removal of the introduced tracer depends on the blood flow rate. The tracers that are used are usually lipophilic (section 1.3.2.), being highly extractable.

Kelly *et al* (1971) have attempted to measure canine tibial diaphyseal blood flow rates by ^{125}I-4-iodoantipyrine (I-Ap) washouts. The formulation they used for deriving cortical blood flow rates $F_{s/Co}$ was,

$$F_{s/Co} = \frac{\lambda_{I-Ap/Co}}{\rho_{Co}} \cdot \frac{C^*(0) - C^*(T)}{\int_{t_0}^{T} C^*(t)dt}$$

where,

- $\lambda_{I-Ap/Co}$ is the partition coefficient (the average bone/blood solubility ratio) for I-Ap in tibial cortical bone.
- ρ_{Co} is the bone specific gravity (g/ml).
- $C^*(t)$ is the count rate at time t, measured by an external detector placed over the bone and $C^*(0)$ is the peak activity count rate at t=0, occurring within a few seconds of the injection at t_0.
- T is the time of the ending of the recording, usually 15 minutes.

$\lambda_{I-Ap/Co}$ and ρ_{Co} (both mean $\pm$ s.d.) were calculated to be 0.150 $\pm$ 0.027 and 1.94 g/ml respectively. In determining $F_{s/Co}$ a shielded 0.75 inch (diam. and thickness) NaI crystal (external detector) was placed over the anterolateral mid-diaphyseal surface of the tibia. The detector was sensibly placed 4-6 cm

from where the tibial nutrient artery (vessel for I-Ap injection) entered the tibia.

Following I-Ap injections, they deduced that $F_{s/Co}$ (mean $\pm$ s.d.) = 0.0152 $\pm$ 0.003 ml/ml bone per minute for 32 washout curves using the formulation. However, further studies that these investigators undertook highlighted the problems of applying washout techniques to bone. They found that count rates after the removal of marrow were 70% of the count rates of the intact bone and attributed this to the marrow independently receiving 30% of the tibial nutrient artery flow. Furthermore, it was found that the uppermost cortical bone could absorb around 40% of potential marrow counts. Their results infact suggested that 50% of the counts that the external detector received may have been attributable to the marrow. Thus cortical flow rates determined specifically from the aforementioned formulation appertaining to the external detection technique are very questionable.

Kelly *et al* (1971) also deduced that the estimates of cortical bone blood flow rates determined by washout of I-Ap were 72.3 $\pm$ 3.7% of the value for pumped perfusion of the whole tibia at a known rate. However, in their calculations, whole volume tibia data were used even though flow rates were specific to the diaphyseal cortex.

Kelly (1973) extended the washout technique to include the marrow. He concluded that the marrow had the same flow rate to partition coefficient ratio as cortical bone because their relative count rates were always similar. He calculated the marrow flow rate $F_{s/M}$ thus,

$$F_{s/M} = \frac{\lambda_{I-Ap/M}}{\lambda_{I-Ap/Co}} \cdot F_{s/Co}$$

$\lambda_{I-Ap/Co}$ (mean $\pm$ s.d.) was found to be 0.62 $\pm$ 0.16 producing $F_{s/M}$ = 0.063 ml/ml

marrow per minute.

To conclude, obtaining flow rates in the diaphysis by the washout of diffusible tracers is very difficult to accomplish. The major problem is interpreting the sources of radiation to the external detector. Additional sources of radiation that could cause interpretation difficulties, other than the mentioned local cortical regions are underlying cortex beneath the marrow, and soft tissue surrounding the bone in general. A further problem to be encountered is recirculation because I-Ap is not completely extractable. Also, difficulties arise in defining the location to place the external detector ; a range of different flow rate measurements could well be obtained simply because there may be flow rate heterogeneity in different regions of the diaphysis.

4.1.3. Indicator fractionation

This technique, which was introduced by Sapirstein (1958), assumes that blood flow rates in all the organs of the body can be determined by cardiac output measurements and the fractions of tracer removed in one passage. Ideally, this technique is only suitable if tracers that are completely extractable and rapidly retained by organs can be used.

Sapirstein (1958) found following intravenous injections of ^{42}K and ^{86}Rb, that these tracers were not completely extractable and recirculated in the bodies of rats and dogs. However, he found that in most organs with the exception of the brain, after killing these animals at various times following injection, the tracer contents were very similar. He concluded from these findings that with the exception of the brain, all organs had extraction ratios for ^{42}K and ^{86}Rb equal to that of the whole body. The equivalence of the extraction ratios of ^{42}K and ^{86}Rb suggested that blood flow rates in the major organs could be

determined ; Kane and Grim (1969) infact extended this technique to hind-limb bone, muscle and skin blood flow studies. However fallibilities to the technique for determining flow rates arise as a consequence of great degrees of variability in back diffusion and recirculation of tracer amongst the organs.

A much more suitable method concerning indicator fractionation is the use of radioactive particles of such a size that they lodge in blood vessels of interest. The technique is well established for many organs and was first described for use in bone by Kane and Grim (1969) in which they used glass microspheres labelled with ^{24}Na.

Bone blood flow measurements using the microsphere technique

Important assumptions involved in the application of the microsphere technique to measure bone blood flow rates after Gross *et al* (1981) and Tothill (1984) are :-

1. the microspheres must mix adequately with arterial blood so that streaming in large arteries does not occur.

2. the microspheres must lodge in one pass through the bone so that shunting of the microspheres through arteriovenous anastomoses does not lead to an underestimation of bone blood flow rates.

3. the microspheres should not cause significant haemodynamic effects i.e. they should not obstruct normal microvascular circulation to the extent that vasomotor responsiveness is altered.

4. the rheological characteristics of the microspheres must not lead to artefactual distortion of regional blood flow rates within the bone.

5. there must be sufficient numbers of microspheres to satisfy statistical considerations.

To satisfy assumption 1., it is usual to inject the microspheres into the left ventricle or left atrium such that the turbulence in the blood mixes them adequately. It has been shown that 15 µm diameter microspheres are of a suitable size for lodging in capillary beds and since microspheres can be labelled with several gamma emitting isotopes such as ^{57}Co, ^{113}Sn, ^{46}Sc, ^{85}Sr and ^{95}Nb which can be separated by differential spectroscopy, repeated measurements of blood flow rates are possible in one animal. Starting a few seconds prior to injection of the microspheres and continuing for 2-3 minutes thereafter, a reference sample of arterial blood is withdrawn at a known constant rate F_{SO} from an artery (surrogate organ SO). At the end of the experiment, the animal is killed and the bones are removed and prepared for counting. The bone blood flow rate F_{Bo} is determined by the equation

$$F_{Bo} = (F_{SO} . C_{Bo}^{*}) / C_{SO}^{*}$$

where C_{Bo}^{*} and C_{SO}^{*} are microsphere counts for a desired period of time in the bone of interest and the surrogate organ respectively. The accuracy of the bone blood flow measurement is dependent on the number of microspheres trapped in the bone and in the blood of the surrogate organ.

4.1.4. Conclusions :- synopsis of bone blood flow measurements

The microsphere technique is the best means of obtaining bone blood flow measurements as compared to the other methods because it is by far the least problematic. The clearance technique in determining bone blood flow measurements is difficult in practice because there do not appear to be any

tracers that meet the requirements of being completely extractable and being able to rapidly bind to bone to minimize back diffusion. These factors additionally apply to tracers used in indicator fractionation techniques. Determining bone blood flow rates by washout of diffusible tracers is probably the most problematic technique of them all. The major difficulty to be encountered with this technique is in the precise interpretation of the gamma rays emanating from the tracer within the bone to the external detector.

TABLE 4-1

Specific flow (ml/min.100 g^{-1}) in the mature canine tibia reported by different authors.

Authors		Regions of the tibia				
		Proximal	Central	Distal	Marrow	WB
Okubo et al.(1979)	(1)	10.6-15.5	3.0	9.4-12.0	-	-
Morris & Kelly (1980)	(2)	11.4	2.3	9.9	7.4	7.8
Schnitzer et al.(1982)	(3)	7.0-14.0	2.0	5.0-12.0	7.0	5.2
Tothill et al.(1987)	(4)	11.0	3.5	7.0	9.0	5.0

Notes ---

WB :- Whole bone
(1) :- Multiple slices through bone ends.
(2) :- 3 equal lengths of bone.
(3) :- Many samples from core & outside of bones.
(4) :- 4 equal lengths of bone, centre 2 combined.

Bearing in mind, the parallel independent nature of the microvasculature in the diaphyseal cortex and marrow, and the metaphyseal and epiphyseal arteries supplying the extremities of bone, table 4-1 illustrates specific blood flow rates in the canine tibia found by various authors using the microsphere technique. There are reasonable agreements in flow rate findings for various regions of the canine tibia between different investigators emphasizing the accuracy and usefulness of the microsphere technique. It can be seen that central regions of the tibia corresponding largely to the diaphyseal cortex have much lower

specific flow rates than the diaphyseal marrow regions. Additionally, blood flow rates to the proximal and distal extremities are much larger in comparison.

4.2. EXPERIMENTAL PROCEDURES

4.2.1. Introduction

Relative distributions of blood flow in regions of the canine tibial diaphysis was investigated for the benefit of modelling tracer uptake. The investigation was carried out using the microsphere technique which has been used to assess regional blood flow distributions in other organs such as the heart (Yipintsoi *et al* 1973). In establishing an experimental protocol, important considerations mainly relating to statistical accuracies of the technique had to be realized.

Firstly, it was found that the proportion of cardiac output supplying the individual tibia in greyhounds was very small, at around 0.16% (Tothill *et al* 1987). This effectively meant that if one million microspheres were injected into the left sides of greyhound hearts, then only 1600 microspheres were likely to be trapped in each tibia. A figure such as 1600 microspheres for the whole tibia was considered much too small to carry out detailed regional distribution of microsphere studies by way of sectioning up the tibia.

The variability of the distribution of microspheres to organs such as the tibia infact approximates a Poisson distribution with the standard deviation being the square root of the number of trapped microspheres. Furthermore, Buckberg *et al* (1971) calculated that for the measurement errors to be within 10% at the 95% confidence levels, a minimum of 384 microspheres must be contained in tissue samples. Consequently, many investigators measuring organ blood flow rates tended to become aware of Buckberg's calculations and ensured that, following expensive large dosage injections of microspheres the minimum sample content of microspheres was around 400. However, it is not essential to satisfy these requirements because perfectly reasonable but less precise

blood flow rate measurements can be obtained in samples containing much fewer microspheres. Generally, measurements can be successfully obtained on samples that contain any number of microspheres no matter how large or small, as long as one is aware of and can interpret the errors that are involved. Earlier investigators using very large microsphere dosages may perhaps have affected the normal vasculature-microvasculature state of their experimental animals.

Another important experimental consideration was resolution - deciding on the sample sizes and the number of samples required for the assessment of diaphyseal blood flow. A compromise had to be obtained between high resolution (many samples) and statistical measurement accuracies involving the number of microspheres within the samples. The question of resolution is important, as highlighted by blood flow studies in the heart where Yipintsoi *et al* (1973) using greater numbers of smaller sized samples obtained different flow distributions to that of Domenech *et al* (1969).

To ensure that reasonable numbers of microspheres would lodge in regions of the canine tibia and to avoid the expense of large dosages, it was decided that the femoral artery would be an appropriate location to inject the microspheres. It was assumed that there would be sufficient turbulence in the femoral artery blood flow to ensure adequate mixing. It was further decided to inject two differently labelled 15 μm microspheres pre and post-ligation of the tibial nutrient artery to assess this artery's contribution to regional tibial flow. As far as resolution was concerned, identifiable bone and marrow samples from the whole tibia that would suitably fit into tubes for counting in an automatic gamma ray sample counter were obtained. Cortical samples were approximately 1 cm in length and of mass 0.5-1.0 g ; marrow samples were typically of mass 0.2-0.7 g. Any problems associated with low sample counts

owing to low numbers of microspheres could be alleviated by combining adjacent samples in the analysis.

4.2.2. The experimental model

The distribution of blood flow in the canine tibial diaphysis was investigated using 3 mature greyhounds which were premedicated and anaesthetised as described in section 2.2.2. Once the greyhounds were anaesthetised, the tibial nutrient artery and the proximal femoral artery were exposed in both hind limbs. Two ties were then loosely placed around both tibial nutrient arteries for ligating these vessels when required. Cannulae were then carefully sutured to the femoral arteries for the injection of the microspheres. Syringes containing the microspheres were placed in an ultrasonic bath to ensure satisfactory mixing.

With the tibial nutrient artery intact, 1.5-3.0 ml of 10 mCi/g ^{113}Sn microspheres (New England Nuclear Corp.) suspended in 0.9% saline with 0.01% Tween-80 surfactant to prevent aggregation, were injected through the cannula into the femoral artery. The tibial nutrient artery was then ligated and 10 mCi/g ^{57}Co microspheres (New England Nuclear Corp.) also in a similar suspension were injected in a similar fashion. The whole procedure was repeated on the other hind limb of the greyhound. Numbers of microspheres associated with each injection were estimated to be between 1.5-2 million. Furthermore, microspheres were injected in the direction of the bloodstream in the first dog but in the opposite direction in the latter two dogs.

Following the injections of the microspheres in both hind limbs, the dogs were sacrificed and both tibiae were removed. The cannulae and syringes that had contained the microspheres were retained and used for assay with standards of

FIGURE 4-1
Sectioning up the
Tibial Diaphysis
(Stripped of Periosteum)

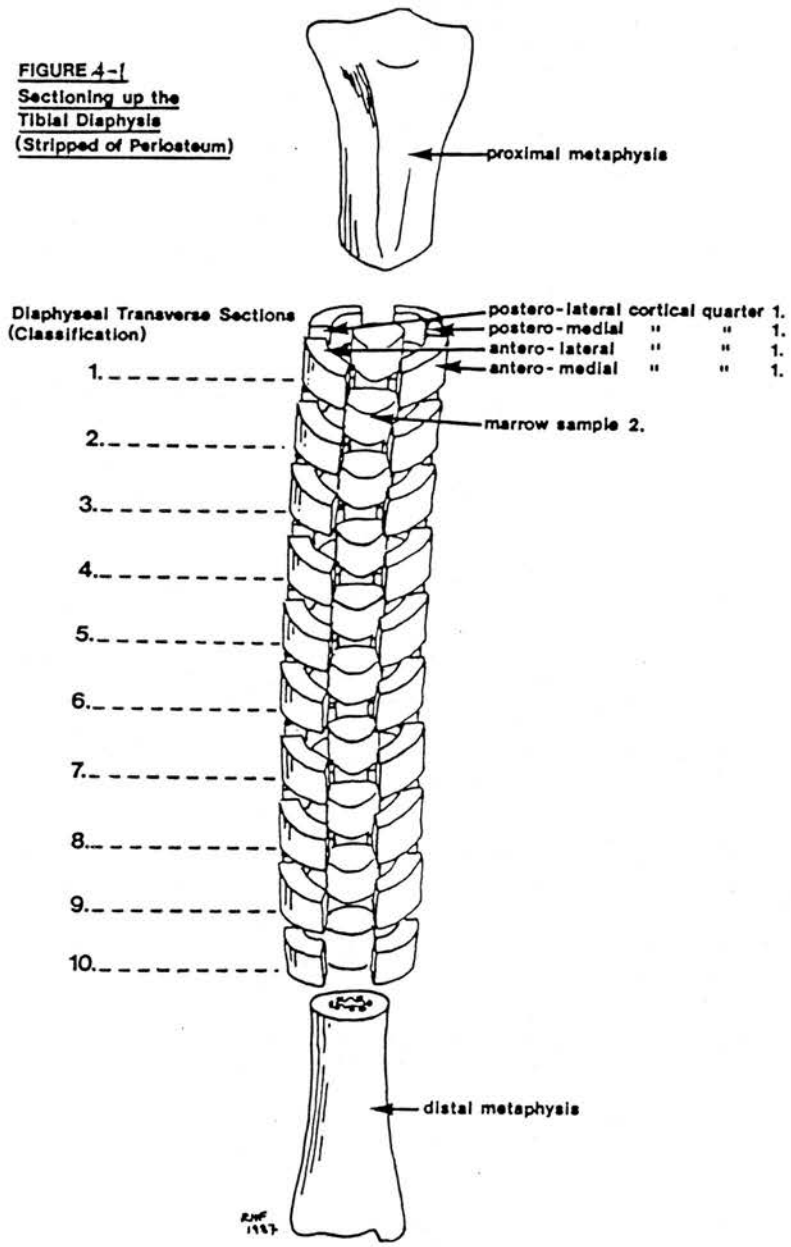

^{113}Sn and ^{57}Co. Count rates for the full syringes of microspheres containing these labels along with their standards had been determined using a scintillation detector prior to experimentation.

4.2.3. Preparation of the bone samples

Periosteum and articular cartilage were removed from all the tibiae using a scalpel and a periosteal elevator. The lengths of each tibiae were then measured and the tibiae were marked so that 4 equal length portions could be identified. The tibiae were then frozen so that fatty marrow could easily be removed from them. Once frozen, 10 equal length transverse sections as illustrated in figure 4-1 were obtained by the use of a hacksaw from the central 2 portions which constituted the diaphysis. The marrow was quickly removed from each of these 10 sections using a spatula, and placed in counting tubes whose mass had already been determined. The mass of the tubes containing the marrow was then obtained so that the mass of the marrow samples could be determined.

Each of the 10 diaphyseal transverse sections of cortex were further sawn into identifiable anatomical quarters as illustrated, using landmarks such as the anterior tuberosity and medial malleolus to assist in the identification. The masses of each of the 40 samples of cortex were determined and the samples were placed in counting tubes.

The two metaphyseal portions of the tibiae were also cut into 10 transverse sections of comparable width to the 10 diaphyseal sections. In these particular sections it was much too difficult to remove marrow because the sections largely contained cancellous bone. Nevertheless, the transverse sections of the metaphyses were systematically sawn up into small identifiable pieces, whose

masses were then determined. The pieces were placed in counting tubes and together with the other bone and marrow samples were counted for ^{113}Sn and ^{57}Co (microspheres) in a dual channel LKB Wallac automatic sample counter. Standards of ^{113}Sn and ^{57}Co were also counted so that the count rates of these isotopes in the samples could be related to count rates in the syringes and cannulae which were determined using a scintillation counter. It was appreciated that there was no significant attenuation of the detectable gamma irradiation from the microspheres within the bone and marrow samples (Gross *et al* 1979).

4.2.4. Measurements obtained from the bone samples

Percentage partitioning of tibial nutrient artery flow Pt to the cortex, Co and marrow, M.

$$Pt_{Co} = \left[\left(\frac{C_{Co}^{*}}{C_{Co}^{*} + C_{M}^{*}}\right)_{113_{Sn}}\right] \times 100 \qquad (4.1)$$

Equation (4.1) describes how Pt_{Co} can be determined using the ^{113}Sn microsphere activities in counts for both the diaphyseal cortex C_{Co}^{*} and marrow C_{M}^{*} with the nutrient artery intact. Pt_{M} for the diaphyseal marrow can be simply calculated thus

$$Pt_{M} = 100 - Pt_{Co} \qquad (4.2)$$

Percentages of total diaphyseal cortex Pc_{Co} and marrow Pc_{M} flow is supplied by the tibial nutrient artery

$$Pc_{Co} = \left\{ 1 - \left[\left(\frac{C_{Co}^{*}}{C_{In}^{*}} \right)_{57Co} \div \left(\frac{C_{Co}^{*}}{C_{In}^{*}} \right)_{113Sn} \right] \right\} \times 100 \qquad (4.3)$$

Pc_{Co} can be determined using equation (4.3) by knowing the activity proportions of the injected dosages of microspheres C_{In}^{*} in the diaphyseal cortex pre (^{113}Sn) and post-ligation (^{57}Co) of the tibial nutrient artery. Pt_{M} can be calculated similarly for diaphyseal marrow using the ^{113}Sn and ^{57}Co marrow activities.

Calculating deposition densities (d_i) and relative deposition densities (rd_i) for each of the samples

To assess the distributions of flow within structural areas of the tibia it is necessary to make measurements relating to the quantity of microspheres per unit mass. The microsphere quantity is directly related to the activity in counts of the particular labels, hence the following definition,

$$\text{deposition density of sample i } (d_i) = \frac{\text{sample i counts } (C_i^{*})}{\text{sample i mass } (g_i)} \qquad (4.4)$$

d_i can be rather a cumbersome quantity especially if large counting times are involved and so it is more beneficial to refer to samples in terms of relative deposition densities rd_i where,

$$\text{relative deposition density of sample i } (rd_i) = d_i / \left(\sum_{i=1}^{n} C_i^{*} / \sum_{i=1}^{n} g_i \right) \qquad (4.5)$$

in which n is the number of samples comprising the structure of interest.

Describing the distribution of relative deposition densities

To assess the distribution of relative deposition densities (blood flow rates) of microspheres within the tibia it is necessary to make relevant measurements concerning spread and peakedness. To achieve this, one can calculate orders (r) of moments (m), i.e.

$$m_r = \left(\sum_{i=1}^{n} g_i (rd_i - \overline{rd})^r\right) / \sum_{i=1}^{n} g_i \qquad (4.6)$$

where $\overline{rd}$ is the mean relative deposition density which is always unity and is calculated as such,

$$\overline{rd} = \left(\sum_{i=1}^{n} g_i rd_i\right) / \sum_{i=1}^{n} g_i \qquad (4.7)$$

If it had been possible to produce samples of exactly the same mass, then the g_i terms may have been omitted from equations (4.6) and (4.7).

From the numerical values of the moments describing the distribution, it is possible to calculate, as illustrated in Spiegel (1972)

$$\text{standard deviation (SD)} = m_2^{\frac{1}{2}} \qquad (4.8)$$

$$\text{percentage relative dispersion (R.D.)} = 100.SD/\overline{rd} = 100.SD \qquad (4.9)$$

$$\text{coefficient of skewness (SK)} = m_3/m_2^{3/2} \qquad (4.10)$$

$$\text{coefficient of kurtosis (KU)} = m_4/m_2^{2} \qquad (4.11)$$

The coefficient of skewness is a measure of the degree of asymmetry of the distribution ; if the distribution is perfectly symmetrical SK = 0. The coefficient of kurtosis (KU) is a measure of the degree of peakedness of the distribution ; for a normal Gaussian distribution KU = 3 (mesokurtic).

Frequency distributions of relative deposition densities

Such distributions can be constructed for regions of the tibia of interest by assigning suitable class intervals Δrd_j to categorize the rd_i values. It is usual to define

$$w_j = \left(\sum_{i=1}^{l} g_i\right) / \left(\Delta rd_j \cdot \sum_{i=1}^{n} g_i\right) \qquad (4.12)$$

where,

- $j = 1,\ldots,nc$ (nc = no. of classes)
- Δrd_j = class interval of jth class
- n = no. of samples comprising structure of interest
- l = no. of samples whose masses g_i corresponds to the rd_i values within the specified class interval
- w_j is the fractional mass per jth class interval width

Such frequency distributions have been constructed by Yipintsoi *et al* (1973) and King *et al* (1985) on microsphere data concerning the heart.

4.2.5. Cortical capillary density measurements

Further investigative work was carried out to measure capillary densities in similar regions of the diaphyseal cortex used to assess microsphere deposition. The purpose of performing these measurements was to examine if possible

FIGURE 4-2 : Sectioning up the canine tibial diaphysis (devoid of periosteum) for the purpose of obtaining transverse diaphyseal sections for capillary density studies.

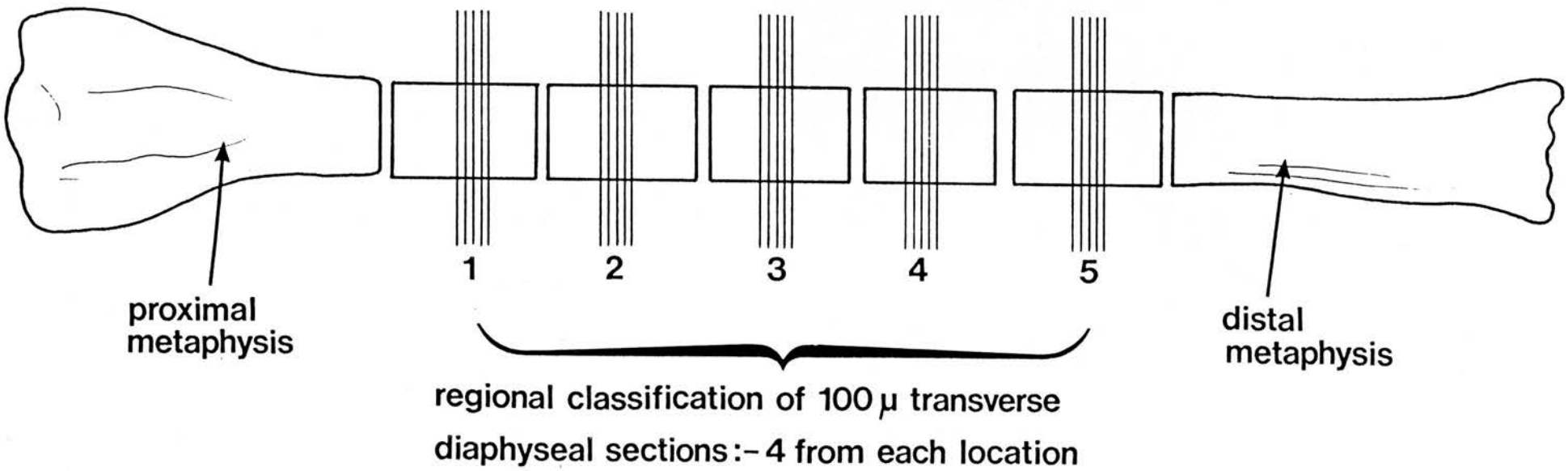

increases and decreases in microsphere deposition densities were attributable to corresponding changes in capillary density. Four tibiae obtained from four greyhounds following sacrifice in M.T.O.D. experiments were used, noting that in the third greyhound, micropaque, insoluble barium sulphate solution was infused into the tibia prior to sacrifice to assist in the identification of the capillaries.

Periosteum and articular cartilage were removed from all the tibiae using a scalpel and a periosteal elevator. The metaphyses of the tibiae corresponding to the outer portions in the microsphere tibiae preparations were discarded leaving a central diaphyseal portion as shown in figure 4-2. A line was scribed on the anterior surface of the diaphyseal portion so that subsequent sections could be identified. The diaphyseal portion was sawn transversely into 5 equal length pieces and the marrow was removed from each piece. Four 100 μm thick adjacent transverse sections were obtained from the centre of each of the 5 pieces by the use of an annular diamond edged saw. All the sections, proximal surface uppermost, were mounted on microscope slides for light microscopy studies.

Capillary density per cm^2 measurements for anatomical quarters in random regions midway between the periosteal and endosteal surfaces were made. These measurements were obtained by noting and counting the capillaries on a square grid via the use of a drawing tube attachment to the microscope.

TABLE 4-2

Deposition density ratios for regions of the canine tibia relative to the diaphyseal cortex set at unity and Pt_{Co}, Pt_{M}. Figures relate to microspheres that were injected pre-ligation of the tibial nutrient artery.
(* :- Upstream direction of injection into the femoral artery).

Dog (Tibia)	Proximal Metaphysis	Diaphyseal Cortex 1-10	Distal Metaphysis	Diaphyseal Marrow 1-10	Whole Tibia	Partitioning of tibial nutrient artery flow (%) Cortex Pt_{Co}	Marrow Pt_{M}	
#1(R)	19.97†	1	13.15†	29.07†	13.47†	15.13†	84.87†	
#1(L)	6.96†	1	1.84†	18.68†	5.02†	21.98†	78.02†	
#2(R) *	3.53	1	4.04	2.84	2.73	71.71	28.29	
#2(L) *	3.05	1	3.27	3.35	2.47	65.97	34.03	
#3(R) *	5.17	1	4.06	7.06	3.97	42.14	57.86	
#3(L) *	4.66	1	2.70	6.87	3.34	43.06	56.94	
Mean±s.d. % c.v (n=4)	4.10±0.98 23.91	1 -	3.52±0.66 18.69	5.03±2.25 44.64	3.13±0.67 21.41	55.72±15.33 27.52	44.28±15.33 34.63	(†:- results not used) (in the calculations)
Okubo et al. (1979)	3.53-5.17	1	3.13-4.00	-	-	-	-	:- Multiple slices through extremities, ratio ranges quoted at metaphyses
Morris & Kelly (1980)	4.96	1	4.30	3.22	3.37	64.11	35.89	:- 3 equal lengths
Schnitzer et al. (1982)	3.50-7.00	1	2.50-6.00	3.50	2.60	62.15	37.85	:- Many samples, ratio ranges quoted at metaphyses
Tothill et al. (1987)	3.14	1	2.00	2.57	1.43	69.08	30.92	:- 4 equal lengths; centre 2 combined
Mean±s.d. %c.v. (n=3)	- -	1 -	- -	3.10±0.48 15.41	2.47±0.98 39.60	65.11±3.57 5.49	34.89±3.57 10.24	

4.3. RESULTS

4.3.1. Blood flow contributions to bone and marrow

Table 4-2 shows microsphere deposition density ratios for regions of the canine tibia relative to the diaphyseal cortex set at unity. The specified regions relate to the way in which the tibia was sectioned up as shown in figure 4-1. Table 4-2 was constructed so that deposition density ratios could be directly compared with appropriate ratios of specific blood flow rate values found in comparable regions by other authors (see also table 4-1). The 6 sets of data in table 4-2 were obtained from the right (R) and left (L) tibiae of the 3 greyhounds.

The deposition density ratios for the diaphyseal marrow tend to be higher than calculated ratios obtained from other authors who injected microspheres into the hearts of dogs. These higher ratios may suggest that following the femoral artery injection, the microspheres were not thoroughly mixed up and have tended to clump slightly in the marrow microvasculature. Lower, more comparable ratios were obtained when the microspheres were injected in an upstream direction into the femoral artery, referring to the 4 sets of results denoted by asterisks in table 4-2. The mean, standard deviation (s.d.) and percentage coefficient of variation (% c.v.) of regional deposition density ratios were determined in 4 out of 6 tibiae. The results concerning both tibiae of dog #1 were ignored because it seemed evident that there had been a large amount of clumping of microspheres in the marrow microvasculature which were probably destined to be trapped in cortical capillary beds. Consequently the deposition density ratios for regions of these tibiae relative to the diaphyseal cortex were far higher than for the other sets of data. As far as the mean deposition density ratios were concerned, there was reasonable

TABLE 4-3

Distribution of microspheres in the canine tibia, pre [PRE] and post-ligation [POST] of the tibial nutrient artery (t.n.a.) and Pc_{Co}, Pc_M, femoral artery injection site. Figures are in terms of the percentage of the injected dosage. The figures in parentheses refer to estimates of no. microspheres/g for the specified regions.

Dog (Tibia)		Proximal Metaphysis		Diaphyseal Cortex 1-10		Distal Metaphysis		Diaphyseal Marrow 1-10		Whole Tibia		Calculated % of t.n.a contribution of flow Cortex Pc_{Co}	Marrow Pc_M
#1(R)	PRE	2.92	(639)	0.13	(32)	0.87	(421)	0.87	(930)	4.79	(431)	17.29 +	49.60 +
	POST	9.19	(1094)	0.11	(14)	2.54	(664)	0.44	(253)	12.28	(580)		
#1(L)	PRE	3.09	(612)	0.45	(88)	0.41	(163)	1.69	(1644)	5.64	(442)	73.73 +	80.52 +
	POST	5.48	(510)	0.12	(11)	0.57	(105)	0.32	(143)	6.49	(233)		
#2(R)	PRE	1.67	(357)	0.41	(101)	0.90	(408)	0.17	(287)	3.15	(276)	76.94	58.05
	POST	1.79	(373)	0.10	(23)	0.17	(73)	0.07	(118)	2.13	(179)		
#2(L)	PRE	1.18	(378)	0.39	(124)	0.75	(406)	0.20	(415)	2.52	(306)	50.26	27.59
	POST	1.76	(305)	0.19	(33)	0.62	(182)	0.15	(162)	2.72	(175)		
#3(R)	PRE	1.44	(279)	0.24	(54)	0.53	(219)	0.35	(381)	2.56	(214)	52.07	44.93
	POST	2.26	(385)	0.12	(23)	0.71	(259)	0.19	(185)	3.28	(228)		
#3(L)	PRE	2.26	(438)	0.36	(84)	0.62	(254)	0.50	(646)	3.74	(314)	68.70	54.53
	POST	1.97	(282)	0.11	(22)	0.42	(128)	0.23	(217)	2.73	(168)		
												61.99±12.97 (n=4)	46.28±13.64 (n=4)

+ :- results not used in the calculations of mean ± s.d. (Pc_{Co} & Pc_M)

R, L refer to right and left tibia of dog # no.

agreement with the calculated ratios obtained from other authors' data in the proximal and distal metaphyses and the tibia as a whole. Thus it would seem that injecting the microspheres into the femoral artery is a reasonable and viable procedure in carrying out detailed deposition density studies or even perhaps detailed regional blood flow studies in the tibia. However, marrow blood flow rate studies may seemingly be problematic as adjudged by the large % c.v. value associated with the mean and s.d. of the mean deposition density ratio. Furthermore, difficulties associated with varying degrees of microsphere entrapment in the marrow have affected the calculations of the partitioning of the nutrient artery flow in table 4-2. The calculated figure of Pt_M = 44.28% and associated % c.v. is much higher than figures deduced from other authors' data. The % c.v. figure associated with Pt_{Co} is also higher in comparison.

Table 4-3 illustrates percentages of the injected dosages of microspheres pre and post-ligation of the tibial nutrient artery in various regions of the tibia. With the tibial nutrient artery intact, 3.73 + 1.26 % (mean + s.d., n=6) of the microspheres injected into the femoral artery lodged in the whole tibia. This figure is about 20-25 times higher than what would have been achieved if the microspheres had been injected into the heart because the tibia in greyhounds has been found to be supplied by 0.16% of cardiac output (Tothill *et al* 1987). In general, the percentage figures cited in table 4-3 should be slightly higher owing to small quantities of microspheres being lost in bone dust and smidgins of marrow during sectioning of the samples.

The numbers of microspheres per g for the various regions of the tibia is also shown in parentheses in table 4-3, to give one an idea of the accuracy of the measurements. Although this quantity may appear small in some instances i.e. 11 microspheres/g (dog #1 ; left tibia post-ligation of tibial nutrient artery) for the diaphyseal cortex, the fact that the masses of these regions are substantial

such as the typical diaphyseal cortex (1-10) being approximately 35 g means that there are certainly enough microspheres to satisfy statistical considerations. It is worth further noting, that in a typical mature greyhound tibia (whole mass approximately 100 g), the masses of the regions so defined in figure 4-1 are ; proximal metaphysis≈35 g, distal metaphysis≈25 g and diaphyseal marrow≈5 g.

In making comparisons between the regional tibial percentages of the injected dosages of microspheres pre and post-ligation of the tibial nutrient artery, the data concerning both tibiae of dog #1 have not been used. This is partly due to the suspected clumping of microspheres in the marrow (pre-ligation of the tibial nutrient artery) as can be appreciated in table 4-2. Furthermore, one can also appreciate from the data that the percentage of the injected dosage post-ligation of the tibial nutrient artery for the whole right tibia is much greater than that for the other sets of data. This is probably caused by an uneven mixing of microspheres which resulted in large disproportionate numbers of microspheres being directed into the metaphyseal arteries.

Paired student's t tests were carried out on the regional percentage dosage figures pre and post-ligation of the tibial nutrient artery with the null hypothesis being that such a ligation caused no difference in the magnitudes of the distributions of microspheres. Omitting the data of dog #1 and using the remaining 4 sets, the only significant result was for the diaphyseal cortex in which it was found that the percentage dosage of microspheres decreased following ligation of the tibial nutrient artery ($P< 0.02$, 3 d.f.). Although it was strongly suspected that the same was true for the diaphyseal marrow, the large variation in the data meant that significance could not be proved ($P<0.1$, 3 d.f. ; rejecting the null hypothesis at 5% level). However one can calculate, using equation (4.3) that the tibial nutrient artery percentage contribution to the

cortex and marrow flow (mean ± s.d., n=4) is 61.99 ± 12.97 and 46.28 ± 13.64 % respectively. A calculated coefficient of variation of 29% appertaining to the latter percentage concerning the marrow is low enough to suggest that the tibial nutrient artery contribution to marrow flow is substantial.

The total number of microspheres to be found in the whole tibia was found to be less than a calculated number based on the product of the tibial content (percentage of injected dosage) and the estimated number of microspheres injected. It was calculated that in a typical batch of 500 µCi (50 mg) ^{113}Sn or ^{57}Co microspheres evenly mixed in 20 ml of saline containing Tween-80, there would be approximately 1.125×10^6 microspheres per ml of suspension. By virtue of the fact that in typical circumstances, 75-80% of a syringe content of isotopes is injected into the bloodstream, meant that approximately 800,000 microspheres were attributed to every 1 ml of microsphere suspension injected. Thus, assuming a 100 g tibia in which 2.5-3.0% of an injected dosage containing 2 ml of microsphere suspension trapped in the whole tibia, then one would expect a figure of approximately 400 microspheres/g whole tibia. One can directly compare this finding to the whole tibia microspheres/g data of dog #3 in table 4-3, in which 2 ml quantities of the microsphere suspension were injected. For the intact tibia in which 2.56 and 3.74% of the injected dose of microspheres were trapped, the number of microspheres/g figures are much less than an estimated figure of 400/g.

The discrepancies in these figures stems right back to the time the microspheres were drawn up into syringes from their containers. Although the containers were well shaken at the time to mix up the microspheres, it seems very likely that the microspheres settled down very quickly in the bottom of their containers during the course of drawing them up into syringes. Table 4-4 shows the great variability in the number of microspheres injected into the

femoral artery blood stream for the stated quantities of the injected suspensions. In general, the actual numbers of microspheres injected into the femoral arteries were between 30-65% of the expected numbers.

TABLE 4-4

Numbers of microspheres (15 μm) injected into the femoral artery bloodstream ; approximate volume of injectate suspension (ml) in parentheses. t.n.a. - tibial nutrient artery, R,L - right, left limb.

Dog	Pre-ligation of t.n.a. ^{113}Sn microspheres	Post-ligation of t.n.a. ^{57}Co microspheres
#1R	789,000 (1.5)	430,000 (1.5)
#1L	658,000 (1.5)	311,000 (1.5)
#2R	746,000 (2.0)	728,000 (2.0)
#2L	1001,000 (3.0)	539,000 (2.0)
#3R	610,000 (2.0)	537,000 (2.0)
#3L	665,000 (2.0) .	490,000 (2.0)

4.3.2. Heterogeneity of blood flow rates in the diaphysis

Heterogeneity of blood flow rates in the cortex

In figure 4-3a, comparisons were made between the rd_i values of 40 corresponding samples of the left and right tibiae of greyhound #3. Also shown are comparisons between the 10 whole diaphyseal transverse sections. It can be seen that apart from 3 outliers, the vast majority of the data points are scattered around an identity line of gradient 1-1 which is constructed at 45° to each axis. This demonstrates that the numerical values of rd_i for each of the samples do actually represent to a reasonable extent the heterogeneity of blood flow rates in the cortex and are not too greatly impaired by measurement errors. If by chance the blood flow rates had been homogeneous

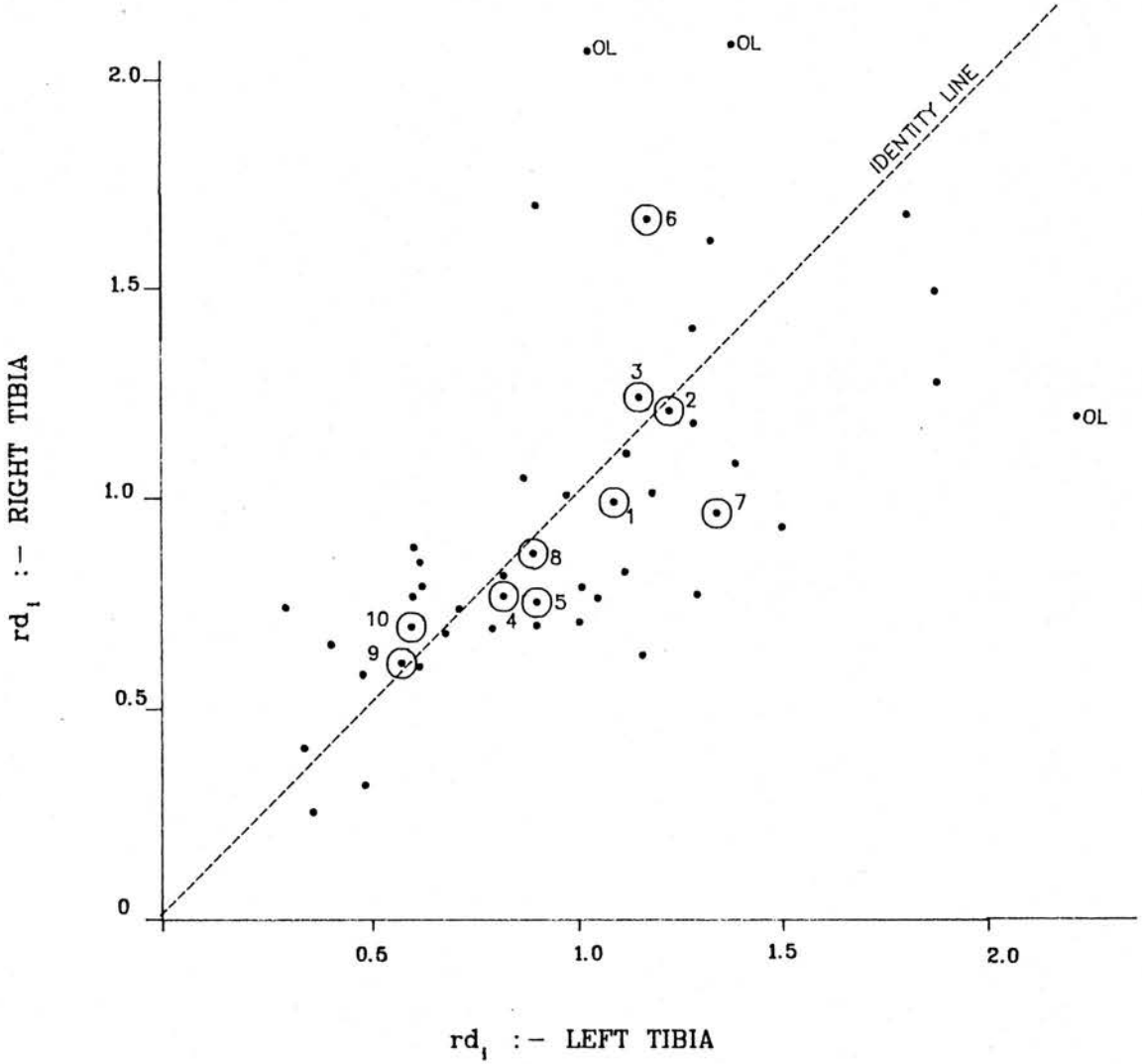

FIGURE 4-3a

Comparison of rd_i values in corresponding pieces of cortex of the left and right tibiae of dog #3.

• ANATOMICAL QUARTERS OF CORTEX (r=0.60)

⊙ WHOLE TRANSVERSE SECTION OF CORTEX (r=0.73)

OL :– OUTLIER

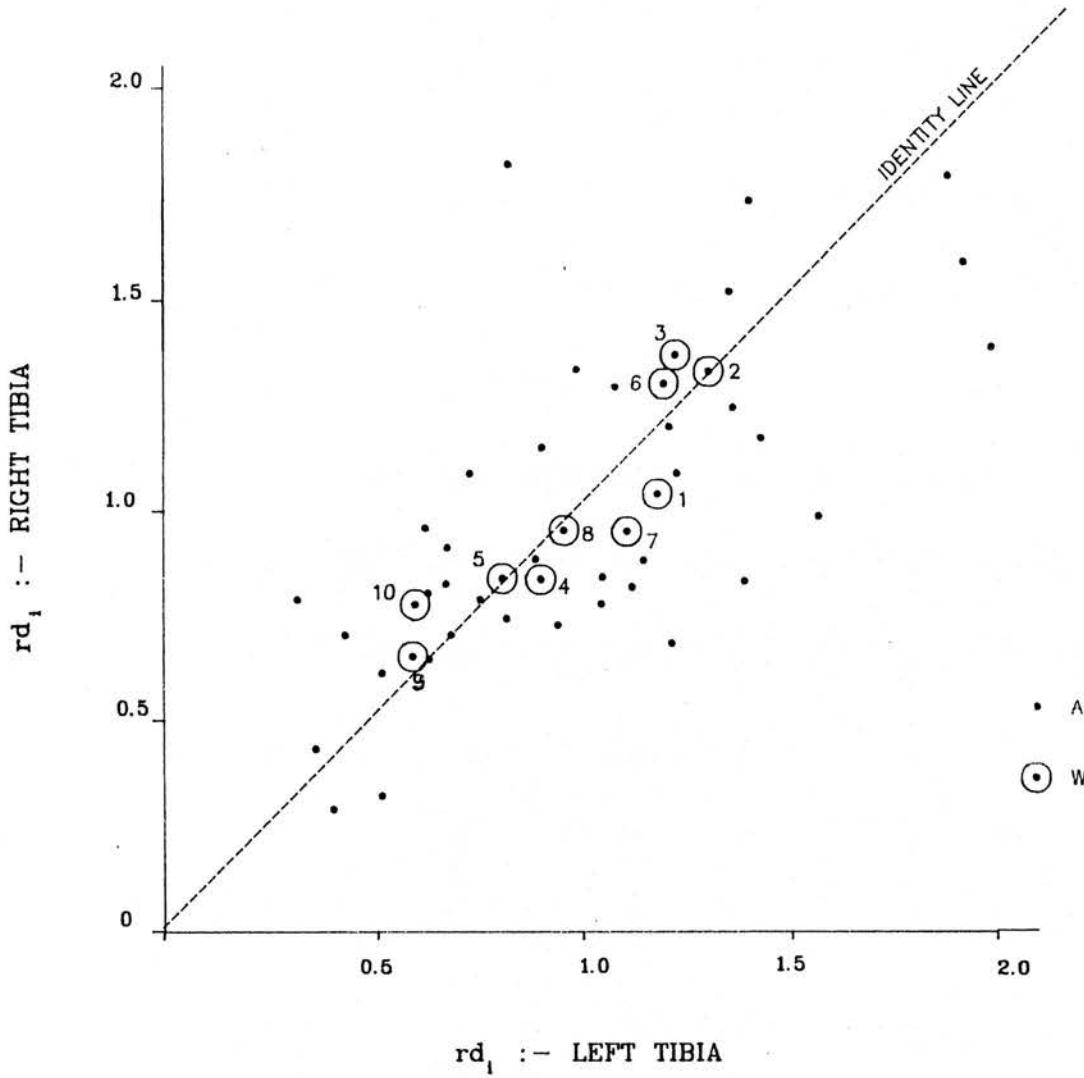

FIGURE 4-3b

Comparison of rd_1 values in corresponding pieces of cortex of the left and right tibiae of dog #3. (3 outliers removed).

throughout the cortex, then all of the rd_i values would have been equal to or in the vicinity of unity for both tibiae, which is not the case. The correlation coefficient r=0.60 for the 40 samples of cortex is lower than such a coefficient r=0.73 for the 10 transverse diaphyseal sections because it is much more difficult to saw up and prepare the smaller sized samples such that corresponding samples from the left and right tibia are of the exact shape and mass. Additionally, the smaller sized samples have fewer microspheres which produces larger errors in the rd_i determinations.

Figure 4-3b illustrates comparisons between the rd_i values for both tibiae of greyhound #3 in a similar fashion to figure 4-3a, but with the main exception of excluding the 3 sample outliers from the analysis. These 3 samples were excluded because their rd_i values were higher than the others owing to suspected microsphere clumping, which is quite conceivable in small sized samples containing relatively low numbers of microspheres. Statistical tests for outliers were not used because the distribution of data was not symmetrical. Removing the outliers from the analysis, produced higher correlation coefficients r=0.69 and r=0.91 concerning the remaining 37 samples and subsequent 10 transverse sections between each tibia.

Similar findings were found for the tibiae of greyhound #1, where large degrees of microsphere clumping in the marrow were suspected. For the 40 samples of cortex and 10 transverse diaphyseal sections, it was found that r=0.45 and r=0.92 respectively, whereas after removing 3 outliers again with comparatively high rd_i values, the correlation coefficients for the remaining 37 samples of cortex and 10 transverse diaphyseal sections were higher at r=0.62 and r=0.92 respectively. However, in greyhound #2 there was no real agreement or strong correlation between the rd_i values of corresponding regions of tibiae. Even after removing 1 outlier, correlation coefficients were

much lower at r=0.25 (39 cortical samples) and r=0.04 (10 transverse sections).

TABLE 4-5

Statistical descriptions of distributions of rd_i values for cortex :- neglecting outliers (40/40).

	Moments						
Dog	m_1	m_2	m_3	m_4	SK	KU	SD
#1R	1.30×10^{-6}	0.39	4.65×10^{-1}	1.12	1.91	7.33	0.63
#1L	1.38×10^{-6}	0.35	3.58×10^{-1}	0.79	1.72	6.41	0.59
#2R	-5.10×10^{-7}	0.22	7.03×10^{-2}	0.14	0.70	2.95	0.46
#2L	1.60×10^{-6}	0.12	2.69×10^{-2}	0.04	0.65	2.78	0.35
#3R	9.36×10^{-7}	0.17	5.78×10^{-2}	0.10	0.82	3.37	0.41
#3L	-5.45×10^{-7}	0.20	6.51×10^{-2}	0.14	0.74	3.43	0.45
mean ± s.d.					1.09±	4.38±	0.48±
(n=6)					0.57	1.97	0.11
% c.v.					52.01	44.90	22.33

TABLE 4-6

Statistical descriptions of distributions of rd_i values for cortex :- allowing for and removing outliers of number OL.

		Moments						
Dog	OL 40	m_1	m_2	m_3	m_4	SK	KU	SD
#1R	6	3.60×10^{-7}	0.15	0.033	0.055	0.58	2.50	0.39
#1L	3	6.81×10^{-7}	0.23	0.113	0.173	0.99	3.16	0.48
#2R	1	5.97×10^{-7}	0.19	0.037	0.082	0.45	2.30	0.43
#2L	1	5.31×10^{-7}	0.12	0.026	0.040	0.61	2.71	0.35
#3R	3	2.56×10^{-6}	0.14	0.024	0.050	0.49	2.72	0.37
#3L	3	9.12×10^{-7}	0.18	0.041	0.091	0.52	2.76	0.43
mean ± s.d						0.61±	2.69±	0.41±
(n=6)						0.20	0.29	0.05
% c.v.						32.43	10.67	12.25
All 6 tibiae (OL=17 from 240 samples)								
		9.46×10^{-7}	0.17	0.050	0.083	0.67	2.91	0.41

Tables 4-5 and 4-6 provide statistical descriptions of the distributions of the rd_i values for each of the 6 tibiae. In table 4-5, the statistical descriptions refer to all the samples of bone, whereas in table 4-6 the descriptions refer to samples in which outliers have been discarded. A further 3 samples other than the 3 aforementioned sample outliers from the right tibia of greyhound #1 were omitted from the analysis because the microspheres to be found in each of them were less than ten in number. Most of the samples which ranged from about 0.5-1.0 g in mass were considered to contain sufficient numbers of microspheres for statistical purposes. It can be appreciated from tables 4-5 and 4-6 that the coefficients of variation associated with skewness, kurtosis and standard deviation for all 6 tibiae are considerably less when outliers are removed from the analysis. From table 4-6, it can be seen that the distributions of rd_i values for each tibia are positively skewed with a relative dispersion (equation (4.9)) of around 40%.

As the numbers of microspheres in the samples were small, statistical investigations were carried to assess what proportions of the observed total variance σ_{Ob}^2 of the distribution of rd_i values were attributable to true flow rate heterogeneity σ_{Het}^2 and the variance associated with the microsphere method of measurement σ_M^2. Firstly, approximate estimates for σ_M^2 were obtained for n cortical bone samples of mass g_i using the following formula,

$$\sigma_M^2 = \left[\frac{\sum_{i=1}^{n} \left\{ g_i \cdot \left(\frac{g_{Co}}{g_i \cdot n_{ms/Co}} \right)^{1/3} \right\}}{\sum_{i=1}^{n} g_i} \right]^2 \qquad (4.13)$$

Equation (4.13) was obtained by assuming that the microspheres were uniformly distributed throughout the cortex with $n_{ms/Co}$ being the total number

of microspheres in the whole of the diaphyseal cortex of mass g_{Co}. By virtue of the fact that microsphere statistics are based on the Poisson distribution with the standard deviation being the square root of the number of trapped microspheres, the square root term in equation (4.13) is the coefficient of variation associated with measurement for each of the samples. The additional g_i terms in equation (4.13) are required because the sample masses are variable.

More realistic estimates though were obtained for σ_M^2 for the samples by using 2 NAG routines G05CCF and G05DDF to produce a non-repeatable Gaussian distribution of random numbers representing numbers of microspheres. By again assuming that the microspheres were uniformly distributed throughout the cortex, numbers of microspheres $\bar{n}_{ms_i}$ and their associated standard deviations $\bar{n}_{ms_i}^{1/2}$ were calculated for each of the bone samples using sample masses. These two quantities for each of the bone samples were used as inputs to the NAG routines which consequently produced new numbers of microspheres $\bar{n}_{ms_i}'$ associated with the bone samples. The NAG routines were used a total of five times and average $\bar{n}_{ms_i}'$ values for each of the bone samples were obtained for each tibia. For these $\bar{n}_{ms_i}'$ values, new relative deposition density distributions associated with the method of measurement were obtained. For ease of explanation, the statistical description of these distributions is referred to as CASE 1.

The whole procedure using the NAG routines was repeated on the experimental microsphere data using actual numbers of microspheres per bone sample n_{ms_i} and associated standard deviations $n_{ms_i}^{1/2}$ as input. The purpose of these actions were to examine and compare the descriptions of the subsequent distributions, in particular the variance ; these descriptions are referred to as CASE 2.

TABLE 4-7

Statistical descriptions of experimental and simulated distributions of relative deposition densities.

Dog	OL/40	SKEWNESS Ob	SKEWNESS CASE 1	SKEWNESS CASE 2	KURTOSIS Ob	KURTOSIS CASE 1	KURTOSIS CASE 2	VARIANCE Ob	VARIANCE CASE 1	σ^{-2} (4.13)	Ob+CASE 1	CASE 2	:- HETEROGENEITY (%) $\{1 - \frac{\text{CASE 1}}{\text{Ob}}\} \times 100$
#1(R)	6	0.576	-5.4×10^{-2}	0.598	2.500	2.762	3.068	0.149	4.1×10^{-2}	4.7×10^{-2}	0.191	0.214	72.15
#1(L)	3	0.993	-9.0×10^{-3}	0.903	3.160	4.380	3.085	0.234	1.7×10^{-2}	1.7×10^{-2}	0.251	0.247	92.82
#2(R)	1	0.453	-7.2×10^{-2}	0.406	2.303	2.926	2.451	0.188	1.4×10^{-2}	1.6×10^{-2}	0.202	0.200	92.50
#2(L)	1	0.607	-0.273	0.514	2.714	3.098	2.686	0.121	1.1×10^{-2}	1.1×10^{-2}	0.132	0.128	90.74
#3(R)	3	0.491	-5.0×10^{-2}	0.614	2.723	3.315	3.321	0.135	3.1×10^{-2}	3.3×10^{-2}	0.166	0.165	77.26
#3(L)	3	0.524	4.3×10^{-2}	0.565	2.757	3.321	2.886	0.181	1.8×10^{-2}	2.0×10^{-2}	0.199	0.194	90.33
Mean± s.d. (n=6)			$(-6.91\pm 10.80) \times 10^{-2}$			3.300 ± 0.572		0.168 ± 0.041	$(2.20\pm 1.17) \times 10^{-2}$	$(2.39\pm 1.32) \times 10^{-2}$	0.190 ± 0.040	0.191 ± 0.041	85.97 ± 8.92

Abbreviations

Ob:- Observed (experimental) distribution of rd_i values.

CASE 1:- Distribution of rd_i values associated with variances in method of measurement.

CASE 2:- Distribution of observed distribution of rd_i values with added variance associated with method of measurement.

(4.13):- Variance $\sigma^{-2}M$ calculated using equation (4.13).

Table 4-7 provides statistical descriptions of the observed distribution of rd_i values and of distributions concerning CASES 1 and 2. For CASE 1, the low magnitudes obtained for the coefficients of skewness, and the coefficients of kurtosis being around 3.3 meant that the distributions were almost Gaussian in shape. The variances associated with CASE 1 were not too dissimilar from variances obtained from equation (4.13), being slightly less in most instances. The reason for this, is that for CASE 1, numbers of microspheres were generated from a Gaussian distribution in which 63% of them would lie within 1 standard deviation of the mean. The most important finding however from table 4-7 was that $\sigma_{Ob}^2 + \sigma_{CASE\ 1}^2 \approx \sigma_{CASE\ 2}^2$. The implication of this finding was that one could readily assume that

$$\sigma_{Obs}^2 \approx \sigma_{Het}^2 + \sigma_{CASE\ 1}^2 \qquad \underline{or}$$

$$\sigma_{Obs}^2 \approx \sigma_{Het}^2 + \sigma_{M}^2 \qquad (4.14)$$

i.e. the factors contributing to the observed variance were proved to be independent of one another. Thus it was possible, as illustrated in the final column of table 4-7 to obtain the percentage of the observed distribution which was attributable to true flow rate heterogeneity. This percentage (mean $\pm$ s.d.) for the 6 tibiae which was found to be 85.97 $\pm$ 8.92 % was considered to be very substantial. The lower percentage figures were associated with bones which had the lowest average number of microspheres/g cortical mass ratios and *vice versa* (see also table 4-3).

Frequency distributions of the observed (experimental) rd_i values for the cortex of each of the tibiae and for the tibiae combined were obtained using equation (4.12). These distributions as illustrated in figure 4-4 were obtained using 4 suitable class intervals Δrd_j of such a size as to cover the entire range of rd_i

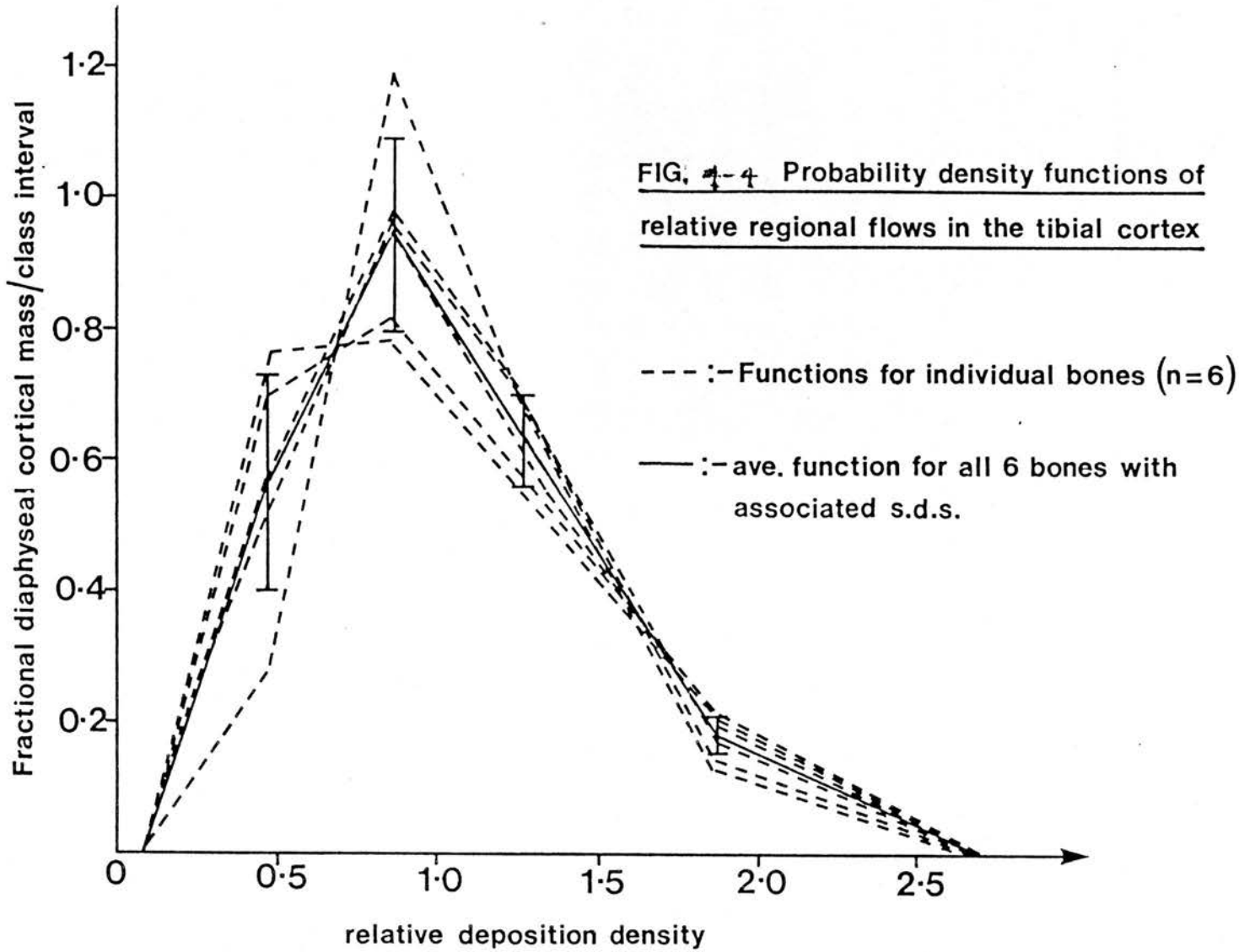

FIG. 4-4 Probability density functions of relative regional flows in the tibial cortex

- - - :- Functions for individual bones (n=6)

—— :- ave. function for all 6 bones with associated s.d.s.

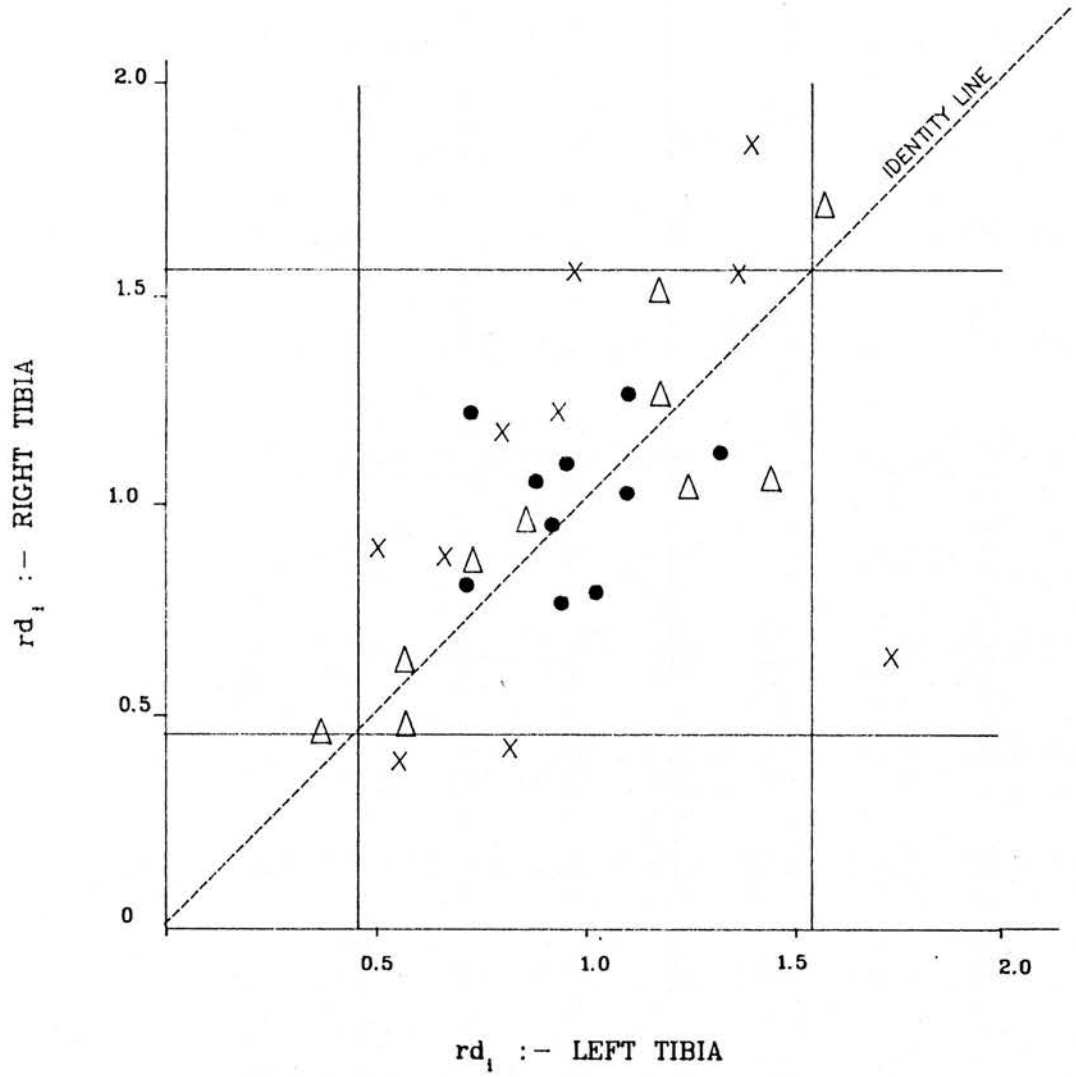

FIGURE 4-5

Comparison of rd_i values in corresponding marrow samples of the left and right tibiae of the same dogs.

CORRELATION COEFFS:

- ● DOG # 1 :- r = 0.12 (n=10)
- X DOG #2 :- r = 0.43 (n=10)
  = 0.83 (n=9)
- Δ DOG # 3 :- r = 0.88 (n=10)

values for all six tibiae and to ensure that reasonable numbers of samples were alloted to each class interval.

One can appreciate from figure 4-4, that the distributions are positively skewed and are not too dissimilar to each other.

Heterogeneity of blood flow rates in the marrow

In figure 4-5, comparisons were made between the rd_i values of 10 corresponding diaphyseal marrow samples in the left and right tibiae of all 3 greyhounds. Apart from greyhound #1 where it was suspected that there was clumping of microspheres in the marrow, there are reasonable scatters of data points along the identity line demonstrating heterogeneities of blood flow rates in the marrow. For greyhound #2, a much higher correlation coefficient was obtained when 1 outlier of a comparatively high rd_i value was removed from the analysis restricting attention to 9 marrow samples. Typical marrow sample masses were 0.2-0.7g and using the figures in table 4-3 relating to the number of microspheres /g for the whole of the diaphyseal marrow, it was certainly believed that there was enough microspheres in the samples to satisfy statistical considerations.

Statistical descriptions of the rd_i values for the marrow samples for each tibia are shown in table 4-8, where it can be seen that the percentage coefficients of variation (% c.v.) associated with measures of skewness, kurtosis and standard deviation in 4 tibiae (excluding the results from dog #1) tend to be higher than for such values for the cortex. This is particularly the case for the coefficient of skewness, where % c.v. was 113.88% owing to 1 out of the 4 distributions being negatively skewed with the remainder being positively skewed.

TABLE 4-8

Statistical descriptions of distributions of rd_i values for marrow (n=10).

Dog	SK	KU	SD	
#1R	-8.29×10^{-2} *	1.79 *	0.17 *	
#1L	1.64×10^{-1} *	2.29 *	0.19 *	
#2R	3.52×10^{-1}	1.84	0.49	
#2L	5.26×10^{-1}	2.08	0.37	
#3R	2.87×10^{-1}	2.06	0.40	
#3L	-1.52×10^{-1}	1.64	0.39	
mean ± s.d. (n=4)	$(2.53 \pm 2.88) \times 10^{-1}$	1.91± 0.21	0.41± 0.05	(* results not used in the calculations)
% c.v.	113.88	10.92	12.39	

4.3.3. Cortical capillary density measurements

Preliminary calculations

The capillaries were counted in a 150x150 mm area of graph paper. Calculations were performed to find the actual area that was observed.

For a 10x eye piece and 10x objective which were used, the following information was known,

1 division (eye piece graticule) was equivalent to a true distance of 11.9×10^{-4} cm.

20 divisions were equivalent to an apparent distance found on graph paper of 27 mm.

$\therefore$

Actual area studied = $\{150 \times (20/27) \times 11.9 \times 10^{-4}\}^2 = 1.748 \times 10^{-2}$ cm^2

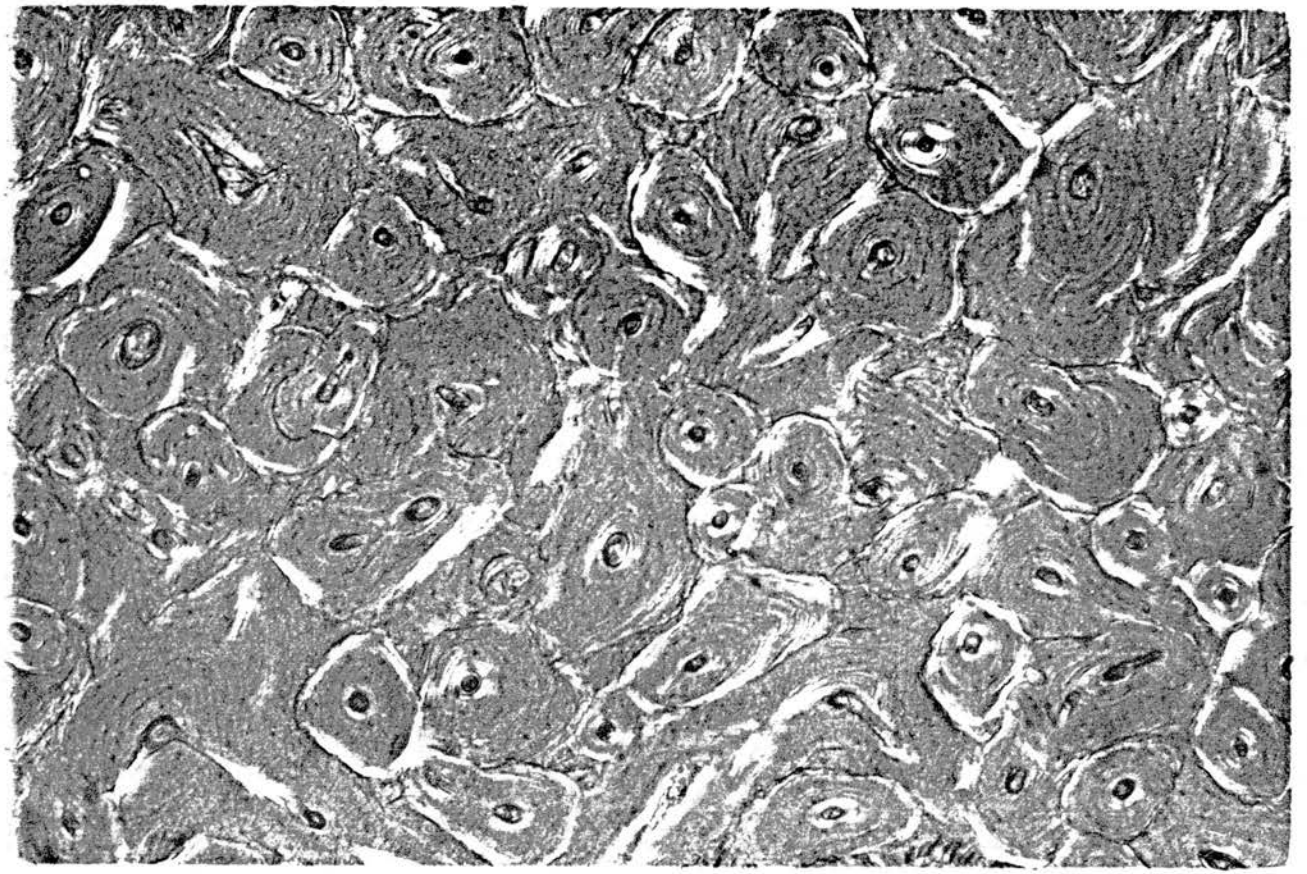

FIGURE 4-6 : Photograph of Haversian systems in a postero-lateral quarter of region 4 (dog 4). Most Haversian systems contain single capillaries.

hence,

$$\text{Capillary density } /cm^2 = \frac{\text{No. capillaries counted: Abbrev. NC}}{1.748 \times 10^{-2}}$$

$$= 57.20 \times NC$$

The vast majority of the capillaries counted were found in the Haversian systems of the cortical bone transverse sections, other capillaries being located in lamellar bone (see figure 4-6).

Results

Capillaries ranging around 45-50 were counted and converted to capillary density/cm^2 measurements. Table 4-9 illustrates these measurements for whole 100 µm transverse cross-sections for different regions of the tibial cortex in 4 greyhounds. The results in each column except where specified otherwise, represent means, s.d.s and percentage coefficients of variation for 12 measurements corresponding to 4 anatomical quarters multiplied by 3 adjacent local cross-sections. Although 4 such cross-sections in various regions were cut from the bones, only 3 were used in the studies ; the other cross-section was a safeguard in case of encountering problems in the preparation of microscope slides.

TABLE 4-9

Capillary density measurements /cm^2 for whole transverse cross-sections of diaphyseal cortex (n=12) ; region 1 is the most proximal. %c.v.s in parentheses.

	D	O		G
	1	2	3 Mp	4
Region				
1	2283 ± 414 (18.11)	3313 ± 435 (13.12)	2412 ± 251 (10.41)	2231 ± 301 (13.49)
2	2155 ± 257 (11.95)	3203 ± 397 (12.39)	2741 ± 305 (11.12)	2274 ± 299 (10.78)
3	2155 ± 145 (6.74)	3403 ± 340 (10.00)	2908 ± 317 (10.90)	2579 ± 213 (8.27)
4	2393 ± 473 (19.75)	3194 ± 399 (12.48)	2860 ± 154 (5.40)	2846 ± 264 (9.29)
5	2159 ± 290 (13.43)	3093 ± 362 (11.69)	2707 ± 328 (12.13)	2221 ± 192 (8.63)
All n=60	2229 ± 339 (15.19)	3241 ± 390 (12.02)	2726 ± 321 (11.77)	2530 ± 364 (14.38)

Using all 4 dogs (n=240)
Capillary density = 2682 ± 510/cm^2 ; %c.v. = 19.02

Mp :- Micropaque infused into capillaries.

From the results there seems to be only small amounts of variation in the capillary density measurements of the anatomical quarters comprising the whole transverse cortical cross-sections. This applies to all 5 transverse regions and to each of the dogs. However, there is more variation when one examines the capillary density measurements based on all 60 locations in each tibia for all 4 dogs ; dog 2 has generally much higher capillary density measurements than dog 1. Combining all the measurements for all 4 dogs produces a capillary density figure (mean ± s.d., n=240) of 2682 ± 510 /cm^2 with a percentage coefficient of variation (% c.v.) value of 19.02 %. It is worth

further noting that the small magnitudes of the percentage coefficients of variation for each region infact approximates to measurement errors if the 45-50 capillaries that were typically counted approximate to a Poisson distribution. It is most possible that lower percentage coefficients of variation may have been obtained if more capillaries had been counted per region.

TABLE 4-10

Capillary density measurements /cm^2 for specific anatomical quarters from all the regional cross-sections (n=15) ; %c.v.s in parentheses.

	D	O		G
	1	2	3 Mp	4
Anatom. quarter				
Antero-lateral	2216 ± 315 (14.22)	2997 ± 332 (11.08)	2631 ± 280 (10.65)	2566 ± 348 (13.55)
Antero-medial	2155 ± 208 (9.66)	3161 ± 270 (8.55)	2593 ± 440 (16.96)	2505 ± 254 (10.14)
Postero-lateral	2349 ± 443 (18.85)	3329 ± 423 (12.71)	2837 ± 234 (8.24)	2452 ± 333 (13.60)
Postero-medial	2197 ± 349 (15.90)	3478 ± 372 (10.68)	2841 ± 226 (7.97)	2597 ± 498 (19.16)

Mp :- Micropaque infused into capillaries.

Table 4-10 illustrates capillary density measurements for specific anatomical quarters from all the regional transverse sections for the tibiae of all 4 dogs. The results in each column represent means, s.d.s and %c.v.s for 15 measurements corresponding to specific anatomical quarters per region multiplied by the 5 regions for each tibia. From the results there appears to be very little variation in the capillary density measurements of the specific anatomical quarters comprising each tibiae, although there may be a slight tendency for capillary densities in posterior portions of the cortex to be larger

than such densities in anterior portions.

The capillary density figure of 2682 / cm^2 seems reasonable in terms of magnitude when compared with the findings of Dallant *et al.* (1986). These investigators studied the microstructure of the medial aspect of the middle third of a human femur (male, 73 years). A figure of 1384 osteons / cm^2 was calculated from their data in which single capillaries were predominant in each of the osteons. Bearing in mind, the cement line radius data between man and dog in table 1-1, it was calculated that osteons in man were approximately twice the size in terms of area as those in dogs. This meant that the capillary density figure of 2682 / cm^2 found for greyhounds that consisted largely of single capillaries in osteons was approximately twice the figure found for man which is reasonable in view of the relative sizes of the osteons.

4.3.4. Conclusions

The experimental model

For the purpose of investigating regional deposition densities of microspheres, it would seem that the femoral artery is a reasonable site for the injection of microspheres, particularly if they are injected upstream to assist with mixing. However, there still may be uncertainties about this site for determining specific bone blood flow rates in the tibia as adjudged by the high marrow deposition densities relative to the cortex ; more experiments should be carried out to try and validate this point.

It was very encouraging to find that following femoral artery injections, 20-25 times more microspheres would lodge in the tibia than would have done if they had been injected into the heart. The larger numbers of microspheres ensured

improved resolution in determining regional deposition densities.

Care however must be taken in estimating the numbers of trapped microspheres in organs such as the tibia. Past estimates based on the percentages of injected doses, may well have been spurious, because great variations in the numbers of microspheres drawn up into syringes was found. Estimates of trapped microspheres are best determined by evaluating the counts in the structure of interest and the counts per microsphere.

Tibial nutrient artery contribution to bone and marrow flow

The tibial nutrient artery percentage contribution to the cortex and marrow flow (mean $\pm$ s.d., n=4) was found to be 61.99 $\pm$ 12.97 % and 46.28 $\pm$ 13.64 % respectively. The figure for the cortex can only be compared with the findings of Tothill *et al.* (1987) whom obtained percentage cardiac output results for 4 equal length pieces of tibiae in 3 greyhounds pre and post-ligation of the tibial nutrient artery. In the 3 left tibiae, their data suggests that the nutrient artery contributes around 80% of total diaphyseal cortical flow. They also found however that in the 3 right tibiae in which the nutrient artery was left intact, the percentage cardiac output results for the whole tibiae for the second administration of microspheres was 25% less than those associated with the first administration of microspheres. Similar systematic decreases were also observed in the femora, humerii and radii as well as the tibiae in 5 greyhounds by Davies *et al.* (1984). These latter investigators also proved from sympathectomy studies that possible damage to the local nerve supplies associated with nutrient artery cannulations would not affect the bone blood flow results over short periods of time up to around 10 min, which is a useful finding in view of M.T.O.D. procedures.

From table 4-3, it would seem that the percentage of the injected dose in the proximal metaphysis actually increases after ligating the nutrient artery. Although there was no evidence of this in data from Tothill *et al.* (1987), the fact that Kelly *et al.* (1971) found that ^{85}Sr deposition was greater in tibiae with cannulated nutrient arteries as opposed to intact tibiae makes this finding seem reasonable. Furthermore, owing to the proximal metaphyseal region being about a third of the whole tibial mass it was found that if the subsequent increases were large enough then the whole tibial content of the percentage dose could increase as a consequence. This however, was never the case as adjudged by the data of Tothill *et al.* (1987). The whole tibial cardiac output figures always decreased after ligating the nutrient artery suggesting that only 30 % of the blood supply to the whole tibia was via the nutrient artery.

The discrepancies in the distributions of microspheres to the metaphyses of the tibia and the bone as a whole following nutrient artery ligation between Tothill *et al.* (1987) and myself may be due to the sites of injection. Clearly more investigative work is required in this area.

Heterogeneity of blood flow rates in the diaphysis and cortical capillary density measurements

The fact that there was evidence of similarities in corresponding cortical bone and marrow samples of the left and right tibiae in most greyhounds emphasized that true flow rate heterogeneity must exist. It was not possible though to attribute the flow rate heterogeneities to any particular regions of the diaphysis. However, the overall picture of blood flow rate heterogeneity appears quite similar for each of the tibial diaphyses, as can be appreciated by the statistical descriptive data and the reasonable degrees of similarity in the frequency distributions of the data.

By statistical simulations it was shown that the variances contributing to the total observed experimental variance were independent of each other. This enabled one to deduce that the variance associated with true flow rate heterogeneity was a very substantial part of the observed variance. This finding was very reassuring in the light of intending to use the observed distributions of rd_i values for purposes of modelling capillary blood flow rates.

From the light microscopy studies, very little variation was observed in the capillary density measurements corresponding to regions for the microsphere studies. This finding suggested that changes in the regional cortical blood flow rates were not attributable to corresponding changes in capillary density i.e. the cortical blood flow rates were truly heterogeneous. For the canine tibia a reasonable estimate for diaphyseal cortical capillary density was found to be $2682 \pm 510 / cm^2$.

CHAPTER 5

MULTICAPILLARY MODELS OF BLOOD-BONE EXCHANGE (SERIES III)

5.1. DEVELOPMENT OF A MULTICAPILLARY MODEL

5.1.1. Concepts of flow-limited & diffusion-limited exchange

From the previous chapter, one can appreciate that there are substantial heterogeneities of blood flow rates in diaphyseal bone capillaries. To illustrate how capillary flow rates may affect the exchange of diffusible tracers one can refer to figure 5-1, in which the clearance (C) i.e.

$$\text{Clearance } (C) = \text{Flow } (F_s) \times \text{Extraction } (E) \qquad (5.1)$$

may be defined as being the minimum volume of blood entering an organ per unit time which could supply the tracer removed per unit time during passage through the organ.

From figure 5-1, one can appreciate that the magnitude of the clearance of tracer tends to increase with convective flow velocity which can be thought of in terms of flow rate. The exchange behaviour of the tracers can suitably be described by 3 processes, which in reference to figure 5-1 relate to the regions described by the Roman numerals.

Region I :- Process of flow-limited exchange

If the flow or the velocity of blood within the capillaries is relatively low, then there is enough time for concentration gradients of tracer between blood and tissue to become dissipated. In this situation, local concentrations of tracer

FIGURE 5-1 : Relationship between the clearance of tracer and flow through a capillary-tissue region.

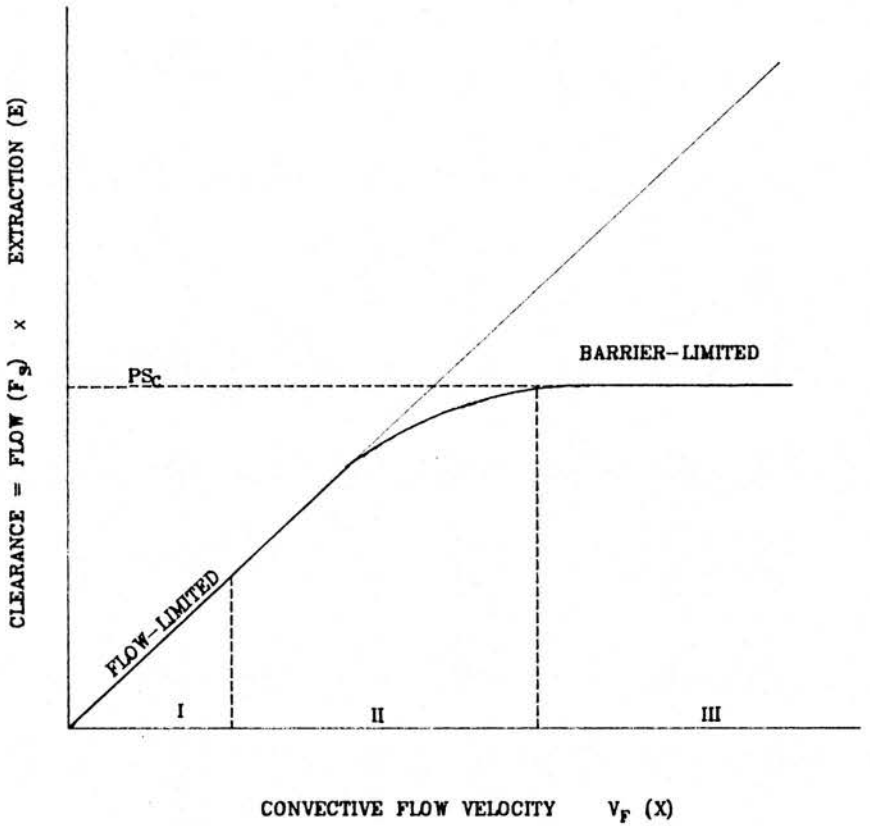

along the capillary approach or achieve equilibrium and the extent of exchange is governed by the flow itself. The extent of the exchange (clearance) tends to increase linearly in direct proportion to flow i.e. the capillary extraction value for the tracer is constant.

Region II :- Process of non-linear diffusion-limited exchange

In this situation, exchange rates are lower than the limit imposed by flow (the sloping line) or by diffusion (horizontal line). Generally as flow rates become increased, greater amounts of tracer are diverted to organs of interest producing higher clearances, but the subsequent increase in the clearances ceases to be proportional to the flow. The reason for this, is that at higher flows, the time available for exchange becomes shorter and there is insufficient time for equilibrium, and concentration differences between the blood and tissue persist whenever either of these is changing. The result of this produces a progressive lowering of the capillary tracer extraction with increasing flow and produces the disproportionate increases in clearance.

Region III :- Process of diffusion-limited exchange

If the flow rates of the tracer become overly high, then subsequent increases in flow do not increase tracer delivery to the tissues. In these situations the exchange of the tracer is actually governed by the properties such as the permeation and surface area of the barrier itself.

One can appreciate that extractions are not constant properties of capillaries for particular tracers and can in some circumstances decrease with flow. It is therefore important to draw careful attention to tracer flow rates when one is

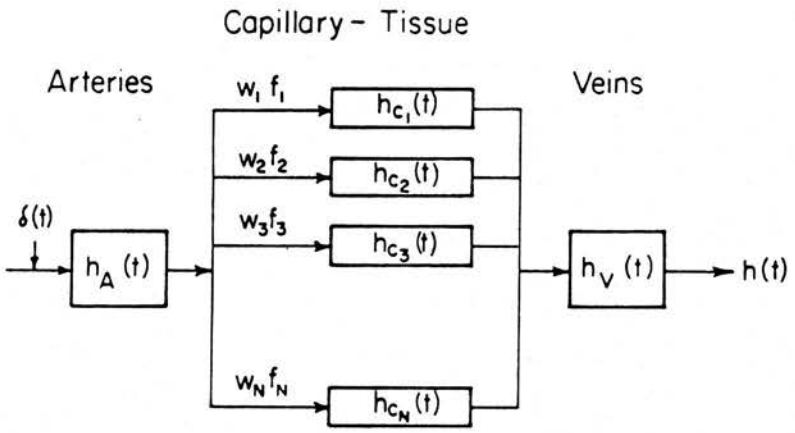

$$h(t) = h_A(t) * \sum_{i=1}^{N} w_i f_i h_{C_i}(t) \Delta f_i * h_v(t)$$

$$h(t) = h_{LV}(t) * h_C(t)$$

FIGURE 5-2 : Heterogeneous flow model III, describing exchange in an organ in which the transport functions of the arteries and veins, $h_A(t)$ and $h_V(t)$ are independent of those in a set of capillary-tissue regions, the $h_{C_i}(t)$ values.

quoting extraction figures for particular organs. For the ^{85}Sr data (table 2-2) from M.T.O.D. techniques, several investigators have obtained E_{max} from differing infusing tracer flow rates which seems unwise. However, McCarthy and colleagues seem to have adopted the more sensible approach by infusing the tracers at constant physiological flow rates. Their E_{max} figures infact tended to have smaller associated coefficients of variation in comparison with other investigators' more averaged E_{max} figures. Furthermore, by using constant infusing flow rates, McCarthy *et al* have proved that the bone seeking tracer ^{99m}Tc-MDP was diffusion limited (McCarthy *et al* 1980 ; McCarthy and Hughes 1983). Other tracers such as ^{85}Sr and ^{18}F also largely appear to be diffusion-limited because their extractions based on clearance techniques using equation (5.1) have tended to vary with flow rates in several bones (Tothill *et al* 1985).

5.1.2. Description of heterogeneous flow model III

The next important step in model development after having alleviated the problem of back diffusion is the incorporation of heterogeneous capillary blood flow rates. Bearing in mind the parallel independent nature of the diaphyseal microvasculature, a model (III) attributable to Bassingthwaighte and Goresky (1984) was developed. The model complete with the large vessels, the arteries (A) and veins (V) is illustrated in figure 5-2.

The transport in the capillary-tissue regions is independent of that in the large vessels such that dispersion and delay in the arterial and venous components of the vasculature are not related to the transit time through the individual capillary. Thus transport functions $h_A(t)$, $h_V(t)$ and $h_C(t)$ appertaining to the arteries, veins and capillaries can be suitably convoluted to produce the total transport function h(t) i.e.

$$h(t) = h_A(t) * \left[\sum_{i=1}^{n} w_i f_i \Delta f_i h_{C_i}(t) \right] * h_V(t) \qquad (5.2)$$

where the weighted summation of all the individual capillary transport functions $h_{C_i}(t)$ values is the overall transport function $h_C(t)$. The weighting function $w_i f_i \Delta f_i$ is composed of w_i, the fraction of the organ having a flow f_i ; the flow f_i, which is the local flow divided by the mean flow for the organ and is dimensionless ; and Δf_i which is the width of the ith class of relative flows.

Capillary volumes V_C (ml) are assumed constant and capillary transit times T_{C_i} (s) can be calculated thus

$$T_{C_i} = V_C / F_i \qquad (5.3)$$

where F_i (ml/s) is the local blood flow rate given by

$$F_i = f_i F_s \qquad (5.4)$$

with F_s (ml/s) being the mean organ flow rate or infusing flow rate.

5.2. MULTICAPILLARY MODELS OF BLOOD-BONE EXCHANGE

5.2.1. Assessment of investigative data for model use

1. Anatomical bone capillary volumes (V_C)

After having obtained capillary density measurements for the canine tibial diaphysis it was now possible to deduce a more realistic value for the total cortical bone capillary volume $V_{C/Co}$ other than the apparent intravascular volume of distribution figure V_C' found from tracer equilibration studies.

It has been found that a large majority of diaphyseal cortical bone capillaries have been confined to Haversian systems with one capillary per Haversian system. If one assumes therefore that the capillary is cylindrical with a radius R_C of 5 µm (table 1-1), then one can calculate using the derived capillary density figure of 2682/cm^2 for all 4 bones (n=240),

Capillary volume/ml cortex (if 1 Haversian system contains one capillary) = 0.0021 ml/ml

For all 6 tibiae the mean diaphyseal cortical mass was found to be 33.313 g which corresponds to a volume of 17.172 ml using a cortical density figure of 1.94 g/ml (Kelly et *et al* 1971). Hence,

Total cortical bone capillary volume $V_{C/Co}$ = 0.0021x17.172 = 0.0362 ml

The figure for $V_{C/Co}$ = 0.0021 ml/ml is about 6.5-7.5 times lower than intravascular volume of distribution V_C' (mean ± s.d.) figures of 0.013 ± 0.002 (Hooper *et al* 1984) and 0.015 ± 0.006 ml/ml (Morris *et al* 1983) found from tracer equilibration studies. The higher V_C' figures most certainly will have

included non-exchanging large vessel volumes.

The total marrow capillary volume $V_{C/M}$ was assumed equal to $V_{C/Co}$ as will be explained later in section 5.2.2.

2. Microsphere derived weighting functions

Such weighting functions have already been found by Bassingthwaighte and colleagues to describe the heterogeneity of flows in the heart for the purpose of modelling tracer uptake. These investigators tended to use 5 capillary systems to represent the whole range of flow heterogeneity in their models as described in figure 5-2 (Bassingthwaighte *et al* 1985 ; Kuikka *et al* 1986). A model infact containing 5 capillary systems was developed to describe blood-bone exchange in which 4 capillary systems were alloted to the cortex and 1 such system alloted to the marrow. Although it has been found that the partitioning of nutrient artery flow to the cortex and marrow is about 2:1, being 65% and 35% respectively, only 1 capillary system alloted to the marrow was considered necessary. This was due to the fact that the marrow blood flow distributions were less peaked as compared to the cortex, and in addition, comparatively large % c.v.s were associated with the descriptive statistics concerning the distribution of marrow flow rates. Essentially the microsphere data concerning the marrow was considered not to be consistent enough to warrant the use of two or more capillary systems in the model. Four capillary systems alloted to the cortex however were considered adequate to describe the distribution of relative regional flows (figure 4-4).

TABLE 5-1

Fractional masses $w_i\Delta f_i$ (i=1,...,4) of the assigned 4 cortical capillary systems (C.S.) for each of the 6 canine tibiae. $n_1,...,n_4$ values represent the number of samples in each class interval Δf_i=(0.4,0.4,0.4,0.8)

Dog (tibia)	C.S. 1 $w_1\Delta f_1$ (n_1)	C.S. 2 $w_2\Delta f_2$ (n_2)	C.S. 3 $w_3\Delta f_3$ (n_3)	C.S. 4 $w_4\Delta f_4$ (n_4)	$\sum_{i=1}^{4} w_i\Delta f_i$ / $(\sum_{i=1}^{4} n_i)$
#1(R)	0.212 (7)	0.385 (14)	0.244 (8)	0.159 (5)	1.0 (34)
#1(L)	0.303 (11)	0.314 (12)	0.214 (9)	0.169 (5)	1.0 (37)
#2(R)	0.276 (10)	0.326 (13)	0.231 (9)	0.167 (7)	1.0 (39)
#2(L)	0.222 (9)	0.387 (15)	0.278 (11)	0.113 (4)	1.0 (39)
#3(R)	0.112 (5)	0.473 (18)	0.274 (9)	0.141 (5)	1.0 (37)
#3(L)	0.229 (9)	0.386 (14)	0.277 (10)	0.108 (4)	1.0 (37)
mean ±	0.226±	0.378±	0.253±	0.143±	1.0
s.d.	0.066	0.057	0.027	0.027	-
c.v.	0.291	0.150	0.109	0.190	0.177

Table 5-1 illustrates the fractional masses of the cortex $w_i\Delta f_i$, having flows within the class Δf_i centred at f_i for each of the 6 tibiae. For the 4 cortical capillary systems (C.S.), the 4 class intervals were 0.4, 0.4, 0.4 and 0.8 with f_i being 0.47, 0.87, 1.27 and 1.87. The sum of the $w_i\Delta f_i$s was unity for each tibia to account for the whole mass of the cortex. One can also observe from table 5-1 that reasonable numbers of samples were alloted to each of the classes which was achieved by extending the latter class interval. The sum of the numbers of samples for each tibia represented the total number of samples after accounting for outliers. Mean and s.d.s were found for the subsequent fractional masses for all 6 dogs. A weighted percentage variance associated with the combination of fractional masses for all 6 tibiae was found to be low at 3.09%. In general there were quite small variations in $w_i\Delta f_i$ for the particular classes in all the dogs.

FIG. 5-3 Cortex/Marrow Multicapillary Model

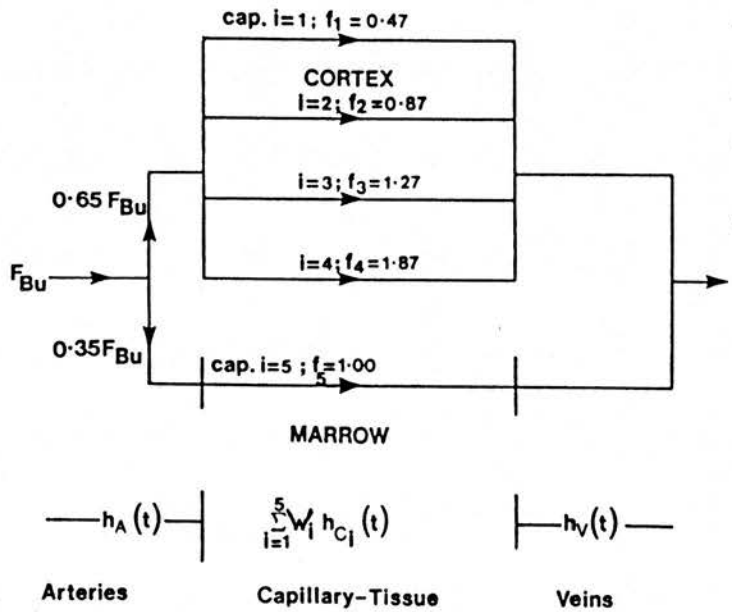

Abbrev.

h(t):- transport function of tracer (s^{-1})
t:- time (s)

F_{Bu}:- infusing buffer flow rate (ml/s)

f_i :- relative regional flow
W_i:- weighting factor

$$h(t) = h_A(t) * [\sum_{i=1}^{5} W_i h_{Ci}(t)] * h_V(t)$$

$$= h_{LV}(t) * h_C(t)$$

To obtain the amount of each tracer entering each capillary system one must consider the $w_i\Delta f_i f_i$ values which summate to unity for all 4 systems. $w_i\Delta f_i f_i$ values for the 4 systems were 0.104, 0.322, 0.314 and 0.260 at flows f_i previously mentioned.

For the 1 capillary system applying to the marrow the analysis was much easier with $f_i=w_i\Delta f_i = w_i\Delta f_i f_i=1.0$. The width of the class interval Δf_i was chosen to be 1.08, being of a suitable size to capture an even spread of marrow rd_i (flow rate) values (see figure 4-5).

5.2.2. Proposition of cortex/marrow (IIIa) and cortex (IIIb) multicapillary models of blood-bone exchange :- Model development as a whole

1. Cortex/marrow model (IIIa)

The general multicapillary model III (figure 5-2) was developed along anatomical and physiological lines into the cortex/marrow multicapillary model (IIIa) as illustrated in figure 5-3 in which 4 capillary systems (i=1,...,4) were assigned to the cortex and 1 capillary system (i=5) to the marrow. Findings from microsphere experiments such as the partitioning of the infusing tracer flow F_{Bu} to the cortex and marrow, and the weighting factors corresponding to the specified local flows f_i were incorporated into model IIIa. The value of V_C=0.0362 ml derived from the capillary density measurements was assigned to each of the capillary systems.

TABLE 5-2

Description of model IIIa parameters

PS_C Capillary permeability-surface area product (cortex and marrow) ml/s.

PS_B Permeability-surface area product - ml/s, applicable to
a) hypothetical bone surface binding pool (^{85}Sr)
b) cellular phase (cortex and marrow) (^{86}Rb)

V_I' Apparent volume of distribution of interstitial fluid (cortex and marrow) ml.

V_B' Apparent volume of distribution - ml. applicable to
a) hypothetical bone surface binding pool (^{85}Sr)
b) cellular phase (cortex and marrow) (^{86}Rb)

Table 5-2 shows important parameters that are associated with model IIIa. Even though there are capillary systems to describe tracer exchange in both the cortex and marrow, it is not feasible to have too many optimizable parameters that relate to the cortex and marrow independently. This is due to the fact that it has been difficult at times to interpret optimized parameter estimates particularly concerning the fourth parameter V_B' in the case of the single capillary model (II). Essentially the outflow data is not refined enough to merit using models with too many structural parameters and therefore many of the parameters in table 5-2 such as PS_C and V_I' relate identically to both the cortex and marrow structures. Indeed, it is the fact that PS_C relates to both cortical and marrow capillaries which prompts the assumption of $V_{C/Co}$ being equal to $V_{C/M}$.

In using the model to optimise ^{86}Rb data, one must realize that the marrow has an interstitial fluid space and cellular elements as well as the cortex. Hence all 4 of the parameters in table 5-2 relate equivalently to the cortex and marrow. In using the model to optimise ^{85}Sr data however, only the PS_C and V_I' parameters are identical for the cortex and marrow. The third phase

concerning the bone surface binding pool is only to be associated with the cortical bone capillaries, thus the parameters PS_B and V_B' apply only to the cortical capillary systems.

2. Cortex model (IIIb)

A cortex model IIIb which was developed, is similar to model IIIa in terms of the 4 cortical weighting factors and 4 local flows f_i, but with the exception of the omission of the marrow capillary system. For this model, the infusing tracer flow F_{Bu} was assumed only to supply the cortex.

Although the cortex model IIIb is not very realistic as compared with the cortex/marrow model IIIa, because it has been established that there is substantial nutrient artery flow to the marrow, it is nevertheless useful for two reasons. Firstly, it will provide information on how extreme the optimizable parameters can become for the diffusible experimental data as much larger proportions of nutrient artery tracer flow is supplied to the cortex. Secondly, one will be able to appreciate the systematic changes in the final optimized parameter estimates for this heterogeneous flow model as opposed to the homogeneous single capillary model II. These systematic changes can then in turn be compared with the findings of Bassingthwaighte *et al.* who fitted a similar model to outflow tracer data from the heart.

Model development as a whole

To provide a complete picture of the models that have been developed to understand tracer exchange in this thesis, one can refer to figure 5-4 which illustrates Krogh-cylinder type models viewed end on.

MODEL I

(CORTEX OR WHOLE BONE)

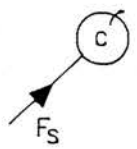

MODEL PARAMETERS

$PS_{C/Co}$ OR $PS_{C/CoM}$

MODEL II

(CORTEX)

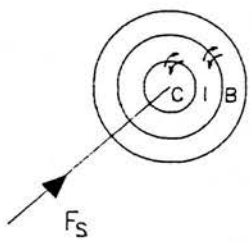

$PS_{C/Co}$. $PS_{B/Co}$. $V'_{I/Co}$. $V'_{B/Co}$

MODEL III

a) (CORTEX AND MARROW)

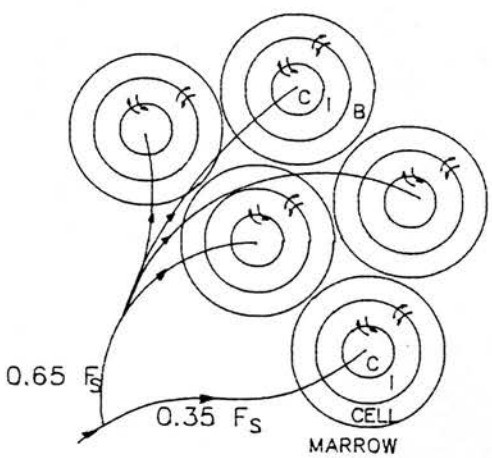

^{85}Sr :-

$PS_{C/CoM}$. $PS_{B/Co}$. $V'_{I/CoM}$. $V'_{B/Co}$

^{86}Rb :-

$PS_{C/CoM}$. $PS_{B/CoM}$. $V'_{I/CoM}$. $V'_{B/Co\,M}$

b) (CORTEX)

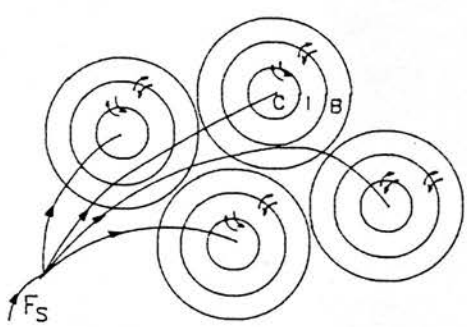

$PS_{C/Co}$. $PS_{B/Co}$. $V'_{I/Co}$. $V'_{B/Co}$

ABBREVIATIONS :-

C :- CAPILLARY ; I :- INTERSTITIAL FLUID

B :- BONE CELL (^{86}Rb)

HYPOTHETICAL BONE SURFACE BINDING POOL (^{85}Sr)

FIGURE 5-4 : Models used to study tracer exchange between blood and bone.

Model I describes the Crone Renkin formulation in which tracer escapes from a homogeneously perfused capillary (C) into an infinite space. This particular model which does not include back diffusion has provided information appertaining only to the capillary permeability-surface area product PS_C. The question as to whether the PS_C findings have applied just solely to cortical capillaries ($PS_{C/Co}$) or to both cortical and marrow capillaries ($PS_{C/CoM}$) as a whole, has always been an unclear and debatable issue.

Model II as described in chapter 3 is a much more informative homogeneous flow single capillary model which allows for back diffusion between two additional finite cumulatively sized cortical bone phases of interstitial fluid (I) and bone (B).

Models IIIa and IIIb as mentioned, accounts for flow rate heterogeneity and back diffusion in describing tracer exchange which is confined solely to the individual cylinder units with no interactions taking place between adjacent units.

5.2.3. Application of model III to experimental data

Introduction

The approach of applying model III to the experimental data is similar to that of the homogeneous model in that a suitable form of the reference tracer transport function $h_R(t)$ is used as model input with proceeding model parameter optimisation to fit the solutions to the transport functions $h_D(t)$ of the diffusible tracers. However, by virtue of the fact that the heterogeneity of flow rates associated with model III results in a range of capillary transit times, means that it is much more difficult to obtain a model input $h_{LV}(t)$ such that

FIGURE 5-5 : Deriving the multicapillary model IIIa input function $h_{LV}(t)$ [LV(1),... values] from outflow reference tracer data $h_R(t)$ [HR(1),... values]. W(1),...,W(5) values represent the weighting functions for each of the 5 capillary systems (C.S.) producing outflow (ofl). See text for further details.

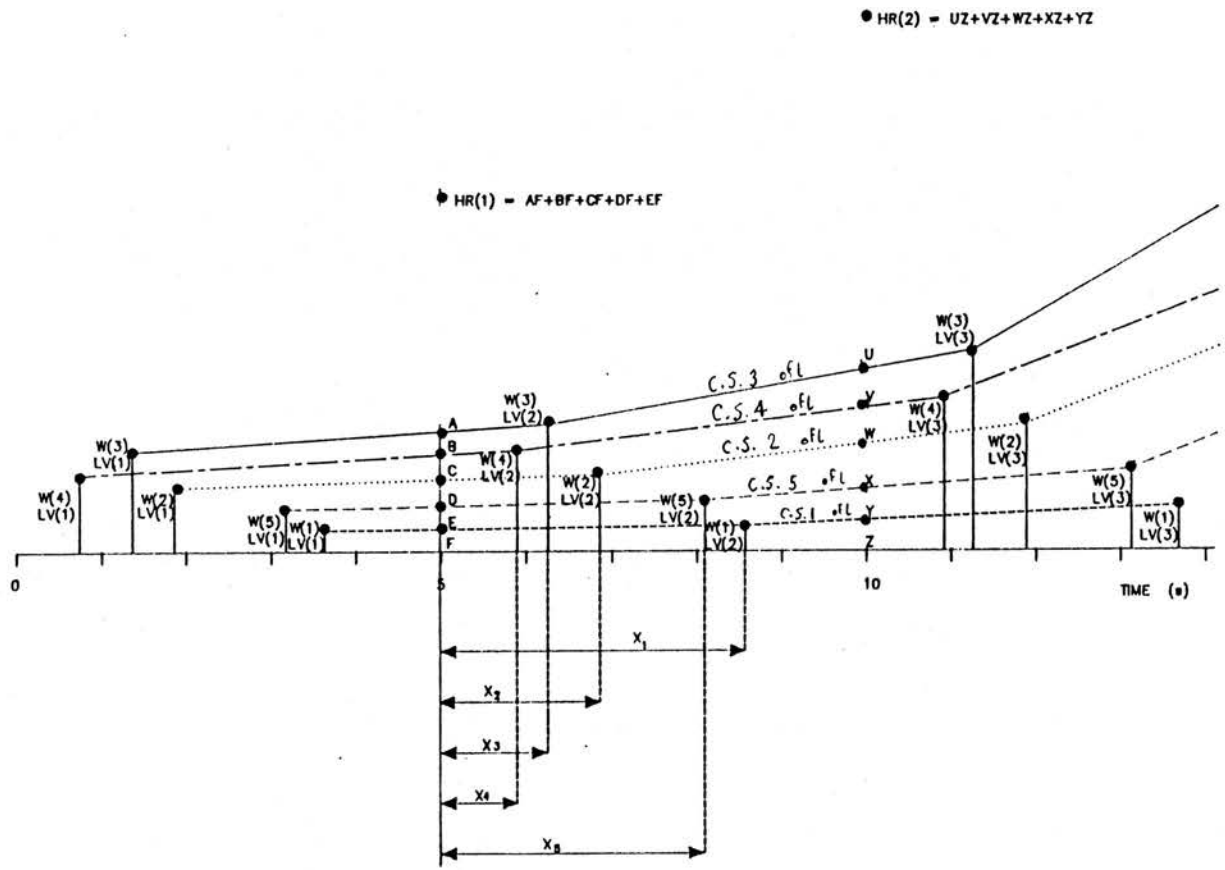

cumulative output from the capillaries (PS_C=0) produces $h_R(t)$. Infact, for an aggregate of non-dispersive capillaries, the distribution of capillary transit times for the reference tracer $h_{C,R}(t)$ is

$$h_{C,R}(t) = \sum w_i f_i (\Delta f_i / \Delta T_{C_i}) \delta(t - T_{C_i}) \qquad (5.5)$$

where $\Delta f_i/\Delta T_{C_i}$ is the interval width in the histogram representation of flows divided by the same for the transit times which can be obtained by use of the equations (5.3) and (5.4). Therefore, for the transport function of the reference tracer $h_R(t)$ one can write,

$$h_R(t) = \left[\sum w_i f_i (\Delta f_i / \Delta T_{C_i}) \delta(t - T_{C_i}) \right] * h_{LV}(t) \qquad (5.6)$$

utilizing equations (3.13) and (5.2). The model input $h_{LV}(t)$ was obtained from equation (5.6) by way of a numerical approach.

Numerical approach to determine $h_{LV}(t)$

Figure 5-5 demonstrates how the model IIIa input $h_{LV}(t)$ can be obtained from the outflow reference $h_R(t)$ data. The objective was to obtain values of $h_{LV}(t)$ represented by LV(1), LV(2),..., LV(N) occurring every 5 s, which would suitably produce model solutions at PS_C=0 resembling those of the reference tracer values HR(1), HR(2),..., HR(60) obtained from blood samples taken every 5 s. Figure 5-5 illustrates this objective for the first two reference tracer values HR(1) and HR(2) in which weighted amounts of tracer outflow (ofl) emerge from the 5 capillary systems (C.S.) at varied transit times. The weighting functions $W(i) = w_i f_i(\Delta f_i/\Delta T_{C_i})$ (i=1,...,5) were (1.423×10^{-2}, 0.1751, 0.3753, 0.3309, 0.1044) and were associated with each of the capillary systems having transit times (s) of (3.549, 1.917, 1.314, 0.892, 3.113). Larger weighting factors were associated

with the shorter capillary transit times and *vice versa*.

To describe how LV( ) values were obtained, one can examine the contributions of the capillary systems at 5 and 10 s corresponding to HR(1) and HR(2) respectively.

At 5 s, the first outflow result HR(1) corresponded to the addition of tracer amounts of magnitudes AF, BF, CF, DF and EF emerging from capillary systems 3, 4, 2, 5 and 1 respectively. The tracer amounts at this time were determined using the principles of similar triangles as such i.e.

$$\text{EF (C.S. 1)} = W(1)LV(2) - (x_1/5)[W(1)LV(2) - W(1)LV(1)]$$

$$\vdots \qquad \vdots \qquad \vdots$$

$$\text{AF (C.S. 5)} = W(5)LV(2) - (x_5/5)[W(5)LV(2) - W(5)LV(1)]$$

in which the quantities W(1)LV(1),...,W(5)LV(1) relate to weighted model input emerging from the capillary systems at the capillary transit times. The quantities W(1)LV(2),...,W(5)LV(2) relate to the weighted model inputs occurring 5 s further on. The $x_1,...,x_5$ values being equal to the appropriate capillary transit times, facilitates the numerical calculations of AF, BF, CF, DF and EF.

By assigning $x_1'=x_1/5,...,x_5'=x_5/5$, HR(1) can be written as

$$HR(1) = LV(1)\left[\sum_{i=1}^{5}(W(i)x_i')\right] + LV(2)\left[\sum_{i=1}^{5} W(i)(1 - x_i')\right]$$

or in more convenient terms as

$$HR(1) = LV(1)K(1,1) + LV(2)K(1,2)$$

where the 2 components i=1 and j=1,2 of the coefficients K(i,j) relate to the 1st outflow result HR(1) and the numbered LV(1) and LV(2) components.

In a similar fashion at 10 s, corresponding to the second outflow result HR(2) consisting of contributions of tracer of magnitudes UZ, VZ, WZ, XZ and YZ, one finds that

$$HR(2) = LV(2)\left[\sum_{i=1}^{5}(W(i)x_i')\right] + LV(3)\left[\sum_{i=1}^{5} W(i)(1 - x_i')\right]$$

or

$$= LV(2)K(2,2) + LV(3)K(2,3)$$

One can now appreciate that K(2,2)=K(1,1) and K(2,3)=K(1,2) or in more general terms K(i,j)=K(i−1,j−1). By extending the analysis for all outflow results HR(1),...,HR(60) one obtains 60 linear simultaneous equations i.e.

$$\begin{aligned}
HR(1) &= K(1,1)LV(1)+K(1,2)LV(2)\\
HR(2) &= \qquad\quad K(2,2)LV(2)+K(2,3)LV(3)\\
&\;\;\vdots\\
HR(60) &= \qquad\qquad\qquad\qquad\qquad\qquad K(60,60)LV(60)+K(60,61)LV(61)
\end{aligned}$$

or in matrix notation one may write

$$\begin{pmatrix} HR(1)\\ HR(2)\\ \vdots\\ HR(60)\end{pmatrix} = \begin{pmatrix} K(1,1) & K(1,2) & & & & \\ & K(2,2) & K(2,3) & & & \\ & & \ddots & \ddots & & \\ & & & & K(60,60) & K(60,61)\end{pmatrix} \begin{pmatrix} LV(1)\\ LV(2)\\ \vdots\\ LV(61)\end{pmatrix}$$

The equations in a matrix form Ax=b where A is a real mxn ($m \leq n$) matrix and b an m element vector, were solved for x i.e. LV( ) by the use of a NAG F04JDF routine. This routine was particularly useful because it minimized the length of the residual vector r=b−Ax in the solving process which alleviated the effects of ill conditioning caused by noisy experimental data values.

The derived $h_{LV}(t)$ values can actually be used as model input to see if the reference outflow profile can be suitably reproduced again. Table 5-3 demonstrates that extremely close agreements can be obtained between the model generated reference values and the actual experimental values, thus validating the method.

TABLE 5-3

Comparison of experimental ($h_R(t)$) and model IIIa ($\hat{h}_R(t)$) produced reference transport function values ($x10^{-6}$ 5 s^{-1}). $\hat{h}_R(t)$ was produced using the derived model IIIa input function $h_{LV}(t)$

Data : ^{125}I-albumin experiment 1.

Time (s)	h_R	$\hat{h}_R$	Time (s)	h_R	$\hat{h}_R$
5	64	64	155	1777	1777
10	441	441	160	1808	1808
15	3487	3487	165	1588	1588
20	16806	16806	170	1581	1581
25	84051	84055	175	827	827
30	116845	116843	180	1427	1427
35	109026	109023	185	1059	1059
40	96118	96115	190	1137	1137
50	65236	65235	200	1025	1025
60	43779	43777	210	795	795
80	20623	20623	230	563	563
100	8247	8246	250	539	539
120	5384	5384	270	537	536
140	2634	2634	290	420	420
150	2190	2189	300	437	437

The described numerical method is a much easier approach of finding $h_{LV}(t)$ other than deconvolution approaches favoured by Bassingthwaighte and colleagues. Achieving deconvolution via Fourier transforms has led to difficulties regarding instability, noise related problems and round off error (Bassingthwaighte 1967). Personal experiences in attempting deconvolution have also produced scaling problems.

TABLE 5-4

Optimisation of heterogeneous model III hypothetical outflow data (generated using PS_C = 0.066 ml/s, PS_B = 0.033 ml/s, V_C' = 0.33ml, V_I' = 1.65 ml, V_B' = 3.3 ml, $\bar{F}_s$ = 0.033 ml/s, T_C = 10s S.S.) using a homogeneous model II of varied V_C' (T_C) parameter (F_s = 0.033 ml/s).

Assigned		Final Parameter Estimates								Fit
V_C' (ml)	T_C (s)	PS_C (ml/s)	% c.v.	PS_B (ml/s)	% c.v.	V_I (ml)	% c.v.	V_B (ml)	% c.v.	C.V.
0.165	5	0.033	0.612	0.019	2.286	1.145	1.429	1.942	1.997	0.0183
0.330	10	0.033	0.610	0.019	2.301	1.154	1.399	1.934	1.998	0.0183
0.825	25	0.033	0.604	0.019	2.347	1.183	1.313	1.909	2.001	0.0183

5.3. INFORMATIVE MODEL SIMULATIONS

5.3.1. Systematic errors in parameter estimates when fitting a single capillary model to heterogeneous data

The choice of an anatomical total capillary volume as opposed to an apparent intravascular volume of distribution

In section 5.2.1, it was found that a total diaphyseal anatomical bone capillary volume obtained from capillary density measurements was infact much lower than a figure used in the homogeneous flow model II, which was based on tracer equilibration studies. Therefore studies were undertaken to investigate the effect of varying V_C' i.e. T_C (F_s constant) on the parameter estimates when optimising the model II to hypothetical data.

Firstly, hypothetical reference and diffusible outflow data were generated for particular parameters using a 5 capillary system heterogeneous model III. Then secondly, the hypothetical reference data was shifted left by varying capillary transit times corresponding to changes in V_C' and used as model II input. Finally, the parameters of model II were optimized such that the solutions or output fit as close as possible to the hypothetical outflow data.

Table 5-4 illustrates the results of these studies in which it is noticeable that as a consequence of using the single capillary model II, the final parameter estimates are much lower than the true parameters which were used to generate the outflow data using the multicapillary model. It would thus seem that in using homogeneous flow models, parameters of the system are underestimated. An important finding regarding the similarities in results in table 5-4 however, is that when using a single capillary model to fit

FIGURE 5-6

7 Class Normal Variation of Flows

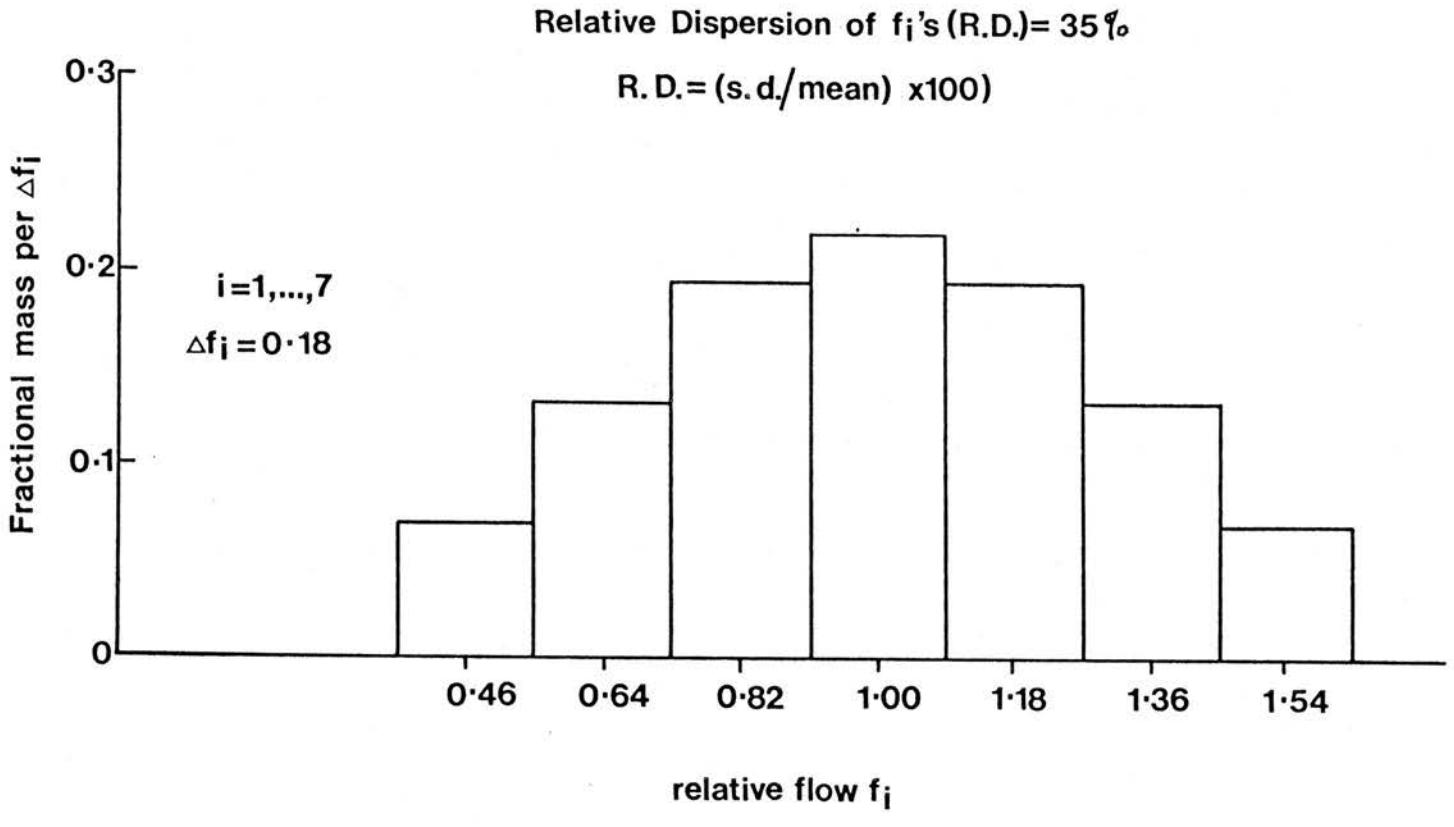

experimental data, the choice of V_C' seems unimportant i.e. the attainable final parameter estimates are independent of V_C' and the shifted capillary transit time. This finding seems reasonable in the light of tracer coronary circulation studies carried out by Rose and Goresky (1976) using a similar model but with different parameters. They found that the process of fitting (optimisation) provided a constant estimate of their parameter V_I'/F_s rather than constant estimates of V_I'/V_C' and T_C.

Errors in the estimation of model II parameters due to heterogeneity of flow

In order to assess the influence of heterogeneity on parameter estimates, a definable 7 class normal or Gaussian distribution of flows was obtained in a similar manner as described by Bassingthwaighte and Winkler (1982). Figure 5-6 illustrates such a distribution of flows in which the relative dispersion of flows f_i is 35% and the common class interval Δf_i is 0.18. Magnitudes of the ordinate axis, the fractional mass/class interval were deduced using statistical tables concerning areas under a normal curve.

Utilizing the illustrated normal distribution of flows in model III, hypothetical reference and diffusible outflow profiles at 5 s intervals were obtained for particular values of the parameters PS_C', PS_B', V_I' and V_B'. These profiles were then suitably used as described, to obtain single capillary model fits with subsequent final parameter estimates. These latter model II parameter estimates were then compared with their true values.

Figure 5-7 illustrates single capillary model fits to heterogeneous data of varied PS_C which for convenience has been expressed as PS_C/F_s. The heterogeneous data was obtained at a relative dispersion of 35% with respective ratios of

FIG. 5-7 **Single-Cap. Fit to Heterogeneous Data of Varied PS_C/F_S**

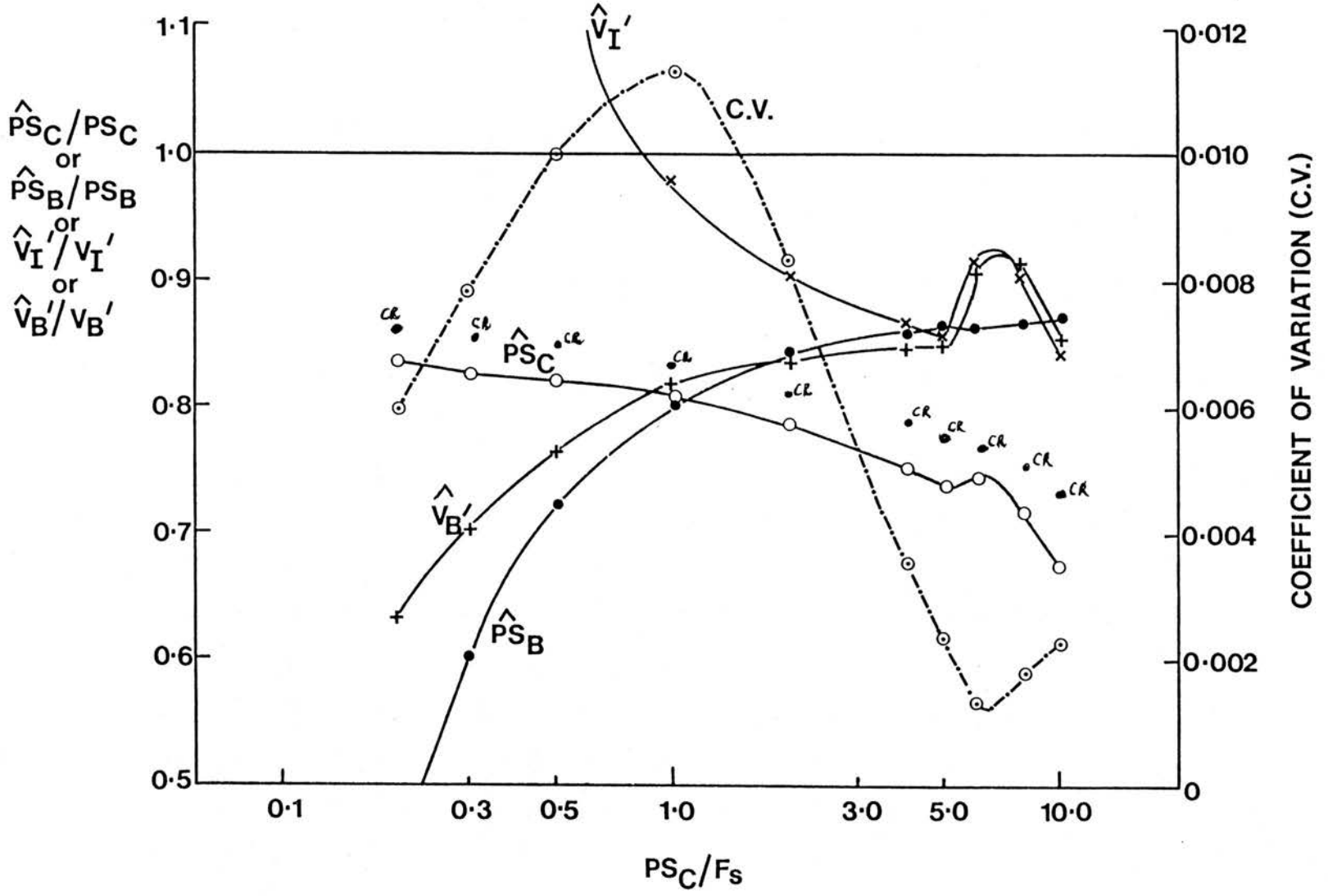

apparent volumes of distribution of interstitial fluid and bone relative to the capillary of 5 and 10 ; the permeability-surface area product for bone was 0.04 ml/s. The parameters with carets or hats denote estimates and those without stand for true values. Thus, by virtue of the fact that most of the parameter ratios were less than unity meant that in the majority of cases, parameters were underestimated.

The degree of underestimation of $\hat{PS}_C$ which implied that calculated maximum extractions would be underestimated, became progressively larger as the PS_C/F_s ratio increased. This was due to the fact that at the larger PS_C/F_s ratios, the exchange was becoming more flow limited, whereas at smaller ratios it was more diffusion-limited, the influence of flow heterogeneity being reduced. The improvement in the estimates of $\hat{PS}_C$ particularly for PS_C/F_s ratios less than unity was contrary to the findings of Levin as quoted in Bassingthwaighte and Winkler (1982). Levin in these circumstances found that for a 2 phase capillary-interstitial fluid system in which $V_I'/V_C' = 5$, with a similar 7 class normal distribution of flows (relative dispersion = 35%), ratios of $\hat{PS}_C/PS_C$ became progressively smaller i.e. $\hat{PS}_C$ became increasingly underestimated. However, Levin's findings seem to be the more unlikely because limiting calculations based on the heterogeneous flow system using the Crone-Renkin formulation ($V_I' = \infty$) have produced systematic underestimations of PS_C (symbols CR in figure 5-7) that resemble in shape the profile of $\hat{PS}_C$ underestimations found by myself.

The profiles for the parameter estimates concerning the third phase, the bone, seemed reasonable in view of the sharply descending parameter ratios $\hat{PS}_B/PS_B$, $\hat{V}_B'/V_B'$ for decreasing PS_C/F_s ratios. This suggests that the smaller amounts of tracer passing through the capillary walls particularly for the high flow rates is increasingly making the third phase of the single capillary model seem invalid.

FIGURE 5-8

Single–Cap. Fit to Heterogeneous Data of Varied V_I'/V_C'

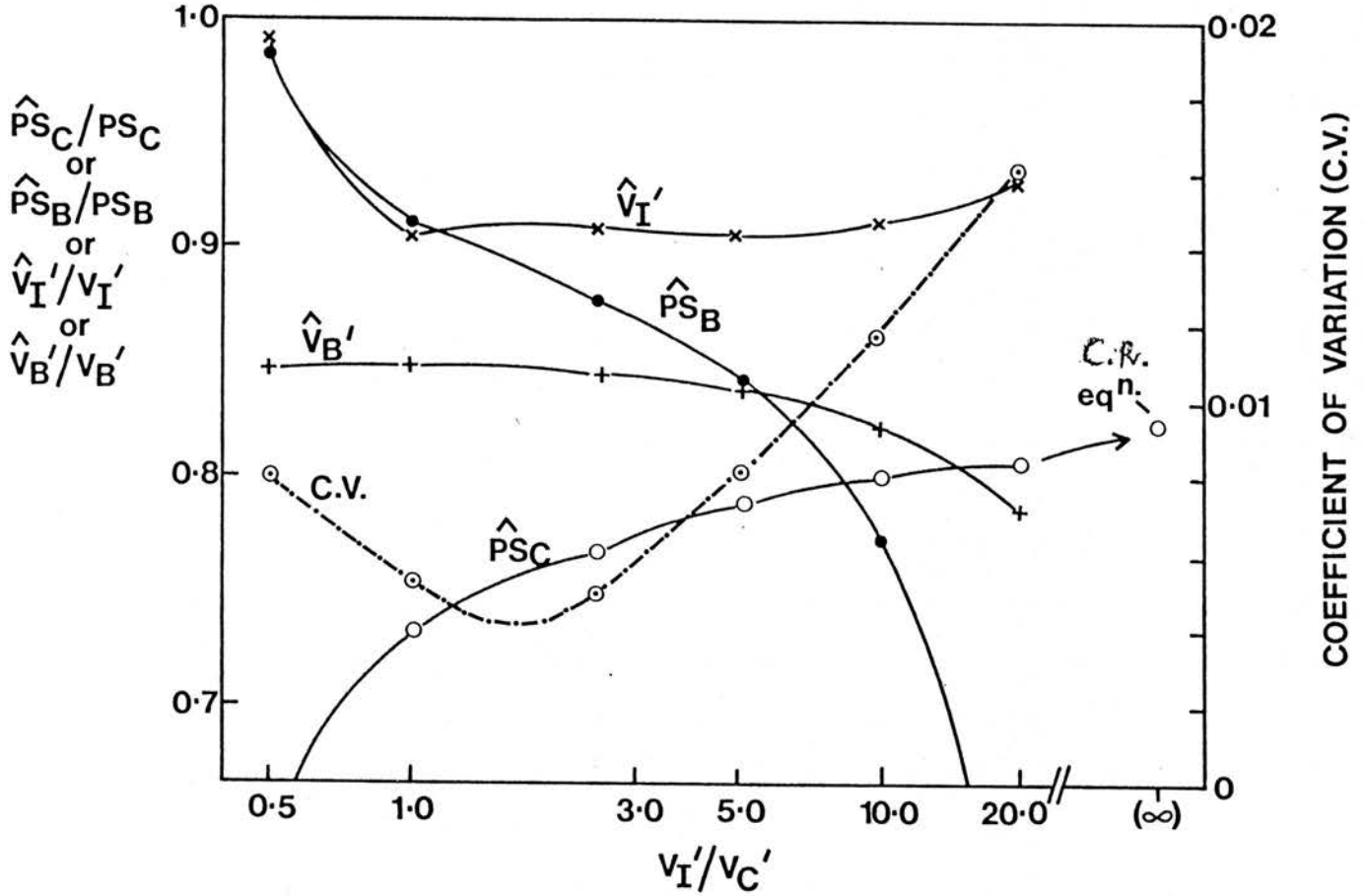

The coefficient of variation (C.V.) figures as illustrated in figure 5-7 were measures of fit with C.V.= $[RSS/(n-1)]^{1/2}/(\Sigma\hat{h}_i/n)$ where RSS is the residual sum of squares based on n=60 samples producing model output $\hat{h}_i$ (i=1,...,n). It would appear that the best fitting is achieved when either very small or large quantities of tracer pass through the capillary walls. There does however seem to be a limit to the goodness of fit when overly large amounts of tracer can pass through the capillary walls as adjudged by the minimum C.V. point of around PS_C/F_s = 6-7 which was responsible for the sudden improvement in all the parameters.

The effect of how the relative dispersion of flows affects the single capillary model II parameter estimates was also investigated. Generally, it was found that larger measures of dispersion caused larger degrees of underestimation in the parameter estimates and larger associated measures of fit and *vice versa*.

Figure 5-8 illustrates single capillary model fits to heterogeneous data of varied V_I' which for convenience has been expressed as V_I'/V_C'. Once again it can be seen that the parameters tend to be underestimated, notably for $\hat{PS}_C$ especially when there is a larger scope for back diffusion with V_I'/V_C' decreasing. For increasing V_I'/V_C' ratios the estimate $\hat{PS}_C$ tended towards a value calculated on the basis of the heterogeneous flow system and the Crone Renkin formulation. Additionally, with increasing V_I'/V_C' ratios, the third bone phase tended to become obsolete with $\hat{PS}_B$ tending towards zero. Estimates of $\hat{V}_I'$ appear to be the most stable in the specified range, not deviating by more than 10% of their true values.

The lowest C.V. values or best measures of fit were obtained for $1.0<V_I'/V_C'<3.0$. This particular range is intermediate to where there is scope for large amounts ($V_I'/V_C'<1.0$) and small amounts ($V_I'/V_C'>3.0$) of back

TABLE 5-5

Effects of noise on the parameter estimates from the multicapillary model III using BMDP PAR, optimising to 60 data values. Starting values are 50% higher than true values. Final values, residual sum of squares (RSS) and coeffs of variation (c.v.) are averaged over given number of runs. In addition, effects of constraining certain parameters to their true values on final parameter estimates. Pre-assigned package values.

Multicapillary model III : 7 capillary systems with flow rates associated with a normal distribution of RD = 35%, V_C' = 0.0362 ml.

Noise Level	No. Runs	PS_C (ml/s)	PS_B (ml/s)	V_I' (ml)	V_B' (ml)	RSS	CPU (s)	% c.v. PS_C	% c.v. PS_B	% c.v. V_I'	% c.v. V_B'
True Values		0.0500	0.0250	1.0000	5.0000	-	-	-	-	-	-
0%	1	0.0500	0.0250	1.0000	5.0014	4.633×10^{-12}	911.38	-	-	-	-
1%	5	0.0501±0.0003	0.0250±0.0001	0.9971±0.0138	4.9671±0.0719	$(2.327\pm0.358)\times10^{-6}$	1052.18±274.97	0.57	0.40	1.39	1.45
5%	5	0.0515±0.0029	0.0250±0.0004	0.9483±0.0370	5.1543±0.3688	$(4.921\pm1.263)\times10^{-5}$	1119.30±261.33	5.59	1.48	3.90	7.15
	5	0.0498±0.0053	0.0243±0.0020	0.9971±0.1277	4.5962±0.3392	$(2.080\pm0.310)\times10^{-4}$	1038.72±398.37	10.68	8.31	12.80	7.38
	5	0.0489±0.0017	0.0244±0.0022	(1.0000 Fixed)	4.5935±0.3447	$(2.179\pm0.290)\times10^{-4}$	917.88±280.08	3.49	9.02	-	7.50
10%	5	(0.0500 Fixed)	0.0252±0.0023	0.9694±0.0457	4.5987±0.3327	$(2.183\pm0.301)\times10^{-4}$	850.82±159.84	-	9.12	4.71	7.23
	5	0.0500±0.0056	(0.0250 Fixed)	0.9861±0.1337	4.5651±0.3920	$(2.144\pm0.312)\times10^{-4}$	917.94±148.87	11.17	-	13.55	8.59
	5	0.0499±0.0054	0.0241±0.0022	1.0079±0.1311	(5.0000 Fixed)	$(2.122\pm0.314)\times10^{-4}$	1072.19±143.11	10.78	9.04	13.00	-

diffusion to take place.

5.3.2. Effects of noise on the parameter estimates

In a similar manner as described in section 3.2.4, a smooth test model curve with pre-assigned parameter values was produced using a lagged normal density curve as input. The curve on this occasion was produced using the more general multicapillary III model with a 7 class normal distribution of flow rates (relative dispersion = 35%) with V_C' = 0.0362 ml, the value obtained from capillary density measurements. The test model curve with varying amounts of noise applied to it simulating experimental variations in isotope activities, was used to test the accuracy of the parameter estimates. The noise was obtained using two NAG routines G05CCF and G05DDF to produce a non-repeatable Gaussian distribution of random numbers which were subsequently added to the test model data. The noise again was defined in terms of the standard deviation ($s.d._p$) calculated at the peak of the response, and optimisation was achieved using a BMDP PAR routine using the lagged normal density input curve and the noisy test model curve.

Table 5-5 illustrates the effects of differing levels of noise on the parameter estimates for 60 values, being comparative to the 60 experimental sample values over a time period of 5 min. The starting values for the optimisation process were 50 % higher than the true pre-assigned parameter values. The results in table 5-5 show the trend of higher coefficients of variation (c.v.) and residual sum of squares (RSS) with higher levels of noise. In contrast with the homogeneous model II noise data of table 3-6, the magnitudes of the coefficients of variation for each of the parameters are much similar. This is particularly the case for the parameters of PS_B and V_I' and occurs principally as a consequence of having much shorter capillary transit times owing to

assigning V_C' = 0.0362 ml in model III as opposed to V_C' = 0.4 ml in the homogeneous model II.

Also illustrated in table 5-5 at the noisiest level ($s.d._p$=10%) are the effects of constraining certain parameters to their true values on the other final parameter estimates. The purpose of constraining the individual parameters was to test the reproducibilty of the remaining parameter estimates, and to observe if CPU times could be reduced, thus enabling more complex models to be used. Although reproducibility was achieved, no significant reduction in CPU times was attained. In a situation of modelling the outflow results of '2 phase' (extravascular) and '3 phase' tracers, reproducibility for 3 phase parameter estimates by for instance constraining a '2 phase' estimate of V_I' could only be achieved if the tracers had equivalent apparent volumes of distribution.

5.4. RESULTS OF MULTICAPILLARY OPTIMISATION TO M.T.O.D. DATA

5.4.1. Fitting the experimental data

Tables 5-6 and 5-7 show the results of final parameter estimates for ^{86}Rb and ^{85}Sr respectively using models IIIa and IIIb after adopting similar policies in the choice of starting values as described in section 3.3.1.

From table 5-6, one can observe that it was possible to fit the two multicapillary models to all of the ^{86}Rb data which was not the case with the homogeneous model II. Data concerning experiment number 3 proved to be the most difficult to fit generally, producing the highest C.V. values and requiring a relatively large 29 increment halvings in the optimisation process involving model IIIa. The C.V. values associated with the individual sets of ^{86}Rb data tended to be very similar for both models.

The fitting of ^{85}Sr data as described in table 5-7 was generally much more improved than using the homogeneous flow model II. Satisfactory fits were obtained in most instances with the exception of using model IIIb with ^{85}Sr data from experiment number 5, in which the pre-assigned maximum number of increment halvings was reached three times. Generally, the fitting for experiment number 5 was difficult with both models, with the PS_B parameter always finishing up equalling the lower bound which was set at zero. It thus appeared that this particular set of ^{85}Sr data, having the lowest PS_C parameter and hence E_{max} value, was more appropriately described by a two phase model. Maybe it is the case that poorly extractable diffusible tracer data from the complex microvascular system is very difficult to model mathematically in terms of three phases, even with multicapillary systems. The evidence for this is provided in figure 5-7 which although demonstrates single capillary model

TABLE 5-6

Parameter estimates of experimental ^{86}Rb data from models IIIa & IIIb using ^{125}I-albumin as input to the model. Maximum increment halvings = 30, otherwise pre-assigned BMDP package values. n_x = (10,10,10,10,10)

Model	Experiment Number	FINAL PARAMETER ESTIMATES								C.V.	CPU time(s)	Largest No. of increment halvings req. (No. times for maximum)	Model II C.V.
		PS_C(ml/s)	(%c.v.)	PS_B(ml/s)	(%c.v.)	V_1' (ml)	(%c.v.)	V_B' (ml)	(%c.v.)				
IIIa	1	0.082	(13.87)	0.014	(8.62)	0.490	(8.53)	1.938	(15.46)	0.215	780.99	4	0.214
	2	0.057	(8.30)	0.0096	(11.12)	0.651	(6.14)	1.804	(20.15)	0.179	1503.04	13	0.181
	3	0.037	(9.20)	0.0070	(35.78)	1.065	(12.89)	L	(L)	0.358	3347.71	29	0.452
	4	0.054	(5.11)	0.022	(5.32)	0.633	(6.52)	3.948	(10.36)	0.158	1342.71	6	0.158
	5	0.018	(2.20)	0.140	(22.81)	3.683	(47.20)	70.248	(76.58)	0.129	3455.48	8	0.197
	6	0.036	(4.45)	0.012	(6.66)	0.626	(5.56)	L	(L)	0.182	3429.14	17	0.180
IIIb	1	0.125	(12.58)	0.025	(8.37)	0.828	(8.73)	3.366	(15.13)	0.214	1307.72	6	
	2	0.089	(7.67)	0.017	(11.08)	1.119	(6.29)	3.116	(19.90)	0.180	1018.35	3	
	3	0.064	(8.73)	0.020	(21.81)	1.700	(14.80)	L	(L)	0.375	5214.92	11	
	4	0.084	(4.72)	0.038	(5.35)	1.102	(6.70)	6.867	(10.37)	0.158	2284.64	8	
	5	0.030	(2.09)	0.288	(33.21)	9.126	(60.48)	115.624	(82.35)	0.133	4708.68	7	
	6	0.058	(4.24)	0.021	(8.13)	1.120	(5.95)	L	(L)	0.180	3442.25	11	

Notes:- L, large values (larger than format specifications of the package)

TABLE 5-7

Parameter estimates of experimental ^{85}Sr data from models IIIa & IIIb using ^{125}I-albumin as input to the model. Maximum increment halvings = 30, otherwise pre-assigned BMDP package values. n_x = (10,10,10,10,10)

Model	Experiment Number	FINAL PARAMETER ESTIMATES								C.V.	CPU time(s)	Largest No. of increment halvings req. (No. times for maximum)	Model II C.V.
		PS_C(ml/s)	(%c.v.)	PS_B(ml/s)	(%c.v.)	V_1' (ml)	(%c.v.)	V_B' (ml)	(%c.v.)				
IIIa	1	0.068	(5.95)	0.031	(3.76)	0.523	(7.90)	8.381	(7.99)	0.100	1396.15	7	0.095
	2	0.063	(6.33)	0.023	(5.97)	0.760	(7.76)	7.905	(13.02)	0.118	807.71	3	0.131
	3	0.030	(10.22)	0.0078	(69.22)	1.407	(21.67)	L	(L)	0.393	2278.33	11	0.407
	4	0.059	(4.18)	0.038	(4.27)	0.684	(8.61)	10 508	(8.31)	0.104	1235.60	9	0.125
	5	0.016	(2.28)	0.000	(0.00)	27.245	(38.73)	0.01	(0.00)	0.219	968.19	6	-
	6	0.036	(2.03)	0.029	(4.78)	1.104	(5.62)	L	(L)	0.088	3134.42	11	0.104
IIIb	1	0.099	(4.00)	0.042	(2.68)	1.093	(4.86)	9.596	(5.93)	0.095	2031.36	7	
	2	0.091	(4.57)	0.032	(5.19)	1.552	(5.35)	8.821	(11.32)	0.130	2103.93	6	
	3	0.050	(9.04)	0.011	(66.82)	2.429	(18.83)	L	(L)	0.395	2392.68	15	
	4	0.083	(2.96)	0.052	(4.07)	1.606	(5.70)	11.490	(7.79)	0.124	1597.32	6	
	5	0.027	(2.81)	0.000	(L)	49.153	(1.75)	0.01	(0.00)	0.232	5467.47	30(3)	
	6	0.057	(1.81)	0.040	(4.99)	2.271	(4.74)	64.307	(51.43)	0.102	1995.23	9	

Notes:- L, large values (larger than format specifications of the package).
Underlined parameter estimates correspond to the lower bounds that were set.

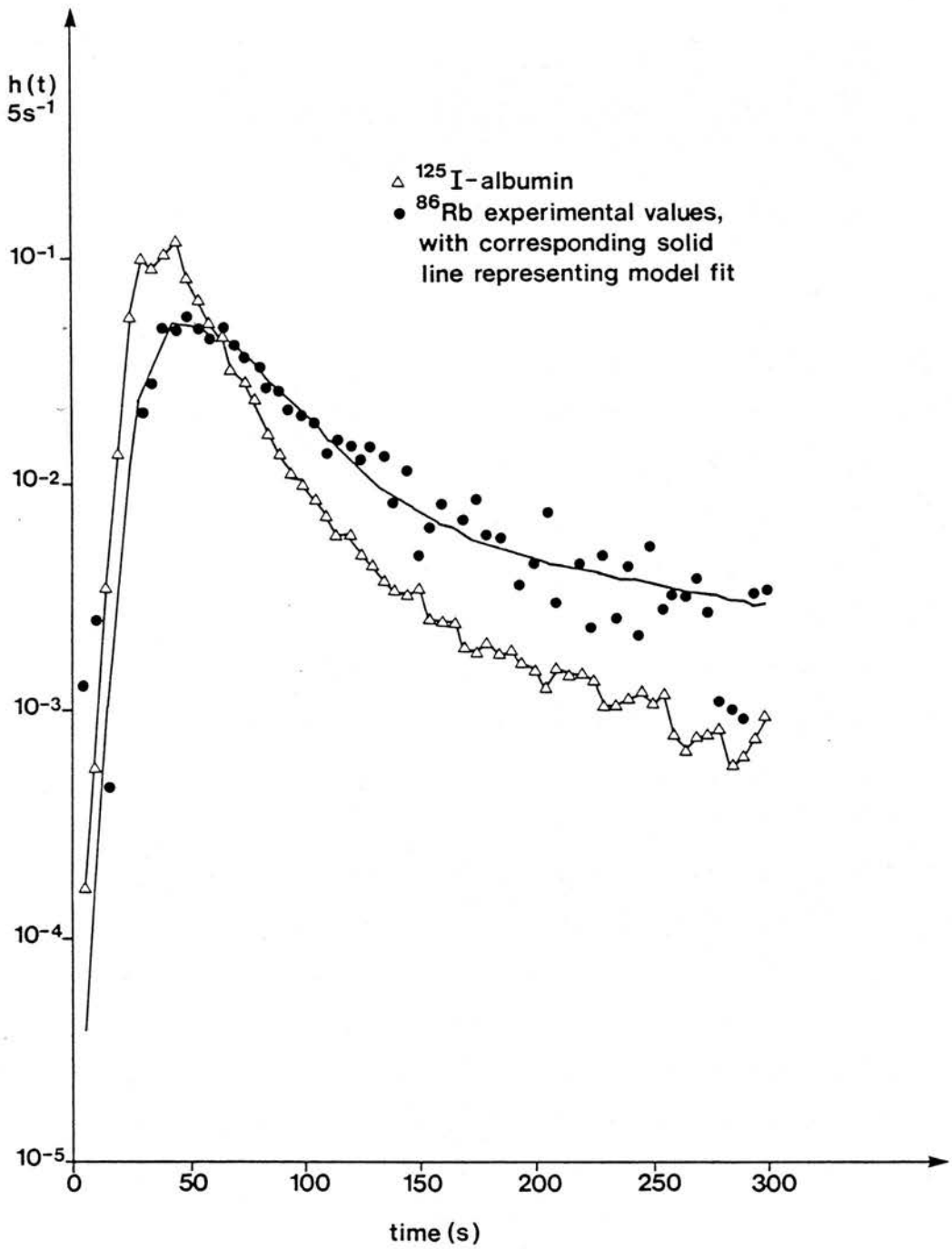

FIGURE 5-9 : Satisfactory model IIIa fit to ^{86}Rb data (experiment number 2) using a suitable form of the ^{125}I-albumin reference tracer outflow data as model input.

fits for noiseless data, shows that there is a tendency for PS_B to approach zero with the PS_C/F_s ratio decreasing.

TABLE 5-8

Mean ± s.d. of measures of fit (C.V.) and necessary CPU times for models II,IIIa and IIIb ; experimental numbers 1,2,4,6.

		Rb-86	Sr-85
Model II		0.183±0.023	0.113±0.017
Model IIIa	C.V.	0.183±0.024	0.103±0.012
Model IIIb		0.183±0.023	0.113±0.017
Model II		65.40±33.46	68.34±36.07
Model IIIa	CPU time (s)	1763.97±1152.47	1643.47±1024.52
Model IIIb		2013.24±1095.94	1931.96±227.63

Table 5-8 shows a comparison between the models in terms of measures of fit (C.V.) and the necessary CPU times to achieve the fits. The means and s.d.s from only 4 sets of data of ^{86}Rb and ^{85}Sr were used in the comparisons owing to fitting problems in the remaining two sets associated with model II. Although it was possible to fit more of the data satisfactorily with the multicapillary models, the C.V.s for all the models associated with the 4 sets of data are very similar, particularly for ^{86}Rb. Figure 5-9, illustrates a satisfactory model IIIa fit to ^{86}Rb data (experiment number 2), in which it can be appreciated that it is the substantial noise particularly in the latter part of the sampling period which causes the similarities in C.V. values i.e. its a case of noise impairing the expected improvement in fit. It is encouraging to observe however in table 5-8, that there seems to be improvements in fit associated with the ^{85}Sr data using the more realistic model IIIa.

The CPU times as described in table 5-8, shows that the more complex multicapillary models take much more time and computing resources to optimise the experimental data. Multicapillary optimisation took around 20-30

times longer to accomplish than single capillary optimisation and had to be achieved in background mode by the submission of queued batch jobs which ran overnight.

5.4.2. Comparison of model extractions & PS_C products

TABLE 5-9

Mean ± s.d. of E_{max} and PS_C for ^{86}Rb and ^{85}Sr (n=6) from different models.

	^{86}Rb	^{85}Sr
MODEL I (Crone-Renkin)		
E_{max}	0.73 ± 0.11	0.76 ± 0.12
PS_C (ml/s)	0.046 ± 0.014	0.052 ± 0.018
MODEL II		
E_{max}	0.73 ± 0.16	0.73 ± 0.16
PS_C (ml/s)	0.050 ± 0.023	0.047 ± 0.019
MODEL IIIa		
E_{max}	0.72 ± 0.17	0.70 ± 0.19
PS_C (ml/s)	0.047 ± 0.022	0.045 ± 0.021
MODEL IIIb		
E_{max}	0.85 ± 0.14	0.83 ± 0.15
PS_C (ml/s)	0.075 ± 0.032	0.066 ± 0.028

Table 5-9 shows the mean and s.d. of various model derived E_{max} and PS_C parameters using all 6 sets of ^{86}Rb and ^{85}Sr data. It can be seen that model IIIa values of PS_C and E_{max}, the latter obtained using equation (2.5) with average flow rates, are quite similar to values derived from models I and II. The expected increases in the PS_C parameter and hence E_{max} associated with multicapillary models were cancelled out by the partitioning of the flows to the cortex and marrow in model IIIa.

One can observe from table 5-9 (model IIIb), that E_{max} and PS_C tends to increase, thus becoming more applicable to cortical capillaries, as larger

proportions of the infusing flow is diverted to the cortex. The percentage increases seem to range between 0-18% (both tracers) and 0-60% (^{86}Rb), 0-47% (^{85}Sr) for E_{max} and PS_C respectively as progressively more than the calculated 65% of the nutrient artery flow supplies the cortex. The mean single capillary model II estimates of PS_C were approximately 0.7 times the model IIIb estimates which is quite similar to a systematic figure of around 0.8 (see figure 5-7 ; appropriate ratio $PS_C/F_s \sim 2\text{-}2.5$) obtained by fitting homogeneous flow models to hypothetical data from a multicapillary system having a normal distribution (relative dispersion = 35%) of flow rates.

5.4.3. Apparent volumes of distribution and PS_B

TABLE 5-10

Mean ± s.d. of V_I', V_B' and PS_B for ^{86}Rb and ^{85}Sr from models II, IIIa and IIIb ; experimental numbers in brackets.

		^{86}Rb	^{85}Sr
MODEL II	V_I' (ml)	0.822 ± 0.116	1.304 ± 0.389
MODEL IIIa	[1,2,4,6]	0.600 ± 0.074	0.768 ± 0.245
MODEL IIIb		1.042 ± 0.143	1.631 ± 0.485
MODEL II	V_B' (ml)	3.452 ± 1.607	7.732 ± 1.082
MODEL IIIa	[1,2,4]	2.564 ± 1.201	8.931 ± 1.386
MODEL IIIb		4.450 ± 2.097	9.969 ± 1.373
MODEL II	PS_B (ml/s)	0.021 ± 0.0075	0.034 ± 0.0070
MODEL IIIa	[1,2,4,6]	0.015 ± 0.0052	0.030 ± 0.0063
MODEL IIIb		0.025 ± 0.0092	0.041 ± 0.0084

Table 5-10 shows the mean ± s.d. values for the parameters V_I', V_B' and PS_B found for the diffusible tracers using various models. For comparison purposes, data appertaining to the quoted experimental numbers was used.

It can be seen that in the vast majority of cases with the only exception being

V_B' (^{85}Sr), the parameter estimates for model IIIa are less than those for the other models. Owing to the improvements in fitting larger proportions of the data, one may additionally calculate using experiment number 3, V_I' (^{86}Rb, n=5) = 0.693 $\pm$ 0.218 ml and V_I' (^{85}Sr, n=5) = 0.896 $\pm$ 0.356 ml (model IIIa). These quantities are best thought of in terms of measures of space in the defined tibial diaphysis bearing in mind that V_I' applies to marrow capillaries as well as cortical ones.

As to be expected from figure 5-7, model IIIb parameter estimates of V_I', V_B' and PS_B are accountably greater than model II predictions. With respect to model IIIa predictions, it appears that V_I', V_B' and PS_B can increase substantially as progressively more than the calculated 65% of the nutrient artery flow supplies the cortex.

5.4.4. Variances in model development ; effect on final parameter estimates (model IIIa)

The major sources of variance in the development of model IIIa and the subsequent parameter estimates, were considered to arise as a consequence of combining data from all the dogs. The variances were considered to stem from,

1. the effects of combining the fractional masses appertaining to the specific ranges of cortical flow rates from each tibia.

2. the effect of choosing Δf_5=1.08 to adequately represent an even spread of marrow rd_i values.

Numerical simulations were carried out to test these effects on the final parameter estimates concerning the ^{86}Rb and ^{85}Sr data of experiment 1. This

TABLE 5-11

Effects of:- 1. the variances in the fractional masses resulting from all 6 tibiae;

2. marrow flow rate class interval Δf_5;

on model IIIa parameter estimates of ^{86}Rb and ^{86}Sr data concerning experiment no. 1

	FRACTIONAL MASSES				FINAL PARAMETER ESTIMATES (^{86}Rb)				FINAL PARAMETER ESTIMATES (^{86}Sr)			
	$w_1 \cdot \Delta f_1$	$w_2 \cdot \Delta f_2$	$w_3 \cdot \Delta f_3$	$w_4 \cdot \Delta f_4$	PS_C(ml/s)	PS_B(ml/s)	V_I' (ml)	V_B' (ml)	PS_C(ml/s)	PS_B(ml/s)	V_I' (ml)	V_B' (ml)
Actual	0.226	0.378	0.253	0.143	0.082	0.014	0.490	1.938	0.068	0.031	0.523	8.381
Simulation												
1	0.171	0.419	0.293	0.117	0.078	0.014	0.476	1.898	0.066	0.030	0.504	8.105
2	0.266	0.394	0.219	0.121	0.080	0.014	0.474	1.886	0.068	0.031	0.488	8.066
3	0.327	0.328	0.226	0.119	0.081	0.014	0.479	1.894	0.069	0.031	0.494	8.170
4	0.286	0.323	0.211	0.180	0.086	0.015	0.514	2.009	0.071	0.031	0.566	8.805
5	0.282	0.304	0.274	0.140	0.082	0.015	0.496	1.952	0.068	0.031	0.534	8.521
Marrow Δf_5=1.08	Mean ± s.d. (n=5)				0.082±	0.014±	0.488±	1.928±	0.068±	0.031±	0.517±	8.333±
	(%c.v.)				0.003	0.0004	0.017	0.052	0.002	0.0002	0.032	0.319
					(3.73)	(2.61)	(3.45)	(2.71)	(2.71)	(0.75)	(6.26)	(3.83)
Marrow Δf_5=0.72	Mean ± s.d. (n=5)				0.081±	0.013±	0.447±	1.775±	0.092±	0.044±	0.248±	7.806±
	(%c.v.)				0.003	0.0003	0.016	0.046	0.007	0.0005	0.005	0.173
					(4.04)	(2.32)	(3.48)	(2.59)	(7.06)	(1.17)	(1.96)	(2.22)

particular set of diffusible tracer data produced the highest extractions, and required comparatively smaller CPU times to achieve optimisation.

Firstly, new cortical fractional masses $w_1\Delta f_1,...,w_4\Delta f_4$ were generated five times by way of using two NAG routines G05CCF and G05DDF which produced a non-repeatable Gaussian distribution of random numbers. Input to these routines were the mean and s.d. of the fractional masses as deduced in table 5-1, notably 0.226 $\pm$ 0.066, 0.378 $\pm$ 0.057, 0.253 $\pm$ 0.027 and 0.143 $\pm$ 0.027.

With each of these sets of new fractional masses, final parameter estimates were obtained for ^{86}Rb and ^{85}Sr data (experiment 1). This exercise was performed ten times, five times with the marrow flow rate class interval Δf_5 set at the pre-assigned value of 1.08 and five times at a reduced interval Δf_5=0.72.

Table 5-11 shows the mean $\pm$ s.d. concerning the results of all the simulations, given in full only for Δf_5=1.08 along with the actual parameter estimates. All 5 sets of the derived cortical masses are shown, in which underlined values lie outside 1 standard deviation from the actual mean. One can appreciate that with marrow Δf_5=1.08, the previously assigned value, the mean and s.d. of the parameter estimates resulting from the five simulations were very close to the actual parameter estimates. However when Δf_5=0.72, two different views of the mean and s.d.s of the parameter estimates emerged from the simulations. For the ^{86}Rb data, the choice of a reduced Δf_5 value caused no real effect on the parameter estimates which all relate equally to marrow and cortical capillaries and surrounding structures ; but this was not the case for the ^{85}Sr data. The effect of decreasing Δf_5 caused substantial increases and decreases in PS_C, PS_B and V_I', V_B' respectively. The reason for the fluctuations in the parameter estimates for ^{85}Sr was entirely due to having a 2 phase capillary-interstitial fluid system for describing ^{85}Sr kinetics in the marrow. The fluctuations in the

^{85}Sr parameter estimates was reassuring, suggesting that the pre-assigned marrow flow rate class interval $\Delta f_5=1.08$ was a sensible choice. This is because intuitively one would expect ^{86}Rb to have a higher PS_C value than ^{85}Sr and have comparable V_I' values. This appeared to be the case with $\Delta f_5=1.08$, but was certainly not the case with $\Delta f_5=0.72$.

5.4.5. Conclusions

Fitting the experimental data

The experimental outflow data for ^{86}Rb and ^{85}Sr in terms of quantity, was modelled far more successfully with the multicapillary models IIIa and IIIb, than with the homogeneous flow model II. For example, it was possible to fit both multicapillary models to all of the ^{86}Rb data, which was not the case with the single capillary model II. As far as ^{85}Sr was concerned, all the outflow data with the exception of experiment number 5, could satisfactorily be fitted with models IIIa and IIIb. The data concerning experiment number 5 was basically difficult to fit because the back diffusion of ^{85}Sr was not substantial until the later stages of the sampling period which was not conducive to the design of the models and resulted in parameter estimates suggesting two phase behaviour. As was observed in section 3.2.2., slower rates of decrease of E_{max} i.e. back diffusion for a particular tracer were always associated with low PS_C and high V' values. This was the case with the final parameter estimates for the ^{85}Sr data of experiment number 5 which produced the lowest and highest values of PS_C and V_I' respectively out of all the data.

Although it was possible to fit more of the data satisfactorily with the multicapillary models, the C.V.s for all the models associated with the data that

was easier to fit were essentially quite similar. This was due to noise in the data which impaired the expected improvements in the fit. The more physiologically accurate multicapillary model IIIa, however produced a lower average C.V. value for ^{85}Sr as opposed to the other models, which was encouraging.

The main disadvantage of using the multicapillary models to fit the experimental data was that very large amounts of CPU time were needed. The problem of reducing the CPU time seems difficult to overcome as adjudged from the noise simulation studies, in which constraining individual parameters caused no appreciable reduction. It would thus seem that more efficient optimisation routines are essential in reducing CPU times, thus enabling more sophisticated mathematical models to be used. Bassingthwaighte and colleagues infact employ sensitivity analysis in fitting their models to data (Bassingthwaighte *et al.* 1982 ; Bassingthwaighte and Chaloupka 1984). Sensitivity analysis has been proven to converge much quicker to final parameter estimates than more standard optimisation routines (Chan and Bassingthwaighte, personal communication).

Comparison of model parameters

After proceeding to great lengths to obtain parameter estimates from the multicapillary models, it would appear that model IIIa predictions of PS_C and hence E_{max} for ^{86}Rb and ^{85}Sr are hardly dissimilar to those obtained from the much simpler Crone Renkin formulation. The expected increase in the PS_C parameter as observed from the simulations involving the homogeneous flow modelling of heterogeneous outflow data, was cancelled out by the partitioning of the flows to the cortex and marrow in model IIIa.*

*The PS_C (^{86}Rb)/PS_C (^{85}Sr) ratio which was equal to 1.04 and not the corresponding free diffusion coefficient ratio of 1.58 suggests that the exchange is flow limited.

Increases however, were observed in the parameter estimates regarding ^{86}Rb and ^{85}Sr when the cortex multicapillary model IIIb was used. It was found that the PS_C parameters for both tracers i.e. PS_C (^{86}Rb) = 0.047 ± 0.022 and PS_C (^{85}Sr) = 0.045 ± 0.021 ml/s (both n=6) could increase by as much as 60% as progressively more than the calculated 65% of the nutrient artery flow supplied the cortex ; subsequent E_{max}s could increase by as much as 18%. Thus it may be the variation in the contributions of nutrient artery flow between greyhounds which may account for the differences in E_{max} and PS_C for each animal.

The systematic increases in PS_C for the tracers associated with model IIIb may be compared with predictions PS_C (Crone) from the Crone Renkin formulation. For ^{86}Rb and ^{85}Sr respectively, it was found that PS_C = (1.60 ± 0.40)PS_C(Crone) and PS_C = (1.28 ± 0.20)PS_C(Crone) :- both mean ± s.d., n=6. These relationships compare favourably with other authors' findings. Bassingthwaighte *et al.* (1985) using a similar model but with 5 pathways found that for D-glucose and L-ascorbate in rabbit heart perfusion studies, the model PS_C = (1.39 ± 0.47)PS_C(Crone). Similarly, Kuikka *et al.* (1986) found that for D- and 2-deoxy-D-glucose in dog heart perfusion studies, the model PS_C = (1.30 ± 0.23)PS_C(Crone).

Kuikka *et al.* (1986) also mentioned that estimates of PS_{pc} relating to their third phase of parenchymal cells were on the average quite similar for both single and multicapillary modelling ; the ratio (single/multiple) was 0.87 ± 0.28 (n=21). Although these investigators incorporated a fifth parameter of intracellular sequestration into their models, the ratio is nevertheless similar to a ratio (PS_B model II/PS_B model IIIb) = 0.81 ± 0.01 (n=8) derived from the successful model fits concerning both ^{86}Rb and ^{85}Sr. Also this ratio agrees with the expected magnitudes of underestimation from the homogeneous model simulation

studies. The agreement between these parameters and the PS_C parameters in addition is reassuring and lends credence to the development of multicapillary models IIIa and IIIb.

The estimates of V_I' and V_B' for both models IIIa and IIIb were not too greatly dissimilar to estimates from model II. Estimates of V_I' for ^{86}Rb and ^{85}Sr were found to be quite similar for the more realistic model IIIa. This is a useful finding in the sense that phenomena such as phase partition coefficients and tracer exclusion that apply to the tracers individually, may well only contribute minimally to the apparent volume of distribution V_I'. Thus the similarities in V_I' for each of the tracers could well to a large extent resemble anatomical volumes V_I, that are equivalent for both tracers, which could lend support to the use of extravascular '2-phase' tracers for determining V_I' which could then be constrained for modelling '3-phase' tracers in desired cases.

Effects of variances in model development on the parameter estimates

From the simulation studies it was found that the variances in the weighting functions for the cortical capillary systems associated with the combining of fractional masses from each tibia, caused no appreciable changes in the parameter estimates for ^{86}Rb and ^{85}Sr derived from model IIIa. However, quite large changes in the parameter estimates particularly for ^{85}Sr (2 phase marrow system) occurred when the class interval of the distribution of marrow flow rates was decreased from the pre-assigned value Δf_5=1.08. The parameter estimates for ^{86}Rb and ^{85}Sr at the pre-assigned class interval corresponding to an even spread of marrow flow rates were the most meaningful though, with PS_C (^{86}Rb) being expectedly greater than PS_C (^{85}Sr) and V_I' being approximately equal for both tracers.

To summarize, the parameter estimates generally are stable to the variances in the cortical weighting factors, and the pre-assigned weighting factor for the marrow seems a sensible choice.

TABLE 5-12

Parameter estimates of experimental ^{85}Sr data before (BP) and after (AP) PTH.
(* 24 hr parathyroidectomy). Maximum increment halvings = 30, V_C' = 0.0362 ml, n_x = (10,10,10,10,10) : Model IIIa

				FINAL PARAMETER ESTIMATES										
Expt No.	E_{net} 300s	E_{max}	(IIIa) E_{max}	PS_C ml/s	(%c.v.)	PS_B ml/s	(%c.v.)	V_I' ml	(%c.v.)	V_B' ml	(%c.v.)	C.V.	CPU Time(s)	LN (NTH)
1BP	0.59	0.77	0.74	0.022	(1.315)	0.030	(5.854)	2.007	(6.549)	121.090	(127.449)	0.092	816.21	9
1AP	0.49	0.73	0.72	0.021	(2.063)	0.033	(4.035)	0.533	(9.078)	21.339	(18.054)	0.100	1762.78	8
2BP	0.49	0.69	0.62	0.016	(3.115)	0.018	(16.349)	2.840	(15.142)	500.000	(-)	0.191	857.25	4
2AP	0.47	0.68	0.62	0.016	(4.694)	0.017	(48.251)	2.221	(25.906)	L	(L)	0.205	1789.40	17
3BP	0.37	0.68	0.60	0.015	(4.836)	0.017	(42.644)	1.591	(25.141)	6.995	(81.354)	0.275	424.15	10
3AP	0.33	0.68	0.54	0.013	(6.107)	0.0060	(70.524)	2.406	(24.665)	500.000	(-)	0.404	1019.01	30(1)
4BP	0.20	0.46	0.13	0.0023	(5.739)	0.000	(-)	500.000	(-)	-		0.202	3166.63	30(6)
4AP	0.19	0.37	0.14	0.0026	(4.558)	0.000	(-)	15.383	(635.638)	-		0.183	2653.29	30(4)
5BP	0.64	0.79	0.68	0.019	(4.748)	0.000	(-)	14.838	(60.117)	-		0.392	3437.45	30(4)
5AP	0.40	0.60	0.44	0.010	(7.283)	0.000	(-)	7.056	(33.450)	-		0.332	559.34	7
6BP	0.44	0.66	0.53	0.013	(5.019)	0.041	(22.105)	0.404	(42.061)	104.180	(280.587)	0.154	3546.78	7
6AP	0.32	0.49	0.36	0.0074	(3.910)	0.043	(44.656)	0.326	(44.159)	23.443	(72.472)	0.072	2073.10	10
7BP	0.41	0.65	0.51	0.012	(3.483)	0.026	(35.465)	1.958	(29.334)	12.160	(69.912)	0.161	1100.46	7
7AP*	0.28	0.56	0.46	0.010	(2.580)	0.0074	(70.433)	1.541	(16.255)	2.380	(94.063)	0.121	343.42	3
8BP	0.29	0.50	0.42	0.0092	(4.708)	0.015	(19.045)	0.611	(24.157)	16.643	(112.748)	0.138	654.30	5
8AP*	0.28	0.49	0.41	0.0088	(3.806)	0.011	(36.724)	1.092	(21.481)	12.722	(241.340)	0.135	906.63	6

LN (NTH) : Largest No. of increment halvings required (No. of times for maximum)

L : Large, value is larger than format specifications of package.

_____ : underlined values are those at parameter bounds.

5.5. RESULTS OF MODEL IIIA OPTIMISATION TO M.T.O.D. DATA CONCERNING PTH

5.5.1. Fitting the experimental data :- final parameter estimates

M.T.O.D. data obtained from parathyroidectomised greyhounds before (BP) and after (AP) the administration of PTH (see section 2.2.2.) was optimized using model IIIa to investigate if there were any substantial changes in the parameter estimates for ^{85}Sr when the bone physiology was effectively perturbed ; no changes in perfusion pressure had been observed due to the PTH.

Table 5-12 shows the results of these parameter estimates along with calculable model I parameters such as E_{max}, and E_{net} at 300 s. Although these latter parameters could be obtained from all 16 sets of data from 8 dogs, it was not possible to achieve this for the model IIIa parameters. Successful fitting as adjudged by low numbers of increment halvings was obtained in 12 out of 16 sets of data. Parameter estimates from the 4 unsuccessful fits tended to support a two phase capillary-interstitial fluid system which was lacking in physiological significance. Analysis of the particular experimental data showed that the highest calculable extractions for ^{85}Sr occurred relatively late in the sampling period which was not conducive to the performance of model IIIa.

Table 5-13 shows mean and s.d.s of the model parameters for ^{85}Sr for comparison purposes, before and after administration of PTH. Student's paired t tests were carried out on all the individual sets of parameters (a) and (b) as described in table 5-13, to test for significance ($P<0.05$).

TABLE 5-13

Comparison of model parameters concerning ^{85}Sr before and after administration of PTH. For model IIIa, experimental numbers used in the analyses in brackets.

	(a) Sr-85 before PTH	(b) Sr-85 after PTH	Sig. between (a) & (b)
MODEL I (n=8)			
E_{max}	0.65±0.12	0.58±0.12	P<0.05 7 d.f.
E_{net} (300 s)	0.43±0.15	0.35±0.10	P<0.05 7 d.f.
MODEL IIIa			
E_{max} [1,2,6,7,8]	0.56±0.12	0.51±0.15	N.S. 4 d.f.
PS_C(ml/s)[1,2,6,7,8]	0.014±0.005	0.013±0.006	N.S. 4 d.f.
PS_B(ml/s)[1,2,6,7,8]	0.026±0.010	0.022±0.015	N.S. 4 d.f.
V_I'(ml) [1,2,6,7,8]	1.564±1.029	1.143±0.769	N.S. 4 d.f.
V_B'(ml) [1,6,7,8]	63.52±57.16	14.97±9.59	P<0.02 3 d.f.*

Notes

Paired student's t test :- * result obtained by normalizing data (a) to unity & scaling in accordance.

Utilizing all 8 sets of data, significant decreases ($P<0.05$) in E_{max} and E_{net} (300 s) for ^{85}Sr were found from model I. It was not possible though to analyse all the data with regard to significance testing of parameter estimates for model IIIa ; only 5 sets of the data in most instances were used owing to difficulties in fitting the other data sets. From the model IIIa ^{85}Sr parameter estimates, no significant changes occurred in PS_C (hence E_{max}), PS_B and V_I' following the administration of PTH.

The lack of significance for model IIIa ^{85}Sr E_{max} is contrary to the findings concerning model I using all 8 sets of data. However, when only the appropriate 5 sets of data were analysed from model I, the suspected decrease in ^{85}Sr E_{max} following PTH administration was not significant whilst the suspected decrease in ^{85}Sr E_{net} (300 s) was still significant ($P<0.05$).

From table 5-12, one can appreciate in experimental numbers 1,6,7,8 that there are noticeable decreases in V_B' following PTH administration, but significance can't readily be proved owing to the large variabilities in magnitude of each of the values. A significant result for V_B' ($P<0.02$, see table 5-13) however can be obtained if the estimates for each dog are scaled by similar factors such that V_B' estimates before PTH were equal to unity. This approach seems reasonable, by virtue of the fact that the outflow data tends to be noisy particularly in the latter outflow samples. This results in large variations in V_B' when optimising data between runs in the same greyhounds and when optimising data from different greyhounds. Furthermore, a decrease in V_B' following PTH administration readily explains the significant decreases in ^{85}Sr E_{net} (300 s), bearing in mind that no significant changes were observed in the other parameters. If V_B' is decreased with the other parameters remaining unchanged then larger effluxes of ^{85}Sr (back diffusion) to the capillaries would result, hence lowering the value of E_{net} (300 s).

5.5.2. Conclusions

Perhaps the most significant finding from modelling the outflow data was the decrease in ^{85}Sr E_{net} (300 s) after the administration of PTH, which strongly suggests an inhibition of ^{85}Sr uptake. However, with model I it was difficult to ascertain whether these changes were attributable to decreases in E_{max} or perhaps some other factors ; the subsequent problems of obtaining appropriate measurements of E_{max} having already been discussed in chapter 2. Therefore in attempting to make realistic conclusions about a very variable physiological system it was better to deal with the more improved model IIIa which was much more adequate than model I.

The fact that only 5 sets of parameter estimates out of a possible 8 sets could

be used for analysis is not disastrous. It merely underlines the problems of interpreting the data from an extremely variable system.

Using the model IIIa, it would appear that the inhibition of ^{85}Sr uptake following PTH is best explained by a decrease in the parameter of V_B', even though it is difficult to attach any statistical significance to this finding. An important question to be answered however, is whether this decrease is due to a reduction in size of the specified apparent volume of distribution of the bone surface binding pool or is due to changes relating to active or asymmetric transport which may manifest themselves in V_B'.

CHAPTER 6

INVESTIGATION OF LARGE VESSEL DISPERSION & ASYMMETRIC TRANSPORT OF TRACER

6.1. LARGE VESSEL DISPERSION

6.1.1. The use of gamma variates to study large vessel dispersion

Throughout the course of using the models, shifted forms of the reference transport function describing the large vessel dispersion in the arteries and veins have been used as model input. The question which arises is how robust are these input functions, and can varying degrees of dispersion in the arterial and venous systems affect their overall forms. Furthermore, can the diffusible tracer outflow profiles be strongly influenced by such dispersion as well. The answer to these questions is provided by the use of gamma variates to study large vessel dispersion.

The gamma variate is essentially another mathematical function that can be used to describe outflow dilution curves (Thompson Jr. *et al* 1964 ; Davenport 1983). The expression for a gamma variate $h(\alpha,\beta;t)$ having parameters α ($\alpha>-1$) and β and an independent variable time t is

$$h(\alpha,\beta;t) = \frac{t^{\alpha} e^{-t/\beta}}{\beta^{\alpha+1} \cdot \int_0^{\infty} x\, e^{-x} dx} \qquad (6.1)$$

If α belongs to the set of positive real integers, then the gamma variate can be simply written as

FIGURE 6-1 : Gamma variate curves of varied α and β parameter values.

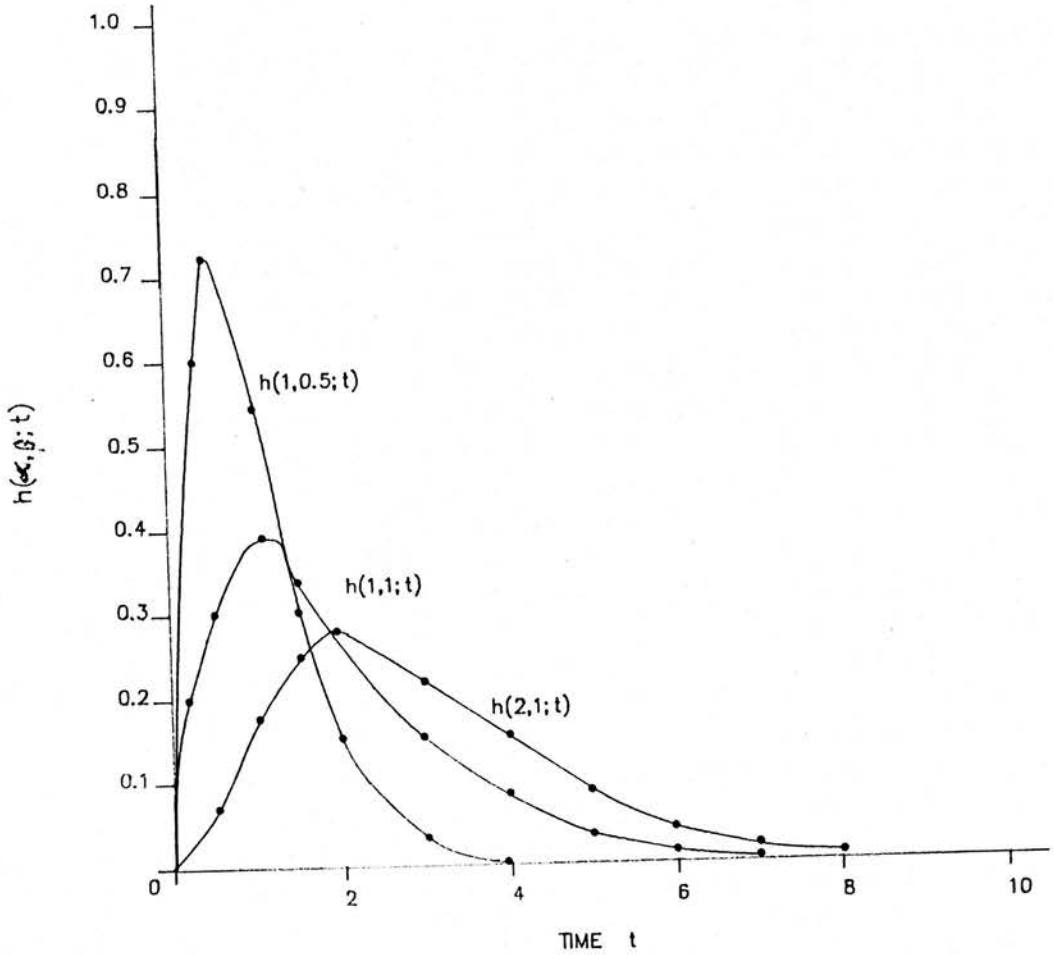

$$h(\alpha,\beta;t) = \frac{t^{\alpha} e^{-t/\beta}}{\beta^{\alpha+1}.\alpha!} \qquad (6.2)$$

Figure 6-1 illustrates gamma variate curves with different parameter values.

The most important result however concerning the gamma variate is

$$h_1(\alpha_1,\beta;t) * h_2(\alpha_2,\beta;t) = h_3(\alpha_1+\alpha_2+1,\beta;t) \qquad (6.3)$$

i.e the convolution of two gamma variates with the same β parameter yields another third gamma variate defined by the same β parameter and an α parameter which is equal to one plus the summation of the α parameters of the other 2 gamma variates. This result also exists when there are time delays t_1 and t_2 i.e.

$$h_1(\alpha_1,\beta;t-t_1)*h_2(\alpha_2,\beta;t-t_2) = h_3(\alpha_1+\alpha_2+1,\beta;t-(t_1+t_2)) \qquad (6.4)$$

From equations (6.3) and (6.4), one can appreciate the usefulness of the gamma variate as opposed to functions such as the lagged normal density function in so far as studying dispersion and delay in components of systems.

6.1.2. Outcome of applying gamma variates to the experimental model

In the context of investigating large vessel dispersion via the reference tracer outflow profile $h_R(t)$, equation (6.4) can be written as,

$$h_A(\alpha_1,\beta;t-T_C)*h_V(\alpha_2,\beta;t-t_V) = h_R(\alpha_1+\alpha_2+1,\beta;t-(T_C+t_V)) \qquad (6.5)$$

where T_C is the capillary transit time and t_V is a delay time for the venous system. The gamma variate $h_A(\alpha_1,\beta;t-T_C)$ essentially represents the tracer emerging from a single capillary system of transit time T_C, having experienced dispersion in the arterial system. Convoluting $h_A(\alpha_1,\beta;t-T_C)$ with a gamma

variate $h_V(\alpha_2,\beta;t-t_V)$ describing dispersion and delay in the venous system, produces the reference outflow gamma variate $h_R(\alpha_1+\alpha_2+1,\beta;t-(T_C+t_V))$. The result (6.5) confirms that the shifted reference tracer outflow profile must always be a robust model input i.e. varying degrees of arterial, venous dispersion and delay as produced by combinational changes of α_1, α_2 and T_C, t_V respectively will not alter its form.

The robustness of the model input was demonstrated by firstly, obtaining a representative gamma variate form of the reference tracer outflow profile. This form represented by $5h_R(7, 5.75; t)$ was obtained by trial and error, juggling the α and β parameters. The constant multiplying figure of 5 was assigned to the gamma variate because typical reference tracer outflow profiles are constructed such that the area beneath them is 5 and not unity as in the case of gamma variates. The choice of an odd number of 7 for the α parameter was deliberate, enabling equal amounts of venous and arterial gamma variate dispersion ($\alpha_1=\alpha_2=3$) to be studied.

With appropriate parameters of the capillary-tissue system kept simple i.e. $PS_C=0$; $V_C'=0.036$ ml, $F_s=0.036$ ml/s producing $T_C=1$ s, a suitable gamma variate $h_A(\alpha_1, 5.75; t)$ was used as model input and the output $h_A(\alpha_1, 5.75; t-1)$ was convoluted with $h_V(\alpha_2, 5.75; t-4)$ for the venous system to produce the reference outflow profile as follows,

$$5[h_A(\alpha_1,5.75,t-1)*h_V(\alpha_2,5.75,t-4)] = 5h_R(7,5.75;t-5) \qquad (6.6)$$

A time delay of 4 s was assigned to the venous system. The convolution was achieved by numerical means using the formulation (Bassingthwaighte 1967)

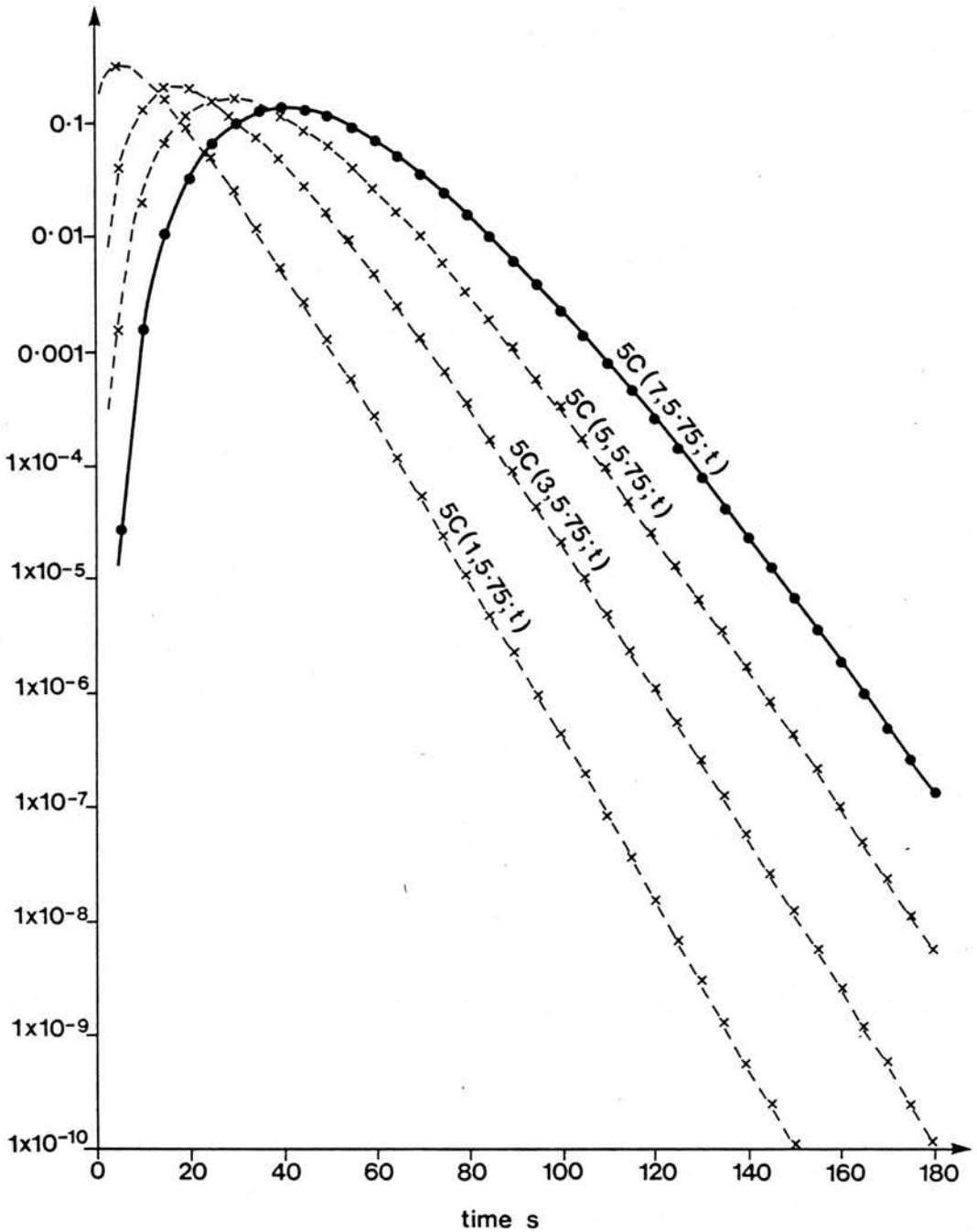

FIGURE 6-2 : Gamma variate profiles simulating dispersion in the arteries and veins, along with a representative reference outflow profile form :- 5C(7, 5.75; t). Profiles are only illustrated between 0 and 180 s.

$$h_{R_n} = \sum_{i=1}^{n} h_{A_i} . h_{V_{n-i+1}} \qquad (6.7)$$

where h_A, h_V and h_R were sequences of pulses of duration Δt = 1 s, and n was the total number of pulses.

Equation (6.6) was found to be satisfied because suitable combinations of $h_A(\alpha_1, 5.75, t-1)$ and $h_V(\alpha_2, 5.75; t-4)$ i.e. $\alpha_1=\alpha_2=3$; $\alpha_1=1$, $\alpha_2=5$ when convoluted exactly reproduced the reference outflow gamma variate values. Figure 6-2 shows these gamma variate forms (without time delays), so that degrees of dispersion can be appreciated.

The whole exercise of using gamma variates as described was repeated again with the exception that $PS_C \neq 0$. It was found that similar combinations of the gamma variates when convoluted, always produced the same numerical output which effectively represented hypothetical diffusible tracer outflow values. It was thus reassuring to find that diffusible outflow data as well as reference outflow data was robust to changes in large vessel dispersion.

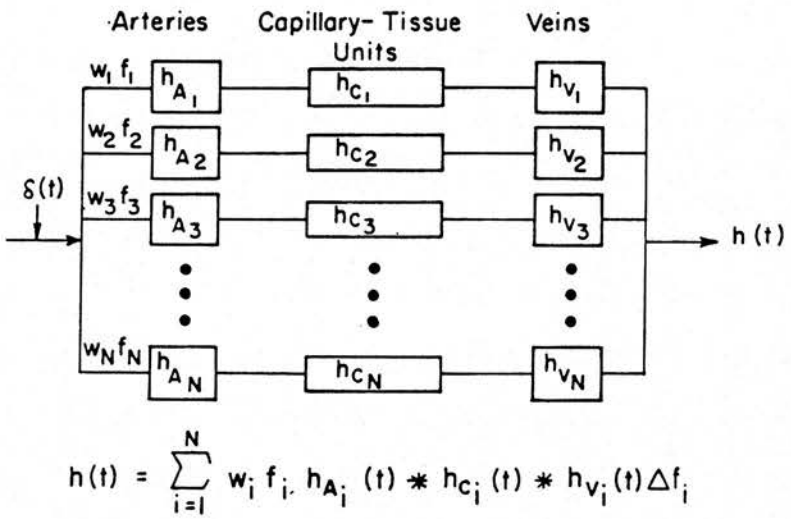

$$h(t) = \sum_{i=1}^{N} w_i f_i \, h_{A_i}(t) * h_{C_i}(t) * h_{V_i}(t) \Delta f_i$$

FIGURE 6-3 : Capillary-tissue transport model IV with specifically defined relationships between transit times in large vessels and in capillaries.

6.2. DEPENDENCE BETWEEN LARGE VESSEL & CAPILLARY TRANSIT TIMES

6.2.1. Description of a time dependent multicapillary model IV

The models that have so far been used, have been such that large vessel transport has been independent of capillary transit times i.e. the input function $h_{LV}(t)$ has been identical in terms of shape at exactly the same values of time t for each of the capillary systems. The identicalness in the shape reflects equal amounts of dispersion and the exactness in time infers that capillaries with varying transit times are associated with large vessels having identical transit times. Apart from the equivalence of dispersion which is difficult to investigate, the latter point concerning the transit times is questionable. Intuitively, one would expect capillaries having the shortest transit times to be associated with large vessels also having the shortest transit times and *vice versa*.

To investigate capillary and large vessel transit times with respect to tracer exchange, a model IV attributable to Rose and Goresky (1976) was employed. Figure 6-3 illustrates this model, in which the microsphere derived weighting functions apply more to large vessel-capillary systems i.e.

$$h(t) = \sum w_i \Delta f_i f_i [h_{LV_i}(t) * h_{C_i}(t)] \qquad (6.8)$$

where

$$h_{LV_i}(t) = h_{A_i}(t) * h_{V_i}(t) \qquad (6.9)$$

Model IV has so far been used with the requisite of the intravascular pathways being non-dispersive i.e. $h_R(t)=\delta(t - (T_{LV} + T_C))$ and the large vessel transit

times T_{LV} being linearly related to T_C (Rose and Goresky 1976 ; Rose *et al* 1977).

6.2.2. The use of model IV in hypothetical studies

Model IV was essentially used to generate hypothetical reference and diffusible outflow data which was consequently optimized with model IIIa to identify systematic changes in parameter estimates associated with exchange when there was a dependence in transit times of the vasculature. The study was undertaken in an attempt to explain the poorer fits of experimental data concerning model IIIa.

The hypothetical model IV data was generated by using delayed forms of weighted lagged normal density curves as input to model IIIa. The lagged normal density curves were similar in terms of shape i.e. the amount of dispersion associated with each capillary system was assumed constant. Furthermore, the magnitude of the delays t_{LV_i} regarded as the sum of arterial t_{A_i} and venous t_{V_i} delays were considered to be proportional to each of the capillary transit times T_{C_i} i.e.

$$t_{LV_i} = K.T_{C_i} \qquad (6.10)$$

To avoid computation difficulties in producing the exact time delays, capillary transit times to one decimal place resembling values associated with the experimental data were used. T_{C_i} values were 3.5, 1.9, 1.3, 0.9 and 3.1 s.

On the basis of average transport behaviour, a mean transit time $\bar{T}$ = 61.2 $\pm$ 9.8 s (F_s = 2 ml/min) was calculated as such, using each of the 60 reference outflow sample values $h_R(t)_i$, at times t_i i.e.

$$\bar{T} = \sum_{i=1}^{60} t_i h_R(t)_i \; / \; \sum_{i=1}^{60} h_R(t)_i \qquad (6.11)$$

Furthermore, an average capillary transit time $\bar{T}_C$ = 1.5 s was calculated using the weighting functions W(i) i.e.

$$\bar{T}_C = \sum_{i=1}^{5} W(i) T_{C_i} \; / \; \sum_{i=1}^{5} W(i) \qquad (6.12)$$

Using $\bar{T}$ and $\bar{T}_C$, a value of K≈40 was deduced from average transit times i.e.

$$K = (\bar{T} - \bar{T}_C) \; / \; \bar{T}_C \qquad (6.13)$$

Hence K values ranging from 1-40 were considered in the generation of the hypothetical outflow data using appropriate microsphere derived weighting factors W(i). For the hypothetical diffusible outflow profiles, typical parameters of PS_C=0.05 ml/s, PS_B=0.025 ml/s, V_I'=1.0 ml, V_B'=5.0 ml and V_C'=0.036 ml were used. Furthermore, hypothetical diffusible outflow profiles were generated such that they simulated ^{86}Rb (3 phases-marrow) and ^{85}Sr (2 phases-marrow) exchange behaviour.

After all of the data had been generated, the hypothetical model IV reference outflow results were suitably modified in accordance with the methods of model IIIa and optimized to the diffusible outflow results using model IIIa.

6.2.3. Systematic errors in parameter estimates when fitting model IIIa to hypothetical data derived from model IV

Figures 6-4 a and b illustrate model IIIa fits to model IV diffusible outflow data of varied K values simulating ^{86}Rb and ^{85}Sr exchange behaviour respectively.

FIGURE 6-4 : Model IIIa fits to hypothetical model IV outflow data concerning 3 and 2 phase marrow capillary systems. The diffusible outflow data was generated using parameters of PS_C=0.05 ml/s, PS_B=0.025 ml/s, V_I'=1.0 ml, V_B'=5.0 ml and V_C'=0.036 ml. Average flow rates, $\bar{F}_{s/Co}$=0.02 ml/s and $\bar{F}_{s/M}$=0.01 ml/s were used in addition.

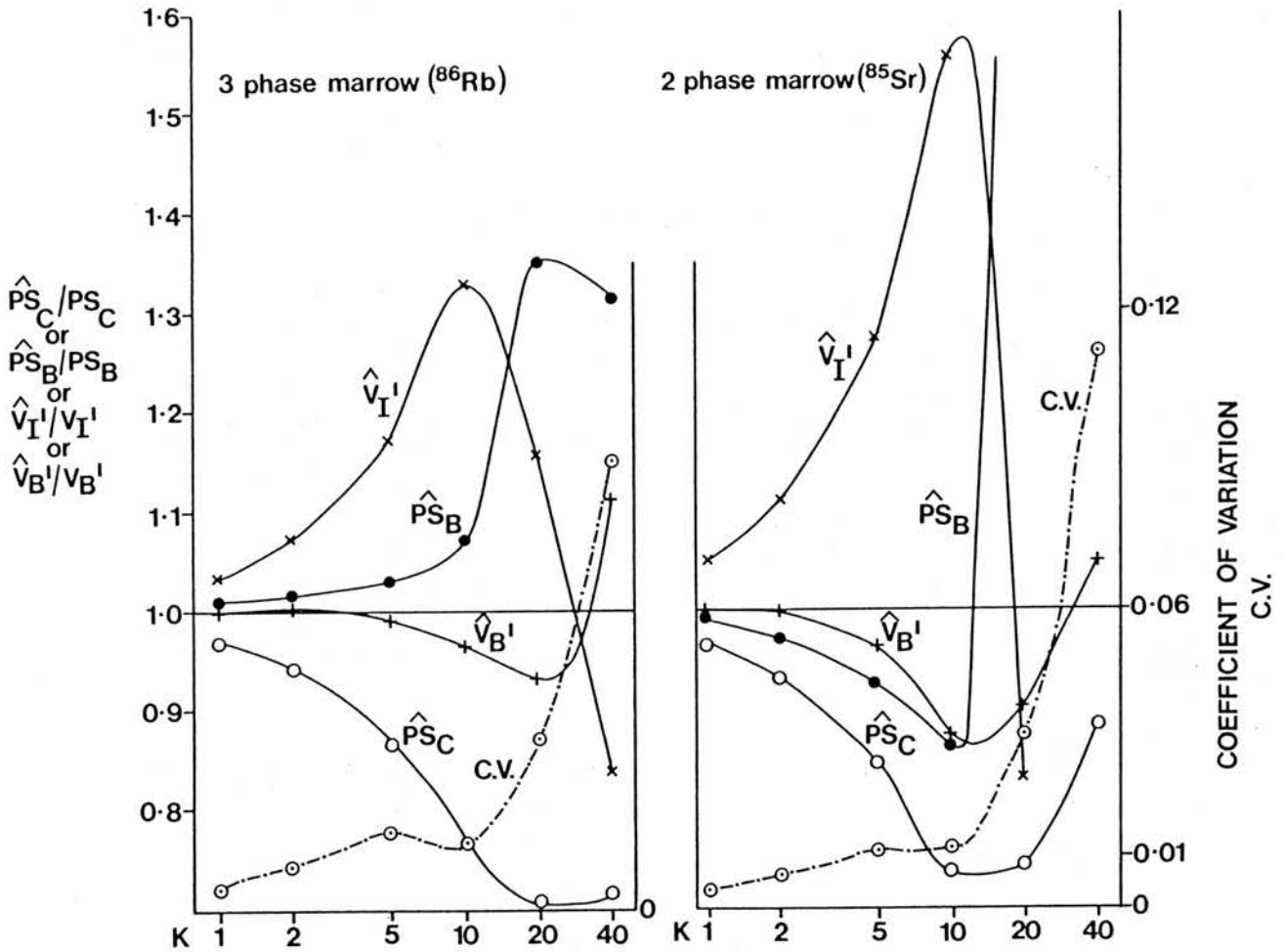

In similar fashion to section 5.3.1. the parameters with carets denoted estimates and those without represented true values.

One can generally observe that the measure of fit deteriorated with increasing K values and the parameter $\hat{PS}_C$ was always underestimated. Additionally, there was a strong tendency for $\hat{V}_I'$ parameters to be overestimated for ranges of K values between 1 and 20. The $\hat{V}_B'$ parameter appeared to be the least affected parameter in terms of systematic changes, whilst the behaviour of the $\hat{PS}_B$ parameter was largely due to the number of phases assigned to the marrow capillary systems. For the 2 phase marrow system the $\hat{PS}_B/PS_B$ ratio became greater than 2.0 for K values exceeding 20.

The systematic decreases and increases of $\hat{PS}_C$ and $\hat{V}_I'$ respectively can be compared with the parameter estimates of ^{14}C-sucrose obtained from a variety of single capillary models by Rose and Goresky (1976). Their parameter estimates of k_s (s^{-1}) and Φ (s^{-1}) were equivalent to PS_C/V_I' and F_s/V_I' respectively. Generally, parameter estimates of Φ and the quantity k_s/Φ were greater for single capillary models of varying capillary and large vessel transit times as opposed to such models in which the capillary transit time was constant and independent of large vessel transit times. This implied that the parameters of PS_C and V_I' were actually larger and smaller respectively for the former model as opposed to the latter which approved the systematic changes in these parameters as observed in figure 6-4.

In conclusion, the systematic changes in the parameters did not explain the poorer fits of experimental data with model IIIa. The two phase behaviour with PS_B tending towards zero, the usual hallmark of poor fitting did not seem apparent from the systematic changes in the parameters. Although fitting for ^{86}Rb was generally successful, the systematic underestimations of PS_B as

illustrated (2 phase marrow capillary system) were not large enough in magnitude to account for PS_B tending towards zero. Furthermore, PS_B tended to be overestimated for K values greater than 10.

6.3. ASYMMETRIC TRANSPORT OF TRACERS

6.3.1. The interpretation of existing parameter estimates

So far, the existing final parameter estimates have been derived from the solutions of the 3 P.D.E.s (equations 3.3) involving passive permeability-surface area PS products and apparent volumes of distribution V'. It has not been feasible as yet, to relate to the true anatomical volumes of distribution for the various tracers because complications arise, owing to effects such as volume exclusion, phase partition coefficients, tracer binding and asymmetric or active transport. It is this latter effect that is of most interest, in so far as how does asymmetric transport, in which permeabilities are different on both sides of the barrier, affect the final parameter estimates in the passive barrier optimisation process. Can the possible changes throw light on existing experimental findings especially for the PTH experiments involving ^{85}Sr, where the other effects such as volume exclusion and phase partition coefficients may or may not be of great importance.

6.3.2. Effects of optimising outflow data involving asymmetric transport with the existing passive barrier models

To investigate asymmetric transport on final parameter estimates, hypothetical diffusible outflow data was generated using a lagged normal density curve as input to the homogeneous model II. Many different sets of data were obtained by varying the parameters $PS_{C/12}$, $PS_{C/21}$, $PS_{B/23}$ and $PS_{B/32}$. $PS_{C/12}$ was the permeability-surface area product for tracer influx across the capillary from phase 1 (vascular) to phase 2 (interstitial fluid) ; *vice versa* for $PS_{C/21}$ describing tracer efflux. Additionally, $PS_{B/23}$ was the permeability-surface area

TABLE 6-1

Optimisation of homogeneous Model II (passive barrier parameters) to hypothetical outflow data (Model II) derived after asymmetric transport in system, in which F_s = 0.033 ml/s, V_C = 0.0362 ml, V_I = 1.0 ml, V_B = 5.0 ml.

Hypothetical Model II outflow data generated using (ml/s)				Model II Optimisation - Passive barrier parameters			
$PS_{C/12}$	$PS_{C/21}$	$PS_{B/23}$	$PS_{B/32}$	PS_C(ml/s)	PS_B(ml/s)	V_I' (ml)	V_B' (ml)
0.06	0.04			0.060	0.037	1.493	7.465
0.08	0.02	0.025	0.025	0.080	0.100	4.000	20.006
0.04	0.06			0.040	0.017	0.667	3.335
0.02	0.08			0.020	0.0063	0.250	1.251
		0.03	0.02	0.050	0.030	1.000	7.465
0.05	0.05	0.04	0.01	0.050	0.040	1.000	20.005
		0.02	0.03	0.050	0.020	1.000	3.335
		0.01	0.04	0.050	0.010	1.000	1.251
0.06	0.04	0.03	0.02	0.060	0.045	1.493	11.142
0.04	0.06	0.02	0.03	0.040	0.013	0.667	2.223

product for tracer influx across the bone surface/bone cell from phase 2 (interstitial fluid) to phase 3 (bone) ; *vice versa* for $PS_{B/32}$. All other parameters of the system such as flow and apparent volumes of distribution were constant. The hypothetical diffusible outflow data was optimized in the usual manner with passive barrier parameters PS_C and PS_B and the apparent volumes of distribution V_I' and V_B'.

Table 6-1 illustrates the effects of asymmetric transport of known barrier conditions on the final optimizable parameter estimates. For the first 4 sets of results in which asymmetric transport was just applicable to the capillary, one can observe that the final parameter estimates for PS_C were exactly equal to the $PS_{C/12}$ parameter describing the influx of tracer across the capillary wall. The picture of parametric changes however became more apparent when asymmetric transport was just confined to the bone i.e. the second set of results. In these circumstances, it was observed that the final parameters of PS_C and PS_B were always exactly equal to their respective influx barrier parameters of $PS_{C/12}$ and $PS_{B/23}$ and the interstitial fluid volume parameter was exactly obtained. Final parameter estimates were also obtained in two instances when asymmetric transport was applying to both the capillary and bone barriers.

Exact relationships between the passive barrier optimisation parameters and the asymmetric transport parameters were consequently deduced as,

$$PS_C = PS_{C/12} \qquad (6.14)$$

$$PS_B = (PS_{C/12} / PS_{C/21}).PS_{B/23} \quad (6.15)$$

$$V_I' = (PS_{C/12} / PS_{C/21}).V_I \quad (6.16)$$

$$V_B' = (PS_{C/12} / PS_{C/21}).(PS_{B/23} / PS_{B/32}).V_B \quad (6.17)$$

The constant V_I and V_B parameters which were used to generate the hypothetical outflow data, were in these circumstances regarded as anatomical volumes with the subsequent apparent volumes of distribution V_I' and V_B' occurring solely as a consequence of asymmetric transport. The relationship between V_I' and V_I was identical to a relationship perceived by Bassingthwaighte and Goresky (1984) which was for a 2 phase capillary-interstitial fluid system.

The aforementioned relationships were exactly obtained even when the procedures were repeated using the multicapillary model IIIa, with 2 and 3 phase marrow capillary systems.

6.3.3. Conclusions

It would appear that the existing parameter estimates of M.T.O.D. data may have information to conceal. Apart from the PS_C parameter which exactly represents the influx of tracer $PS_{C/12}$ through the capillary walls, the other three parameters actually represent to an extent the various types of barrier exchange processes involved in asymmetric transport.

The relationship for V_I' in terms of $PS_{C/12}$ and $PS_{C/21}$ was a very useful finding, even though it was surprising that properties of the adjacent third phase were not involved. Similarities in the V_I' parameters for differing diffusible tracers would tend to infer that their individual influxes and effluxes through the capillary walls were similar, and that passive transport processes either side of the wall were very likely. One would then be able to deduce information about other properties of the system i.e. the PS_B parameter would accurately predict the influx of tracer $PS_{B/23}$ to the bone phase. If similarities in V_I' were obtained for a particular diffusible tracer in control states and states where the bone physiology had been perturbed, then any significant differences in either PS_B or V_B' would reflect active transport between the interstitial fluid and bone phases. However, if similarities in V_I' did not exist between the states i.e. the influx or efflux of tracer through the capillaries had been changed, then it would be very difficult to make measurements of uptake mechanisms beyond the capillary wall.

Examining the final parameter estimates for ^{86}Rb and ^{85}Sr in view of these findings, suggests that tracer effluxes from the interstitial fluid to the capillary are by passive diffusion which has already been established for influxes in the opposite direction (Kelly and Bassingthwaighte 1977). The similarities in the V_I' parameters for both tracers as obtained from the more realistic model IIIa makes this suggestion reasonable. One can therefore further conclude by virtue of the fact that PS_B is larger for ^{85}Sr than ^{86}Rb, that uptake to the bone surface occurs more rapidly than cellular uptake.

Examining the ^{85}Sr final parameter estimates from the PTH experiments, one may conclude from the similarities in V_I' parameters, that PTH does not impair the passive diffusion transport properties of ^{85}Sr either side of the capillary wall. Furthermore, similarities in the PS_B parameters suggests that tracer

influxes to the bone surface are not impaired by PTH in addition. The speculated decreases in V_B' following PTH however, may suggest that the bone surface for ^{85}Sr uptake has been reduced or that active transport processes concerning effluxes from the bone to the interstitial fluid may increase.

CHAPTER 7

CONCLUSIONS & FUTURE WORK

In concluding this thesis, it may be useful to consider to what extent the objectives of the thesis, as set out on page 24 have been met.

Assessing the first objective, it can be concluded that the existing information on ^{85}Sr and ^{86}Rb uptake from M.T.O.D. techniques is not as clear cut as may have seemed. Problems relating to back diffusion and heterogeneous capillary blood flow rates have posed difficulties in interpreting the venous outflow results for the purpose of making measurements. However, it is evident from single capillary modelling that maximum instantaneous extractions obtained from M.T.O.D. data provide the best estimates of actual bone capillary extractions and subsequent PS_C products for diffusible tracers. Thus from tables 2-2 and 2-3 it would seem that E_{max} figures of approximately 0.7-0.8 (^{85}Sr) and 0.7 (^{86}Rb) respectively are the most realistic. ^{85}Sr is retained in greater amounts compared with ^{86}Rb as judged from E_{net} (5 min) figures of 0.48 ± 0.11 and 0.38 ± 0.11 respectively.

Passive diffusion is certainly the mechanism for the transport of tracer analogues of bone across the capillaries. Investigators such as Davies et al. (1976) and Kelly and Bassingthwaighte (1977) have shown that ratios of PS_C products, notably for ^{85}Sr and $Na^{18}F$ with ^{14}C-Sucrose are in close agreement with corresponding ratios of free diffusion coefficients. This is not the case when the tracers of

^{42}K and ^{86}Rb are considered. Complications may arise owing to ^{42}K and ^{86}Rb uptake to endothelial cells and differing uptake rates to cellular types in the marrow and cortex.

Parathyroid hormone (PTH) does not appear to impair the passive diffusion of ^{85}Sr across bone capillaries. ^{85}Sr E_{max} figures have never been significantly different in various states of parathyroidism. However from M.T.O.D. procedures performed on parathyroidectomised greyhounds (McCarthy and Hughes, unpublished data), ^{85}Sr E_{net} (5 min) values were significantly lowered after administering PTH one minute prior to sampling. This finding suggests that PTH exerts a rapid and direct effect on blood-bone disequilibrium inhibiting the uptake of ^{85}Sr to the matrix.

As described in chapter 3, a simple homogeneous flow model (single capillary model II) of uniform flow rates was developed to further interpret the ^{85}Sr and ^{86}Rb outflow data. The model which described tracer exchange to Haversian systems comprising the cortex, proved to be of use in experimental design. From noise simulation studies, it was found that many samples and long counting times were necessary to provide structural information beyond the capillary wall.

Although the model II predictions for E_{max} for ^{86}Rb and ^{85}Sr were similar to maximum instantaneous extractions obtained from the outflow data, a suggested modification to the Crone-Renkin equation to obtain PS_C products is $PS_C=-F_s\log_e(1-1.12E_{max})$; where E_{max} is an averaged instantaneous extraction figure up to the peak of the

reference outflow profile. The modified equation applying to ^{85}Sr and ^{86}Rb may be of use in M.T.O.D. procedures applied to other organs as well as the tibia. Further studies involving model II have also revealed that fractional escape rates are not suitable for obtaining PS_B for diffusible tracers in bone. This is because it is too difficult to obtain fractional escape rates representing constant bone-blood effluxes by virtue of the facts that the interstitial fluid space is not negligibly small as compared with the bone phase, and that in addition there is flow rate heterogeneity. Ratios of apparent volumes of distribution, $V_I'/V_C'=3.95\pm1.18$ (n=4) and $V_B'/V_C'=23.43\pm3.28$ (n=3) for ^{85}Sr were greater than corresponding ratios $V_I'/V_C'=2.49\pm0.35$ (n=4) and $V_B'/V_C'=10.46\pm4.87$ (n=3) for ^{86}Rb. These figures emphasize the much greater capacity for longer term ^{85}Sr retention compared with ^{86}Rb. It was impossible to obtain parameter estimates from all 6 sets of data. These parameters were susceptible to experimental noise and the adequacy of model fitting.

With the intention of improving the model to fit more of the data, the third objective was to assess blood flow contributions to the tibial diaphysis. The microsphere technique was employed and microsphere deposition densities were analysed in the cortex and marrow following injection into the femoral artery. The tibial nutrient artery, a substantial afferent supply vessel contributed 65% and 35% of its flow to the cortex and marrow respectively ; blood flow rates in these structures were found to be heterogeneous. For the diaphyseal cortex in particular, the distribution of relative deposition densities (rd_i values) corresponding to relative

regional blood flow rates was positively skewed with a relative dispersion of around 40%. High correlation coefficients between the rd_i values for corresponding pieces of cortex in the left and right tibia further emphasized the flow rate heterogeneity ; statistical studies revealed minimal impairment from measurement errors. Studies involving light microscopy, suggested that the cortical flow rates were not attributable to particular changes in capillary density which remained relatively uniform at 2682±510 capillaries/cm^2 (4 tibiae ; 240 observations).

In view of the heterogeneities observed in the flow studies as mentioned, objective 4 was accomplished by incorporating flow rate heterogeneity and back diffusion for the cortical and marrow capillary systems. The resulting more complex model IIIa as described in chapter 5 was the most realistic model employed to fit the outflow data. Tracer exchange was assumed to be confined to the diaphysis in view of tracers being injected into the tibial nutrient artery.

Parameter estimates for PS_C from model IIIa were similar for ^{86}Rb and ^{85}Sr, being 0.047±0.022 and 0.045±0.021 ml/s (both n=6) respectively. The $PS_C(^{86}Rb)/PS_C(^{85}Sr)$ ratio which was equal to 1.04 and not the corresponding free diffusion coefficient ratio of 1.58 suggested that the exchange was flow limited. The PS_C products were similar to Crone-Renkin predictions of 0.046±0.014 (^{86}Rb) and 0.052±0.018 ml/s (^{85}Sr) using maximum instantaneous extractions and whole infusing buffer flow rates. Although systematic increases in the PS_C parameter associated with flow rate heterogeneity have been

observed (Kuikka et al. 1986), the effect was not observed owing to the partitioning of the flows to the cortex and marrow. Further studies which revealed that the PS_C products could increase by as much as 60% as progressively more than the calculated 65% of the nutrient artery flow supplied the cortex may account for the differences in PS_C between the dogs.

Similarities in the model IIIa V_I' parameters (both n=5) of 0.69±0.22 (^{86}Rb) and 0.90±0.36 ml diaphysis (^{85}Sr) which reflects individualistic tracer phenomena such as phase partition coefficients and asymmetric transport, suggests that tracer effluxes from the interstitial fluid to the capillary is by passive diffusion ; Kelly and Bassingthwaighte (1977) have already established that passive diffusion describes the tracer influxes in the opposite direction. The cited value of V_B'=2.56±1.20 ml of diaphysis (n=3) for ^{86}Rb applying to bone and marrow cells suggests that approximately 10% of the diaphysis constitutes a cell phase. Generally, the model IIIa parameter estimates for ^{86}Rb and ^{85}Sr were believed to be robust in view of the simulation studies involving the stability of parameter estimates to the variances in the weighting factors for the cortical capillary systems. The assigned weighting factor f_5=1.08 for the marrow was considered a sensible choice.

Although it was possible to fit more of the outflow data satisfactorily with model IIIa as opposed to the single capillary model II, parameter estimates particularly V_B' and PS_B were unstable at times. Remedying this problem requires the reduction of experimental noise particularly in the latter outflow samples, and

improved model development. One may well be advised to inject larger quantities of the tracers in future work involving modelling the results of M.T.O.D. studies, to try and alleviate the effects of noise. Future consideration of tracer exchange to canaliculi-lacunae and a more detailed approach to osteon geometry may well make the model more suitable for fitting the data. In addition, future development of more efficient optimisation routines with rapid convergence as has been investigated by Bassingthwaighte and colleagues would be an important requisite in reducing CPU times. This is especially in view of the fact that no significant reduction in CPU times following optimisation, were observed when parameters were constrained to fixed values.

Examining the model findings from outflow data concerning parathyroidectomised dogs and PTH, it would appear that PTH inhibits ^{85}Sr uptake following PTH administration. Using model IIIa, this inhibition is best explained by way of a decrease in the parameter of V_B' even though it is difficult to attach any statistical significance to this finding. In view of the statistically insignificant changes in the other parameter estimates and in the light of the asymmetric (active) transport investigations on parameter estimates (chapter 6), it would appear that PTH does not impair the passive diffusion transport properties of ^{85}Sr either side of the capillary wall and ^{85}Sr influxes to the bone surface. The speculated V_B' decrease following PTH however may suggest that the bone surface for ^{85}Sr uptake has been reduced or that an active transport process prevails in pumping out the ^{85}Sr from the bone to blood at increased rates.

Reassuringly, in view of the large vessel studies involving gamma variates (chapter 6), it would seem that model inputs are robust in terms of arterial and venous dispersion. It would appear that comparing the final parameter estimates from all the experimental greyhounds was justifiable.

I. APPENDIX : SOLVING THE MODEL EQUATIONS BY ANALYTICAL METHODS

1. Solution of a 2 compartment (segment) system

Suppose we have a 2 compartment system as shown below, with subscripts 1 and 2 referring to each of the compartments.

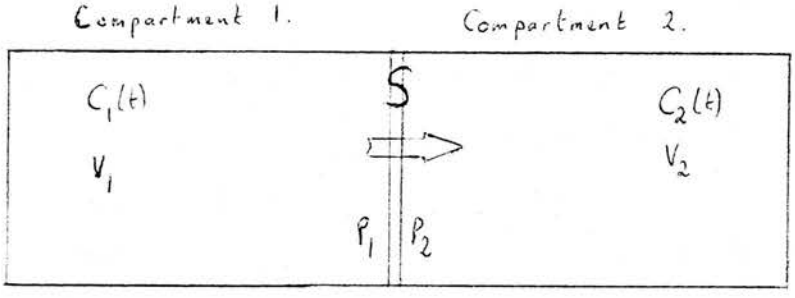

Nomenclature :-

- C(t) :- Conc. (g/ml) as a function of time t (s).
- V :- volume (ml).
- q(t) :- flux or amount (g) as a function of time t.
- S :- surface area of partition or barrier (cm^2).
- P :- permeability (cm/s).

Boundary conditions are :-

$$C_1(0) = C_0 \qquad (A1.1)$$

$$C_2(0) = 0 \qquad (A1.2)$$

$$C_1(\infty) = \gamma C_2(\infty) = \frac{V_1 \gamma}{(\gamma V_1 + V_2)} C_0 \qquad (A1.3)$$

$$(\because C_0 V_1 = C_1(\infty) V_1 + C_2(\infty) V_2)$$

Conservation of mass.

when the transport across the barrier is active i.e. $P_1 \neq P_2$, in particular,

$$\gamma = P_2 / P_1 \qquad (A1.4)$$

and

$$K_1 = P_1 S \qquad (A1.5a)$$

$$K_2 = P_2 S \qquad (A1.5b)$$

Simultaneous O.D.E.s regarding tracer exchange w.r.t. time are

Compartment 1. : $V_1 \dot{C}_1(t) = K_1(\gamma C_2(t) - C_1(t))$ (A1.6)

Compartment 2. : $V_2 \dot{C}_2(t) = K_1(C_1(t) - \gamma C_2(t))$ (A1.7)

To solve O.D.E.s (A1.6) and (A1.7), one must obtain single variable O.D.E.s in $C_1(t)$ and $C_2(t)$. To obtain an equation described solely in terms of $C_1(t)$ one can proceed by firstly differentiating (A1.6) w.r.t. time t.

$$\Rightarrow V_1 \ddot{C}_1(t) = K_1 \gamma \dot{C}_2(t) - K_1 \dot{C}_1(t) \qquad (A1.8)$$

Substituting for $\dot{C}_2(t)$ from (A1.7) into (A1.8) one obtains

$$V_1 \ddot{C}_1(t) = (K_1^2 \gamma / V_2).(C_1(t) - \gamma C_2(t)) - K_1 \dot{C}_1(t) \qquad (A1.9)$$

Substituting for $C_2(t)$ from (A1.6) into (A1.9) one obtains

$$V_1 \ddot{C}_1(t) = (K_1^2 \gamma / V_2) C_1(t) - (K_1^2 \gamma^2 / V_2).(V_1 \dot{C}_1(t) + K_1 C_1(t))(1/K_1 \gamma) - K_1 \dot{C}_1(t)$$

which reduces to

$$\ddot{C}_1(t) + (K_1 / V_1 V_2)(V_2 + \gamma V_1) \dot{C}_1(t) = 0 \qquad (A1.10)$$

The solution of O.D.E. (A1.10) is of the form

$$C_1(t) = A + B e^{-\alpha t} \qquad (A1.11)$$

where

$$\alpha = (K_1 / V_1 V_2)(V_2 + \gamma V_1) \qquad (A1.12)$$

and A, B are constants.

By applying boundary conditions (A1.1) and (A1.3), equation (A1.11) becomes

$$C_1(t) = (C_0/(\gamma V_1 + V_2))(\gamma V_1 + V_2 e^{-\alpha t}) \qquad (A1.13)$$

The corresponding equation for $C_2(t)$ applying similar methods is

$$C_2(t) = (C_0 V_1/(\gamma V_1 + V_2))(1 - e^{-\alpha t}) \qquad (A1.14)$$

2. Extending the solution to solve model P.D.E.s (3.3))

Referring to section 3.1.3., the objective is to solve equations (3.4) which are described in terms of flux q i.e. q(t)=V.C(t). Thus from equation (A1.13)

$$q_1(t) = (C_0 V_1/(\gamma V_1 + V_2)).(\gamma V_1 + V_2 e^{-\alpha t}) \qquad (A1.15)$$

The change in flux Δq_1 during a time interval Δt can be written as,

$$\Delta q_1 = q_1(t+\Delta t) - q_1(t) \qquad (A1.16)$$

Thus,

$$\Delta q_1 = (C_0 V_1/(\gamma V_1 + V_2)).(\gamma V_1 + V_2 e^{-\alpha\Delta t} e^{-\alpha t} - \gamma V_1 - V_2 e^{-\alpha t})$$

$$\Rightarrow \Delta q_1 = (C_0 V_1 V_2/(\gamma V_1 + V_2)).e^{-\alpha t}(e^{-\alpha\Delta t} - 1) \qquad (A1.17)$$

(short digression :- equation (A1.13) - (A1.14)

$$\Rightarrow C_1(t) - \gamma C_2(t) = C_0 e^{-\alpha t} \qquad (A1.18))$$

Substituting equation (A1.18) in equation (A1.17)

$$\Rightarrow \Delta q_1 = (C_1(t) - \gamma C_2(t)).(V_1 V_2/(\gamma V_1 + V_2)).(e^{-\alpha\Delta t} - 1)$$

$$\Rightarrow \Delta q_1 = V_1 \left[\frac{\gamma V_1 C_1(t) + \gamma V_2 C_2(t) - \gamma V_1 C_1(t) - V_2 C_1(t)}{(\gamma V_1 + V_2)} \right]$$

$$\cdot \left[1 - e^{-\alpha \Delta t} \right] \qquad (A1.19)$$

One can now revert to the notation of section 3.1.3. in which compartments 1. and 2. are now represented by segments j, representing the capillary (C) and interstitial fluid (I) respectively. Furthermore, $qr_{CI_j} \equiv q_1$, $V_C'/n_x \equiv V_1$, $V_I'/n_x \equiv V_2$ and α is defined using equations (A1.12) and (A1.5a).

Firstly, dealing with the exponential term...

$$\alpha \Delta t = (P_1 S_C / n_x) \cdot (n_x^2 / V_C' V_I') \cdot (1/n_x) \cdot (V_I' + \gamma V_C') \cdot \Delta t$$

$$= P_1 S_C \Delta t \cdot \left((1/V_C') + (\gamma / V_I') \right)$$

Now equation (A1.19) becomes

$$\Delta qr_{CI_j} = \frac{V_C'}{n_x} \left\{ 1 - \exp \left[-\Delta t P_1 S_C \cdot \left(\frac{1}{V_C'} + \frac{\gamma}{V_I'} \right) \right] \right\}$$

$$\cdot \left\{ \frac{\gamma}{(\gamma V_C' + V_I')} \left[V_C' C_{C_j}(t+) + V_I' C_{I_j}(t) \right] - C_{C_j}(t+) \right\} \qquad (A1.20)$$

* For a case of passive transfer, one may write the passive permeability :- $P = P_1 = P_2$; additionally from equation (A1.4), $\gamma = 1$. Carrying out these amendments to equation (A1.20) produces the solution as given by equation (3.5).

* The terms between the second braces {} of equation (A1.20) are incorrect in Bassingthwaighte's solution (Bassingthwaighte, 1974).

II. APPENDIX : OBTAINING LAGGED NORMAL DENSITY CURVES FOR SIMULATION STUDIES

Lagged normal density curves r(t) can be obtained by convoluting a first-order exponential process p(t) with a normal density curve q(t) (Bassingthwaighte *et al.* 1966) i.e.

$$r(t) = p(t) * q(t) \qquad (A2.1)$$

in which p(t) is defined as such,

$$\left.\begin{aligned} p(t) &= (1/\tau).e^{-t/\tau} \quad \text{for } t \geq 0 \\ p(t) &= 0 \quad \text{for } t < 0 \end{aligned}\right\} \qquad (A2.2)$$

where τ is a time constant (s), and q(t) as

$$\left.\begin{aligned} q(t) &= (1/\sigma(2\pi)^{1/2}).e^{-1/2[(t-t_c)/\sigma]^2} \quad \text{for } t \geq 0 \\ q(t) &= 0 \quad \text{for } t < 0 \end{aligned}\right\} \qquad (A2.3)$$

where t_c (s) is a time corresponding to the centre of symmetry and σ is the standard deviation.

The lagged normal density curve r(t) whose shape and position in time is described by the parameters σ, τ and t_c was achieved by a numerical form of the convolution equation (A2.1), in particular after Bassingthwaighte (1967)

$$r_n = \sum_{i=1}^{n} p_n \cdot q_{n-i+1} \qquad (A2.4)$$

where p,q and r were sequences of pulses of duration Δt = 1 s, and n was the total number of pulses i.e. $p_n = p[(n - 0.5).\Delta t]$, similarly for q_n and r_n.

In view of optimising r(t) to a particular set of ^{125}I-albumin reference data, time

t was defined between 1 and 60 s which was one fifth of the experimental sampling period. The reference outflow data, instead of being defined at times of t=5,10,...,300 s was instead defined at times of t=1,2,...,60 s, so that r(t) of unit area could fit such an outflow profile which are typically constructed such that the area beneath them is 5.

Owing to limitations in the goodness of fit to the particular set of outflow data, the lagged normal density curve r(t) was optimized using a NAG E04FDF routine to the first 20 outflow values (t=1,...,20 s) in which the parameters were found to be σ=1.92, τ=3.36 s and t_c=4.88 s. Using these parameters, a suitably smooth lagged normal density form, $r_R(t)$ of the reference outflow profile was obtained as follows in which the convoluting functions were exactly defined as

$$p_R(t) = (1/\tau).e^{-t'/\tau} \qquad \begin{matrix} t'=t & \text{for } 0 \le t \le 24\,s \\ t'=24 & \text{for } 24 < t \le 60\,s \end{matrix} \Big\} \quad (A2.5)$$

and

$$q_R(t) = (1/\sigma(2\pi)^{1/2}).e^{-1/2\,[(t''-t_c)/\sigma]^2} \qquad \begin{matrix} t''=t & \text{for } 0 \le t \le 40\,s \\ t''=40 & \text{for } 40 < t \le 60\,s \end{matrix} \Big\} \quad (A2.6)$$

The specified conditions associated with time t in equations (A2.5) and (A2.6) were found by trial and error to provide accurate $r_R(t)$ forms of the reference outflow profile, especially in view of the tail region. Generally, 'pure' lagged normal density curves which adequately fit the peaks of such profiles, decrease too greatly and consequently do not fit the tail.

Once $r_R(t)$ values at times of t=1,2,...,60 s had been obtained, the values were then attributed to times of 5,10,...,300 s for the purpose of model simulation studies.

III. APPENDIX : DESCRIPTION OF NAG SUBROUTINES & BMDP PAR

Important subroutines/packages used extensively throughout the course of the research are mentioned as follows :-

NAG G05CCF and NAG G05DDF subroutines

The NAG G05CCF subroutine sets the basic number generator routine NAG G05CAF to a non-repeatable initial state, in which this latter subroutine usually produces pseudo-random numbers taken from a uniform distribution between 0 and 1. If however, it is called in conjunction with the NAG G05DDF subroutine, then subsequent random numbers can be obtained from a normal distribution of definable mean and standard deviation. These particular subroutines are useful in noise and statistical simulation studies.

NAG E04FDF subroutine

This subroutine is an easy-to-use algorithm for finding an unconstrained minimum of a sum of squares of M nonlinear functions in N variables ($M \geqslant N$). No derivatives are required.

It is intended for functions which are continuous and which have continuous first and second order derivatives, although it will usually work even if the derivatives have occasional discontinuities.

The NAG E04FDF subroutine was used to fit a lagged normal density curve to part of the ^{125}I-albumin reference outflow data (appendix 2) , with M = 20 (t=1,...,20 s) and N = 3 (σ, τ and t_c).

NAG F04JDF subroutine

This subroutine finds the minimal solution of a linear least squares problem,

Ax=b, where A is a real mxn ($m \leq n$) matrix and b is an m element vector. The solution vector x is found after the residual vector r=b-Ax is minimized.

This subroutine was used to find the multicapillary model input $h_{LV}(t)$, with m=60 and n=61.

BMDP PAR

BMDP PAR is a derivative-free nonlinear regression package that estimates the parameters of a nonlinear function by least squares. It is more superior to the NAG E04FDF subroutine, in the sense that upper and lower bounds can be specified on the individual parameters or for arbitrary linear combinations of the parameters.

The nonlinear function is fitted by a Pseudo-Gauss-Newton iterative algorithm. The termination criterion for the algorithm is given by

$$\left| \frac{RSS^{(k+1)} - RSS^{(k)}}{RSS^{(k+1)}} \right| < C$$

for five successive values of k, where $RSS^{(k)}$ is the residual sum of squares at step k, and C is the value of the convergence criterion. If the RSS increases between two iterations, the increment size is halved and the RSS is recomputed and tested against the RSS at the previous iteration. This halving is repeated until the RSS is less than that of the previous halving or the maximum number of halvings is reached.

A tolerance criterion is used to guard against round-off errors in critical portions of the computations.

Pre-assigned package values (see overleaf).

- Convergence criterion (C) : 1×10^{-5}
- Tolerance criterion : 1×10^{-8}
- Maximum number of iterations : 50
- Maximum number of increment halvings : 50

IV. APPENDIX : COMPUTER PROGRAMS

Important computer programs which were used throughout the course of the research are listed below. In most instances, the nomenclature between the programs and that as quoted in the main body of the text, conforms.

Programs

A4-1 : Fits a lagged normal density function to part of the reference outflow data.

A4-2 : Generates a lagged normal density form of the reference outflow data.

A4-3 : Generates random numbers for noise simulation studies.

A4-4 : Obtains model input $h_{LV}(t)$ from heterogeneous flow output.

A4-5 : Generates hypothetical outflow data from a single or multicapillary system.

A4-6 : Optimizes multicapillary model IIIa to M.T.O.D. data.

A4-7 : Typical BMDP control program which is used in conjunction with program A4-6.

A4-1

```
C
C     OPTIMISATION FOR LAGGED NORMAL DENSITY FNS.
C
C     PROG:  SM WILLANS  15.03.85
C
C  Initial Declaration
C
      INTEGER  M,N,LW
      PARAMETER  (M = 20 ,N = 3 ,
     +            LW = 7*N + N*N + 2*M*N + 3*M +
     +                 N*(N - 1)/2 )
C
C  Scalars in Common
C
      DOUBLE PRECISION  DT
      INTEGER  NI
C
C  Arrays in Common
C
      DOUBLE PRECISION  RR(20),T(20),IOAL(20)
C
C  Local Scalars
C
      DOUBLE PRECISION  FSUMSQ
      INTEGER  I,IFAIL,J,LIW
C
C  Local Arrays
C
      DOUBLE PRECISION  W(LW),X(3)
      INTEGER  IW(1)
C
C  Common Blocks
C
      COMMON /INPUT/ NI,DT,IOAL,T
      COMMON /OUTPUT/ RR
C
C  Specifying Values for NAG E04FDF
C
      IFAIL = 1
      LIW = 1
C
C  Inputting the Constants & Experimental Values
C
      READ (5,*) NI
      READ (5,*) DT
C
      READ (4,*) (T(I) ,I = 1,M)
      READ (9,*) (IOAL(I) ,I = 1,M)
C
C  Input the Initial Estimates
C
      READ (10,*) (X(I) ,I = 1,N)
C
      CALL E04FDF(M,N,X,FSUMSQ,IW,LIW,W,LW,IFAIL)
C
C  Outputting the Results
C
      WRITE (6,'(3X,''On Exit ,Sum of Squares = '',
     +       E15.5)') FSUMSQ
      WRITE (6,'(3X,''At The Point '',3(2X,E15.5))')
     +       (X(I) ,I = 1,N)
C
      WRITE (7,'(3X,''On Exit ,Sum of Squares = '',
     +       E15.5)') FSUMSQ
      WRITE (7,'(3X,''At The Point '',3(2X,E15.5))')
     +       (X(I) ,I = 1,N)
      WRITE (7,*) ' '
      WRITE (7,'(3X,''Final Iteration No. '',I4)') NI
      WRITE (7,*) ' '
      DO 50  I = 1,M
        WRITE (7,599) T(I),RR(I),IOAL(I)
  599   FORMAT (3X,F6.2,2X,2(2X,E15.5))
   50 CONTINUE
C
      END
C
```

A4-1 Cont.

```
      SUBROUTINE LSFUN1(M,N,XC,FVECC)
C
C  Scalar Arguements
C
      INTEGER  M,N
C
C  Array Arguements
C
      DOUBLE PRECISION  FVECC(M),XC(N)
C
C  Arrays in Common
C
      DOUBLE PRECISION  RR(20),T(20),IOAL(20)
C
C  Local Scalars
C
      DOUBLE PRECISION  Q
      INTEGER  I,J,L
C
C  Local Arrays
C
      DOUBLE PRECISION  QR(20),PR(20),
     +                  HA(20),HB(20)
C
C  Scalars in Common
C
      DOUBLE PRECISION  DT
      INTEGER  NI
C
      COMMON /INPUT/ NI,DT,IOAL,T
      COMMON /OUTPUT/ RR
C
C
      NI = NI + 1
      WRITE (8,*) ' '
      WRITE (8,'(3X,''Iteration No. '',I3)') NI
      WRITE (8,'(3X,''XC(1) = '',E15.5)') XC(1)
      WRITE (8,'(3X,''XC(2) = '',E15.5)') XC(2)
      WRITE (8,'(3X,''XC(3) = '',E15.5)') XC(3)
      WRITE (8,*) ' '
      DO 60  I = 1,M
        Q = 0.5D0*(((T(I) - XC(2))/XC(1))**2)
        HA(I) = DEXP(-Q)/(DSQRT(2.0D0*3.142D0)*XC(1))
        HB(I) = DEXP(-T(I)/XC(3))/XC(3)
   60 CONTINUE
C
C  Evaluation of Areas for Recursive Convolution Integral
C
      DO 70  I = 1,M
        QR(I) = HA(I)*DT
        PR(I) = HB(I)*DT
   70 CONTINUE
C
C  Recursive Convolution Integral
C
      DO 80  I = 1,M
        RR(I) = 0.0D0
        DO 90  J = 1,I
          L = I - J + 1
          RR(I) = QR(J)*PR(L) + RR(I)
   90   CONTINUE
   80 CONTINUE
      DO 100  I = 1,M
        FVECC(I) = RR(I) - IOAL(I)
        WRITE (8,600) T(I),RR(I),IOAL(I),FVECC(I)
  600   FORMAT (3X,F6.2,2X,3(2X,E15.5))
  100 CONTINUE
      RETURN
      END
```

A4-2

```
C      LAGGED NORMAL DENSITY VALUES
C        OBTAINED BY CONVOLUTION
C
       DIMENSION  QR(60),RR(61),HA(61),HB(61),PR(60)
C
C  Specifying the Shape Variables
C
       READ (5,*) SG
       READ (5,*) TC
       READ (5,*) TR
       READ (5,*) DT
C
C  Obtaining Values of Normal Density Fn(HA) & 1st
C  Order Exponential Fn(HB) at DT sec intervals.
C
       DO 60  I = 1,60
         T = FLOAT(I) - 0.5
         TT = FLOAT(I) - 0.5
         IF(T.GT.40.0)  T = 40.0
         IF(TT.GT.24.0)  TT = 24.0
         Y = ((T - TC)/SG)**2
         YY = -0.5*Y
         A = EXP(YY)
         B = SQRT(2.0*3.1416)*SG
         HA(I) = A/B
         HB(I) = EXP(-TT/TR)/TR
         WRITE (7,*) T,HA(I),HB(I)
   60  CONTINUE
C
C      Evaluation of Areas for Recursive Convolution Integral
C
       DO 70  I = 1,60
         QR(I) = HA(I)*DT
         PR(I) = HB(I)*DT
   70  CONTINUE
C
C      Recursive Convolution Integral
C
C
       DO 80  I = 1,60
         RR(I) = 0.0
         DO 90  J = 1,I
           L = I - J + 1
           RR(I) = QR(J)*PR(L) + RR(I)
   90    CONTINUE
   80  CONTINUE
C
C      Outputting the Values
C
       WRITE (6,*) SG,TC,TR
C
       T = 0.0
       DO 100  I = 1,60
         WRITE (6,*) T,RR(I)
         WRITE (8,*) RR(I)
         T = T + 5.0
  100  CONTINUE
       END
```

A4-3

```
C     RANDOM NUMBER GENERATOR (GAUSSIAN DISTRIBUTION)
C
C     PROG  SM WILLANS  14:04:85
C
C  Local Scalars
C
      DOUBLE PRECISION  F,H(100),SD,OUTPUT
      INTEGER  I,J,M,NP
C
C  Function References
C
      DOUBLE PRECISION  G05DDF
C
C  Inputting Variables
C
      READ (5,*) NP
      READ (5,*) M
      READ (5,*) F
C
      READ (4,*) (H(I) , I = 1,NP)
C
      WRITE (6,*) ' '
      WRITE (6,'(2X,''G05DDF Results'')')
      WRITE (6,*) ' '
C
      CALL G05CBF
      DO 100  I = 1,NP
        SD = F*SQRT(H(I))
        WRITE (6,*) SD
          OUTPUT = G05DDF(H(I),SD)
          WRITE (6,*) H(I),OUTPUT
          WRITE (6,*) OUTPUT
  100 CONTINUE
      END
```

A4-4

```
      PROGRAM TO OBTAIN MODEL INPUT FROM
      HETEROGENEOUS FLOW OUTPUT

      PROG:  SM WILLANS  11:08:86

Scalars in Common --

      INTEGER  I,J,MC,MF,MR

Local Scalars --

      INTEGER  IFAIL,IRANK,LWORK,M,N,NRA
      DOUBLE PRECISION  SIGMA,TOL

Local Arrays --

      DOUBLE PRECISION  A(61,62),B(61),WORK(4000)

Inputting Constants --

      READ (5,*) M
      READ (5,*) N
      READ (5,*) MC
      READ (5,*) MF
      READ (5,*) MR

      READ (18,*) (B(I), I = 1,N)

Setting up the coefficient A matrix --

      DO 60  I = 1,M
        DO 70  J = 1,N
          A(I,J) = 0.0D0
70      CONTINUE
60    CONTINUE

      READ (19,*) ((A(I,J), J = 1,MC), I = 1,MR)

Calculation of matrix A coefficients --

      DO 79  I = MR+1,M
        MF = MF + 1
        MC = MC + 1
        DO 80  J = MF,MC
          A(I,J) = A(I-1,J-1)
80      CONTINUE
79    CONTINUE

      NRA = 61
      TOL = 5.0D-07
      LWORK = 4000
      IFAIL = 0

      CALL F04JDF(M,N,A,NRA,B,TOL,SIGMA,IRANK,WORK,
     *            LWORK,IFAIL)

      DO 45  I = 1,N
        WRITE (6,*) I,B(I)
        WRITE (8,*) B(I)
45    CONTINUE
      END
```

A4-5

```
C     PROG. TO GENERATE HYPOTHETICAL OUTFLOW DATA USING
C     EITHER A SINGLE OR MULTICAPILLARY SYSTEM.
C
C     PROG: SM WILLANS  06.02.86
C
C     Arrays used--
C
      REAL      CB(105),CC(105),CI(105),
     +          QRBI(105),QRCI(105),QRIB(105),QRIC(105),
     +          ENT(85),Y(85),ZC(105),FI(5),WT(5),R(6000),RR(85),RRR(85)
      INTEGER   NX(5)
C
C     Model variables--
C
      REAL      A1,A2,B1,B2,DT,FC,PSB,PSC,T,
     +          TC,VB,VI,ZM,ZR
      INTEGER   I,J,K,M,N,NDC
C
C     Model constants--
C
      REAL      FS,VC
C
C     Control variables--
C
      REAL      DTT,FF,PP,TR
      INTEGER   II,IJ,ITC,L
C
C     I/P IS SPECIFIED EVERY 5 SECONDS
C
C     O/P IS SPECIFIED EVERY 5 SECONDS
C
C     Input Desired Variables--
C
      READ (5,*) PSC
      READ (5,*) PSB
      READ (5,*) VI
      READ (5,*) VB
      READ (5,*) NDC
      READ (5,*) N
C
      READ (9,*) (ENT(I), I = 1,N+1)
      READ (10,*) (WT(I), I = 1,NDC)
      READ (11,*) (NX(I), I = 1,NDC)
      READ (12,*) (FI(I), I = 1,NDC)
C
C     Specifying constants--
C
      FS = 0.0217
      VC = 0.0362
C
C     Setting up Array for Results
C
      DO 75  I = 1,85
        RR(I) = 0.0
        RRR(I) = 0.0
75    CONTINUE
C
C     Large outer loop for the capillaries--
C
      DO 900  K = 1,NDC
C
        IF(K.EQ.NDC) FS = 0.01163
        DO 85  I = 1,5000
          R(I) = 0.0
85      CONTINUE
C
        M = NX(K) + 1
C
        DO 200  I = 1,N
          Y(I) = ENT(I)
200     CONTINUE
C
        FC = FS*FI(K)
        TC = VC/FC
        DT = TC/FLOAT(NX(K))
        ZR = PSC/FLOAT(NX(K))
        ZM = PSB/FLOAT(NX(K))
C
C     Setting up Initial Values--
C
        DO 300  J = 2,M
          CC(J) = 0.0
          CI(J) = 0.0
          CB(J) = 0.0
300     CONTINUE
```

A4-5 cont.

```
C
C  ITC IS O/P CONTROL FACTOR FOR CAP. TRANSIT TIME
C  FF IS O/P CONTROL FACTOR FOR 5 SECOND INTERVAL
C  PP IS I/P CONTROL FACTOR
C  IJ AIDS IN OBTAINING TIMES EVERY 5 SECONDS
C
      ITC = 0
      FF = 5.0
      II = 1
      IJ = 1
      L = 1
      PP = 5.0
      T = 0.0
C
C  Segmental Tracer Amounts--
C
  700 DO 400  J = 2,M
        CC(2) = Y(II)
C
        A1 = DT*ZR*(FLOAT(NX(K))/VC + FLOAT(NX(K))/VI)
        A2 = (1.0 - EXP(-A1))*(((VC*CC(J) + VI*CI(J))/
     .       (VC + VI)) - CC(J))
        QRCI(J) = (VC*A2)/FLOAT(NX(K))
        QRIC(J) = -QRCI(J)
C
        B1 = DT*ZM*(FLOAT(NX(K))/VB + FLOAT(NX(K))/VI)
        B2 = (1.0 - EXP(-B1))*(((VB*CB(J) + VI*CI(J))/
     .       (VI + VB)) - CI(J))
        QRIB(J) = (VI*B2)/FLOAT(NX(K))
        QRBI(J) = -QRIB(J)
C
  400 CONTINUE
C
C  Calc New Segmental Concentrations--
C
      DO 500  J = 2,M
        CC(J) = CC(J) + FLOAT(NX(K))*QRCI(J)/VC
        CI(J) = CI(J) + FLOAT(NX(K))*(QRIC(J) + QRIB(J))/VI
        CB(J) = CB(J) + FLOAT(NX(K))*QRBI(J)/VB
  500 CONTINUE
C
C  Sliding the Segments (Convection)
C
      DO 600  J = 2,M
        ZC(J) = CC(J)
  600 CONTINUE
      DO 650  J = 2,M
        CC(J+1) = ZC(J)
  650 CONTINUE
C
      ITC = ITC + 1
      T = T + DT
C
C  Testing for emergence
C
      IF(ITC.GE.NX(K)) GO TO 16
      GO TO 17
   16 CC(M+1) = CC(M+1)*WT(K)
      R(IJ) = CC(M+1)
C
C  Collating the Results
C
   17 TR = T - FF
      IF(TR.LT.0.0) GO TO 18
      RR(L) = R(IJ) - TR*(R(IJ) - R(IJ-1))/DT
      IF(R(IJ-1).EQ.0.0.AND.TR.NE.0.0) RR(L) = 0.0
      RRR(L) = RRR(L) + RR(L)
C
      IF(K.LT.NDC) GO TO 19
      WRITE (6,*) L,FF,RRR(L)
      WRITE (8,*) FF,RRR(L)
C
   19 FF = FF + 5.0
      L = L + 1
      IF(L.GT.N) GO TO 900
   18 IJ = IJ + 1
C
C  Calculating input values--
C
   20 IF(T.GE.PP) GO TO 21
      Y(II) = Y(II) + DT*(ENT(II+1) - ENT(II))/5.0
      GO TO 700
C
   21 DTT = T - PP
      II = II + 1
      Y(II) = Y(II) + DTT*(ENT(II+1) - ENT(II))/5.0
      PP = PP + 5.0
      GO TO 700
  900 CONTINUE
      END
```

```
      OPTIMISATION OF DATA USING
      HETEROGENEOUS MULTICAPILLARY MODEL IIIA
      (125-I-A1- Reference is Input)

      PROG: SM WILLANS  17:06:86

Scalar arguements --

      INTEGER  IPASS,KASE,N,NPAR,NVAR
      DOUBLE PRECISION  F,XLOSS

Local scalars --

      DOUBLE PRECISION  A1,A2,B1,B2,DT,DTT,FC,FF,FS,
     +                  PP,RR,RRR,TC,VC,W1,W2,W3,XN,ZR,ZM
      INTEGER  I,IJ,J,K,LL,M,NDC

Local arrays --

      DOUBLE PRECISION  CB(65,5),CC(65,5),CI(65,5),
     +                  FI(5),QRBI(65),QRCI(65),QRIB(65),QRIC(65),
     +                  R(6000,5),T(5),TR(5),V(3,5),WT(5),ZC(65)
      INTEGER  IJJ(6),ITC(6),NX(6)

Common blocks --

      COMMON /CONCS/ CC,CI,CB,R,V
      COMMON /TIMING/ T
      COMMON /SYNCH/ IJJ,ITC,FF,PP

Specifying local constants --

      FS = 0.0217D0
      VC = 0.0362D0
      NDC = 5
      RRR = 0.0D0

      WT(1) = 1.4229D-02
      WT(2) = 0.17514D0
      WT(3) = 0.37533D0
      WT(4) = 0.33094D0
      WT(5) = 0.10435D0

      FI(1) = 0.47D0
      FI(2) = 0.87D0
      FI(3) = 1.27D0
      FI(4) = 1.87D0
      FI(5) = 1.00D0

      NX(1) = 10
      NX(2) = 10
      NX(3) = 10
      NX(4) = 10
      NX(5) = 10

Simplified terms --

      W1 = VC
      W2 = P(3)
      W3 = P(4)

Large outer loop for capillaries --

      DO 900  K = 1,NDC

Setting up initial values --

      XN = DBLE(NX(K))
      M = NX(K) + 1

      IF(K.EQ.NDC) FS = 0.011630D0
      IF(KASE.NE.1) GO TO 12
      DO 10  J = 2,M
        CC(J,K) = 0.0D0
        CI(J,K) = 0.0D0
        CB(J,K) = 0.0D0
10    CONTINUE
      DO 15  I = 1,5000
        R(I,K) = 0.0D0
15    CONTINUE

      V(2,K) = X(2)
      V(3,K) = X(3)
      ITC(K) = 0
      FF = 5.0D0
      T(K) = 0.0D0
      IJJ(K) = 1
      PP = 5.0D0

12    FC = FS*FI(K)
      TC = W1/FC
      DT = TC/XN
      ZR = P(1)/XN
      ZM = P(2)/XN
      IJ = IJJ(K)
```

IF(K.EQ.NDC) ZM = 0.000 (for ^{85}Sr data)

A4-6 cont.

```
C
C  ITC IS O/P CONTROL FACTOR FOR CAP. TRANSIT TIME
C  FF IS O/P CONTROL FACTOR FOR 5 SECOND INTRVAL
C  PP IS I/P CONTROL FACTOR
C  IJ AIDS IN OBTAINING TIMES EVERY 5 SECONDS
C
      LL = 2
      IF(KASE.EQ.1) GO TO 700
      V(LL,K) = V(LL+1,K)
      V(3,K) = X(3)
C
  700 DO 400 J = 2,M
        CC(2,K) = V(LL,K)
C
        A1 = DT*ZR*(XN/W1 + XN/W2)
        A2 = (1.0D0 - DEXP(-A1))*(((W1*CC(J,K) + W2*CI(J,K))/
     +       (W1 + W2)) - CC(J,K))
C
        QRCI(J) = (W1-A2)/XN
        QRIC(J) = -QRCI(J)
C
        B1 = DT*ZM*(XN/W3 + XN/W2)
        B2 = (1.0D0 - DEXP(-B1))*(((W3*CB(J,K) + W2*CI(J,K))/
     +       (W2 + W3)) - CI(J,K))
C
        QRIB(J) = (W2*B2)/XN
        QRBI(J) = -QRIB(J)
C
  400 CONTINUE
C
C  Calc. new segmental concentrations --
C
      DO 500  J = 2,M
        CC(J,K) = CC(J,K) + XN*QRCI(J)/W1
        CI(J,K) = CI(J,K) + XN*(QRIC(J) + QRIB(J))/W2
        CB(J,K) = CB(J,K) + XN*QRBI(J)/W3
  500 CONTINUE
C
C  Sliding the segments (convection) --
C
      DO 600  J = 2,M
        ZC(J) = CC(J,K)
  600 CONTINUE
C
      DO 650  J = 2,M
        CC(J+1,K) = ZC(J)
  650 CONTINUE
C
      ITC(K) =ITC(K) + 1
      T(K) = T(K) + DT
C
C  Testing for emergence --
C
      IF(ITC(K).GE.NX(K)) GO TO 16
      GO TO 17
   16 CC(M+1,K) = CC(M+1,K)*WT(K)
      R(IJ,K) = CC(M+1,K)
C
C  Collating the results --
C
   17 TR(K) = T(K) - FF
      IF(TR(K).LT.0.0D0) GO TO 18
      RR = R(IJ,K) - TR(K)*(R(IJ,K) - R(IJ-1,K))/DT
      IF(R(IJ-1,K).EQ.0.0D0.AND.TR(K).NE.0.0D0) RR = 0.0D0
      RRR = RRR + RR
C
      GO TO 21
   18 IJ = IJ + 1
C
C  Calculating input values --
C
      IF(T(K).GE.FF) GO TO 21
      V(LL,K) = V(LL,K) + DT*(X(LL+1) - X(LL))/5.0D0
      GO TO 700
C
   21 DTT = T(K) - PP
      LL = LL + 1
      V(LL,K) = V(LL,K) + DTT*(X(LL+1) - X(LL))/5.0D0
      IJJ(K) = IJ + 1
      IF(K.NE.NDC) GO TO 900
C
      FF = FF + 5.0D0
      PP = PP + 5.0D0
      F = RRR
C
  900 CONTINUE
```

A4-7

```
/PROBLEM        TITLE IS 'HETERO MODEL 4/1 RB1101'.

/INPUT          VARIABLES ARE 4.
                FORMAT IS FREE.
                UNIT=14.
                CASE=60.

/VARIABLE       NAMES ARE EXPTH,ALI1,ALI2,ALI3.

/REGRESS        DEPENDENT IS EXPTH.
                PARAMETERS ARE 4.
                ITERATIONS ARE 200.
                HALVINGS ARE 50.

/PARAMETER      INITIAL ARE 0.05,0.02,0.5,2.0.
                MINIMUMS ARE 0.001,0.0005,0.01,0.01.
                NAMES ARE PSCAP,PSCEBO,VINT,VCEBO.

/END
```

BIBLIOGRAPHY

Alvarez, O.A. and Yudilevich, D.L. (1969) Heart capillary permeability to lipid insoluble molecules. J. Physiol. **202**, 45-58.

Atkinson, P.J. and Hallsworth, A.S. (1982) The spatial structure of bone. In: Harrison, R.J. and Navaratman, V. (eds.), Progress in Anatomy, Vol 2, Cambridge University Press, 179-198.

Bassingthwaighte, J.B., Ackerman, F.H. and Wood, E.H. (1966) Applications of the lagged normal density curve as a model for arterial dilution curves. Circ. Res. **18**, 398-415.

Bassingthwaighte, J.B. (1967) Circulatory transport and the convolution integral. Mayo Clin. Proc. **42**, 137-154.

Bassingthwaighte, J.B., Knopp, T.J. and Hazelrig, J.B. (1970) A concurrent flow model for capillary-tissue exchanges. In: Crone, C. and Lassen, N.A. (eds.), Capillary Permeability, Copenhagen : Munksgaard (Alfred Benzon Symp. 2), 60-80.

Bassingthwaighte, J.B. (1974) A concurrent flow model for extraction during transcapillary passage. Circ. Res. **35**, 483-503.

Bassingthwaighte, J.B. (1982) Cellular influx and efflux in the heart. Fed. Proc. **41**, 3040-3044.

Bassingthwaighte, J.B., Chaloupka, M. and Goldstein, A.A. (1982) Optimisation using sensitivity functions for fitting models to data. Mathematics and Computers in Simulations XXIV, North Holland Publishing Company, 502-506.

Bassingthwaighte, J.B. and Winkler, B. (1982) Kinetics of blood to cell uptake of radiotracers. In: Columbetti, L.G. (ed.), Biological Transport of Radiotracers, Cleveland, Ohio : CRC Press, 97-146.

Bassingthwaighte, J.B. and Chaloupka, M. (1984) Sensitivity functions in the estimation of parameters of cellular exchange. Fed. Proc. **43**, 180-184.

Bassingthwaighte, J.B. and Goresky, C.A. (1984) Modelling in the analysis of solute and water exchange in the microvasculature. In: Handbook of Physiology - The Cardiovascular System IV, American Physiological Society, Bethesda, U.S.A., 549-626.

Bassingthwaighte, J.B., Kuikka, J.T., Chan, I.S., Arts, T. and Reneman, R.S. (1985) A comparison of ascorbate and glucose transport in the heart. Am. J. Physiol. **249**, H141-H149.

Brånemark, P-I. (1959) Vital microscopy of bone marrow in rabbit. Scand. J. Clin. and Lab. Invest. Vol **11**-Suppl. 38.

Brommage, R. and Neuman, W.F. (1979) Passive accumulation of magnesium, sodium, and potassium by chick calvaria. Calcif. Tissue Int. **28**, 57-63.

Brookes, M. (1971) The blood supply of bone : an approach to bone biology. Butterworths (pub.), London.

Buckberg, G.D., Luck, J.C., Payne, D.B., Hoffman, J.I.E., Archie, J.P. and Fixler, D.E. (1971) Some sources of error in measuring regional blood flow with radioactive microspheres. J. Appl. Physiol. **31**, 598-604.

Burkinshaw, L., Marshall, D.H., Oxby, C.B., Spiers, F.W., Nordin, B.E.C. and Young, M.M. (1969) Bone turnover model based on a continuously expanding exchangeable calcium pool. Nature, Lond. **222**, 146-148.

Cañas, F., Terepka, A.R. and Neuman, W.F. (1969) Potassium and milieu interieur of bone. Am. J. Physiol. **217**, 117-120.

Charkes, N.D., Brookes, M. and Makler Jr., P.T. (1979) Studies of skeletal tracer kinetics : II Evaluation of a five-compartment model of [^{18}F] fluoride kinetics in rats. J. Nucl. Med. **20**, 1150-1157.

Chinard, F.P., Vosburgh, G.J. and Enns, T. (1955) Transcapillary exchange of water and of other substances in certain organs of the dog. Am. J. Physiol. **183**, 221-234.

Cofield, R.H., Bassingthwaighte, J.B. and Kelly, P.J. (1975) Strontium-85 extraction during transcapillary passage in tibial bone. J. Appl. Physiol. **39**, 596-602.

Cohen, J. and Harris, W.H. (1958) The three-dimensional anatomy of Haversian systems. J. Bone and Jt. Surg. **40A**, 419-434.

Cohn, S.H., Bozzo, S.R., Jesseph, J.E., Constantinides, C., Huene, D.R. and Gusmano, E.A. (1965) Formulation and testing of a compartmental model for calcium metabolism in man. Rad. Res. **26**, 319-333.

Cooper, R.R., Milgram, J.W. and Robinson, R.A. (1966) Morphology of the osteon : an electron microscopic study. J. Bone and Jt. Surg. **48A**, 1239-1271.

Copp, D.H. and Shim, S.S. (1965) Extraction ratio and bone clearance of ^{85}Sr as a measure of effective bone blood flow. Circ. Res. **16**, 461-467.

Crone, C. (1963) The permeability of capillaries in various organs as determined by the use of the 'indicator diffusion' method. Acta Physiol. Scand. **58**, 292-305.

Dallant, P., Meunier, A., Christel, P.S. and Sedel, L. (1986) Semi-automatic image-analysis applied to the quantification of bone microstructure. J. Biomed. Eng. **8**, 320-328.

Davenport, R. (1983) The derivation of the gamma-variate relationship for tracer dilution curves. J. Nucl. Med. **24**, 945-948.

Davies, D.R., Bassingthwaighte, J.B. and Kelly, P.J. (1976) Transcapillary exchange of strontium and sucrose in canine tibia. J. Appl. Physiol. **40**, 17-22.

Davies, R., Tothill, P., Hooper, G., Fleming, R.H., McCarthy, I.D. and Hughes, S.P.F. (1984) The early effects of sympathectomy on bone blood flow. Calcif. Tissue Int. **36**, 622-624.

Döhler, J.R., Robertson, S. and Hughes, S.P.F. (1986) The effect of sympathomimetic drugs on bone capillaries. Arch. Orthop. Trauma Surg. **105**, 62-65.

Domenech, R.J., Hoffman, J.I.E., Noble, M.I.M., Saunders, K.B., Henson, J.R. and Subijanto, S. (1969) Total and regional coronary blood flow measured by radioactive microspheres in conscious and anaesthetised dogs. Circ. Res. **25**, 581-596.

Doty, S.B. and Schofield, B.H. (1972) Metabolic and structural changes within osteocytes of rat bone. In: Calcium, Parathyroid Hormone and the Calcitonins, Proc. Parathyroid Conf., 4th, Chapel Hill, North Carolina, 1971. Amsterdam : Excerpta Med. Found., 353-364. (Int. Congr. Ser. 243).

Frederickson, J.M., Honour, A.J. and Copp, D.H. (1955) Measurement of initial bone clearance of ^{45}Ca from blood in the rat. Fed. Proc. **14**, 49.

Goresky, C.A. (1963) A linear method for determining liver sinusoidal and extravascular volumes. Am. J. Physiol. **204**, 626-640.

Groer, P.G. and Marshall, J.H. (1973) Mechanisms of calcium exchange at bone surfaces. Calc. Tiss. Res. **12**, 175-192.

Gross, P.M., Heistad, D.D. and Marcus, M.L. (1979) Neurohumoral regulation of blood flow to bones and marrow. Am. J. Physiol. **237**, H440-H448.

Gross, P.M., Marcus, M.L. and Heistad, D.D. (1981) Current concepts review : measurement of blood flow to bone and marrow in experimental animals by means of the microsphere technique. J. Bone and Jt. Surg. **63A**, 1028-1031.

Guller, B., Yipintsoi, T., Orvis, A.L. and Bassingthwaighte, J.B. (1975) Myocardial sodium extraction at varied coronary flows in the dog : estimation of capillary permeability by residue and outflow detection. Circ. Res. **37**, 359-378.

Harrison, G.E., Howells, G.R. and Pollard, J. (1967) Comparative uptake and elution of ^{45}Ca, ^{85}Sr, ^{133}Ba and ^{223}Ra in bone powder. Calcif. Tiss. Res. **1**, 105-113.

Hooper, G., McCarthy, I.D., Wootton, R. and Hughes, S.P.F. (1984) Fluid spaces in the canine tibia. In: Arlet, J., Ficat, R.P. and Hungerford, D.S. (eds.), Bone Circulation, Williams and Wilkins (pub.), Baltimore, U.S.A., 204-206.

Hughes, S.P.F., Davies, D.R., Bassingthwaighte, J.B., Knox, F.G. and Kelly, P.J. (1977) Bone extraction and blood clearance of diphosphonate in the dog. Am. J. Physiol. **232**, H341-H347.

Hughes, S.P.F., Davies, D.R., Khan, R.A.A. and Kelly, P.J. (1978) Fluid space in bone. Clin. Orthop. **134**, 332-341.

Hughes, S.P.F. and Blount, M. (1979) The structure of capillaries in cortical bone. Ann. R. Coll. Surg. Engl. **61**, 312.

Johnson, L.C. (1963) Morphologic analysis in pathology : The kinetics of disease and general biology of bone. In: Frost, H.M. (ed.), Henry Ford Hospital - International Symposium - Bone Biodynamics, Churchill, J. and A. (pub.), London, U.K., 543-654.

Jowsey, J. (1966) Studies of Haversian systems in man and some animals. J. Anat. **100**, 857-864.

Kane, W.J. and Grim, E. (1969) Blood flow to canine hind-limb bone, muscle, and skin. J. Bone and Jt. Surg. **51A**, 309-322.

Kelly, P.J. (1966) Measurement of oxygen saturation in arterial and venous blood of bone in normal puppies and in puppies with arteriovenous fistula. Mayo Clin. Proc. **41**, 95-102.

Kelly, P.J., Yipintsoi, T. and Bassingthwaighte, J.B. (1971) Blood flow in canine tibial diaphysis estimated by iodoantipyrine-^{125}I washout. J. Appl. Physiol. **31**, 38-47.

Kelly, P.J. (1973) Comparison of marrow and cortical bone blood flow by ^{125}I-labelled 4-iodoantipyrine (I-Ap) washout. J. Lab. Clin. Med. **81**, 497-505.

Kelly, P.J. and Bassingthwaighte, J.B. (1977) Studies on bone ion exchanges using multiple-tracer indicator-dilution techniques. Fed. Proc. **36**, 2634-2639.

Kelly, P.J. (1983) Pathways of transport in bone. In: Geiger, S.R. (ed.) The Cardiovascular System. Part 1 : Peripheral Circulation and Organ Blood Flow, Vol. 3, Ch. 12, American Physiological Society, Bethesda, U.S.A., 371-396.

Kety, S.S. (1951) Theory and applications of exchange of inert gas at lungs and tissues. Pharmacol. Rev. **3**, 1-40.

King, R.B., Bassingthwaighte, J.B., Hales, J.R.S. and Rowell, L.B. (1985) Stability of heterogeneity of myocardial blood flow in normal awake baboons. Circ. Res. **57**, 285-295.

Kuikka, J., Levin, M. and Bassingthwaighte, J.B. (1986) Multiple tracer dilution estimates of D- and 2-deoxy-D-glucose uptake by the heart. Am. J. Physiol. **250**, H29-H42.

Lassen, N.A. and Crone, C. (1970) The extraction fraction of a capillary bed to hydrophilic molecules : theoretical considerations regarding the single injection technique with a discussion of the role of diffusion between laminar streams (Taylor's effect). In: Crone, C. and Lassen, N.A. (eds.), Capillary Permeability, Copenhagen : Munksgaard, (Alfred Benzon Symp. 2), 48-59.

Lemon, G.J., Davies, D.R., Hughes, S.P.F., Bassingthwaighte, J.B. and Kelly, P.J. (1980a) Transcapillary exchange and retention of fluoride, strontium, EDTA, sucrose, and antipyrine in bone. Calcif. Tissue Int. **31**, 173-181.

Lemon, G.J., Maltby, B., Davies, D.R., Hughes, S.P.F., Bassingthwaighte, J.B. and Kelly, P.J. (1980b) Transcapillary exchange and washout of ^{42}K compared with ions and molecules that concentrate in bone. (Abstract). Trans. 26th Annu. Meet. Orthop. Res. Soc. **5**, 49.

Lemon, G.J., Bassingthwaighte, J.B. and Kelly, P.J. (1982) Influence of parathyroid state on calcium uptake in bone. Am. J. Physiol. **242**, E146-E153.

Levin, M., Kuikka, J. and Bassingthwaighte, J.B. (1980) Sensitivity analysis in optimisation of time-distributed parameters for a coronary circulation model. Med. Prog. Technol. **7**, 119-124.

Little, S.E. and Bassingthwaighte, J.B. (1983) Plasma-soluble marker for intraorgan regional flows. Am. J. Physiol. **245**, H707-H712.

Lopez-Curto, J.A., Hughes, S.P.F., Kelly, P.J. and Bassingthwaighte, J.B. (1976) Interstitial fluid space in bone. (Abstract.) Fed. Proc. **35**, 850.

Lopez-Curto, J.A., Bassingthwaighte, J.B. and Kelly, P.J. (1980) Anatomy of the microvasculature of the tibial diaphysis of the adult dog. J. Bone and Jt. Surg. **62A**, 1362-1369.

Makler Jr., P.T. and Charkes, N.D. (1980) Studies of skeletal tracer kinetics IV. Optimum time delay for Tc-99m(Sn) methylene diphosphonate bone imaging. J. Nucl. Med. **21**, 641-645.

Maltby, B., Lemon, G.J., Bassingthwaighte, J.B. and Kelly, P.J. (1982) Exchange of potassium and strontium in adult bone. Am. J. Physiol. **242**, H705-H712.

Marshall, J.H. (1964) Theory of alkaline earth metabolism. J. Theoret. Biol. **6**,386-412.

Martin, P. and Yudilevich, D.L. (1964) A theory for the quantification of transcapillary exchange by tracer-dilution curves. Am. J. Physiol. **207**, 162-168.

McCarthy, I.D., Hughes, S.P.F. and Orr, J.S. (1980) An experimental model to study the relationship between blood flow and uptake for bone-seeking radionuclides in normal bone. Clin. Phys. Physiol. Meas. **1**, 135-143.

McCarthy, I.D. and Hughes, S.P.F. (1983) The role of skeletal blood flow in determining the uptake of ^{99m}Tc-methylene diphosphonate. Calcif. Tissue Int. **35**, 508-511.

McCarthy, I.D. and Hughes, S.P.F. (1986) Inhibition of bone cell metabolism increases strontium-85 uptake. Calcif. Tissue Int. 386-389.

McLean, F.C. (1957) The parathyroid hormone and bone. Clin. Orthop. **9**, 46-60.

Miller, S.C., Bowman, B.M., Smith, J.M. and Jee, W.S.S. (1980) Characterisation of endosteal bone-lining cells from fatty marrow bone sites in adult beagles. Anat. Rec. **198**, 163-173.

Morris, M.A. and Kelly, P.J. (1980) Use of tracer microspheres to measure bone blood flow in conscious dogs. Calcif. Tissue Int. **32**, 69-76.

Morris, M.A., Lopez-Curto, J.A., Hughes, S.P.F., An, K-N., Bassingthwaighte, J.B. and Kelly, P.J. (1983) Fluid spaces in canine bone and marrow. Microvasc. Res. **23**, 188-200.

Nelson Jr., G.E., Kelly, P.J., Peterson, L.F.A. and Janes, J.M. (1960) Blood supply of the human tibia. J. Bone and Jt. Surg. **42A**, 625-636.

Neuman, W.F. and Neuman, M.W. (1958) The chemical dynamics of bone mineral. University of Chicago Press, Chicago.

Neuman, W.F. (1969) The milieu interieur of bone : Claude Bernard revisited. Fed. Proc. **28**, 1846-1850.

Okubo, M., Kinoshita, T., Yukimura, T., Abe, Y. and Shimazu, A. (1979) Experimental study of measurement of regional bone blood flow in the adult mongrel dog using radioactive microspheres. Clin. Orth. Rel. Res. **138**, 263-270.

Parfitt, A.M. (1984) The cellular basis of bone remodelling : The quantum concept reexamined in light of recent advances in the cell biology of bone. Calcif. Tissue Int. **36**, S37-S45.

Parsons, J.A., Neer, R.M. and Potts Jr.,J.T. (1971) Initial fall of plasma calcium after intravenous injection of parathyroid hormone. Endocrinology **89**, 735-740.

Pasternak, H.S., Kelly, P.J. and Owen Jr., C.A. (1968) Metabolic rate in tibia of normal and thyrotoxic dogs. J. Lab. & Clin. Med. **71**, 240-246.

Pinto, M.R. and Kelly, P.J. (1984) Age-related changes in bone in the dog : fluid spaces and their potassium content. J. Orthop. Res. **2**, 2-7.

Posner, A.S. (1978) The chemistry of bone mineral. Bull. Hosp. Joint Dis. **39**, 126-144.

Ramp, W.K. and Neuman, W.F. (1971) Some factors affecting mineralisation of bone in tissue culture. Am. J. Physiol. **220**, 270-274.

Reeve, J., Veall, N. and Wootton, R. (1978) Problems in the analysis of dynamic tracer studies. Clin. Sci. Mol. Med. **55**, 225-230.

Renkin, E.M. (1955) Effects of blood flow on diffusion kinetics in isolated perfused hind-legs of cats. Am. J. Physiol. **183**, 125-136.

Renkin, E.M. (1959) Transport of potassium-42 from blood to tissue in isolated mammalian skeletal muscles. Am. J. Physiol. **197**, 1205-1210.

Renkin, E.M. (1977) Multiple pathways of capillary permeability. Circ. Res. **41**, 735-743.

Rhinelander, F.W. (1968) The normal microcirculation of diaphyseal cortex and its response to fracture. J. Bone and Jt. Surg. **50A**, 784-800.

Rose, C.P. and Goresky, C.A. (1976) Vasomotor control of capillary transit time heterogeneity in the canine coronary circulation. Circ. Res. **39**, 541-554.

Rose, C.P., Goresky, C.A. and Bach, G.G. (1977) The capillary and sarcolemmal barriers in the heart - an exploration of labelled water permeability. Circ. Res. **41**, 515-533.

Rose, C.P., Goresky, C.A., Bélanger, P. and Chen, M-J. (1980) Effect of vasodilation and flow rate on capillary permeability surface product and interstitial space size in the coronary circulation. Circ. Res. **47**, 312-328.

Rowland, R.E. (1966) Exchangeable bone calcium. Clin. Orthop. and Rel. Res. **49**, 233-248.

Sapirstein, L.A. (1958) Regional blood flow by fractional distribution of indicators. Am. J. Physiol. **193**, 161-168.

Schnitzer, J.E., McKinstry, P., Light, T.R. and Ogden, J.A. (1982) Quantitation of regional chondroosseous circulation in canine tibia and femur. Am. J. Physiol. **242**, H365-H375.

Silverman, M. and Trainor, C. (1982) *In vivo* determination of cellular uptake in the kidney. Fed. Proc. **41**, 3054-3060.

Spiegel, M.R. (1972) Moments, skewness and kurtosis. In: Theory and problems of statistics, Schaum's outline series : McGraw-Hill Book Company, 89-98.

Talmage, R.V. (1969) Calcium homeostasis - calcium transport - parathyroid action. Clin. Orthop. **67**, 210-224.

Talmage, R.V. (1970) Morphological and physiological considerations in a new concept of calcium transport in bone. Am. J. Anat. **129**, 467-476.

Tancredi, R.G., Yipintsoi, T. and Bassingthwaighte, J.B. (1975) Capillary and cell wall permeability to potassium in isolated dog hearts. Am. J. Physiol. **229**, 537-544.

Thompson Jr., H.K., Starmer, C.F., Whalen, R.E. and McIntosh, H.D. (1964) Indicator transit time considered as a gamma variate. Circ. Res. **14**, 502-515.

Tothill, P. (1984) Review : Bone blood flow measurement. J. Biomed. Eng. **6**, 251-256.

Tothill, P. and Hooper, G. (1984) Invalidity of single-passage measurements of the extraction of bone-seeking tracers in rats and rabbits. J. Orthop. Res. **2**, 75-79.

Tothill, P., Hooper, G., McCarthy, I.D. and Hughes, S.P.F. (1985) The variation with flow-rate of the extraction of bone-seeking tracers in recirculation experiments. Calcif. Tissue Int. **37**, 312-317.

Tothill, P., Hooper, G., McCarthy, I.D. and Hughes, S.P.F. (1987) The pattern of distribution of blood flow in dog limb bones measured using microspheres. Submitted to Clin. Phys. Physiol. Meas. In press.

Trueta, J. and Harrison M.H.M. (1953) The normal vascular anatomy of the femoral head in adult man. J. Bone and Jt. Surg. **35B**, 442-461.

Weinman, D.T., Kelly, P.J., Owen, C.A. and Orvis, A.L. (1963) Skeletal clearance of ^{47}Ca and ^{85}Sr and skeletal blood flow in dogs. Proc. Mayo Clin. **38**, 559-570.

Wootton, R. (1974) The single-passage extraction of ^{18}F in rabbit bone. Clin. Sci. Mol. Med. **47**, 73-77.

Yipintsoi, T., Dobbs Jr., W.A., Scanlon, P.D., Knopp, T.J. and Bassingthwaighte, J.B. (1973) Regional distribution of diffusible tracers and carbonized microspheres in the left ventricle of isolated dog hearts. Circ. Res. **33** 573-587.

Yudilevich, D.L. and Smaje, L.H. (1976) Serial barriers to blood-tissue transport in the cat salivary gland using single passage multiple tracer dilution. In: Grayson, J. and Zingg, W. (eds.), Transport mechanisms, disease states. Microcirculation II,. Plenum (pub), New York, U.S.A., 79-81.

PRESENTATIONS & PUBLICATIONS

Presentations

A distributed model to analyse mineral exchange between blood and bone. 5th Int. Conf. Mechanics in Medicine & Biology, Bologna, Italy, July 1986.

Optimisation of a multicapillary model of blood-bone exchange to multiple tracer outflow dilution data. British Microcirculation Society, London, Apr. 1987. (Abstract to be published).

Assessment of blood flow in the canine tibial diaphysis using the microsphere technique. 4th Int. Symp. on Bone Circulation, Toulouse, France, Sept. 1987. (Paper to be published).

A multicapillary distributed model of blood-bone exchange to analyse multiple tracer outflow dilution data. 4th Int. Symp. on Bone Circulation, Toulouse, France, Sept. 1987. (Paper to be published).

Publication

S.M. Willans & I.D. McCarthy, Distributed model of blood-bone exchange, J. Biomed. Eng. 8, 235-243, 1986.

DISTRIBUTED MODEL OF BLOOD–BONE EXCHANGE

S.M. Willans and I.D. McCarthy

Received December 1985; accepted February 1986

ABSTRACT

An understanding of bone physiology obtained from a knowledge of fluid spaces and their associated barriers may lead to better management of bone pathologies. Such information can be obtained by mathematically modelling the results of multiple tracer outflow dilution techniques, which in our case were performed on the canine tibia. Hence, a computer model was developed to describe the exchange processes of tracers between blood and bone. Capillary permeability, bone binding and the vascular, interstitial fluid and bone volumes of distribution were used as parameters in the equations describing the system, which also used published morphometric bone data. Parameter estimates were then derived by the use of optimization procedures.

Keywords: Musculoskeletal system, bone, mathematical model, ion exchange

INTRODUCTION

The application of compartment analysis to the study of solute and water exchange in tissue is limited. The assumptions of compartment analysis are that each compartment is wholly and instantaneously mixed, the system is in a steady state with respect to the mother substance, and the volumes and exchange rates between compartments are constant. It is usually the first assumption that is the problem. Indicator dilution curves show that plasma is not an instantaneously mixed compartment. Along capillaries of the organ of interest there are usually axial concentration gradients; these have led to the incorporation of some degree of structure into the modelling of exchange processes, particularly in the coronary and hepatic circulation. The uses of these distributed models have been reviewed by Bassingthwaighte and Goresky[1].

Mathematical models that describe ion exchange between blood and bone have generally been limited in terms of physiological and anatomical considerations. The majority employ a compartment analysis and attempt to measure rate constants in bone for large exchangeable pools[2]. Invariably in such models, parameters such as permeable capillary walls, capillary configurations and blood flow have not been considered. The models have been prescribed for long term exchange (hours to days) and very few have dealt with short term exchange (minutes).

Diffusion has been shown to be the mechanism for the movement of ions across bone capillaries[3–5]. A number of investigators have applied multiple tracer outflow dilution (MTOD) techniques to canine tibiae and have calculated extractions $E(t)$ from transport functions $h(t)$ of reference (R) and diffusible (D) tracers. The formula used was,

$$E(t) = \frac{h_R(t) - h_D(t)}{h_R(t)} \quad (1)$$

where $h(t)$ represents the fraction of the injected dose appearing in the outflow per unit time. Capillary permeability–surface area PS_C products for diffusible tracers have been obtained from maximum extractions E_{max} and solute flows F_s using the equation derived independently by Renkin[6] and Crone[7].

$$PS_C = -F_s \log_e (1 - E_{max}) \quad (2)$$

Permeability ratios of ^{85}Sr and ^{99m}Tc labelled ethane-1-hydroxy-1,1-diphosphonate (^{99m}Tc-EHDP) with ^{14}C-sucrose were in close agreement with corresponding ratios of free diffusion coefficients, suggesting a passive diffusion process taking place[4,5]. Further studies reveal that bone has an extravascular-extracellular fluid space[8–10], the size of which considerably influences the ion exchange between blood and bone. Back diffusion, referring to the return of diffusible tracer to flowing blood without recirculation, has been shown from theoretical and experimental extraction profiles and must be seriously considered in theoretical models.

This paper describes a simple homogeneous capillary–interstitial fluid–bone model to interpret the kinetics of short term ion exchange in the canine tibia. Assumptions made in the development of the equations are explicitly discussed. Theoretical outflow dilution curves were developed and used as input to examine the effects of varying model parameters, which were further studied by derivation of impact functions. The effect of noise superimposed on the theoretical curves was used to study parameter estimations. Finally, optimization procedures were used to fit the model to experimental data.

Department of Orthopaedic Surgery, University of Edinburgh, Medical School Buildings, Teviot Place, Edinburgh EH8 9AG, UK
Reprints from Dr I.D. McCarthy

0141–5425/86/030235–09 $3.00

The model utilizes venous blood count data from MTOD techniques[11]. In short, the radioactive tracers ^{125}I-albumin, ^{86}Rb and ^{85}Sr were injected simultaneously, via a cannulated tibial nutrient artery, into bicarbonate buffer which was perfused through the bone at a constant rate of 2.0 ml/min. Blood samples containing the tracer washout were taken immediately from the ipsilateral femoral vein; the sample collection time was 5 s with 60 samples being collected over a 5 min period. Quantitative values of volumes of distribution and permeability–surface area products for the diffusible tracers ^{86}Rb and ^{85}Sr, were obtained from the model using the reference tracer ^{125}I-albumin as input. ^{86}Rb and ^{85}Sr were used because the former is a tracer for potassium and enters bone cells, and the latter exchanges with calcium in the hydroxyapatite. These quantitative values were compared with extraction data, and fluid space measurements made from tracer equilibration studies.

MODELLING METHOD

Anatomical investigations of the tibial diaphysis of adult dogs have shown that the blood flows through the microvasculature of the cortex and marrow are in parallel[12]. In this respect it is reasonable to treat the cortex and marrow independently, as has been the case in bone blood flow determinations using microspheres[13]. The bulk of arterial blood to the tibial diaphysis is supplied by a single nutrient artery and the major portion of venous drainage has been found to be via small venules through the cortex into periosteal veins.

With regard to modelling, the parallel, independent nature of the microvasculature simplifies the exchanges of tracers in the bone considerably. In this paper, interest is centred solely on the cortex, with the model describing tracer kinetics in parallel arrays of Haversian systems, which are assumed to contain the exchanging vessels of cortical bone. A Haversian system is a cylindrical unit which contains a central Haversian canal, within which is a capillary. Their morphometric dimensions, as given in *Table 1*, influence some of the assumptions which follow; Volkmann canals that connect neighbouring Haversian systems and lamellar bone have not been considered. Exchange between the Haversian canal and osteocytes within the bone matrix is facilitated by canaliculi, fine channels of approximately 0.1–1.0 μm diameter[16].

The model is composed of a number of parallel idealized tissue units which consist of concentric

Table 1 Morphometric measurements of Haversian systems in long bones of dogs and man

Description	Measurement (x 10^{-4} cm)		Reference
	Dog	Man	
Cement line radius (R_{CL})	(77 ± 19)	(112 ± 25)	14 : 14
Haversian canal radius (R_{HC})	(14 ± 6)	25	14 : 15, 16
Haversian canal length (L_{HC})	—	5000	: 15, 16
Capillary radius (R_C)	5	5	—

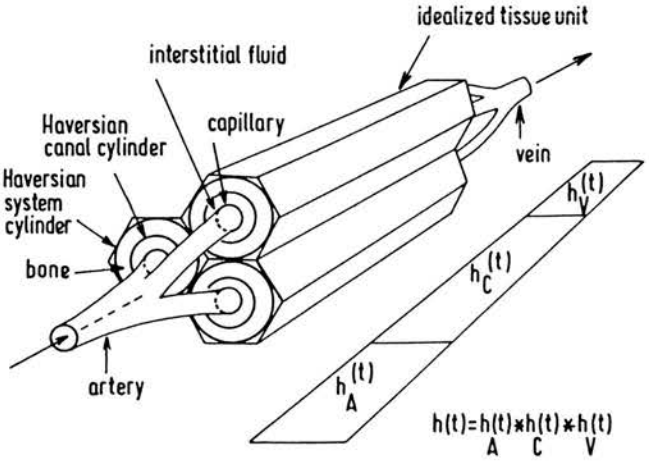

Figure 1 Parallel, hexagonal idealized tissue units responsible for tracer exchange, shown with artery and vein. These units consist of concentric cylinders of capillary, Haversian canal and Haversian system. The volume between the latter cylinder and the boundary of the hexagonal tissue unit is negligible. Flows in adjacent capillaries and volumes in each tissue unit are equal, such that there are no concentration gradients across the interface between units

cylinders of capillary–interstitial fluid–bone. These units can be thought of in terms of Krogh cylinders subjected to equal blood flows, such that there are no concentration gradients across the interfaces (see *Figure 1*). The following assumptions have been made.

1. The system to be modelled is considered to be uniform and straight geometrically, such that radial fluxes are independent of axial fluxes and the system is radially symmetric.
2. The system is assumed to be linear and stationary, to ensure mass conservation when there is no consumption of tracer.
3. Permeable boundaries have negligible thickness so that tracer does not accumulate there and have axially uniform permeability–surface area products.
4. Capillary tracer movement is described by a flat velocity profile, which is reasonable in view of small bone capillary diameters being typically of the order of 10 μm. Flat velocity profiles allow much easier solutions to the model.
5. Convection is assumed to occur only in the capillaries.
6. Radial diffusion is adjudged to be rapid on the basis of short relaxation times (τ) regarding the distance between a bone capillary and the extremities of a Haversian canal. For example

$$\tau = (R_{HC} - R_C)^2/D = 0.04 \text{ s}$$

using a typical effective diffusion coefficient $D = 2.0 \times 10^{-5}$ cm^2/s. This assumes that binding occurs only on the surface of the Haversian canal and that binding on internal canalicular and lacunar surfaces can be ignored.

7. Axial diffusion is assumed to be negligible because the transit times for the vessels are short in comparison with relaxation times for diffusion along the axial distances involved.

As a result of these assumptions, the concentrations of solute in capillary, (C), interstitial fluid, (I), and bone, (B) can be described by three partial differential equations.

For the capillary of length L(cm), subject to a solute flow F_s (ml/s),

$$\left.\begin{aligned}
\frac{\partial C_C(x,t)}{\partial t} &= \frac{PS_C}{V'_C}\,[C_I(x,t) - C_C(x,t)] \\
&\quad - \frac{F_s L}{V'_C}\,\frac{\partial C_C(x,t)}{\partial x}
\end{aligned}\right\}$$

For the interstitial fluid

$$\left.\begin{aligned}
\frac{\partial C_I(x,t)}{\partial t} &= \frac{PS_C}{V'_I}\,[C_C(x,t) - C_I(x,t)] \\
&\quad - \frac{PS_B}{V'_I}\,[C_I(x,t) - C_B(x,t)]
\end{aligned}\right\} \quad (3)$$

For the bone

$$\left.\begin{aligned}
\frac{\partial C_B(x,t)}{\partial t} &= \frac{PS_B}{V'_B}\,[C_I(x,t) - C_B(x,t)]
\end{aligned}\right\}$$

where PS is a passive permeability–surface area product (ml/s), V' is apparent volume of distribution (ml) and $C(x, t)$ is concentration (units of choice) as a function of axial position x (cm) and time t (s). The apparent volume of distribution represents the anatomical volume accessible to the tracer multiplied by a factor which accounts for the compounded effects of parameters such as volume exclusion, phase partition coefficients, tracer binding and asymmetric transport across boundaries. The concentrations are defined in terms of apparent volume of distribution. The notation of PS_B and V'_B has been used for bone. These parameters apply to bone cells and to a hypothetical pool representing bone surface binding, when describing the kinetics of ^{86}Rb and ^{85}Sr respectively.

The equations were solved by a numerical technique described by Bassingthwaighte[17]. Firstly, they were reduced to ordinary differential equations by dividing the phases up into a number of segments n_x along the vessel such that each equation described tracer exchange across a permeable barrier in a segment. The equations were then solved in finite difference form using analytical solutions. Thus, solute fluxes across each permeable barrier in each segment during a time interval Δt were calculated, where $\Delta t = T_C/n_x$, with T_C being the capillary transit time. These solutions of solute flux were used to calculate new segmental concentrations. Then, the process of convection was achieved by sliding the capillary concentration values along by one segment in the direction of flow. The concentration in the n_xth segment then became the capillary outflow concentration. The processes of successively calculating fluxes and concentrations, then sliding capillary concentrations by one segment were repeated up to a prescribed time, to meet the demands of a lengthy continuous input and changing concentration gradients. All the calculations were accomplished on the University of Edinburgh's BUSH (ICL 2988) computer system using a program written in Fortran 77.

To permit applications of the model to experimental data from bone, it neglects any contributions due to bone marrow; this assumption is reasonable in data from the perfused tibia because of the much higher proportion of cortex to marrow. Also, one should consider the transport functions (probability density function of transit times) of the arteries and veins $h_A(t)$ and $h_V(t)$, as well as the capillaries for the whole system (see *Figure 1*). The transport function of the whole system is the convolution of the arterial, transcapillary and venous transport functions

$$h(t) = h_A(t) * h_C(t) * h_V(t) \quad (4)$$

or

$$h(t) = h_C(t) * h_{LV}(t) \quad (5)$$

where $h_C(t)$ is the impulse response of the capillary tissue cylinder and $h_{LV}(t)$ is a large vessel transport function.

For MTOD techniques which involve inflow injections and outflow sampling one can write

$$C_{Out}(t) = C_{In}(t) * h(t) = \int_0^t C_{In}(\alpha)\, h(t-\alpha)\, d\alpha \quad (6)$$

where $C_{In}(t)$ and $C_{Out}(t)$ are inflow and outflow concentrations respectively which can be expressed in terms of variable counts. α is a variable used for the integration.

For the purposes of this homogeneous model, it is assumed that all capillary transit times are equal, and that the large vessel transit times for each capillary unit are identical. The transport function $h_R(t)$ of an intravascular reference tracer such as ^{125}I-albumin can then be written

$$h_R(t) = h_{LV}(t - T_C) \quad (7)$$

when the transit times T_C of the capillaries are the same. The reference transport function shifted left by one capillary transit time is used as input to the model. Parameters of the model may then be optimized such that the solutions or output fit the transport functions $h_D(t)$ of diffusible tracers. The parameters in question are PS_C, PS_B, V_I' and V_B'. Their final estimates will provide an insight into the role of barriers and fluid spaces in bone for diffusible tracers.

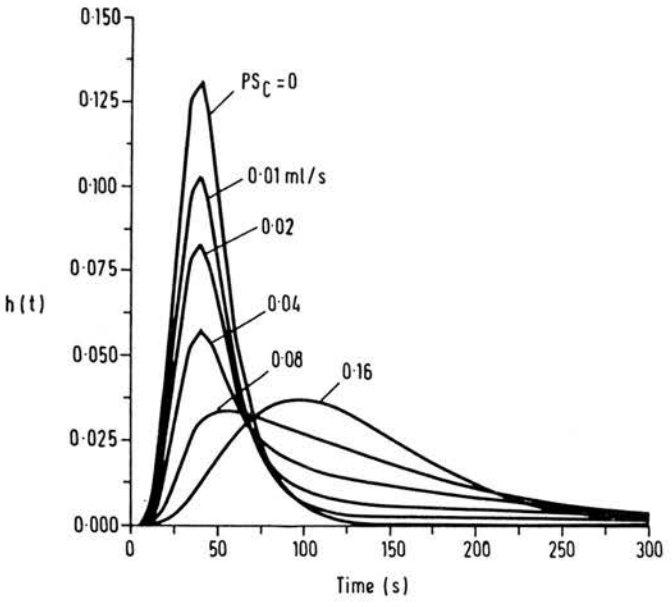

Figure 2 Responses of the model specified as $h(t)$, representing solutions every 5 s for changes in PS_C, with $PS_B = 0$, $F_s = 0.04$ ml/s, $V_I'/V_C' = 8.0$ and $T_C = 10$ s

RESULTS

Simulation of outflow curves from varying the parameters

To appreciate the behaviour of the model it is necessary to examine the responses as a consequence of varying the parameters. A smooth input function was used in this simulation study, obtained using a NAG E04FDF minimization routine to fit a lagged normal density curve to experimental ^{125}I-albumin reference data.

Figure 2 shows the responses of the model to changes in PS_C; the response for $PS_C = 0$ is simply the input function appearing after the capillary transit time. The effect of PS_C is considerable, the peak of the response decreases with increasing PS_C. Also, the tail portions of the responses become more substantial, demonstrating increasing amounts of solute returning to the vascular system i.e. back diffusion. *Figure 3* illustrates the positive extractions which can be calculated from these responses using equation (1). The maximum extraction always occurs at the capillary transit time and decreases as higher concentrations of solute are established in the interstitial fluid space. The rate of decrease is principally governed by the magnitudes of PS_C and V_I'. Smaller PS_C and higher V_I' values always produce slower rates of decrease and vice versa. Responses of the model for changes in V_I'/V_C' are shown in *Figure 4*. The responses for changes in PS_B and V_B'/V_C' are not as apparent when compared to the other parameters, although they do play a decisive role in the modelling of bone.

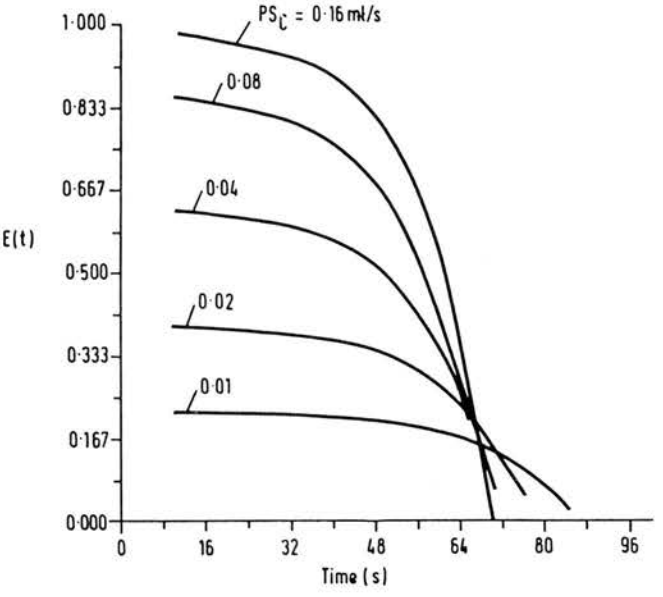

Figure 3 Positive extractions calculated from the responses in *Figure 2*

Impact functions

Impact functions are useful in demonstrating the effects of parameter estimations on the model. Consider the three partial differential equations, equation (3), in the form of a general functional relationship given by

$$\hat{f} = \hat{f}(t; PS_C, PS_B, V_I', V_B') \qquad (8)$$

where $\hat{f}$ is the function calculated for values of an independent variable, time t. The impact function for each parameter is a measure of the change in $\hat{f}$ caused by a perturbation of that parameter. For example, the impact function $\Delta\hat{f}_{PS_C}{}^2$ caused by a

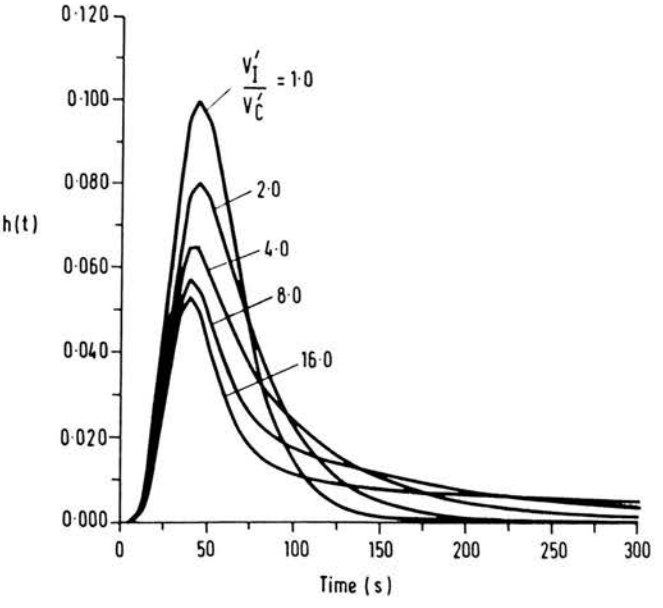

Figure 4 Responses of the model specified as $h(t)$, representing solutions every 5 s for changes in V_I'/V_C', with $PS_C = 0.04$ ml/s, $PS_B = 0$, $F_s = 0.04$ ml/s and $T_C = 10$ s

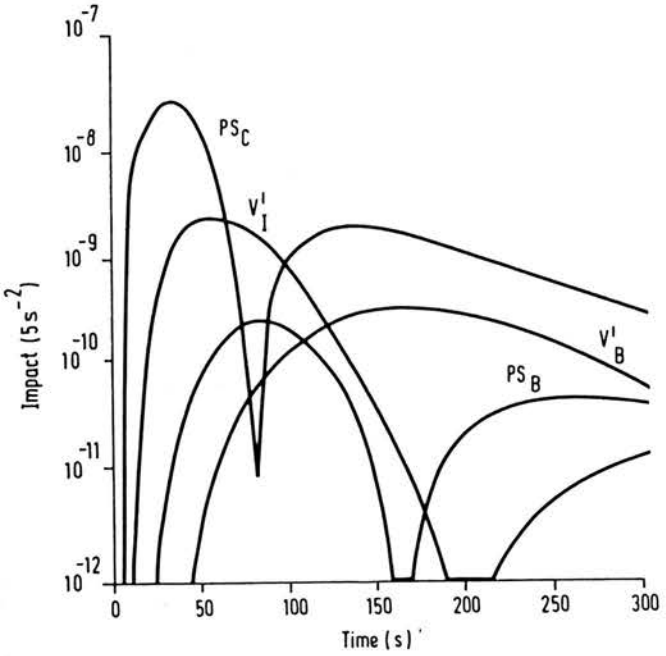

Figure 5 Impact functions (log scale) derived every 5 s, caused by 1% perturbations to the parameters $PS_C/F_s = PS_B/F_s = 1.0$ and $V'_I/V'_C = V'_B/V'_C = 7.5$

perturbation ΔPS_C applicable to the PS_C product is

$$\Delta \hat{f}^2_{PS_C} = [\hat{f}(t; PS_C + \Delta PS_C, PS_B, V'_I, V'_B) - \hat{f}(t; PS_C, PS_B, V'_I, V'_B)]^2 \quad (9)$$

Figure 5 illustrates the impact functions of each of the parameters over the experimental time range for a smooth input function, the size of the perturbations are 1% of the parameter values. It is interesting to observe the considerable effect of PS_C, particularly for early times when extractions are positive. The impact function for V'_B is larger in magnitude over the last half of the time range and emphasizes why so many venous blood count samples have to be taken. The maximum value for each impact function gives one a good idea of the relative accuracies involved in obtaining parameter estimates.

Effects of noise on the parameter estimates

A smooth test model curve with pre-assigned parameter values was produced using a lagged normal density curve as input. The test model curve with varying amounts of noise applied to it, was used to test the accuracy of parameter estimates. The noise was obtained using two NAG routines G05CCF and G05DDF, to produce a non-repeatable Gaussian distribution of random numbers which was subsequently added to the test model data. Noise was defined in terms of standard deviation (s.d.$_p$) calculated at the peak of the response. Optimization was achieved using a BMDP package (see Appendix). *Table 2* illustrates the effects of noise on the parameter estimates using 50% high initial estimates for the optimization routine. These results show the trend of higher coefficients of variation (c.v.) and residual sum of squares (*RSS*) with higher levels of noise. They also suggest that estimations of PS_C are relatively accurate in comparison with the other parameters, and show that for accurate estimations many samples and long counting times are necessary.

Fitting the experimental data

Tables 3 and *4* show the results for parameter estimates of experimental ^{86}Rb and ^{85}Sr data respectively; lower bounds as well as starting values are shown because they were required to prevent negative estimates and model solutions exceeding the computational range. Starting values were picked close to the limit nearer zero, as advised in the BMDP literature. The choice of a starting value for PS_C was found to be very influential in obtaining quick and meaningful results from the package. A PS_C value slightly less than an experimental value calculated from equations (1) and (2) was found to be the most suitable. The number of increment halvings cited in the tables gives an indication of the adequacy of the model, the higher the value the less adequate the model (see Appendix).

The fitting of data for experiments 3 and 5 is not very good, indicated by the fact that the pre-assigned maximum number of increment halvings has been reached several times. The CPU times and c.v.s for these experiments are also generally higher than for the others. For ^{85}Sr data, experiment 5, the final values shown represent the last parameter estimates which were obtained

Table 2 Effects of noise on the parameter estimates using BMDP PAR. Final values, residual sum of squares (*RSS*) and coefficients of variations (c.v.) are averaged over given number of runs. No bounds or constraints applied. Pre-assigned package values. $T_C = 10$ s, $n_x = 10$

Noise level (s.d.$_p$)	Number of runs	Parameter vector $\left(\frac{PS_C}{F_s}, \frac{PS_B}{F_s}, \frac{V'_I}{V'_C}, \frac{V'_B}{V'_C}\right)$			c.v.	*RSS*
		Starting values	Final values	True values		
0%	1	1.50, 1.50, 11.25, 11.25	1.00, 1.00, 7.50, 7.50	1.00, 1.00, 7.50, 7.50	—	2.95×10^{-14}
1%	5	1.50, 1.50, 11.25, 11.25	1.01, 1.01, 7.55, 7.52	1.00, 1.00, 7.50, 7.50	0.25, 2.24, 1.15, 0.84	1.86×10^{-7}
5%	5	1.50, 1.50, 11.25, 11.25	1.01, 1.05, 7.50, 7.64	1.00, 1.00, 7.50, 7.50	0.50, 9.05, 4.94, 5.66	5.25×10^{-6}
10%	5	1.50, 1.50, 11.25, 11.25	1.01, 1.08, 7.05, 7.88	1.00, 1.00, 7.50, 7.50	3.70, 19.95, 12.54, 12.24	2.10×10^{-5}

Table 3 Parameter estimates of experimental ^{86}Rb data using ^{125}I-albumin as input to the model. Maximum increment halvings = 100, otherwise pre-assigned BMDP package values. T_C = 10 s, n_x = 10

Experiment number	Parameter vector $\left(\frac{PS_C}{F_s}, \frac{PS_B}{F_s}, \frac{V'_I}{V'_C}, \frac{V'_B}{V'_C}\right)$			c.v.	*RSS*	CPU time (s)	Largest number of increment halvings required (No. of times for maximum)
	Starting values	Lower bounds	Final values				
1	1.818, 0.303, 1.515, 1.515	0.030, 0.000, 0.030, 0.030	2.527, 0.621, 1.964, 7.935	11.089, 8.595, 8.682, 15.057	4.425×10^{-4}	38.46	5
2	1.818, 0.303, 1.515, 1.515	0.030, 0.000, 0.030, 0.030	1.870, 0.409, 2.654, 7.367	6.877, 11.215, 6.247, 20.005	3.575×10^{-4}	37.07	3
3	1.061, 0.303, 1.515, 1.515	0.030, 0.000, 0.030, 0.030	0.897, 0.094, 2.720, 1.780	10.203, 137.663, 13.143, 11.867	5.764×10^{-4}	611.17	100(6)
4	1.212, 0.303, 1.515, 1.515	0.030, 0.000, 0.030, 0.030	1.770, 0.936, 2.661, 16.066	4.212, 5.613, 6.608, 10.309	1.423×10^{-4}	80.70	8
5	0.757, 0.303, 1.515, 1.515	0.030, 0.000, 0.030, 0.030	0.691, 0.330, 36.785, 16.394	0.856, 20.242, 13.752, 188.090	1.413×10^{-4}	504.87	100(4)
6	0.909, 0.303, 1.515, 1.515	0.030, 0.000, 0.030, 0.030	1.258, 0.518, 2.664, L	3.784, 6.874, 5.631, L	5.808×10^{-5}	105.36	7

L: Large, value is larger than format specifications of package

Table 4 Parameter estimates of experimental ^{85}Sr data using ^{125}I-albumin as input to the model. Maximum increment halvings = 100, otherwise pre-assigned BMDP package values. T_C = 10 s, n_x = 10

Experiment number	Parameter vector $\left(\frac{PS_C}{F_s}, \frac{PS_B}{F_s}, \frac{V'_I}{V'_C}, \frac{V'_B}{V'_C}\right)$			c.v.	*RSS*	CPU time (s)	Largest number of increment halvings required (No. of times for maximum)
	Starting values	Lower bounds	Final values				
1	2.121, 0.303, 1.515, 1.515	0.030, 0.015, 0.303, 0.303	2.052, 1.042, 2.644, 22.498	3.550, 2.827, 4.811, 5.906	5.480×10^{-5}	118.76	11
2	1.970, 0.303, 1.515, 1.515	0.030, 0.015, 0.303, 0.303	1.909, 0.770, 3.714, 20.712	4.103, 5.357, 5.323, 11.362	1.271×10^{-4}	67.27	8
3	1.212, 0.303, 1.515, 1.515	0.030, 0.015, 0.303, 0.303	0.985, 0.094, 7.189, 2.064	3.134, 174.690, 5.495, 5.980	3.875×10^{-4}	926.87	100(9)
4	1.818, 0.303, 1.515, 1.515	0.030, 0.015, 0.303, 0.303	1.764, 1.279, 3.934, 27.072	2.639, 4.329, 5.604, 7.909	6.592×10^{-5}	52.11	5
5	0.606, 0.303, 1.515, 1.515	0.030, 0.015, 0.303, 0.303	0.618*, 0.015*, 121.062*, 292.623*	NA, NA, NA, NA	1.790×10^{-4}*	—	100(3)
6	0.909, 0.303, 1.515, 1.515	0.030, 0.015, 0.303, 0.303	1.242, 0.964, 5.501, 149.542	1.701, 5.221, 4.788, 51.606	1.434×10^{-5}	35.23	2

* Last values obtained for an incomplete run. NA: not available

before the program failed; failure was due to very high parameter estimates of V'_I and V'_B which caused some of the exponential terms in the analytical solution to be out of computational range. The CPU time has not been cited and the c.v.s are not available because the run was incomplete; additional runs using different starting values could not remedy the situation, hence the model is unsatisfactory for this data. *Figure 6* shows the poor model fit to ^{86}Rb data of experiment 3. The fitting of data for experiments 1, 2, 4 and 6 was considered satisfactory in view of smaller c.v.s, CPU times and numbers of increment halvings used. *Figures 7a* and *b* illustrate the fitting of the model to ^{86}Rb and ^{85}Sr data respectively, of experiment 4.

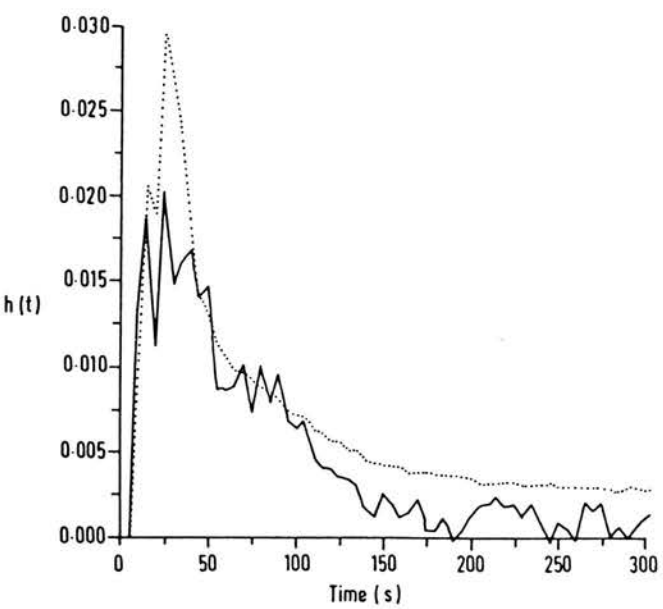

Figure 6 Poor model fit (dotted line) to ^{86}Rb data of experiment 3 (solid line). Fitting is performed at 5 s multiples for 300 s

Comparison of experimental and theoretical extractions and PS_c products

Table 5 shows mean and standard deviations of experimental and theoretical maximum extractions E_{max} and PS_C which were calculated from equations 1 and 2 for both of the diffusible tracers using the six sets of data (n = 6). The theoretical and

Table 5 Mean and s.d. of E_{max} and PS_C for ^{86}Rb and ^{85}Sr (n = 6)

	^{86}Rb	^{85}Sr
Experimental		
E_{max}	0.73 ± 0.11	0.76 ± 0.12
PS_C (ml/s)	0.046 ± 0.014	0.052 ± 0.018
Theoretical		
E_{max}	0.73 ± 0.16	0.73 ± 0.16
PS_C (ml/s)	0.050 ± 0.023	0.047 ± 0.019

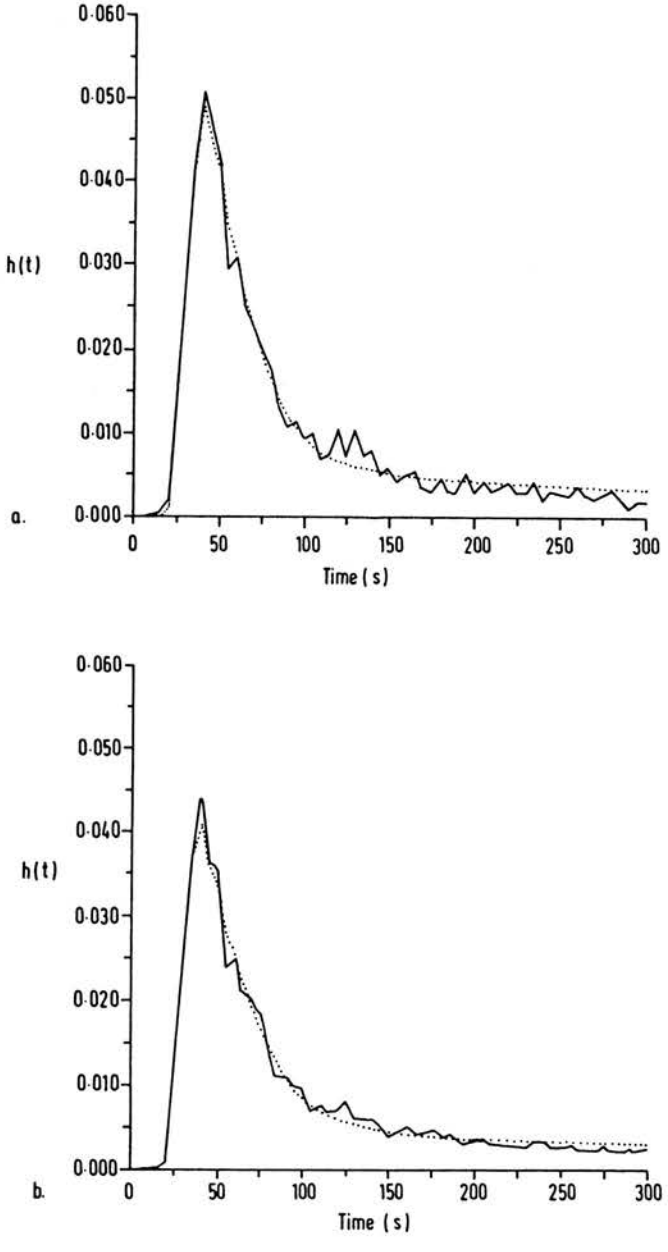

Figure 7 Satisfactory model fits (dotted lines) to, **a**, ^{86}Rb and, **b**, ^{85}Sr data of experiment 4 (solid lines). Fitting is performed at 5 s multiples for 300 s

experimental values were quite similar for each of the tracers and suggest that sensible values for E_{max} were found from experimental extraction data.

Permeability ratios (P_{Rb}/P_{Sr}) were found by dividing the PS_C product of ^{86}Rb with that of ^{85}Sr. The theoretical and experimental ratios (P_{Rb}/P_{Sr}) were found to be 1.04 ± 0.11 and 0.90 ± 0.11 respectively. These values fall short of the free diffusion coefficient ratio (D_{Rb}/D_{Sr}) of 1.58, where[18] $D_{Rb} = 2.10 \times 10^{-5}$ and[19] $D_{Sr} = 1.33 \times 10^{-5}$ cm^2/s in water at 25°C. This is probably due to an underestimation of PS_C for ^{86}Rb which may suggest that part of the ^{86}Rb is being taken up by the endothelial cells forming the capillary wall.

Table 6 Mean and s.d. of V_I'/V_C' and V_B'/V_C' for ^{86}Rb and ^{85}Sr. Experimental numbers used in parentheses

	^{86}Rb	^{85}Sr
V_I'/V_C'	2.49 ± 0.35 (1, 2, 4, 6)	3.95 ± 1.18 (1, 2, 4, 6)
V_B'/V_C'	10.46 ± 4.87 (1, 2, 4)	23.43 ± 3.28 (1, 2, 4)

Apparent volumes of distribution

Table 6 shows the mean ± s.d. values of parameter estimates V_I'/V_C' and V_B'/V_C' found for the diffusible tracers. The ratios quoted were calculated from the parameter estimates of satisfactory experimental fits and represent apparent volumes of distribution. The larger V_I'/V_C' ratio for ^{85}Sr compared to ^{86}Rb suggests that the interstitial fluid is more accessible to ^{85}Sr, if one assumes equal accessibilities for the tracers in the bicarbonate buffer flowing through the capillaries.

DISCUSSION

The model was developed to interpret the results of MTOD techniques to provide constructive information about ion exchange in bone. Although the model far from resembles the complex structure of bone, it is considerably more advanced than the compartment models which have preceded it. When optimization procedures were used to derive parameter values by fitting to experimental data, the model was able to provide satisfactory fits in the majority of cases.

The similar experimental and theoretical E_{max} values (*Table 5*) found for ^{86}Rb and ^{85}Sr can be compared with values from other authors. The mean E_{max} for ^{86}Rb is similar in magnitude to a value of $E_{max} = 0.84 \pm 0.05$ ($n = 4$) found by Alvarez and Yudelivich[18] who studied the heart. The mean E_{max} for ^{85}Sr is in reasonable agreement with values of $E_{max} = 0.69 \pm 0.11$ ($n = 14$)[4], $E_{max} = 0.75 \pm 0.10$ ($n = 3$)[5] and $E_{max} = 0.82 \pm 0.06$ ($n = 5$)[11] found for normal canine tibiae.

The experimental permeability ratios (P_{Rb}/P_{Sr}) calculated from E_{max} using equations 1 and 2 were found to be lower than theoretical ratios. These findings are consistent when compared with the higher theoretical estimates of PS_C found by Guller *et al.*[20], when they fitted a similar model to experimental dilution curves obtained for sodium in perfused dog hearts. The experimental ratios are lower because the Renkin and Crone formula, equation (2), does not account for back diffusion which may have occurred before the onset of venous sampling. This effect would reduce extractions and hence permeabilities calculated from the venous blood samples. The low permeability ratio found for ^{86}Rb and ^{85}Sr as compared with their free diffusion coefficient ratio could be due to the model. It would be interesting to see whether the difference in the ratios is reduced if a heterogeneous flow

model is used. Alternatively, the low permeability ratio may be due to an underestimation of PS_C for ^{86}Rb caused by uptake to endothelial cells comprising the capillary wall.

The ratios of apparent volumes of distribution (*Table 6*) can only be directly compared to other ratios if the same tracers were used under the same experimental conditions. Nevertheless, the V_I'/V_C' ratios found for ^{86}Rb and ^{85}Sr are about the same order of magnitude compared with $V_I'/V_C' = 2.20 \pm 1.35$ calculated from data[9] in which ^{99m}Tc-albumin (plasma), ^{99m}Tc-labelled red blood cells, and ^{14}C-sucrose (extravascular) tracers were used. The ratio of $V_B'/V_C' = 10.46 \pm 4.87$ for ^{86}Rb, with V_B' being applicable to bone cells, agrees quite favourably with $V_B'/V_C' = 6.00 \pm 1.15$ (mature dogs) and $V_B'/V_C' = 6.00 \pm 1.30$ (old dogs) calculated from data[21] in which ^{99m}Tc-labelled red blood cells were used. The latter V_B'/V_C' ratios may be low as V_B' was estimated just from osteocyte measurements. The high V_B'/V_C' ratio for ^{85}Sr indicates that it must be absorbed by the large bone surface area.

The fact that some of the experimental data could not be adequately described by the model, indicates that modifications need to be developed. Firstly, it has been assumed that blood flow in the tibia is homogeneous, in reality, there is a distribution of flows whose heterogeneity should be considered. Bassingthwaighte and Goresky[1], have reported that PS_C is consistently underestimated when a similar homogeneous model is used to fit heterogeneous data, and the error increases with increasing heterogeneity. Secondly, dispersion in large vessels should be studied. Although it seems that parameter estimates are relatively robust to changes in input function, the appropriate form of the input function should be examined. Thirdly, radial diffusion gradients have been ignored and the relative importance of binding in the canalicular system must be considered.

Experimentally, it may be possible to improve the accuracy of parameter estimates by using more tracers. For example, ^{14}C-sucrose is not taken up by bone cells, nor does it bind to bone. If an outflow dilution curve for ^{14}C-sucrose were developed, it could be used to estimate V_I'; this value could then be used as a constraint in the estimates for ^{86}Rb and ^{85}Sr data. More complex models could be studied, but again this would probably require additional tracers in the bolus to provide sufficiently accurate parameter estimates.

Despite these provisos, the development of a distributed model is an important step in being able to understand the physiological mechanisms behind the kinetic information derived from outflow dilution experiments applied to bone.

ACKNOWLEDGEMENTS

S.M. Willans was in receipt of an Edinburgh University, Faculty of Medicine Scholarship. The authors would like to thank Professor S.P.F. Hughes and Mr R.H. Fleming for their assistance in the experimental work, which was funded by the Medical Research Council.

REFERENCES

1 Bassingthwaighte, J.B. and Goresky, C.A. Modelling in the analysis of solute and water exchange in the microvasculature. In: *Handbook of Physiology - The Cardiovascular System IV* American Physiological Society; Bethesda, USA 1984, 549–626
2 Groer, P.G. and Marshall, J.H. Mechanisms of calcium exchange at bone surfaces. *Calc. Tiss. Res.* 1973, **12**, 175–92
3 Cofield, R.H., Bassingthwaighte, J.B. and Kelly, P.J. Strontium-85 extraction during transcapillary passage in tibial bone. *J. Appl. Physiol.* 1975, **39**, 596–602
4 Davies, D.R., Bassingthwaighte, J.B. and Kelly, P.J. Transcapillary exchange of strontium and sucrose in the canine tibia. *J. Appl. Physiol.* 1976, **40**, 17–22
5 Hughes, S.P.F., Davies, D.R., Bassingthwaighte, J.B., Knox, F.G. and Kelly, P.J. Bone extraction and blood clearance of diphosphonate in the dog. *Am. J. Physiol.* 1977, **232**, H341–7
6 Renkin, E.M. Transport of potassium-42 from blood to tissue in isolated mammalian skeletal muscles. *Am. J. Physiol.* 1959, **197**, 1205–10
7 Crone, C. The permeability of capillaries in various organs as determined by the use of the 'indicator diffusion' method. *Acta Physiol. Scand.* 1963, **58**, 292–305
8 Hughes, S.P.F., Davies, D.R., Khan, R.A.A. and Kelly, P.J. Fluid space in bone. *Clin. Orthop.* 1978, **134**, 332–341
9 Morris, M.A., Lopez-Curto, J.A., Hughes, S.P.F., An, K.N., Bassingthwaighte, J.B. and Kelly, P.J. Fluid spaces in canine bone and marrow. *Microvasc. Res.* 1983, **23**, 188–200
10 Hooper, G., McCarthy, I.D., Wooton, R. and Hughes, S.P.F. Fluid spaces the canine tibia, In: *Bone Circulation,* (Eds. J. Arlet, R.P. Ficat and D.S. Hungerford), Williams and Wilkins: Baltimore, USA, 1984, 204–206
11 McCarthy, I.D. and Hughes, S.P.F. Serial barriers to blood-bone exchange in the normal canine tibia Submitted to *Am. J. Physiol.*
12 Lopez-Curto, J.A., Bassingthwaighte, J.B. and Kelly, P.J. Anatomy of the microvasculature of the tibial diaphysis of the adult dog. *J. Bone Jt Surg* 1980, **62A**, 1362–9
13 Morris, M.A. and Kelly, P.J. Use of tracer microspheres to measure bone blood flow in conscious dogs. *Calcif. Tissue Int.* 1980, **32**, 69–76
14 Jowsey, J. Studies of Haversian systems in man and some animals. *J. Anat.* 1966, **100**, 857–864
15 Johnson, L.C. Morphologic analysis in pathology: The kinetics of disease and general biology of home, In: *Henry Ford Hospital - International Symposium - Bone Biodynamics,* J. and A. Churchill Ltd: London, UK, 1963, 543–654
16 Atkinson, P.J. and Hallsworth, A.S. The spatial structure of bone. In: *Progress in Anatomy,* (Eds. R.J. Harrison and V. Navaratman), Vol 2, Cambridge University Press, 1982, 179–198
17 Bassingthwaighte, J.B. A concurrent flow model for extraction during transcapillary passage. *Circ. Res.* 1974, **35**, 483–503
18 Alvarez, O.A. and Yudelivich, D.L. Heart capillary permeability to lipid insoluble molecules. *J. Physiol.* 1969, **202**, 45–58
19 Maltby, B., Lemon, G.J., Bassingthwaighte, J.B. and Kelly, P.J. Exchange of potassium and strontium in adult bone. *Am. J. Physiol.* 1982, **242**, H705–H712
20 Guller, B., Yipintsoi, T., Orvis, A.L. and Bassingthwaighte, J.B. Myocardial sodium extraction at varied coronary flows in the dog: estimation of capillary permeability by residue and outflow detection. *Circ. Res.* 1975, **37**, 359–378
21 Pinto, M.R. and Kelly, P.J. Age related changes in bone in the dog: fluid spaces and their potassium content. *J. Orthop. Res.* 1984, **2**, 2–7

APPENDIX

BMDP PAR

BMDP PAR is a derivative-free nonlinear regression package that estimates the parameters of a nonlinear function by least squares. Upper and lower bounds can be specified on the individual parameters or for arbitrary linear combinations of the parameters.

The nonlinear function is fitted by a Pseudo–Gauss–Newton iterative algorithm. The termination criterion for the algorithm is given by

$$\left| \frac{RSS^{(k+1)} - RSS^{(k)}}{RSS^{(k+1)}} \right| < C$$

for five successive values of k, where $RSS^{(k)}$ is the residual sum of squares at step k and C is the value of the convergence criterion. If the *RSS* increases between two iterations, the increment size is halved and the *RSS* is recomputed and tested against the *RSS* at the previous iteration. This halving is repeated until the *RSS* is less than that of the previous halving or the maximum number of halvings is reached.

A tolerance criterion is used to guard against round-off errors in critical portions of the computations.

Pre-assigned package values

Convergence criterion (C)	1×10^{-5}
Tolerance criterion	1×10^{-8}
Maximum number of iterations	50
Maximum number of increment halvings	5